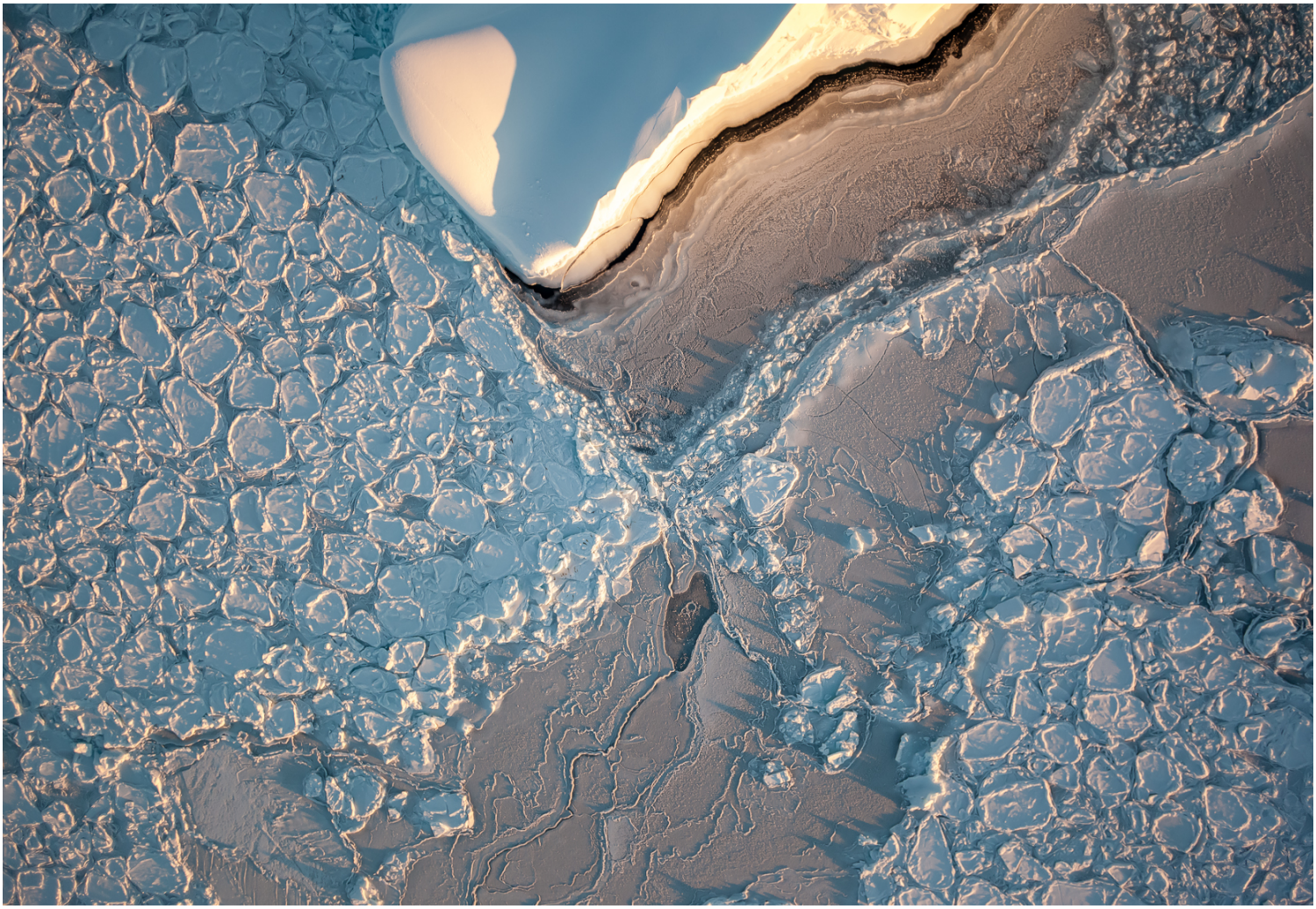

Incorporation mechanisms of iron and organic matter into newly-formed sea ice

by

Julie Janssens
B.Sc., M.Sc.

Submitted in partial fulfilment of the requirements for the Degree of
Doctor of Philosophy in Quantitative Antarctic Science

University of Tasmania (UTAS)
Institute for Marine and Antarctic Studies (IMAS)
Australian Antarctic Division (AAD)
Antarctic Climate & Ecosystems Cooperative Research Centre (ACE CRC)

November, 2016

Incorporation mechanisms of iron and organic matter into newly-formed sea ice

By

Julie Janssens
B.Sc., M.Sc.

Under the supervison Dr. Delphine Lannuzel, Dr. Klaus Meiners and Dr. Ben Galton-fenzi

Submitted in partial fulfilment of the requirements for the Degree of Doctor of Philosophy in Quantitative Antarctic Science

University of Tasmania (UTAS)
Institute for Marine and Antarctic Studies (IMAS)
Australian Antarctic Division (AAD)
Antarctic Climate & Ecosystems Cooperative Research Centre (ACE CRC)

November, 2016

Australian Government
Department of the Environment and Energy
Australian Antarctic Division

Declaration of originality

I declare that this thesis contains no material which has been accepted for a degree or diploma by the University or any other institution, except by way of background information and duly acknowledged in the thesis, and to the best of my knowledge and belief no material previously published or written by another person except where due acknowledgement is made in the text of the thesis, nor does the thesis contain any material that infringes copyright.

Signed:

Julie P. J. Janssens

Date: November 3rd, 2016

Authority of access statement

The publisher of the paper comprising Chapter 2 holds the copyright for that content, and access to the material should be sought from the journal. The remaining non published content of this thesis may be made available for loan and limited copying in accordance with the *Copyright Act 1968*.

Signed:

Julie P. J. Janssens

Date: November 3rd, 2016

ABSTRACT

Sea ice plays a critical role in the global ocean, including polar biogeochemical cycles and ecosystems. Importantly, sea ice serves as temporal reservoir for key nutrient iron (Fe), which is known to limit primary productivity in large parts of the Southern Ocean. Iron released from melting sea ice contributes to the formation of important phytoplankton blooms, and the carbon drawdown in the marginal ice zone. Although the importance of sea ice as a source of Fe for the Southern Ocean has been clearly established, the processes leading to the high levels of Fe in sea ice have yet to be identified and quantified. In this study, the mechanisms responsible for Fe enrichment in sea ice are explored through observations, including *in situ* ice-growth experiments, laboratory ice-growth experiments, and one-dimensional numerical modelling.

A combination of natural young ice sampling and *in situ* ice-growth experiments conducted under trace metal clean conditions during a winter voyage in the Weddell Sea shows that enrichment of Fe and organic matter starts at the very first stages of sea ice formation. Results show that physical processes occurring during sea ice growth are responsible for early enrichment of both Fe and organic matter into newly formed sea ice. The particle size plays a key role, with bigger particles exhibiting higher enrichment indices (EI). Dissolved compounds behaved conservatively with salt, except dissolved Fe (DFe) and ammonium, which were enriched in the ice compared to concentrations in the underlying seawater. Differential behavior of DFe and particulate Fe (PFe) is observed for the first time during sea ice formation, suggesting a decoupling throughout the whole year.

The role of organic matter (particulate organic carbon and extracellular polymeric substances (EPS)) as a carrier for Fe is then investigated using laboratory ice growth experiments. The form of organic matter determines its entrapment rate in forming

sea ice. The quality of organic matter also influences its association with Fe, and therefore the EI of Fe. Biogenic PFe is preferentially enriched compared to lithogenic PFe. Higher EI for biogenic PFe are explained by a combination of factors, such as size and association to EPS. Organic ligands are thought to drive the enrichment of DFe into forming sea ice.

Finally, a Fe-biogeochemical component was added to the Louvain-la-Neuve sea Ice Model (LIM-1D) to explore the initial entrapment of Fe in young sea ice, and to identify the biological and physical mechanisms driving the Fe dynamic in older sea ice. LIM-1D is a one-dimensional (vertical) biogeochemical sea ice model configured to reproduce the typical thermodynamic regimes of first-year Antarctic sea ice. By implementing the model with an entrapment factor for PFe and an adsorption rate for DFe it is possible to reproduce the high DFe and PFe concentrations observed in young sea ice. The activation of biological processes is then needed in order to reproduce Fe pattern observed in older sea ice. Specifically, it is crucial to better constrain the parameters regulating the fluxes between pools of Fe. This represents a first step toward an improved representation of sea ice biogeochemical processes in order to introduce them in Earth System Models used for climate simulations.

A Papy

Acknowledgments

First I would like to thank my three extraordinary supervisors, Dr. Delphine Lannuzel, Dr, Klaus Meiners and Dr. Ben Glaton-Fenzi. Thank you for all your advice and support and for your guidance and encouragement over the past four years. I feel very lucky to have you. As a child I had a dream to travel to Antarctica, and thanks to you Delphine and Klaus, that dream came true more than once. I don't think I could thank you enough for trusting me and sending me on (and through) the ice.

I also received great support during my PhD from Dr. Pier van der Merwe (your knowledge and patience with the FIA are truly incredible Pier) and Dr. Ashley Townsend (ICP-guru). It was a pleasure to work with you and I learnt so much from you. Dr. Martin Vancoppenolle, thank you for the model, thank you for collaborating with us, and thank you for all your funny e-mails when discussing serious questions. It has been really fun to work with you in between hemispheres.
Seb, je sais pas trop comment te remercier pour tout ce que tu as fait pour moi ces derniers mois. Je crois toujours que ce dernier chapitre ne serait pas sorti sans ton aide et tes cafés (et le tiramisu de Claire). Et si tu doutes encore, demande autours de toi, je fais ton apologie!
A special thank you goes to Wenneke Ten Hout (you just make everything so much easier Wen) and Simon Wotherspoon (aka Spoon), your help has been invaluable.
More generally I would like to thank the IMAS and ACE CRC crew who created such a fun work environment.
Jean-Louis, thank you for infecting me with your sea ice virus at first and then "sending" me to Tassie. I wont forget where it all started!

I don't think this PhD adventure would have been the same without the three Antarctic adventures. I met some truly amazing people in each trip, and will forever be grateful to have been able to share these adventures with them. A huge thanks to all the SIPEX folks and crew of the Aurora Australis. A big shout out to Molly, Fanny (possibly the two best cabin-mates you can have!), Arnout, Olivier and Anne-Ju for making each trip on the ice so much fun despite the un-countable issues we had all the time. It was a pleasure to share all these giggles with you. Klaus I will always be indebted to you for showing us the rudiment of sea ice sampling despite your very much-overbooked schedule as a Chief Scientist. This first meeting with the "White Continent" was such a unique experience, and certainly wouldn't have been the same without you.
Another huge thank you goes out to the AWECS folks and crew of the Polarstern. Braving the Antarctic winter (and the German gastronomy) with you all was certainly an unforgettable experience. Janne, Anne-Mari, Jean-Louis, Bruno, Gerhard (thanks) for keeping an eye on me during the entire cruise), Jeroen (Bedankt Jeroen voor onze tijd in de bubble met de Grote David), Daiki and Christiane the whisky tastes so much better when drunk out of an ice core! A special thank you goes out to Priska, Michelle

and the CTD monkeys for keeping me entertained all day and night, and providing some good coffees!
The third and last Antarctic thank you is to the Davis folks. The science party was pretty much another dream team: Pat(s), Klaus, Arnout, Florian, Marie, Naoya, Pettra, Rob(s) and Mark, I cant thank you enough for the time spent on the ice, in the lab and in the bar. Clive thanks for filling up for me when I couldn't. Sharon, I don't think the twice-daily meetings would have been the same without you. I sure could count on the giggles to keep us going. Thank you for making everything easier for us. Mark, you are the best Yellow-Hagg-taxi-driver I have ever met, and VLZ ~~Casey~~ Davis had an overtone with you. Also, a big thank you to the boys: Mizza, Scotty, Nei(ie)l, Karloto, Hayden, Mick, Adam, Cam, Kirck, and co. You are an awesome bunch of very entertaining cool cats! And now I can say I have met some real Aussies! Seb a special thanks for you for feeding us so well, and for the special brunch on the ice. This experience really moved me!

To keep going with the Antarctic theme: A big thank you to The Young Antarctic Scientists (YAS) team: Guy, Eva, Tom, Pearse, Ben, Merel, Nick, Mana, Molly, Tom, Margaux and David. It was very rewarding to share our Antarctic experience with the kids, and what a team to do it with!

Finally, a big thanks to the 4th floor of bâtiment D, ULB, for welcoming me during my two Belgian stays. You have a very special team there.

Now I need to thanks these people from behind the scene, family and friends from here and the other side of the planet. This wouldn't have been possible without your smiles, giggles, support and amazingness of each and every one of you.
To the Southern Hemispherians: Thank you for all the Tasmanian adventures and making Tassie life here so enjoyable. The "first generation" just made it so easy to come back after my internship and start the PhD: Molly, Alyce, Eva, Mana, Mauro, Lucho, Ramossito (sorry for your reproductive fitness), Andre and Nicole, Manu (le Père). Tania, Daniela, Claudio, Roland, Vero, Mono, Fabien, Lara, Eric and Ceci, Axel and Malou and Sjoerd.
The "second generation" made it so easy to stay: Thibaut (le petit frère), Wally, Tom and Christine, Malindicious, Lavy (also, a massive thank you for reading through my thesis!), Bibi et Anicee (merci pour le support belge, je me sens moins seule depuis que vous êtes la!), Maddy, Ari and Joan, the Papas, Pearse, Seb(s), Delphi, Sandra, Indi, Martin(s), Nico and Anthony, Rominou et Melanouille, Andreas, Jimmy(s), Margausita (I still think my parents didn't tell me about you being my second sister!), Nina, Karine, Manon, and all the others that I can't name here. A massive thank you for Saga (le Mère) and Fluffy, I wouldn't be the same if without you.
Matt, thank you for being my first (and most favourite) Australian friend, thanks for being the only one trusting my driving skills.

These acknowledgments wouldn't be complete without thanking my early morning buddies from Bucks: Stumpy, Lucy, Meaghan, Fi, Boof, Laura, Abbie and Christie, … The early morning sunrises on the Derwent, and weekends at Lake Barrington were always worthwhile with you! Keep pushing hard girls!
Thank you to Channel 10 for providing some good entertainment on late Thursday nights (and thank you to Moisi for sharing that for 2 years!)
Hats off to all the housemates I had the privilege to live with. Alyce (I still can't believe you survived two years with me! This is a world record, well done), Pattra, Gen, Matthias and Anna, Michal and Dani and Yuko. Thank you for feeding me, not only with food, but also with love, support and care during these four years.
Guys, I feel so lucky to have you all, and will never be able to express all my gratitude. You are a second family for me here! Keep rocking the world my friends!

Un mega thanks aux amis Belch's: Martin, Aline, Milou, Coralie (j'aurais jamais pu survivre sans tes réapprovisionnement en Côte d'Or), Marine, Chavo, Fish, Anne-Ju, Amandine, Batman, Melissma, Demi-Poney et les "Affreux" de Belgique. C'est chouette de savoir que je peux toujours compter sur vous pour des retours folkloriques et éthyliques. Vous n'avez pas failli à votre tâche! Milou, big up à ce voyage extraordinaire dans l'hiver patagonien! Hats off to the visitors pour avoir fait le voyage (et pour la plupart, merci à leur labos respectifs pour financer le voyage): Celia, Momo, Martin, Zhou-Zhou, Brice, Melissa et bien sur Batman. Ca fait toujours chaud au coeur de voir vos bouilles de ce côté-ci.
Merci aux 9 filles du 8+ et Olivier! Cette course, ca restera un des temps fort de ces 4 dernières années. Merci d'avoir cru en moi et de m'avoir intégrée dans l'équipe. (Et big up à l'UNB en général, qui rendait ces épopées belges toujours un peu plus spéciales)

Time has come to thanks the VIP area! First, la crazy Kipet. Tout ca n'aurait pas été aussi haut en couleurs sans toi! Kipet et Kipiss on encore de belles années devant elles.
Claudio, my dear BC, maybe?! Coolah!
And last but not least, these three, who were here from the very start of the adventure: Mana, Manu, and Sally (it just feels like you have always been here). You bring so much joy and happiness into my life that I can't express it! I don't think I can express how I feel about you three, and how grateful I am towards your unconditional support, uncountable coffees, teas and beers, gins, chats, laughs and giggles, and much more. I have learnt so much about life, gastronomy, friendship, French methods, Australian/New-Zealander reasoning, slang, and Japanese traditions. You guys truly made the lunch breaks and this entire adventure so special (plus I don't think I would have survived the last six-or-so months without you).

My final thanks goes out to my Family from the Northen Hemisphere. A vous tous, la Famille de de l'autre côté, sur qui je peux toujours compter: Les bruxellois: Mamy,

Papitou, Sophie, Paul, Michel et les deux d'jeuns: Baboo, Eesha; et les liégeois: Youri, Anne, Philou et Guy.
Et enfin, les derniers remerciements et pensées vont à ceux à qui je fais la vie dure depuis maintenant 29 ans: Les Janssens: Papa, Maman et Céline. Mes remerciements vont au delà de ce que je peux écrire ici (puis bon, Maman, tu risquerais d'encore verser une larme), mais honnêtement, rien de tout cela n'aurait été possible sans vous. Merci!

Statement of Co-authorship

The following collaborators contributed to the publication of the work undertaken as part of this thesis:

(1) ***Julie Janssens (candidate)*** - Institute for Marine and Antarctic Studies (IMAS), University of Tasmania, Hobart, Australia; Antarctic Climate and Ecosystems Cooperative Research Centre (ACE CRC), University of Tasmania, Hobart, Australia; Australia Antarctic Division (AAD), Kingston, Tasmania.
(2) ***Delphine Lannuzel*** - Institute for Marine and Antarctic Studies (IMAS), University of Tasmania, Hobart, Australia; Antarctic Climate and Ecosystems Cooperative Research Centre (ACE CRC), University of Tasmania, Hobart, Australia.
(3) ***Klaus M. Meiners*** - Australian Antarctic Division (AAD), Kingston, Australia; Antarctic Climate and Ecosystems Cooperative Research Centre (ACE CRC), University of Tasmania, Hobart, Australia.
(4) ***Jean-Louis Tison*** - Glaciology Unit, Département Géosciences, Environnement, Société, Université Libre de Bruxelles, Belgium.
(5) ***Gerhard S. Dieckamnn*** – Alfred-Wegener-Institut Helmholtz-Zentrum für Polar und Meeresforschung, Bremerhaven, Germany
(6) ***Bruno Delille*** – Unité d'Océanographie Chimique, MARE, Université de Liège, Belgium.
(7) ***Fanny Chever*** – Ocean and Earth Science, National Oceanography Centre Southampton, University of Southampton, United Kingdom.
(8) ***Pier C. van der Merwe*** - Antarctic Climate and Ecosystems Cooperative Research Centre (ACE CRC), University of Tasmania, Hobart, Australia.
(9) ***Arnout Roukearts*** – Analytical, Environmental & Geo-Chemistry, Vrije Universiteit van Brussel, Brussels, Belgium.
(10) ***Anne-Julie Cavagna*** - Analytical, Environmental & Geo-Chemistry, Vrije Universiteit van Brussel, Brussels, Belgium.
(11) ***Ashley T. Townsend*** – Central Science Laboratory, University of Tasmania, Hobart, Australia.

(12) ***Andrew R. Bowie*** – Institute for Marine and Antarctic Studies (IMAS), University of Tasmania, Hobart, Australia; Antarctic Climate and Ecosystems Cooperative Research Centre (ACE CRC),

PAPER 1 (Chapter 2):

1. **Janssens J,** Meiners K.M., Tison J.-L., Dieckmann G.S., Delille B. and Lannuzel D. 2016. Incorporation of iron and organic matter into young Antarctic sea ice during its initial growth stages, *Elementa Science of the Anthropocene* 4: 000123, 2016, doi: 10.12952/journal.elementa.000123

Janssens J. 70% *Meiners K.M. 10%, Tison J.-L. 4%, Dieckmann G.3%, Delille B. 3% and Lannuzel D.10%*

JJ, KMM and DL designed the project. JJ, KMM, JT, GD, BD and DL contributed to the field and laboratory analysis. JJ took the lead role in data analysis, manuscript preparation and reviews, with DL, KMM, BB, DG and JT assisting in manuscript drafting.

PAPER 2 (Appendix):

2. Lannuzel D., Chever, F., van der Merwe P.C, **Janssens, J.,** Roukaerts A., Cavagna, A.J., Townsend A.T., Bowie A.R. and Meiners, K. 2014a Iron biogeochemistry in Antarctic pack ice during SIPEX-2, *Deep Sea Research II Top Stud Oceanogr*, 131:111-122. doi: 10.1016/j.dsr2.2014.12.003.

Lannuzel D. 55%, Chever, F 10%., van der Merwe P 5%., ***Janssens, J. 5%,*** *Cavagna, A.J. 5%, Roukaerts A. 5%, Townsend A. 5%, Bowie A. 5% and Meiners, K* 5%

DL designed the project and analysed the samples. FC, JJ, AC, AR and KM collected the samples and field data. DL took the lead role in data analysis, manuscript preparation and reviews, with FC, PvdM, JJ, AC, AR, AB and KM contributing to the revision of the manuscript.

We, the undersigned, agree with the above stated, "proportion of work undertaken" for each of the above published peer reviewed manuscript contributing to this thesis:

Signed

Dr. Delphine Lannuzel
Primary Supervisor
Institute for Marine and Antarctic Studies (IMAS)
University of Tasmania

Date: 23.04.2017

Signed:
(Neil Holbrook, A/HOS)
on behalf of

Pr. Nathan Bindoff
Head of School
Institute for Marine and Antarctic Studies (IMAS)
University of Tasmania

Date: 26/4/2017

Signed:

Julie Janssens
PhD Candidate
Institute for Marine and Antarctic Studies (IMAS)
University of Tasmania

Date: 23.04.2017

TABLE OF CONTENT

List of figures

List of tables

CHAPTER 1

Introduction

1.1 General context

Carbon dioxide (CO_2) is the primary driver of recent climate changes (IPCC report. 2013). The atmospheric concentration of CO_2 has increased from 270 ppm in the 1750's to over 400 ppm at present (http://www.esrl.noaa.gov/gmd/ccgg/trends/). The world ocean plays a key role in the regulation of the Earth's climate by transferring the carbon form the atmosphere into the ocean. The transfer of carbon from the atmosphere to the ocean occurs through the physical and the biological pumps of carbon demonstrated in Figure 1.1.

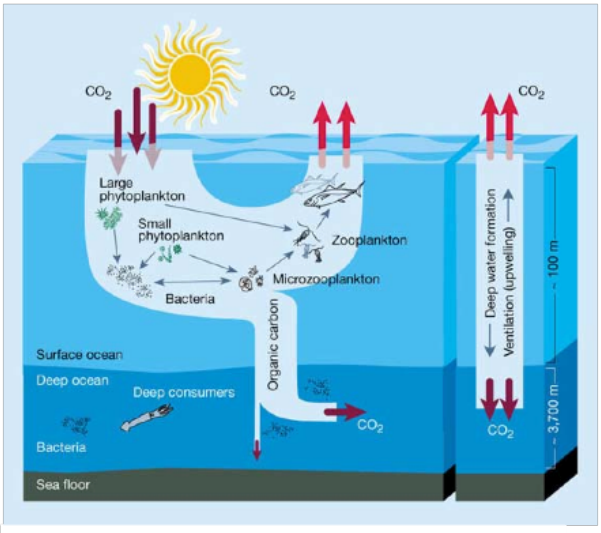

Figure 1.1 Schematic of the biological (left) and physical (right) carbon pump in the ocean (from Chisholm, 2000)

The uptake of carbon by the ocean primarily happens through physical processes where CO_2 is dissolved into cold waters and downwelled into the deep ocean via the

physical pump (also called the solubility pump). This process is especially efficient in the Southern Ocean, whereby the formation of sea ice initiates the sinking of cold saline CO_2 rich waters to the depths via the formation of Antarctic Bottom water. Sequestration of CO_2 is also induced by the fixation of CO_2 by primary producers, followed by a fraction of produced organic matter sinking into the deep waters, referred to as the biological pump.

The Southern Ocean represents only 10% of the world ocean but is responsible for sequestering 25% of the atmospheric CO_2 (Takahashi et al., 2002). The net primary production (NPP) is the amount of carbon capture by plants through photosynthesis. The global NPP has been estimated at 104.9 gigatons of carbon per year (Field et al., 1998). Although marine phytoplankton represents only 0.2% of the global plant biomass, its contribution to the global NPP is equal to the contribution from the terrestrial biomass (Field et al., 1998). Each year, approximately 16 gigatons of the organic carbon produced through photosynthesis by phytoplankton is exported to the deep ocean (Falkowski et al., 1998), and isolated from the atmosphere for thousands of years (Chisholm, 2000).

The efficiency of the biological pump in the Southern Ocean is constrained by interactions between silicate limitation (Brzezinski et al., 2003), grazing on phytoplankton (Atkinson et al., 2001; Dubischar and Bathmann, 1997), light availability (Mitchell and Holm-Hansen, 1990; Nelson and Smith, 1991), and iron supply to surface waters (Martin et al., 1990; Lancelot et al., 1993; de Baar et al., 1995; Smetacek et al., 2012).

1.1.1 The role of iron in the ocean and the iron hypothesis

Iron (Fe), which is one of the main elements of the Earth crust (Taylor, 1964), is a vital nutrient for marine life, and therefore a key player in the carbon cycle. This

essential micro-nutrient is used by phytoplankton and sea-ice algae in metabolic processes (e.g., in electron transport chains in photosynthesis and respiration, and in chlorophyll synthesis Raven et al., 1999; Tortell et al., 1999; Michel and Pistorius, 2004). Approximately 80 % of the biological requirement of Fe by phytoplankton is used for metabolism associated to photosynthesis (Raven et al., 1999). In the Southern Ocean, light and Fe co-limit primary production (de Baar et al., 2005; Lancelot et al., 1993).

The Fe limitation in the Southern Ocean is referred to as the "iron hypothesis" and was initially proposed by Martin (1990). Ice core records demonstrate that the atmospheric CO_2 concentrations were higher during the interglacial periods compared to the glacial periods. Further examination of aeolian dusts particles in ice cores suggests that the supply of Fe to the ocean was higher during glacial periods, boosting the biological pump in the Southern Ocean and delivering more CO_2 to the deep sea, consequently decreasing the concentration of CO_2 in the atmosphere (Martin, 1990). Model calculations have attributed the 30% difference of atmospheric CO_2 concentrations observed between the interglacial-glacial periods to the enhanced primary production (Falkowski et al., 1998). More recently, a number of artificial Fe fertilisations experiments have confirmed that addition of Fe to the surface ocean enhances primary productivity in the Southern Ocean. While it was shown that addition of Fe increases the growth rate of phytoplankton, increased carbon export to the deep ocean was observed in a small subset of these experiments (Boyd et al., 2007).

1.1.2 High-nutrients, low-chlorophyll ocean

In Fe-deficient waters, phytoplankton is unable to take advantage of the macro-nutrient-rich (phosphate, silicic acid and nitrate) environment it lives in. These

regions are known as a high-nutrient, low-chlorophyll area (HNLC). The Southern Ocean is the largest HNLC area in the world ocean (Boyd and Ellwood, 2010), however Fe limitation (sub-nano molar level of Fe) is also observed in different parts of the global ocean: the subarctic Pacific, the equatorial Pacific and the Southern Ocean (Figure 1.2). Together they represent 40% of the global ocean.

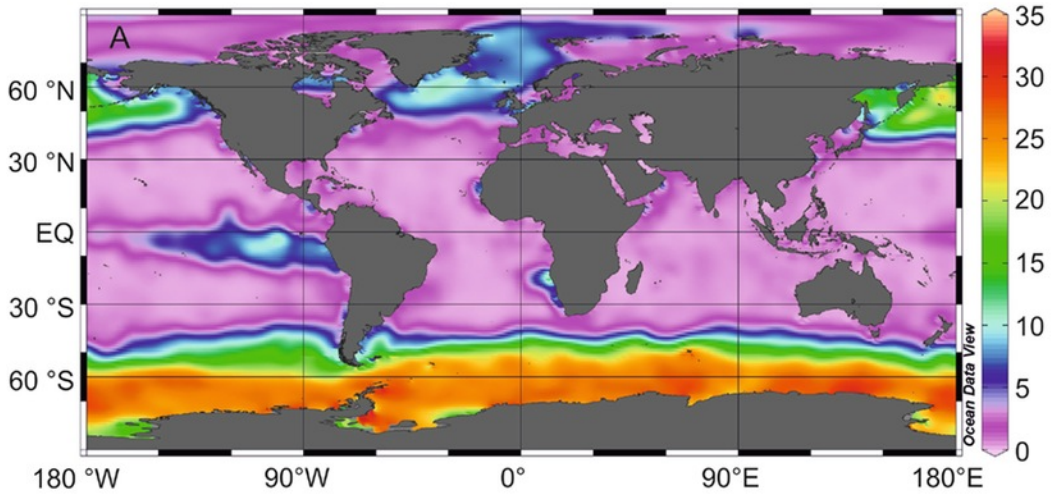

Figure 1.2 Annual average surface water nitrate concentrations (μmol L^{-1}). The nitrate distribution was obtained using data from the World Ocean Atlas 2009. The three main HNLC regions are the Southern Ocean, the Equatorial Pacific and the Sub-Arctic Pacific (Gledhill and Buck, 2012)

1.1.3 Sources of Fe in the Southern Ocean

Primary sources of Fe in the Southern Ocean include continental shelf advection and sediment resuspension (e.g., Bowie et al., 2009; de Jong et al., 2012, 2015; Johnson et al., 1999; Sedwick et al., 2000; Westerlund and Öhman, 1991), upwelling, vertical diffusion and deep winter mixing (Blain et al., 2007; de Baar et al., 1995; de Baar and de Jong, 2001; Hoppema et al., 2003; Loscher et al., 1997; Tagliabue et al., 2014), atmospheric dust depositions and extraterrestrial dusts (Boyd and Mackie, 2008; Boyd et al., 2004; Cassar et al., 2007; Johnson, 2001). Due to the remoteness of the Southern Ocean, continental dust depositions are extremely low (Gao et al., 2013, 2001; Jickells et al., 2005; Wagener et al., 2008; Winton et al., 2016). Nonetheless,

dust depositions might be important locally. De Jong et al. (2015) showed that depositions from the McMurdo Dry Valley and the Mount Erebus volcano are a substantial supply of dissolved Fe (DFe) to the nearby sea ice and surface waters.

Although melting icebergs also contribute to replenish the Antarctic waters with Fe (de Baar and de Jong, 2001; Duprat et al., 2016; Hoppema et al., 2003; Lin et al., 2011), it is believed that it does not significantly contribute to the flux of DFe in the upper mixed layer, and therefore has a limited impact on the natural Fe fertilisation of the Southern Ocean (de Jong et al., 2015). More recently hydrothermal vents have been shown to contribute to the DFe pool of the Southern Ocean (Klunder et al., 2011; Resing et al., 2015; Tagliabue et al., 2010). Dominant sources differ in space and time. Vertical advection dominates in the open ocean (de Jong et al., 2015), while lateral fluxes dominate in the continental shelf (de Jong et al., 2012). Supply of particulate Fe (PFe) to the coastal area, including land-fast sea ice, is dominated by sedimentary inputs (de Jong et al., 2013; Grotti et al., 2005; van der Merwe et al., 2011; Noble et al., 2013). Melting of glacial ice is thought to be a major source of DFe in the Ross Sea (Gerringa et al., 2015; Sherrell et al., 2015). Recent analysis of Fe in continental and marine ice from the Amery Ice Shelf confirms this finding in the East Antarctic sector (Herraiz-Borreguero et al., 2016). Based on future rates of ice shelf basal melt, this fertilization pathway is likely to increase, with important implications for the Southern Ocean productivity and CO_2 drawdown.

1.1.4 Role of sea ice as an ocean fertiliser

Sea ice is not a new source of Fe but it acts as a spatial and temporal reservoir of Fe (e.g., Lancelot et al., 2009; Lannuzel et al., 2010; Sedwick and DiTullio, 1997). Sea ice meltwaters contribute to up to 70% of the total Fe input in the Antarctic surface waters during spring (Lannuzel et al., 2007), and Fe released from sea ice contributes

to the formation of intense algal blooms observed in the marginal ice zone in spring (Lancelot et al., 2009; Lannuzel et al., 2010, 2007; Sullivan et al., 1993). Recent studies estimated the seasonal release of Fe from melting fast ice might support 85% of the local primary production in the Ross Sea (de Jong et al., 2013).

Similarly, Lannuzel et al. (2014a) highlighted the importance of sea ice as a biogenic PFe supplier to Antarctic surface waters. These authors estimated that the flux of sea-ice derived lithogenic and biogenic PFe is an order of magnitude higher than the flux of DFe. They calculated that the melting of sea ice sustains up to 40% of the primary productivity in the East Antarctic sector (Lannuzel et al., 2014a). The importance of sea ice as Fe supplier for Southern Ocean surface waters increases with distance to the Antarctic continent and the shelf-break zone (Lannuzel et al., 2016).

Sea ice extent and volume is predicted to reduce in the future due to climate change (e.g., Arzel et al., 2006; Smith et al., 2012). However, sea ice cover in the Southern Ocean has expanded slightly since the late 1970's (e.g., Parkinson and Cavalieri, 2012; Stammerjohn et al., 2012). Important regional trends exist: increase in sea ice extent has been observed in the Ross sea, the Weddell sea and the Indian Ocean sector, but a decrease in sea ice extent was observed in the Bellinghausen/Amundsen sea sector (Parkinson and Cavalieri, 2012; Stammerjohn et al., 2012).

Sea ice plays an important role in the physics, the biogeochemical cycles and the ecology of the Southern Ocean. Sea ice formation is a major driver of the global ocean overturning circulation (e.g., Rintoul et al., 2001). The albedo of sea ice is higher than the albedo of the open ocean, reflecting 50 to 70 % of the incoming solar radiation (e.g., Brandt et al., 2005). The ecology of the Southern Ocean is also relying on the presence of sea ice as a source of food for higher trophic level (e.g., Flores et al., 2012; Nicol et al., 2008), and foraging and breeding ground for iconic Antarctic

species, such as penguins and seals (Kooyman and Burns, 1999). The presence of a sea ice cover impacts the biogeochemical cycles such as CO_2 exchanges between the ocean and the atmosphere (Delille et al., 2007; Nomura et al., 2010), the Fe cycles (e.g., Lannuzel et al., 2010), and the sulphur cycle with sea ice being a major source of dimethyl sulfide (Stefels et al., 2007; Trevena and Jones, 2012). Possible implication and feedbacks mechanisms of changes in sea ice on these cycles are currently poorly understood. To evaluate this impact, it is essential to fully understand and quantify the present-day biogeochemical processes associated to sea ice growth and melt cycles.

1.2 Challenges and strategies

Antarctic sea ice forms from very low Fe-concentration seawater and because formation of sea ice rejects impurities, the first data reporting high Fe concentrations in sea ice raised questions (Grotti et al., 2005, 2001; Lannuzel et al., 2014a, 2014b, 2008, 2007; van der Merwe et al., 2011a, 2011b, 2009; Noble et al., 2013). Despite growing body on Antarctic sea ice biogeochemistry, the mechanisms leading to Fe enrichment in sea ice remain poorly understood.

The co-occurrence of high concentrations of Fe and organic matter in sea ice (de Jong et al., 2013, 2015; Grotti et al., 2005; Lannuzel et al., 2014a, 2014b, 2008, 2007; van der Merwe et al., 2011a, 2011b, 2009) suggests coupled processes leading to their enrichments. The aim of the thesis is to elucidate and quantify the pathways leading to Fe and organic matter enrichment in sea ice. In this work, we use a multi-pronged approach, combining field experiment data, laboratory ice-growth data and one-dimensional (1-D) modelling.

1.3 Sea ice formation processes

1.3.1 Macro-scale

Sea ice forms through freezing of seawater. Through contact with the cold atmosphere, Antarctic seawater temperature drops down to the freezing point (~ -1.8°C for a salinity of 35 S_P). Crystals of frazil ice then start to form on the surface of the ocean or at depth (up to 30 m deep in the water column (Penrose et al., 1994)). These ice crystals, being more buoyant that seawater, begin to rise towards the surface to accumulate at the surface of the ocean where they form a soupy layer of "grease ice" or accumulate at the bottom of an existing ice cover (Horner et al., 1992). Crystals of frazil ice are 2 to 4 mm in size and can have various shapes from spicules-like to platelet-like. These crystals form the so-called granular ice (Figure 1.3). In calm conditions, crystals of frazil ice continue to accumulate, and form a continuous elastic and transparent cover of "nilas" (~ 0.10 m thick). Nilas continues to develop into "grey ice" (0.10-0.15 m thick). In turbulent conditions, crystals of frazil ice are compressed in pancake ice. Pancake ice is circular piece of ice that can grow to few meters in diameter and a couple of tens of centimetres in thickness (Lange et al., 1989; Maykut, 1985). Pancakes raft and ridge under the action of waves and wind. They form an ice sheet once consolidated together.

Once the water is isolated from the atmosphere, the latent heat required for the freezing of seawater is extracted from the ice itself, and congelation ice starts to develop downward under the surface ice layer (Figure 1.3). The growth rate is determined by the temperature gradient in the ice cover and its effective conductivity. Crystals of congelation ice (or columnar ice) grow slower than frazil ice, theoretically rejecting impurities more efficiently than frazil ice. Growth of crystals of columnar ice is only possible in one direction and a geometric selection occurs. This results in

vertically elongated and prismatic crystals that can grow up to several centimetres in diameters and tens of centimetres in length. Sea ice continues to grow through the winter period. Young ice is defined as the stage between nilas and first-year ice, and can be up to 0.3 m thick. As young ice grows, it becomes the so-called first-year ice. As indicated by its name, first-year ice is not older than one year and has a thickness of 0.3 to up to 2 m (or more). Thermodynamics alone do not determine the ice thickness. Internal stress and external forces (wind, currents) play an important role in the formation of ridges and rafting of sea ice.

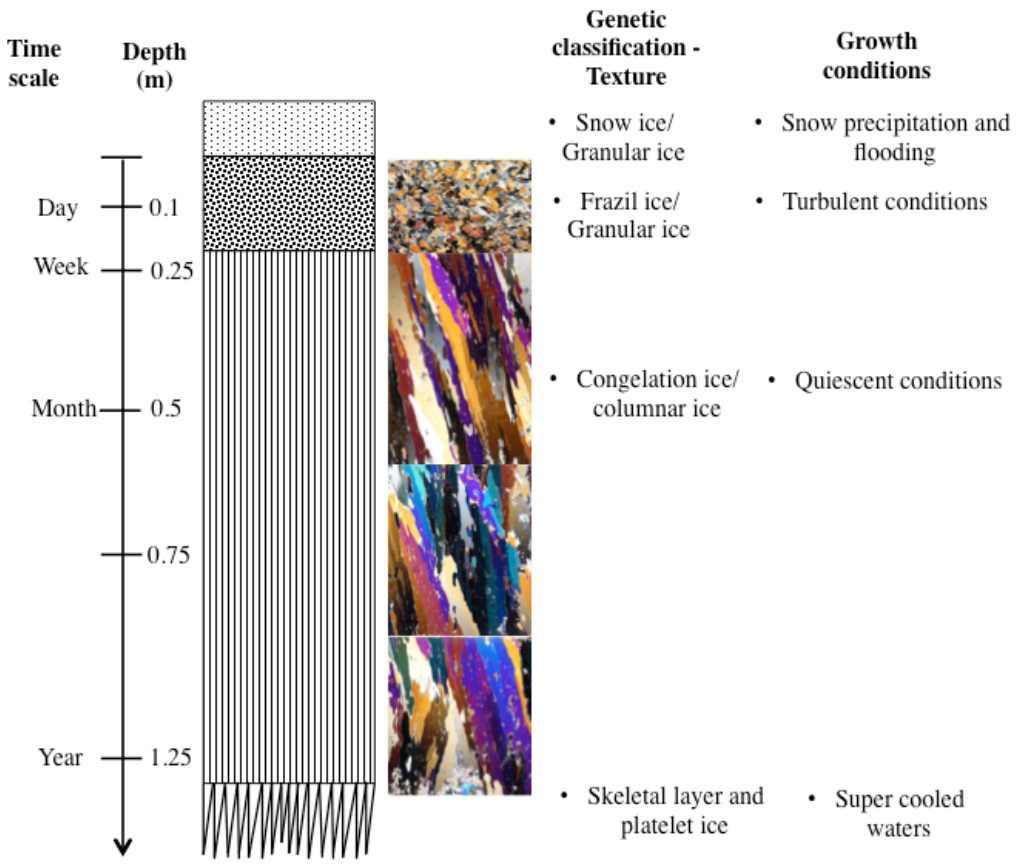

Figure 1.3 Illustration summarizing the main ice textures, growth conditions and timescales for first year sea ice (adapted from Eicken, 2003). Photos from J-L Tison and J Janssens.

Depending on its location, fast ice refers to the sea ice that fasts along the coast of Antarctica and stays attached to the shore. Fast ice is often anchored by grounded icebergs. Pack ice refers to the floating sea ice not attached to the continent. Pack ice is usually more rafted and ridged than the fast ice because it has formed in a more turbulent environment under the action of winds, currents and waves. In Antarctic waters, fast ice can be more than a year old, while pack ice is usually first-year ice (multi-year pack ice is found in the western part of the Weddell Sea, Hellmer et al., 2006) and fully melt each spring-summer.

There are three other ice classes found in Antarctic sea ice according to the presence of snow on top on the ice cover, the presence of melting ice or the formation of ice due to super cooled waters. The former two usually occur later in the season. Snow ice forms when there is negative freeboard (ice depressed below sea level) due to the thick snow cover on top of the ice sheet. The seawater infiltrates the snow and forms snow ice when the saturated snow refreezes (Fritsen et al., 1998). Like frazil ice, crystals of snow ice are granular in shape (Figure 1.3). Measurements of stable water isotopes ($\delta^{18}O$) are used to distinguish the seawater-derived granular ice from the snow ice (Eicken, 1998; Lange et al., 1989). Superimposed ice refers to refrozen snow meltwater on top of the ice cover. Platelet ice forms in the water column along the Antarctic coastline, usually underneath an ice shelf or an existing sea ice cover (Dieckmannn and Hellmer, 2010).

1.3.2 Micro-scale

Sea ice is a heterogeneous and porous media consisting of a matrix of pure solid ice and liquid saline phase, known as brines. When sea ice forms, only few species of ions and molecules with specific charge and size can be incorporated in the ice crystal lattice (e.g., fluorine, ammonium and some gases). Most of the impurities present in

seawater (e.g., Na^+, Cl^-, K^+, Ca^{2+}, Mg^{2+}) are rejected from the forming ice crystals because of electric charges and size constraints (Petrich and Eicken, 2010), and become concentrated in the brine inclusions within the ice matrix. As the ice grows and cools, brines become more concentrated. They start to move downward and under gravity drainage are eventually expulsed from the ice into the ocean and replaced with seawater through convection. Ahead of the advancing ice interface, the skeletal layer is composed of parallel vertical ice crystals (Figure 1.3). The skeletal layer is highly porous and small amount of seawater can be trapped between the growing crystals and incorporated in the ice. Niedrauer and Martin (1979) have observed convective movements in the skeletal layer (Figure 1.4) and the brine channels.

1.3.3 Mechanisms of incorporation of Fe and organic matter into sea ice

Although during formation sea ice rejects impurities, sea ice still holds a large reservoir of organic matter (dissolved and particulate) (e.g., Aslam et al., 2012; Norman et al., 2011; Thomas et al., 2001; Underwood et al., 2010; Zhou et al., 2014), microorganisms (e.g., Becquevort et al., 2009), and Fe (e.g., Grotti et al., 2005; Lannuzel et al., 2014a, 2010, 2008, 2007; de Jong et al., 2013; 2015) compared to parent seawater. Sea ice genesis can lead to the enrichment of biogenic and lithogenic materials through a combination of physical and biological processes that are currently not fully understood.

1.3.3.1 Initial incorporation of impurities

Although processes leading to Fe enrichment have not been specifically studied, van der Merwe et al., (2009) suggest that Fe and extracellular polymeric substances (EPS) are co-incorporated into the ice, helped by the sticky properties of EPS.

Once crystals of frazil ice have formed at depth in the water column, they rise up to the surface. During their ascent they scavenge and harvest impurities such as microorganisms, detritus or organic matter (Dethleff, 2005; Garrison et al., 1989; Osterkamp and Gosink, 1983; Reimnitz et al., 1993; Weeks and Ackley, 1982). Alternatively, impurities can act as nuclei to favour ice formation (Knopf et al., 2010). Crystals of frazil accumulate at the surface, and particles can be concentrated by wave field pumping through the freshly formed layer of frazil ice (Lindemann et al., 1997), or the action of Langmuir cells circulation (Martin and Kauffman, 1981). These particles then become attached to, or trapped in between, the ice crystals (Weissenberger and Grossmann, 1998). These processes are schematised in Figure 1.4. Bigger particles (or aggregated particles) are more enriched in sea ice compared to smaller particles (Gradinger and Ikävalko, 1998; Riedel et al., 2007; Von Quillfeldt et al., 2003). Although, physical processes do not seem to lead to the enrichment of bacteria in sea ice, bacteria can be attached to algae and EPS, and then concentrated in the ice layer by physical processes explained above (Grossmann and Dieckmann, 1994; Meiners et al., 2003; Riedel et al., 2007; Weissenberger and Grossmann, 1998). The potential role of EPS coating in the bacteria incorporation has been specifically highlighted (Riedel et al., 2007), but remains unclear.

1.3.3.2 Accumulation in columnar ice

Once a layer of consolidated ice is formed, exchanges of salts and nutrients between the ice and the seawater are controlled by convection (e.g., fluid movement induced by strong salinity gradients across the ice/water interface (Vancoppenolle et al., 2010). Lannuzel et al. (2010) proposed that these mechanisms are responsible for aggregation of living and dead microorganisms (and associated Fe) at the seawater sea ice boundary and subsequent incorporation into sea ice as the ice grows.

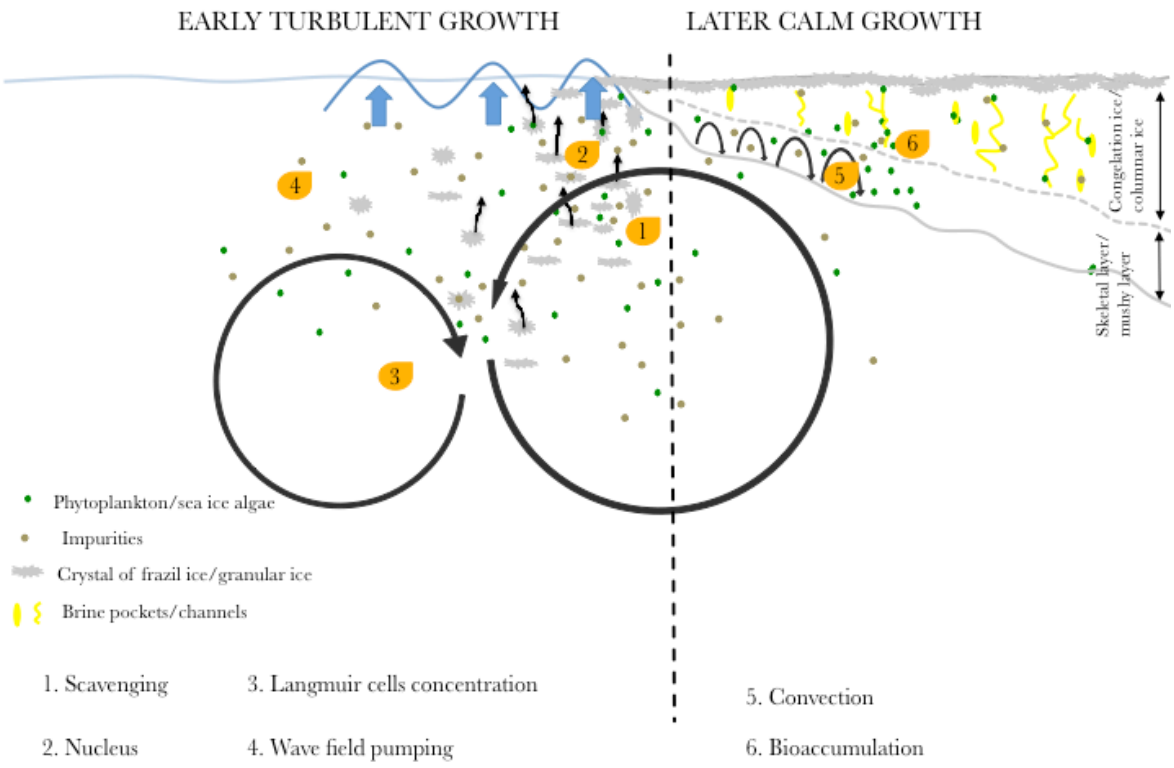

Figure 1.4 Schematic of the proposed mechanisms of particles entrapment in forming sea ice.

Organic matter, and associated Fe in columnar ice can built-up from the continuous development of algae at the bottom of sea ice (Lizotte, 2003; Spindler, 1994). The colonization mechanisms would allow the retention and migration of organic matter (living and decaying) and Fe towards the internal layers as the ice continues to thicken (Lannuzel et al., 2010; Noble et al., 2013, Figure 1.4).

So far, no clear relationship has been found between the ice texture and the enrichment in organic matter and Fe. This suggests that frazil ice does not incorporate more Fe and organic matter than granular ice (see ice texture in Dumont et al., 2009; Lannuzel et al., 2007; van der Merwe et al., 2009b), which is counterintuitive considering the physical processes of sea ice formation (illustrated in Figure 1.4).

1.4 Sea ice biogeochemistry

The unique physical structure of sea ice and the processes influencing its formation and decay determine the biology and chemistry of the sea ice matrix. Sea ice with a columnar ice crystal texture is believed to be permeable when the brine volume is > 5%, i.e., when the ice temperature is above -5°C and the bulk ice salinity > 5 ("Rules of Fives", Golden et al., 1998). Therefore, the interior of the sea ice is rarely isolated from seawater and exchanges between sea ice and the ocean occur from late spring to autumn. For ice with a granular sea ice texture, the permeability threshold is thought to be around a brine volume of 10 % (Saenz and Arrigo, 2012; Meiners and Michel, 2017). These exchanges are constrained by the molecular diffusion across the diffusive boundary layer (especially in young ice or porous rotten ice, Thomas et al., 2010), brine convection (Vancoppenolle et al., 2010), and advective processes (Thomas and Dieckmann, 2009). Microorganisms are greatly influenced by the chemistry of the medium surrounding them, and in turn, can modify it. A good example is the alteration of the salt retention and habitability of sea ice by EPS produced by sea ice algae or bacteria in the ice (Krembs et al., 2011).

1.4.1 Iron in sea ice

1.4.1.1 Overview of Fe measurements in Antarctica

Martin (1990) was the first to suggest that sea ice could be a source of Fe for Fe-depleted Southern Ocean surface waters. Following this, few Fe measurements have supported this hypothesis (Boye et al., 2001; de Baar and de Jong, 2001; de Jong et al., 1998; Loscher et al., 1997; Westerlund and Öhman, 1991) but it is only in 2001 that the first Fe profile in a sea-ice core was made (Grotti et al., 2001). Reason for this early very sparse data was the extremely challenging nature of sampling under trace

metal clean conditions in polar environments, and the lack of standardized procedure for sea ice sampling. The number of Fe measurements in sea ice has considerably increased over the past 2 decades following the development of trace metal sampling procedures by Lannuzel et al. (2006) for sea ice, brine and associated seawater.

Despite this, data are still sparsely distributed around the Antarctic continent and locations principally reflect the accessibility of the different sampling sites. The Australian East Antarctic sector between 90°E and 150°E is undoubtedly the most studied (Figure 1.5, Table 1.1). Among all these studies, only two focused on the temporal evolution of the distribution of Fe of a particular ice floe through time: Ice Station POLarstern (ISPOL) in Weddell Sea pack ice (Lannuzel et al., 2008) and a time-series of fast ice at Casey Station (van der Merwe et al., 2011a). Other studies display spatial variation of Fe concentrations in sea ice (Lannuzel et al., 2014a, 2007; van der Merwe et al., 2009).

Current Fe measurements are not representative of all the seasons. Sampling is indeed limited by the schedule of scientific cruises and the active Antarctic season, with very few, if any, studies in autumn and austral winter (Table 1.1). Autumn and early winter Fe concentrations in sea ice have not been available but are crucial to fully understand the biogeochemical Fe cycle associated to sea ice. Table 1.1 summarises currently available information including Fe concentration ranges and locations of study sites. A full review of Fe studies in sea ice can be found in Lannuzel et al. (2016).

Table 1.1 List of the Antarctic sea ice data currently available in the literature (Adapted from Lannuzel et al., 2016)

Voyage ID	Sector	Year	Months	Type of ice	DFe (nmol. L^{-1})	PFe (nmol.L^{-1})	TDFe (nmol.L^{-1})	References
PNRA	Western Ross Sea	1997/1998	Nov	Fast ice	ND	718 - 7,091	ND	Grotti et al., 2001
ANT XVI/3	South Atlantic	1999	March - May	Pack ice	0.22 - 4.36	ND	ND	Boye et al., 2001
PNRA	Western Ross Sea	2000/2001	Nov - Jan	Fast ice	1.07 - 5.98	26 - 1,162	ND	Grotti et al., 2005
Scott Base	Ross Sea	2003	January	Fast ice	2.2 - 109	9 - 1,854	10 - 1,178	de Jong et al., 2013
ARISE	South Pacific	2003	Sept - Oct	Pack ice	2.6 - 26	ND	3.3 - 65.8	Lannuzel et al., 2007
ISPOL	Weddell Sea	2004/2005	Nov - Jan	Pack ice	0.7 - 36.8	2.0 - 141.2	2.3 - 97.8	Lannuzel et al., 2008
SIPEX	South Pacific	2007	Sept - Oct	Pack and fast ice	0.2 - 14.4	ND	1.2 - 378	van der Merwe et al., 2011b
SIMBA	Bellingshausen Sea	2007	Sept - Oct	Pack ice	1.1 - 30.2	ND	2.8 - 77.7	de Jong et al., 2015
Casey	South Pacific	2009	Nov	Fast ice	2.1 - 8.1	40.4 - 6, 828	33.8 - 4,240	van der Merwe et al., 2011a
Mc Murdo	Ross Sea	2009	Nov	Fast ice	ND	12 - 9,318	ND	Noble et al., 2013
SIPEX 2	South Pacific	2012	Sept - Nov	Pack ice	0.9 - 17.4	0.04 - 990	ND	Lannuzel et al., 2014a

The physical and chemical forms under which Fe exists dictate its accessibility for microorganisms (Bruland and Rue, 2001). To understand the processes discussed in this thesis, it is important to understand the forms of Fe present in sea ice, as a mean to approximate its bio-availability for polar micro-organisms.

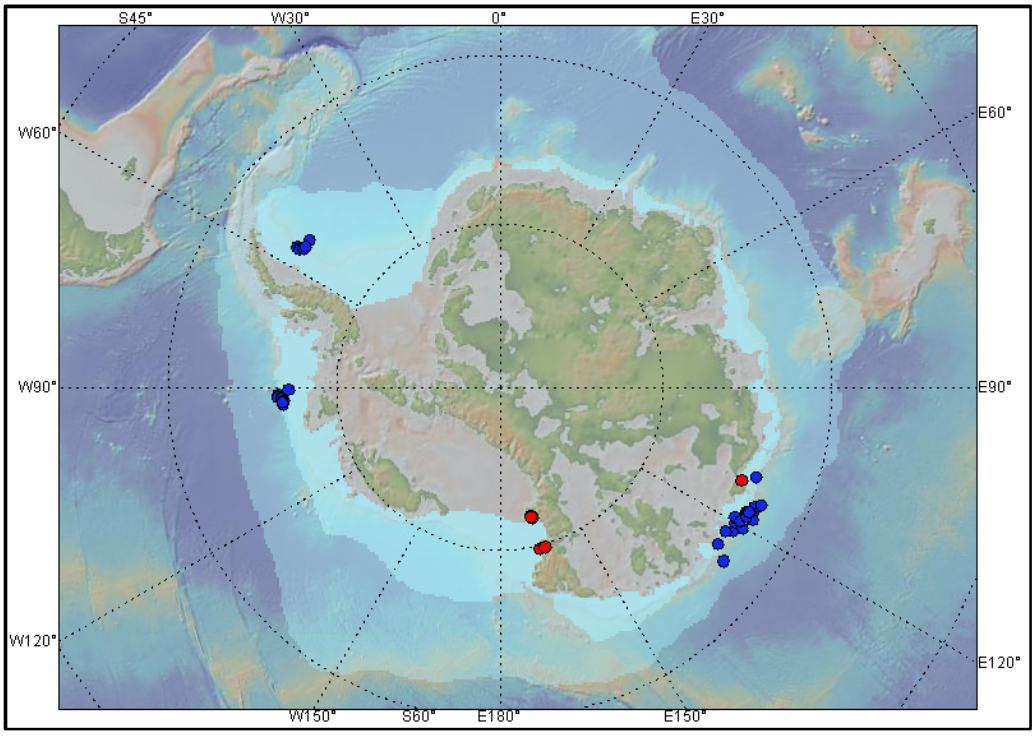

Figure 1.5 Locations of fast (red dots) and pack (blue dots) ice cores (Lannuzel et al., 2016). The blue shaded colors represent the mean (1979-2007) maximal (September) and minimal (March) sea ice extent

1.4.1.2 Physical fractionation

The physical speciation of Fe is based on an arbitrary size classification, which allows comparison between studies. Iron in the ocean and in sea ice actually exists in a continuum of size from the soluble fraction (sFe < 0.02 μm) to the particulate fraction (PFe > 0.2 or 0.4 μm). The dissolved fraction is operationally defined, and traditionally seen as the fraction passing through polycarbonate (PC) membranes filters of 0.2 or 0.4 μm pore size, and includes the sFe and the colloidal Fe (0.02 < cFe < 0.2 or 0.4 μm). Total dissolvable Fe (TDFe) commonly refers to the unfiltered

sample acidified to pH 1.8 for 6 months. TDFe measurements represent the leachable Fe fraction and do not include highly refractory Fe species. A strong acid leach (such as hydrofluoric acid, HF) is needed to recover this fraction. The PFe is the fraction retained on membrane filters of 0.2 – 0.4 μm porosity.

1.4.1.3 Chemical speciation: redox state and organic complexion

Iron exists under two oxidation states, Fe (II) and Fe (III). In oxygenated seawater, Fe (III) species largely dominate. Fe (III) is thermodynamically more stable than Fe (II), and tends to adsorb onto particles and form complexes. (Oxy)-hydroxide formed from Fe (III) have a very low solubility in seawater (Liu and Millero, 2002; Millero et al., 1995), and are accordingly not readily bioavailable for macro-organisms (Kuma et al., 1996). Fe (III) is therefore easily removed from the surface waters by sedimentation of Fe particles (de Baar and de Jong, 2001; Sunda, 2001). Fe (II) is more soluble in seawater and is assumed to be the most bioavailable form of Fe in seawater (Shaked and Lis, 2012), however Fe(II) is rapidly oxidised by O_2 or hydrogen peroxide (H_2O_2). It is commonly accepted that DFe is more bioavailable than PFe. Processes keeping the Fe in its dissolved form will therefore enhance Fe bioavailability. Although inorganic Fe is the preferred form of Fe for micro-organisms uptake, organic complexion of Fe minimises the formation of (oxy)-hydroxide particles and therefore increases its residence time in the surface water or in the ice, rendering it more bio-available for phytoplankton uptake (Johnson et al., 1997; Sunda and Huntsman, 1997). Over 99% of DFe in the ocean is complexed to organic ligands (e.g., Boye et al., 2001a; Rue and Bruland, 1995). More recently, similar results have been found for DFe in sea ice (Boye et al., 2001a; Lannuzel et al., 2015). Lannuzel et al. (2015) have highlighted the importance of organic complexation in Antarctic fast ice, maintaining DFe at much higher levels than seawater concentrations and regulating

the solubility threshold between DFe and PFe in the ice. It is expected that pack ice also exhibits organic complexation of Fe > 99%.

Few studies suggested that EPS act as weak Fe-binding organic ligands (Benner, 2011; Hassler et al., 2011a; Lannuzel et al., 2015; van der Merwe et al., 2009). Iron bound to EPS from natural marine bacteria was also more available to phytoplankton than Fe bound to siderophores (Hassler et al., 2011a, 2011b) The exact nature of EPS and organic ligands in seawater is currently unknown but there are evidences that the majority of ligands are of microbial origin (Geider, 1999).

1.4.1.4 Fe-cycle associated to sea ice

When sea ice forms in winter, it accumulates Fe to much higher concentrations than the concentrations found in seawater (global DFe concentrations in shelf seawaters of the Southern Ocean: DFe = 0.61 ± 1.14 nmol L^{-1}, and DFe concentration off shelf seawaters DFe = 0.38 ± 0.55 nmol L^{-1} (Tagliabue et al., 2012), median DFe concentration in pack ice DFe = 4.4 nmol L^{-1} (Lannuzel et al., 2016)). Pack ice and fast ice have been found to be enriched in all form of Fe (PFe, DFe, sFe and TDFe) compared to seawater (Boye et al., 2001; de Jong et al., 2013, 2015, 1998; Grotti et al., 2005, 2001; Lannuzel et al., 2014a, 2008, 2007; Loscher et al., 1997; van der Merwe et al., 2011a, b, 2009). While DFe seems to be relatively homogenous between pack ice and fast ice (Lannuzel et al., 2010) both lithogenic and biogenic PFe, and TDFe concentrations are higher in fast ice by a factor ~7 (Lannuzel et al., 2016).

Biological processes (via autothrophic and heterotrophic activities - (Lannuzel et al., 2010, 2008), and physical processes (such as percolation of DFe contained in brine, temperature and sea ice formation processes - de Jong et al., 2007) regulate the fractionation of Fe between PFe and DFe in the ice. It is therefore likely that the Fe

initially incorporated under a specific form in autumn will not be released in the same form in spring. Studies of the release of Fe during spring melt have shown that DFe, together with salinity and dissolved organic carbon (DOC), is released first, followed by PFe and particulate organic carbon (POC) (Figure 1.6, Lannuzel et al., 2013; van der Merwe et al., 2009). This decoupling is likely due to PFe retention within the brine channels. Exopolysaccharides have been proposed to be responsible of the attachment of PFe to the walls of the brines inclusions in the sea ice matrix (Juhl et al., 2011; van der Merwe et al., 2009). Similarly, comparing measured and theoretically derived DFe concentrations in the brines, Lannuzel et al. (2016) found that only 10% of the DFe is truly dissolved in the brine system. The rest is retained in the ice, through attachment to surfaces.

Once sea ice melts, the fate of Fe in seawater below is likely dictated by its physical and chemical speciation (Lannuzel et al., 2016; Schallenberg et al., 2015). For particles of identical composition, smaller particles will remain in suspension for longer than large particles. Similarly, Fe bound to organic ligands has been found to stay longer in suspension than organically-free Fe that tends to form oxy-hydroxide and sink (Waite, 2001). Phytoplankton and bacteria can take DFe up, and remineralized PFe (Figure 1.6). Dissolved Fe can also scavenge onto particles (Lannuzel et al., 2016), and PFe can be exported to the deep ocean (Figure 1.6). At end of summer, fraction of the Fe released by sea ice stays in suspension in the surface water, associated with microorganisms and detritus (Lannuzel et al., 2010). This pool, supplemented by various other sources, is then available for entrapment into newly forming sea ice in autumn (Figure 1.6).

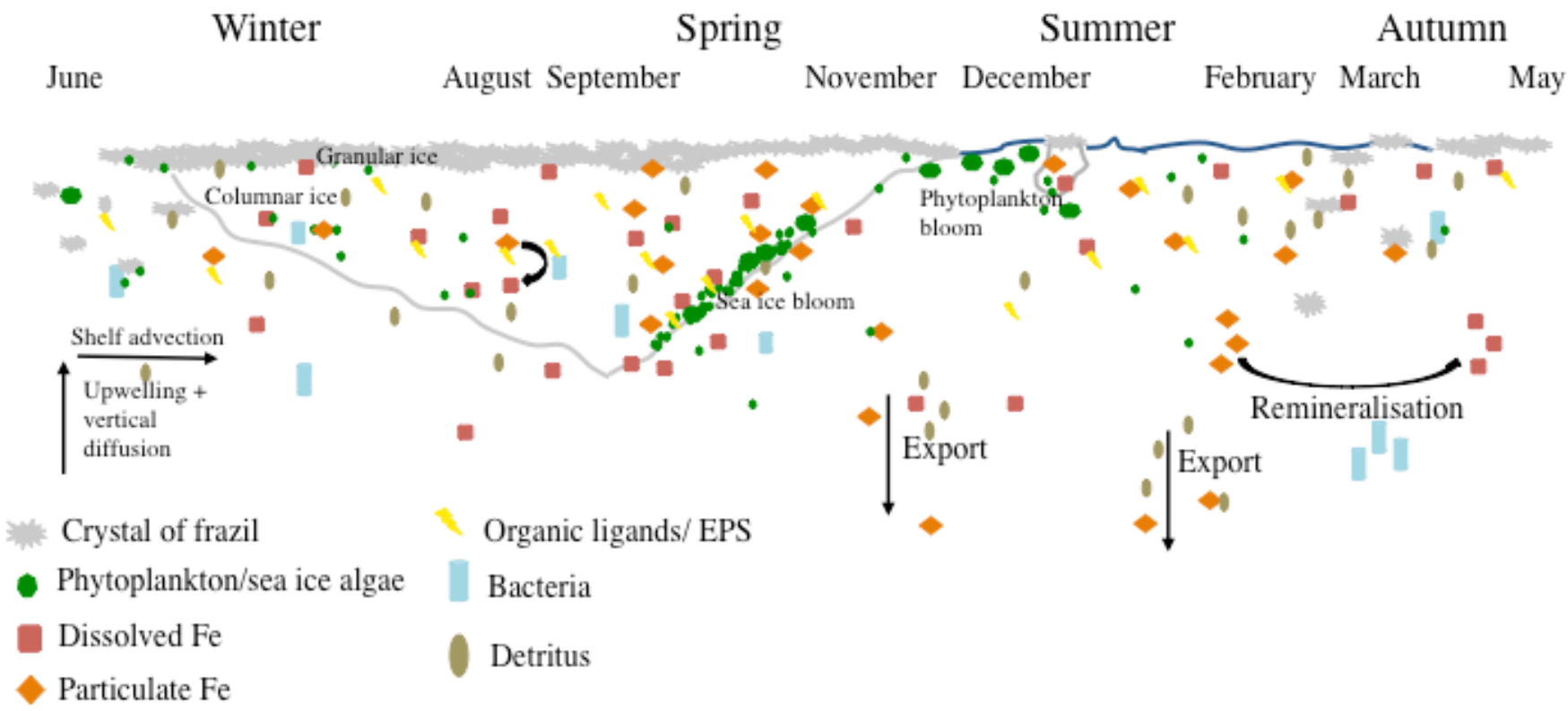

Figure 1.6 Schematic of the seasonal Fe cycle associated to sea ice in the seasonal ice zone. The black arrows represent the main sources and sinks of Fe (remineralization, export, shelf advection, upwelling and vertical diffusion) in the seasonal ice zone. Size of the objects are not representatives of scale.

Iron-enriched sea ice drift induces a redistribution of matter from where it has been trapped in the first place and therefore, can strongly influence the biogeochemical cycles in the Southern Ocean by potentially seeding Fe-limited surface water in offshore areas (Lancelot et al., 2009; Lannuzel et al., 2010; Sullivan et al., 1993). The role of sea ice formation in governing Fe availability in the Southern Ocean is not yet fully understood. It is therefore important to understand the relationship between sea ice formation and Fe biogeochemistry, and clarify the temporal storage and transport of Fe by the ice.

1.4.2 Dissolved and particulate organic matter and extracellular polymeric substances

Organic matter is an essential component of the marine food web and carbon cycle (e.g., Pomeroy et al., 2007). Organic matter in the ocean is mainly composed of biomass of living microorganisms and detrital non-living compounds derived from dead microorganisms or excreted by living microorganisms. Organic matter is principally composed of carbohydrates, lipids, protein and nucleic acids, and can be remineralized as CO_2 by heterotrophic organisms. Organic matter occurs in a range of size from nanometres to millimetres (Verdugo et al., 2004). Like Fe, the distinction between dissolved (DOM) and particulate (POM) organic matter is purely operational and depends on the filter porosity. Dissolved organic matter is traditionally defined as the fraction passing through a membrane of between 0.2 and 0.7 μm of porosity (Thomas et al., 2010). Particulate organic matter is the fraction retained on these filters. Practically, GF/F or quartz filters of porosity 0.7 μm are used.

Transparent exopolysaccharides (TEP) are an important class of compound at the interface between particulate organic carbon (POC) and dissolved organic carbon (DOC). TEP are gel-like substances formed by accretion of DOC and/or EPS

produced by phytoplankton and bacteria in the form of mucus or gels (Ewert and Deming, 2013; Verdugo et al., 2004). Extracellular polymeric substances are composed of polysaccharides and are rich in carbohydrates and can also contain nucleic acids, proteins and lipids. The negatively charged surface of EPS (due to a high content of poly-anionic sugars) is stabilised by the presence of cations K^+ and Ca^{2+} (Kloareg and Quatrano, 1988; Verdugo et al., 2004). This composition could explain the tendency of EPS to adsorb trace elements like Fe (Mancuso Nichols et al., 2005; Passow, 2002). The sticky properties of EPS determine the interaction of EPS with other components of the marine environment (Passow, 2002).

Extracellular polymeric substances have received a lot of attention recently because of their ecological importance (Aslam et al., 2012; Krembs et al., 2011; Meiners et al., 2004, 2003, 2008). Extracellular polymeric substances in sea ice are thought to act as cryoprotectant (e.g., Krembs et al., 2002), to be important in buffering the salinity (e.g., Ewert and Deming, 2011), to increase sea ice habitability (Krembs et al., 2011), and play a role in attachment and locomotion of microorganisms (Krembs et al., 2011, 2002; Krembs and Deming, 2008; Meiners et al., 2004, 2003). More recently they have been proposed to play a role in the entrapment of Fe into sea ice (van der Merwe et al., 2009), and in keeping the DFe in solution (Lannuzel et al., 2015).

1.5 Laboratory sea ice formation experiments

Sea ice is a challenging environment to sample and sampling in the field is mainly destructive. Polar marine field studies require an extremely high logistical effort, are time consuming and expensive, and often limited to measurement during spring/summer. Moreover, the study of physical, chemical and biological properties of sea ice is extremely difficult due to the complex interactions between them. Sea ice

is also characterised by a high spatial and temporal variability and heterogeneity (e.g., Meiners et al., 2012). Based on these reasons, it is very difficult to examine a specific process or the fate of a chosen parameter. In this context, laboratory ice growth experiments are of particular interest. The main arguments for use of ice tank experiments are: (1) they provide highly controllable conditions and separation of the physico-chemical-biological processes during sea ice growth, (2) their reproducibility, and (3) their cost-effectiveness. Furthermore, Antarctic and Arctic field data can be refined and compared to the laboratory-based data. Laboratory ice-growth experiments however have their limitations (e.g., temporal and scale limitation, ice thickness, walls effects), but nonetheless are a powerful way to study sea ice processes and refine field data.

1.5.1 A brief review of main laboratory ice growth experiments

Laboratory controlled ice-growth experiments show variations in size of the tank, source-solution used, type of ice formed (granular vs columnar), and studied processes. Early ice tank experiments had special emphasis on the understanding of the properties and mechanisms of growing sea ice. Entrapment processes occurring during sea ice formation have been in the spotlight since the first ice tank formation experiments (Eicken et al., 1998; Garrison et al., 1989; Martin et al., 1995; Reimnitz et al., 1993). Later, biological aspects and interaction between microorganisms and sea ice as their living environment have been studied (e.g., Ewert and Deming, 2011; Krembs et al., 2011; Weissenberger, 1998).

The INTERICE (I-V) experiments were a series of large-scale sea ice formation in controlled conditions investigating different aspects of ice formations. The primary focus of INTERICE I and II was on abiotic processes such as bulk salinity development in growing sea ice (Cottier et al., 1999), the influence of brine channel

evolution on the sea ice algae development (Krembs et al., 2001), the influence of waves and current in the incorporation of algae in sea ice (Weissenberger and Grossmann, 1998), and the first measurements of oxygen using micro-optode (Mock et al., 2002). A biological component was added in INTERICE III, IV and V. INTERICE III investigated the biological processes occuring during sea ice formation (Thomas and Wilkinson, 2001). Gas composition and content in sea ice were investigated and main findings can be found in Verbeke (2005). INTERICE IV (Thomas et al., 2009) explored the fractionation of biogeochemical component (Geilfus et al., 2012; Thomas, et al., 2009), the production of calcium carbonate during sea ice formation (Papadimitriou et al., 2004), and the production of dissolved EPS (dEPS) and bacterial growth during sea ice formation (Aslam et al., 2011). Zhou et al., (2014) studied the effect of riverine DOM on the sea ice biogeochemistry and bacterial activity during the INTERICE V experiment, while Jørgensen et al. (2015) found that sea ice formation processes can increase the bioavailability of dissolved organic material not only in the brines but also in the seawater below.

Over the past decade, other large-scale ice tank experiments have flourished and such facilities exist now in Canada (SERF – Sea-ice Environmental Research Facility) and in the United States (CRREL – Cold Regions Research and Engineering Laboratory). Despite the relative abundance of studies on sea ice growth and its impact on biogeochemical cycles, to our knowledge, no tank studies have investigated the processes leading to the enrichment of Fe in forming sea ice. This thesis constitutes the first step forward in addressing this gap.

1.5 Modelling sea ice

"*Understanding how sea-ice processes contribute to marine biogeochemistry is essential to accurately predict past, present and future climate change responses of marine ecosystems in both polar and global oceans*." (Steiner et al., 2016).

Numerical modelling is the only means to study large-scale processes in a changing environment. Changes in sea ice (Arzel et al., 2006; Massom et al., 2013; Stammerjohn et al., 2012) are expected to drastically affect biogeochemical cycles, including the Fe cycle, in the polar oceans. These changes in biogeochemical cycles remain very difficult to predict (Vancoppenolle et al., 2013), and could in return impact the global ocean and climate system.

Sigman et al. (2010) proposed that the strengthening of the Southern Ocean CO_2 uptake in glacial periods was caused by a stronger Fe supply, leading to a more efficient use of the nutrients. During these periods, winter sea ice cover was also more important (e.g., Gersonde et al., 2005; Stephens and Keeling, 2000), potentially impacting the Fe delivery to surface waters during melting period. It is therefore crucial to understand the role of Fe and the annual cycle of sea ice formation and retreat on the pelagic ecosystem, and more largely as an ocean fertiliser.

Models representing the Earth system are numerous and various (e.g., Flato et al., 2013 and references therein). Unfortunately sea ice is usually represented as an inert impermeable layer between the ocean and the atmosphere in these models (Vancoppenolle et al., 2013). Sea ice biogeochemical models are comparatively relatively poorly developed, and therefore poorly represented in global models. There is urgent need for further development of sea-ice biogeochemical models and coupling with global models.

Modelling is an essential step towards the quantification of the Fe budget associated to sea ice. While numerical models have been developed to quantify sediment incorporation into sea ice (e.g., Sherwood, 2000), these have not been adopted to test hypothesis on the incorporation of Fe and biological material into sea ice. At present, only a few sea ice biogeochemical models exist (e.g., Arrigo et al., 1993; Moreau et al., 2015, 2014; Saenz and Arrigo, 2012; Tedesco et al., 2010; Tedesco and Vichi, 2012; Vancoppenolle et al., 2010), and are mainly focused on a N-P formulation (Sarmiento and Gruber, 2005; Tedesco et al., 2010). Before being added in large-scale global biogeochemical models and global Earth System Models (ESM), Fe processes have to be implemented in one-dimensional models.

1.6.1 Modelling Fe in sea ice

To our knowledge, only two modelling studies have addressed Fe biogeochemical processes associated to sea ice. Lancelot et al. (2009) highlighted the importance of DFe stored in sea ice for phytoplankton blooms in the Southern Ocean using the 3-dimensional biogeochemical model SWAMCO (Sea Water Microbial Community model) coupled to the ocean-sea-ice model NEMO-LIM (Nucleus for European Modelling of the Ocean – Louvain-la-Neuve Ice Model). However, they were not able to quantify the influence of melting sea ice as a Fe source for surface waters because they used a very simple parameterisation due to a lack of understanding of the mechanisms associated with sea-ice Fe capture and release to the ocean. Sea ice Fe concentrations were reached by simply pumping the Fe in the seawater until a fix concentration was reached in the ice.

Similarly, Wang et al. (2014) demonstrated the important role of Fe released by sea ice in boosting of phytoplankton growth in the marginal ice zone in polar oceans. In their Community Earth System Model (CESM) model, Fe was incorporated into sea

ice as a passive tracer. Once in the ice, biological processes, chemical reactions and Fe speciation were not considered. Simulated Fe concentrations were not able to reproduce high Fe concentrations found in sea ice, likely due to missing mechanisms of Fe entrapment.

The study from Lancelot et al. (2009) only considered DFe, whereas Wang et al. (2014) did not distinguish between the dissolved and particulate fraction of Fe in sea ice. Yet, Lannuzel et al. (2014a) showed that 70% of the PFe stored in the ice could become bioavailable for phytoplankton once released in the water column, highlighting the potential importance of PFe. It is therefore crucial to differentiate the Fe size pools and represent the interactions between the pools of Fe accurately in a sea-ice model. There is also a requirement for an improved representation of exchanges between the ice and the ocean (Lancelot et al., 2009; Wang et al., 2014).

1.7 Research questions and outline

1.7.1 Research questions

This thesis uses three different methods to address key knowledge gaps in the understanding of the incorporation of Fe into newly forming sea ice and subsequent biogeochemical cycling. Specifically, these questions are:

i. What are the pathways leading to Fe and organic matter enrichment in newly formed sea ice?

ii. What is the role of organic matter as a carrier of Fe in sea ice?

iii. Is it possible to model the initial enrichment of Fe in sea ice, and physical and biological processes driving the Fe dynamics in sea ice?

1.7.2 Organisation of the thesis

Chapter 2 describes the *in situ* ice-growth experiments used to identify the pathways leading to the enrichment of organic matter and iron into newly formed sea ice. Experimental data are combined with results from natural young ice sampled during a winter cruise in the Weddell Sea.

Chapter 3 focuses on the specific role of organic matter and sea ice algae on the incorporation efficiency of Fe into sea ice. Sea ice is grown from different source solutions to isolate the role of organic matter and algae in the enrichment of Fe, and investigate the influence of the initial Fe concentrations in the seawater.

Chapter 4, using results from previous chapters and data from the literature, presents an implementation of a halo-thermodynamic sea ice model (LIM 1-D) with an initial enrichment of Fe during the first stages of ice growth. Iron is added as new biogeochemical component to the model to study the main mechanisms driving the Fe dynamic in un-deformed first year pack ice.

Chapter 5 summarises the main findings of this thesis and outline future research directions.

References

Arrigo KR, Kremer JN, Sullivan CW. 1993. A simulated Antarctic fast ice ecosystem. *J Geophys Res* 98:6929–6946. doi:10.1029/93JC00141

Arzel O, Fichefet T, Goosse H. 2006. Sea ice evolution over the 20th and 21st centuries as simulated by current AOGCMs. *Ocean Model* 12:401–415. doi:10.1016/j.ocemod.2005.08.002

Aslam SN, Cresswell-Maynard T, Thomas DN, Underwood GJC. 2012. Production and Characterization of the Intra-and Extracellular Carbohydrates and Polymeric Substances (EPS) of Three Sea-Ice Diatom Species, and Evidence for a Cryoprotective Role for EPS. *J Phycol* 48:1494–1509.

Aslam SN, Underwood GJC, Kaartokallio H, Norman L, Autio R, Fischer M, Kuosa H, Dieckmann GS, Thomas DN. 2011. Dissolved extracellular polymeric substances (dEPS) dynamics and bacterial growth during sea ice formation in an ice tank study. *Polar Biol* 35:661–676. doi:10.1007/s00300-011-1112-0

Atkinson A, Whitehouse MJ, Priddle J, Cripps GC, Ward P, Brandon MA. 2001. South Georgia, Antarctica: A productive, cold water, pelagic ecosystem. *Mar Ecol Prog Ser* 216:279–308. doi:10.3354/meps216279

Becquevort S, Dumont I, Tison J-L, Lannuzel D, Sauvée M-L, Chou L, Schoemann V. 2009. Biogeochemistry and microbial community composition in sea ice and underlying seawater off east Antarctica during early spring. *Polar Biol* 32:879–895. doi:10.1007/s00300-009-0589-2

Benner R. 2011. Loose ligands and available iron in the ocean. *Proc Natl Acad Sci U. S. A.* 108:893–894. doi:10.1073/pnas.1018163108

Blain S, Quéguiner B, Armand L, Belviso S, Bombled B, Bopp L, Bowie A, Brunet C, Brussaard C, Carlotti F, et al. 2007. Effect of natural iron fertilization on carbon sequestration in the Southern Ocean. *Nature* 446:1070–1074.

Bowie AR, Lannuzel D, Remenyi TA, Wagener T, Lam PJ, Boyd PW, Guieu C, Townsend AT, Trull TW. 2009. Biogeochemical iron budgets of the Southern Ocean south of Australia: Decoupling of iron and nutrient cycles in the subantarctic zone by the summertime supply. *Global Biogeochem Cycles* 23:1–14. doi:10.1029/2009GB003500

Boyd P, Mackie D. 2008. Comment on "The Southern Ocean biological response to aeolian iron deposition". *Science* 319:159; author reply 159. doi:10.1126/science.1149884

Boyd PW, Ellwood MJ. 2010. The biogeochemical cycle of iron in the ocean. *Nat Geosci* 3:675–682. doi:10.1038/ngeo964

Boyd PW, Jickells T, Law CS, Blain S, Boyle EA, Buesseler KO, Coale KH, Cullen JJ, de Baar HJW, Follows M, et al. 2007. Mesoscale iron enrichment

experiments 1993-2005: Synthesis and future directions. *Science* 315:612–617. oi: 10.1126/science.1131669

Boyd PW, McTainsh G, Sherlock V, Richardson K, Nichol S, Ellwood M, Frew R. 2004. Episodic enhancement of phytoplankton stocks in New Zealand subantarctic waters: Contribution of atmospheric and oceanic iron supply. *Global Biogeochem Cycles* 18:1–23. doi:10.1029/2002GB002020

Boye M, Van Den Berg CMG, de Jong JTM, Leach H, Croot P, de Baar HJW. 2001. Organic complexation of iron in the Southern Ocean. *Deep Res Part I Oceanogr Res Pap* 48:1477–1497. doi:10.1016/S0967-0637(00)00099-6

Brandt RE, Stephen GW, Worby AP, Grenfell TP. 2005. Surface albedo of the Antarctic sea ice zone. *J Clim* 18:3606–3622. doi:10.1175/jcli3489.1

Bruland KW, Rue EL. 2001. Iron: analytical methods for the determination of concentrations and speciation., in: Turner, D.R., Hunter, K.A. (Eds.), The Biogeochemistry of Iron in Seawater. John Wiley & Sons Ltd, West Sussex, pp. 255–289.

Brzezinski MA, Dickson M-L, Nelson DM, Sambrotto R. 2003. Ratios of Si, C and N uptake by microplankton in the Southern Ocean. *Deep Res Part II Top Stud Oceanogr* 50:619–633. doi:10.1016/S0967-0645(02)00587-8

Cassar N, Bender ML, Barnett BA, Fan S, Moxim WJ, Levy II H, Tilbrook B. 2007. The Southern Ocean biological response to aeolian iron deposition. *Science* 317:1067-1070. doi:10.1126/science.1144602

Chisholm SW. 2000. Stirring times in the Southern Ocean. *Nature* 407:685–687. doi:10.1038/35037696

Cottier F, Eicken H, Wadhams P. 1999. Linkages between salinity and brine channel distribution in young sea ice. *J Geophys Res* 104:15,859-15,871. doi:10.1029/1999jc900128

de Baar HJW, Boyd PW, Coale KH, Landry MR, Tsuda A, Assmy P, Bakker DCE, Bozec Y, Barber RT, Brzezinski MA, Buesseler KO, Boyé M, Croot PL, Gervais F, Gorbunov MY, Harrison PJ, Hiscock WT, Laan P, Lancelot C, Law CS, Levasseur M, Marchetti A, Millero FJ, Nishioka J, Nojiri Y, van Oijen T, Riebesell U, Rijkenberg MJA, Saito H, Takeda S, Timmermans KR, Veldhuis MJW, Waite AM, Wong CS. 2005. Synthesis of iron fertilization experiments: From the iron age in the age of enlightenment. *J Geophys Res Ocean* 110:1–24. doi:10.1029/2004JC002601

de Baar HJW, de Jong JTM. 2001. Distributions, Sources and Sinks of Iron in Seawater. (in) The biogeochemistry of iron in seawater. Eds: Turner DR, Hunter KA. IUPAC Series on Analytical and physical chemistry of environment systems, Wiley. pp:123–253.

de Baar HJW, de Jong JTM, Bakker DCE, Loscher BM, Veth C, Bathmann U,

Smetacek V. 1995. Imporance of iron for plankton blooms and carbon dioxide drawdown in the Southern Ocean. *Lett to Nat* 373:412–415. doi:10.1038/373412a0

de Jong J, Schoemann V, Lannuzel D, Croot P, de Baar H, Tison J-L. 2012. Natural iron fertilization of the Atlantic sector of the Southern Ocean by continental shelf sources of the Antarctic Peninsula. *J Geophys Res Biogeosciences* 117:G01029. doi:10.1029/2011JG001679

de Jong J, Schoemann V, Maricq N, Mattielli N, Langhorne P, Haskell T, Tison J-L. 2013. Iron in land-fast sea ice of McMurdo Sound derived from sediment resuspension and wind-blown dust attributes to primary productivity in the Ross Sea, Antarctica. *Mar Chem* 157:24–40. doi:10.1016/j.marchem.2013.07.001

de Jong J, Schoemann V, Tison J-L, Becquevort S, Masson F, Lannuzel D, Petit J, Chou L, Weis D, Mattielli N. 2007. Precise measurement of Fe isotopes in marine samples by multi-collector inductively coupled plasma mass spectrometry (MC-ICP-MS). *Anal Chim Acta* 589:105–119. doi:10.1016/j.aca.2007.02.055

de Jong JTM, den Das J, Bathmann U, Stoll MHC, Kattner G, Nolting RF, de Baar HJW. 1998. Dissolved iron at subnanomolar levels in the Southern Ocean as determined by ship-board analysis. *Anal Chim Acta* 377:113–124. doi:10.1016/S0003-2670(98)00427-9

de Jong JTM, Stammerjohn SE, Ackley SF, Tison J-L, Mattielli N, Schoemann V. 2015. Sources and fluxes of dissolved iron in the Bellingshausen Sea (West Antarctica): The importance of sea ice, icebergs and the continental margin. *Mar Chem* 177:518–535. doi:10.1016/j.marchem.2015.08.004

Delille B, Jourdain B, Borges AV, Tison J-L, Delille D. 2007. Biogas (CO_2, O_2, dimethylsulfide) dynamics in spring Antarctic fast ice. *Limnol Oceanogr* 52:1367–1379. doi:10.4319/lo.2007.52.4.1367

Dethleff D. 2005. Entrainment and export of Laptev Sea ice sediments, Siberian Arctic. *J Geophys Res Ocean* 110:1–17. doi:10.1029/2004JC002740

Dieckmann GS, Hellmer HH. 2010. The importance of sea ice: an overview. (in) Sea ice. Eds. Thomas D, and Dieckamm GS. Wiley-Blackwell. pp:1-22

Dubischar CD, Bathmann UV. 1997. Grazing impact of copepods and salps on phytoplankton in the Atlantic sector of the Southern Ocean. *Deep Sea Res Part II Top Stud Oceanogr* 44:415–433. doi:10.1016/s0967-0645(96)00064-1

Dumont I, Schoemann V, Lannuzel D, Chou L, Tison J-L, Becquevort S. 2009. Distribution and characterization of dissolved and particulate organic matter in Antarctic pack ice. *Polar Biol* 32:733–750. doi:10.1007/s00300-008-0577-y

Duprat LPAM, Bigg GR, Wilton DJ. 2016. Enhanced Southern Ocean marine productivity due to fertilization by giant icebergs. *Nat Geosci* 9:219–221.

doi:10.1038/ngeo2633

Eicken H. 2003. Sea Ice: An Introduction to its Physics, Chemistry, Biology and Geology. John Wiley & Sons.

Eicken H, Weissenberger J, Bussman I, Freitag J, Shuster W, Valero Delgado F, Evers KU, Jochmann P, Krembs C, Gradinger R, Lindemann F, Cottier F, Hall R, Wadhmas P, Reisemann M, Kousa,H, Ikävalko J, Leonard GH, Shen H, Ackley SF, Smedsrud LH. 1998. Ice-tank studies of physical and biological sea-ice processes. (in) Ice in Surface Waters, Eds: Shen, Balkema, Rotterdam

Ewert M, Deming JW. 2013. Sea ice microorganisms: environmental constraints and extracellular responses. *Biology* 2:603–628. doi:10.3390/biology2020603

Ewert M, Deming JW. 2011. Selective retention in saline ice of extracellular polysaccharides produced by the cold-adapted marine bacterium Colwellia psychrerythraea strain 34H. *Ann Glaciol* 52:111–117. doi:10.3189/172756411795931868

Falkowski PG, Barber RT, Smetacek V. 1998. Biogeochemical controls and feedbacks on ocean primary production. *Science* 281:200–206. doi:10.1126/science.281.5374.200

Field CB, Behrenfeld MJ, Randerson JT, Falkowski P. 1998. Primary production of the biosphere: Integrating terrestrial and oceanic components. *Science* 281:237–240. doi:10.1126/science.281.5374.237

Flato G, Marotzke J, Abiodun E, Braconnet P, Chou S. et al. 2013. Evaluation of climate models, (in) Climate Change 2013: The physical Science basis. Contribution of working group I to the fifth assessment report of the intergovernmental panel on climate change. Cambridge, UK, and New York, NY, USA: Cambridge University Press: pp. 741-882

Flores H, van Franeker JA, Siegel V, Haraldsson M, Strass V, Meesters EH, Bathmann U, Wolff WJ. 2012. The association of Antarctic krill Euphausia superba with the under-ice habitat. *PLoS One* 7. doi:10.1371/journal.pone.0031775

Fritzen CH, Ackley SF, Kremer JN, Sullivan CW. 1998. Flood freeze cycles and microbial dynamics in Antarctic pack ice. (in): Antarctic Sea ice biological processes, Interactions and variability. Eds. Lizotte MP and Arrigo KR, American Geophysical Union, Washington, DC

Gao Y, Kaufman YJ, Tanre D, Kolber D, Falkowski PG. 2001. Seasonal distribution of aeolian iron flux to the global ocean. *Geophys Res Lett* 28:29–32. doi:10.1029/2000gl011926

Gao Y, Xu G, Zhan J, Zhang J, Li W, Lin Q, Chen L, Lin H. 2013. Spatial and particle size distributions of atmospheric dissolvable iron in aerosols and its input to the Southern Ocean and coastal East Antarctica. *J Geophys Res Atmos*

118:12634–12648. doi:10.1002/2013JD020367

Garrison DL, Close AR, Reimnitz E. 1989. Algae concentrated by frazil ice: evidence from laboratory experiments and field measurements. *Antarct Sci* 313–316. doi:10.1017/S0954102089000477

Geider RJ. 1999. Complex lessons of iron uptake. *Natur*e 400:815–816. doi: 10.18578/bnf.942178180

Geilfus N-X, Delille B, Verbeke V, Tison J-L. 2012. Towards a method for high vertical resolution measurements of the partial pressure of CO_2 within bulk sea ice. *J Glaciol* 58:287–300. doi:10.3189/2012JoG11J071

Gerringa LJA, Laan P, van Dijken GL, van Haren H, de Baar HJW, Arrigo KR, Alderkamp AC. 2015. Sources of iron in the Ross Sea polynya in early summer. *Mar Chem* 177:447-459. doi:10.1016/j.marchem.2015.06.002

Gersonde R, Crosta X, Abelmann A, Armand L. 2005. Sea-surface temperature and sea ice distribution of the Southern Ocean at the EPILOG Last Glacial Maximum - A circum-Antarctic view based on siliceous microfossil records. *Quat Sci Rev* 24:869–896. doi:10.1016/j.quascirev.2004.07.015

Gledhill M, Buck KN. 2012. The organic complexation of iron in the marine environment: A review. *Front Microbiol* 3:1–17. doi:10.3389/fmicb.2012.00069

Golden KM, Ackley SF, Lytle VI. 1998. The percolation phase transition in sea Ice. *Science* 282:2238–2241. doi: 10.1126/science.282.5397.2238.

Gradinger R, Ikävalko J. 1998. Organism incorporation into newly forming Arctic sea ice in the Greenland Sea. *J Plankton Res* 20:871–886. doi:10.1093/plankt/20.5.871

Grossmann S, Dieckmann GS. 1994. Bacterial standing stock, activity, and carbon production during formation and growth of sea ice in the Weddell Sea, Antarctica. *Appl Environ Microbiol* 60:2746–2753. doi:10.1007/bf00170244

Grotti M, Soggia F, Abelmoschi ML, Rivaro P, Magi E, Frache R. 2001. Temporal distribution of trace metals in Antarctic coastal waters. *Mar Chem* 76:189–209. doi:10.1016/S0304-4203(01)00063-9

Grotti M, Soggia F, Ianni C, Frache R. 2005. Trace metals distributions in coastal sea ice of Terra Nova Bay, Ross Sea, Antarctica. *Antarct Sci* 17:289–300. doi:10.1017/s0954102005002695

Hassler CS, Alasonati E, Mancuso Nichols CA, Slaveykova VI. 2011. Exopolysaccharides produced by bacteria isolated from the pelagic Southern Ocean — Role in Fe binding, chemical reactivity, and bioavailability. *Mar Chem* 123:88–98. doi:10.1016/j.marchem.2010.10.003

Hassler CS, Schoemann V, Nichols CM, Butler ECV, Boyd PW. 2011. Saccharides enhance iron bioavailability to Southern Ocean phytoplankton. *Proc Natl Acad Sci .U.S.A* 108:1076–1081. doi:10.1073/pnas.1010963108

Hellmer HH, Hass C, Dieckmann GS, Schroder M. 2006. Sea Ice Feedbacks Observed in Western Weddell Sea. *EOS, Trans Am Geophys union* 87:2–4. doi:10.1029/2006eo180001

Herraiz-Borreguero L, Lannuzel D, van der Merwe P, Treverrow A, Pedro JB. 2016. Large flux of iron from the Amery Ice Shelf marine ice to Prydz Bay, East Antarctica. *J Geophys Res Ocean* 121:1–14. doi:10.1002/2016JC011687

Hoppema M, de Baar HJW, Fahrbach E, Hellmer HH, Klein B. 2003. Substantial advective iron loss diminishes phytoplankton production in the Antarctic Zone. *Global Biogeochem Cycles* 17:1–11. doi:10.1029/2002GB001957

Horner R, Ackley SF, Dieckmann GS, Gulliksen B, Hoshiai T, Legendre L, Melnikov IA, Reeburgh WS, Spindler M, Sullivan CW. 1992. Ecology of sea ice biota. 1. Habitat, terminology, and methodology. *Polar Biol* 12:417–427. doi:10.1007/bf00243113

Jickells TD, An ZS, Andersen KK, Baker AR, Bergametti G, Brooks N, Cao JJ, Boyd PW, Duce RA, Hunter KA, Kawahata H, Kubilay N, laRoche J, Liss PS, Mahowald N, Prospero JM, Ridgwell AJ, Tegen I, Torres R. 2005. Global iron connections between desert dust, ocean biogeochemistry, and climate. *Science* 308:67–71. doi:10.1126/science.1105959

Johnson KS, 2001. Iron supply and demand in the upper ocean: Is extraterrestrial dust a significant source of bioavailable iron? *Global Biogeochem Cycles* 15:61–63. doi:10.1029/2000GB001295

Johnson KS, Chavez FP, Friederich GE. 1999. Continental-shelf sediment as a primary source of iron for coastal phytoplankton. *Nature* 398:697–700. doi:10.1038/19511

Johnson KS, Gordon RM, Coale KH. 1997. What controls dissolved iron concentrations in the world ocean? *Mar Chem* 57:137-161. doi" 10.1016/s0304-4203(97)00043-1

Jørgensen L, Stedmon CA, Kaartokallio H, Middelboe M, Thomas DN. 2015. Changes in the composition and bioavailability of dissolved organic matter during sea ice formation. *Limnol Oceanogr* 60:817–830. doi:10.1002/lno.10058

Juhl AR, Krembs C, Meiners KM. 2011. Seasonal development and differential retention of ice algae and other organic fractions in first-year Arctic sea ice. *Mar Ecol Prog Ser* 436:1–16. doi:10.3354/meps09277

Kloareg B, Quatrano RS. 1988. Structure of the cell walls of marine algae and ecophysiological functions of the matrix polysaccharides. *Oceanogr. Mar Biol*

Annu Rev 26:259–315.

Klunder MB, Laan P, Middag R, de Baar HJW, van Ooijen JC. 2011. Dissolved iron in the Southern Ocean (Atlantic sector). *Deep Res Part II Top Stud Oceanogr* 58:2678–2694. doi:10.1016/j.dsr2.2010.10.042

Knopf DA, Alpert PA, Wang B, Aller JY. 2010. Stimulation of ice nucleation by marine diatoms. *Nat Geosci* 4:88–90. doi:10.1038/ngeo1037

Kooyman G, Burns J. 1999. Weddell Sea versus emperor Penguin: Boss of the Ross sea. *Am Zool* 39.

Krembs C, Deming JW. 2008. The role of exopolymers in microbial adaptation to sea ice, (in) Psychrophiles: From Biodiversity to Biotechnology. Eds: Margesin R, Schinner F, Marx JC, Gerday C. Springer-Verlag, New-Yortk, pp. 247–264.

Krembs C, Eicken H, Deming JW. 2011. Exopolymer alteration of physical properties of sea ice and implications for ice habitability and biogeochemistry in a warmer Arctic. *Proc Natl Acad Sci U.S.A* 108:3653–8. doi:10.1073/pnas.1100701108

Krembs C, Eicken H, Junge K, Deming JW. 2002. High concentrations of exopolymeric substances in Arctic winter sea ice: implications for the polar ocean carbon cycle and cryoprotection of diatoms. *Deep Sea Res Part I Oceanogr Res* 49:2163–2181. doi:10.1016/S0967-0637(02)00122-X

Krembs C, Mock T, Gradinger R. 2001. A mesocosm study of physical-biological interactions in artificial sea ice: effects of brine channel surface evolution and brine movement on algal biomass. *Polar Biol* 24:356–654. doi:10.1007/s003000000219

Kuma K, Nishioka J, Matsunaga K. 1996. Controls on iron(III) hydroxide solubility in seawater: The influence of pH and natural organic chelators. *Limnol Oceanogr* 41:396–407. doi:10.4319/lo.1996.41.3.0396

Lancelot C, de Montety A, Goosse H, Becquevort S, Schoemann V, Pasquer B, Vancoppenolle M. 2009. Spatial distribution of the iron supply to phytoplankton in the Southern Ocean: a model study. *Biogeosciences Discuss* 6:4919–4962. doi:10.5194/bgd-6-4919-2009

Lancelot C, Mathot S, Veth C, de Baar H. 1993. Factors controlling phytoplankton ice-edge bloomsin the marginal ice-zone of the northwestern Weddel Sea during sea-ice retreat 1988 field observations and mathematical modelling. *Polar Biol* 13:377–387. doi:10.1007/bf01681979

Lange MA, Ackley SF, Wadhams P, Dieckmann GS, Eicken H. 1989. Development of sea ice in the Weddell Sea. *Ann Glaciol* 12:92–96.

Lannuzel D, Chever F, van der Merwe PC, Janssens J, Roukaerts A, Cavagna A-J, Townsend AT, Bowie AR, Meiners KM. 2014a. Iron biogeochemistry in

Antarctic pack ice during SIPEX-2. *Deep Sea Res Part II Top Stud Oceanogr* 131:111-122. doi:10.1016/j.dsr2.2014.12.003

Lannuzel D, de Jong J, Schoemann V, Trevena A, Tison J-L, Chou L. 2006. Development of a sampling and flow injection analysis technique for iron determination in the sea ice environment. *Anal Chim Acta* 556:476–483. doi:10.1016/j.aca.2005.09.059

Lannuzel D, Grotti M, Luisa AM, van der Merwe P. 2015. Organic ligands control the concentrations of dissolved iron in Antarctic sea ice. *Mar Chem* 174:120-130. doi:10.1016/j.marchem.2015.05.005

Lannuzel D, Schoemann V, de Jong J, Chou L, Delille B, Becquevort S, Tison J-L. 2008. Iron study during a time series in the western Weddell pack ice. *Mar Chem* 108:85–95. doi:10.1016/j.marchem.2007.10.006

Lannuzel D, Schoemann V, de Jong J, Pasquer B, van der Merwe P, Masson F, Tison J-L, Bowie A. 2010. Distribution of dissolved iron in Antarctic sea ice: Spatial, seasonal, and inter-annual variability. *J Geophys Res* 115:G03022. doi:10.1029/2009JG001031

Lannuzel D, Schoemann V, de Jong J, Tison J-L, Chou L. 2007. Distribution and biogeochemical behaviour of iron in the East Antarctic sea ice. *Mar Chem* 106:18–32. doi:10.1016/j.marchem.2006.06.010

Lannuzel D, Schoemann V, Dumont I, Content M, de Jong J, Tison J-L, Delille B, Becquevort S. 2013. Effect of melting Antarctic sea ice on the fate of microbial communities studied in microcosms. *Polar Biol* 36:1483–1497. doi:10.1007/s00300-013-1368-7

Lannuzel D, van der Merwe PC, Townsend AT, Bowie AR. 2014b. Size fractionation of iron, manganese and aluminium in Antarctic fast ice reveals a lithogenic origin and low iron solubility. *Mar Chem* 161:47–56. doi:10.1016/j.marchem.2014.02.006

Lannuzel D, Vancoppenolle M, van der Merwe P, de Jong J, Meiners KM, Grotti M, Nishioka J, Schoemann V. 2016. Iron in sea ice: Review and new insights. *Elem Sci Anthr* 4:130. doi:10.12952/journal.elementa.000130

Lin H, Rauschenberg S, Hexel CR, Shaw TJ, Twining BS. 2011. Free-drifting icebergs as sources of iron to the Weddell Sea. *Deep Res Part II Top Stud Oceanogr* 58:1392–1406. doi:10.1016/j.dsr2.2010.11.020

Lindemann F, Holemann JA, Korablev A, Zachek A. 1997. Particle entrainment into newly forming sea ice - Freeze-up studies in October 1995. (in) Land-Ocean Systems in the Siberian Arctic: Dynamics and History. Eds: Kassens H, Bauch HA, Dmitrenko IA, Eicken H, Hubberten H-W, Melles M, Thiede J, Timokhov LA. Springer Berlin, Berlin, doi:10.1007/978-3-642-60134-7_12. pp: 113–125.

Liu X, Millero FJ. 2002. The solubility of iron in seawater. *Mar Chem* 77:43–54.

doi:10.1016/S0304-4203(01)00074-3

Lizotte M. 2003. The microbiology of sea ice. (in) Sea Ice: An Introduction to Its Physics, Chemistry, Biology and Geology. Eds: Thomas DN, Dieckmann GS. Blackwell Science Ltd. pp:184–210.

Loscher BM, de Baar HJW, de Jong JTM, Veth C, Dehairs F. 1997. The distribution of Fe in the Antarctic Circumpolar Current. *Deep Sea Res Part II Top Stud Oceanogr* 44:143–187. doi:10.1016/S0967-0645(96)00101-4

Mancuso Nichols C, Garon Lardière S, Bowman JP, Nichols PD, Gibson JAE, Guézennec J. 2005. Chemical characterization of exopolysaccharides from Antarctic marine bacteria. *Microb Ecol* 49:578–589. doi:10.1007/s00248-004-0093-8

Martin JH. 1990. Glacial-interglacial CO_2 change: the iron hypothesis. *Paleoceanography* 5:1–13. doi:10.1029/pa005i001p00001

Martin JH, Gordon RM, Fitzwater SE. 1990. Iron in Antarctic waters. *Nature* 345:156–158. doi:10.1038/345156a0

Martin S, Drucker R, Fort M. 1995. A laboratory study of frost flower growth on the surface of young sea ice. *J Geophys Res* 100:7027–7036. doi:10.1029/94JC03243

Martin S, Kauffman P. 1981. A field and laboratory study of wave damping by grease ice. *J Glaciol* 27:283–313.

Massom R, Reid P, Stammerjohn S, Raymond B, Fraser A, Ushio S. 2013. Change and Variability in East Antarctic Sea Ice Seasonality, 1979/80-2009/10. *PLoS One* 8:e64756. doi:10.1371/journal.pone.0064756

Maykut GA. 1985. The ice environment. (in) Sea Ice Biota. Eds: Honer R. Boca Raton, FL (USA), pp. 21–82.

Meiners K, Brinkmeyer R, Granskog MA, Lindfors A. 2004. Abundance, size distribution and bacterial colonization of exopolymer particles in Antarctic sea ice (Bellingshausen Sea). *Aquat Microb Ecol* 35:283–296. doi:10.3354/ame035283

Meiners K, Gradinger R, Fehling J, Civitarese G, Spindler M. 2003. Vertical distribution of exopolymer particles in sea ice of the Fram Strait (Arctic) during autumn. *Mar Ecol Prog Ser* 248:1–13. doi:10.3354/meps248001

Meiners KM, Krembs C, Gradinger R. 2008. Exopolymer particles: microbial hotspots of enhanced activity in Arctic fast ice (Chukchi Sea). *Aquat Microb Ecol* 52:195–207. doi:10.1073/pnas.1100701108

Meiners KM, Michel C. 2017. Dynamics of nutriments, dissolved organic matter and exopolymers in sea ice. (in) Sea Ice, 3rd Edition. Eds: Thomas, DN. ISBN:

9781118778388

Meiners KM, Vancoppenolle M, Thanassekos S, Dieckmann GS, Thomas DN, Tison J-L, Arrigo KR, Garrison DL, McMinn A, Lannuzel D, van der Merwe P, Swadling KM, Smith Jr WO, Melnikov I, Raymond B. 2012. Chlorophyll a in Antarctic sea ice from historical ice core data. *Geophys Res Lett* 39:L21602. doi:10.1029/2012GL053478

Michel K, Pistorius E. 2004. Adaptation of the photosynthetic electron transport chain in cyanobacteria to iron deficiency: The function of IdiA and IsiA. *Physiol Plantarum* 120:36–50. doi:10.1111/j.0031-9317.2004.0229.x

Millero FJ, Yao W, Aicher J. 1995. The speciation of Fe (II) and Fe (III) in natural waters. *Mar Chem* 50:21–39. doi:10.1016/0304-4203(95)00024-I

Mitchell GB, Holm-Hansen O. 1990. Observations an modeling of the Antarctic phytoplankton crop in relation to mixing depth. *Deep Sea Res Part II Top Stud Oceanogr* 38:981–1007. doi:10.1016/0198-0149(91)90093-u

Mock T, Dieckmann GS, Haas C, Krell A, Tison J-L, Belem AL, Papadimitriou S, Thomas DN. 2002. Micro-optodes in sea ice: A new approach to investigate oxygen dynamics during sea ice formation. *Aquat Microb Ecol* 29:297–306. doi:10.3354/ame029297

Moreau S, Vancoppenolle M, Delille B, Tison J-L, Zhou J, Kotovitch M, Thomas DN, Geilfus N-X, Goosse H. 2015. Drivers of inorganic carbon dynamics in first-year sea ice: A model study. *J Geophys Res Ocean* 120:471–495. doi:10.1002/2014JC010388

Moreau S, Vancoppenolle M, Zhou J, Tison J-L, Delille B, Goosse H. 2014. Modelling argon dynamics in first-year sea ice. *Ocean Model* 73:1–18. doi:10.1016/j.ocemod.2013.10.004

Nelson DM, Smith WO. 1991. The role of light and major nutrients. *Limnol Oceanogr* 36:1650–1661. doi:10.4319/lo.1991.36.8.1650

Nicol S, Worby A, Leaper R. 2008. Changes in the Antarctic sea ice ecosystem: potential effects on krill and baleen whales. *Mar Freshw Res* 59:361–382. doi:10.1071/MF07161

Niedrauer TM, Martin S. 1979. An experimental study of brine drainage and convection in Young Sea ice. *J Geophys Res* 84:1176. doi:10.1029/JC084iC03p01176

Noble AE, Moran DM, Allen AE, Saito MA. 2013. Dissolved and particulate trace metal micronutrients under the McMurdo Sound seasonal sea ice: basal sea ice communities as a capacitor for iron. *Front Chem* 1. doi:10.3389/fchem.2013.00025

Nomura D, Yoshikawa-Inoue H, Toyota T, Shirasawa K. 2010. Effects of snow,

snowmelting and refreezing processes on air-sea-ice CO_2 flux. *J Glaciol* 56:262–270. doi:10.3189/002214310791968548

Norman L, Thomas DN, Stedmon CA, Granskog MA, Papadimitriou S, Krapp RH, Meiners KM, Lannuzel D, van der Merwe P, Dieckmann GS. 2011. The characteristics of dissolved organic matter (DOM) and chromophoric dissolved organic matter (CDOM) in Antarctic sea ice. *Deep Sea Res Part II Top Stud Oceanogr* 58:1075–1091. doi:10.1016/j.dsr2.2010.10.030

Osterkamp TE, Gosink JP. 1983. Frazil ice formation and ice cover development in interior Alaska streams. *Cold Reg Sci Technol* 8:43–56. doi:10.1016/0165-232X(83)90016-2

Papadimitriou S, Kennedy H, Kattner G, Dieckmann GS, Thomas DN. 2004. Experimental evidence for carbonate precipitation and CO_2 degassing during sea ice formation. *Geochim Cosmochim Acta* 68:1749–1761. doi:10.1016/j.gca.2003.07.004

Parkinson CL, Cavalieri DJ. 2012. Antarctic sea ice variability and trends, 1979-2010. *Cryosphere* 6:871–880. doi:10.5194/tc-6-871-2012

Passow U. 2002. Transparent exopolymer particles (TEP) in aquatic environments. *Prog Oceanogr* 55:287–333. doi:10.1016/s0079-6611(02)00138-6

Penrose JD, Conde M, Pauly TJ. 1994. Acoustic detection of ice crystals in Antarctic waters. *J Geophys Res Ocean* 99:12573–12580. doi: 10.1029/93jc03507

Petrich C, Eicken H. 2010. Growth, structure and properties of sea ice. (in) Sea Ice. Eds: Thomas DN, Dieckmann GS. Wiley-Blackwell, Oxford, pp. 23–77.

Pomeroy LR, Williams PJ leB, Azam F, Hobbie JE. 2007. The Microbial Loop. *Oceanography* 20:28–33. doi: 10.5670/oceanog.2007.45

Reimnitz E, Clayton JR, Kempema EW, Payne JR, Weber WS. 1993. Interaction of rising frazil with suspended particles: tank experiments with applications to nature. *Cold Reg Sci Technol* 21:117–135. doi:10.1016/0165-232X(93)90002-P

Raven PH, Evert RF, Eichhorn SE. 1999. Biology of plants, 6th ed. Freeman Co. New York

Resing JA, Sedwick PN, German CR, Jenkins WJ, Moffett JW, Sohst BM, Tagliabue A. 2015. Basin-scale transport of hydrothermal dissolved metals across the South Pacific Ocean. *Nature* 523:200–203. doi:10.1038/nature14577

Riedel A, Michel C, Gosselin M, LeBlanc B. 2007. Enrichment of nutrients, exopolymeric substances and microorganisms in newly formed sea ice on the Mackenzie shelf. *Mar Ecol Prog Ser* 342:55–67. doi:10.3354/meps342055

Rintoul SR, Hughes C, Olbers D. 2001. The Antarctic circumpolar current system. (in) Ocean Circulation and Climate, Vol. 77. Eds: Siedler G, Church JA. pp.

271–302.

Rue EL, Bruland KW. 1995. Complexation of iron (III) by natural organic ligands in the Central North Pacific as determined by a new competitive ligand equilibration/adsorptive cathodic stripping. *Mar Chem* 50:117–138. doi:10.1016/0304-4203(95)00031-L

Saenz BT, Arrigo KR. 2012. Simulation of a sea ice ecosystem using a hybrid model for slush layer desalination. *J Geophys Res Ocean* 117:1–20. doi:10.1029/2011JC007544

Sarmiento JL, Gruber N. 2005. Ocean Biogeochemical dynamics. Princeton University Press Princeton, Princeton, New Jersey and Los Angeles, California.

Schallenberg C, van der Merwe P, Chever F, Cullen JT, Lannuzel D, Bowie AR. 2015. Dissolved iron and iron(II) distributions beneath the pack ice in the east antarctic (120°E) during the winter/spring transition. *Deep Sea Res Part II Top Stud Oceanogr* 131:96-110. doi:10.1016/j.dsr2.2015.02.019

Sedwick PN, DiTullio GR, Mackey DJ. 2000. Iron and manganese in the Ross Sea, Antarctica: Seasonal iron limitation in Antarctic shelf waters. *J Geophys Res* 105:11321. doi:10.1029/2000JC000256

Sedwick PN, DiTullio R. 1997. Regulation of algal blooms in Antarctic shelf waters by the release of iron from melting sea ice. *Geophys Res Lett* 24:2515–2518. doi:10.1029/97GL02596

Shaked Y, Lis H. 2012. Disassembling iron availability to phytoplankton. *Front Microbiol* 3:1–26. doi:10.3389/fmicb.2012.00123

Sherrell RM, Lagerström ME, Forsch KO, Stammerjohn SE, Yager PL. 2015. Dynamics of dissolved iron and other bioactive trace metals (Mn, Ni, Cu, Zn) in the Amundsen Sea Polynya, Antarctica. *Elem Sci Anthr* 3:71. doi:10.12952/journal.elementa.000071

Sherwood CR. 2000. Numerical model of frazil ice and suspended sediment concentrations and formation of sediment laden ice in the Kara Sea. *J Geophys Res Ocean* 105:14061–14080. doi:10.1029/2000jc900037

Sigman DM, Hain MP, Haug GH. 2010. The polar ocean and glacial cycles in atmospheric CO_2 concentration. *Nature* 466:47–55. doi:10.1038/nature09149

Smetacek V, Klaas C, Strass VH, Assmy P, Montresor M, Cisewski B, Savoye N, Webb A, d'Ovidio F, Arrieta JM, Bathmann U, Bellerby R, Berg GM, Croot P, Gonzalez S, Henjes J, Herndl GJ, Hoffmann LJ, Leach H, Losch M, Mills MM, Neill C, Peeken I, Röttgers R, Sachs O, Sauter E, Schmidt MM, Schwarz J, Terbrüggen A, Wolf-Gladrow D. 2012. Deep carbon export from a Southern Ocean iron-fertilized diatom bloom. *Nature* 487:313–319. doi:10.1038/nature11229

Smith KL, Polvani LM, Marsh DR. 2012. Mitigation of 21st century Antarctic sea ice loss by stratospheric ozone recovery. *Geophys Res Lett* 39:2–7. doi:10.1029/2012GL053325

Spindler M. 1994. Notes on the biology of sea ice in the Arctic and Antarctic. *Polar Biol* 14, 319–324. doi:10.1007/BF00238447

Stammerjohn S, Massom R, Rind D, Martinson D. 2012. Regions of rapid sea ice change: An inter-hemispheric seasonal comparison. *Geophys Res Lett* 39:L06501. doi:10.1029/2012GL050874

Stefels J, Steinke M, Turner S, Malin G, Belviso S. 2007. Environmental constraints on the production and removal of the climatically active gas dimethylsulphide (DMS) and implications for ecosystem modelling. *Biogeochem* 83:245–275. doi:10.1007/978-1-4020-6214-8_18

Steiner N, Deal C, Lannuzel D, Lavoie D, Massonnet F, Miller LA, Moreau S, Popova E, Stefels J, Tedesco L. 2016. What sea-ice biogeochemical modellers need from observers. *Elem Sci Anthr* 1–22. doi:10.12952/journal.elementa.000084

Stephens BB, Keeling RF. 2000. The influence of Antarctic sea ice on glacial-interglacial CO_2 variations. *Nature* 404:171–174. doi:10.1038/35004556

Sullivan CW, Arrigo KR, McClain CR, Comiso JC, Firestone J. 1993. Distributions of phytoplankton blooms in the Southern Ocean. *Science* 262:1832–1837. doi:10.1126/science.262.5141.1832

Sunda WG. 2001. Bioavailability and bioaccumulation of iron in the sea. (in) The Biogeochemistry of Iron in Seawater. Eds: Turner DR, Hunter KH. IUPAC Series on Analytical and physical chemistry of environment systems, Wiley. pp: 41–84.

Sunda WG, Huntsman SA. 1997.Interrelated influence of iron, light and cell size on marine phytoplankton growth. *Nature* 390:389-392.

Tagliabue, A., Bopp, L., Dutay, J.-C., Bowie, A.R., Chever, F., Jean-Baptiste, P., Bucciarelli, E., Lannuzel, D., Remenyi, T., Sarthou, G., Aumont, O., Gehlen, M., Jeandel, C., 2010. Hydrothermal contribution to the oceanic dissolved iron inventory. *Nat Geosci* 3:252–256. doi:10.1038/ngeo818

Tagliabue A, Mtshali T, Aumont O, Bowie AR, Klunder MB, Roychoudhury AN, Swart S. 2012. A global compilation of dissolved iron measurements: Focus on distributions and processes in the Southern Ocean. *Biogeosciences* 9:2333–2349. doi:10.5194/bg-9-2333-2012

Tagliabue A, Williams RG, Rogan N, Achterberg EP, Boyd PW. 2014. A ventilation-based frameworkd for dissolved Iron in the Ocean. *Geophys Res Lett* 41:7227–7236. doi:10.1002/2014GL061066

Takahashi T, Sutherland SC, Sweeney C, Poisson A, Metzl N, Tilbrook B, Bates N, Wanninkhof R, Feely RA, Sabine C, et al. 2002. Global sea--air CO_2 flux based on climatological surface ocean pCO_2, and seasonal biological and temperature effects. *Deep Sea Res Part II Top Stud Oceanogr* 49:1601–1622. doi:10.1016/s0967-0645(02)00003-6

Taylor SR. 1964. Abundance of chemical elements in the continental crust : a new table. *Geochim Cosmochim Acta* 28:1273–1285. doi:10.1016/0016-7037(64)90129-2

Tedesco L, Vichi M. 2012. LIM1D-BFMSI : a new advanced model of the sea ice ecosystem, in: conference poster, IPY.

Tedesco L, Vichi M, Haapala J, Stipa T. 2010. A dynamic Biologically Active Layer for numerical studies of the sea ice ecosystem. *Ocean Model* 35:89–104. doi:10.1016/j.ocemod.2010.06.008

Thomas DN, Kattner G, Kennedy HA, Dieckmann GS. 2001. Dissolved organic matter in Antarctic sea ice. *Ann Glaciol* 33:297-303. doi:http://dx.doi.org/10.3189/172756401781818338

Thomas DN, et al. 2009. INTERICE 4, Final report.

Thomas DN, Wilkinson J. 2001. INTERICE 3, ARCTELAB, Final Report, July 2001 (unpublished)

Thomas DN, Papadimitriou S, Michel C. 2010. Biogeochemistry of Sea ice. (in): Sea ice. Eds: Thomas D, Dieckamm GS. Wiley-Blackwell. pp:425-468

Tortell PD, Maldonado MT, Granger J, Price NM. 1999. Marine bacteria and biogeochemical cycling of iron in the oceans. *FEMS Microbiol Ecol* 29:1–11. doi:10.1016/s0168-6496(98)00113-5

Trevena A, Jones G. 2012. DMS flux over the Antarctic sea ice zone. *Mar Chem* 134–135:47–58. doi:10.1016/j.marchem.2012.03.001

Underwood GJC, Fietz S, Papadimitriou S, Thomas DN, Dieckmann G. 2010. Distribution and composition of dissolved extracellular polymeric substances (EPS) in Antarctic sea ice. *Mar Ecol Prog Ser* 404:1–19. doi:10.3354/meps08557

van der Merwe P, Lannuzel D, Bowie AR, Meiners KM. 2011a. High temporal resolution observations of spring fast ice melt and seawater iron enrichment in East Antarctica. *J Geophys Res* 116:G03017. doi:10.1016/2010JG001628

van der Merwe P, Lannuzel D, Mancuso Nichols CA, Meiners K, Heil P, Norman L, Thomas DN, Bowie AR. 2009. Biogeochemical observations during the winter–spring transition in East Antarctic sea ice: Evidence of iron and exopolysaccharide controls. *Mar Chem* 115:163–175. doi:10.1016/j.marchem.2009.08.001

van der Merwe P, Lannuzel D, Bowie AR, Mancuso Nichols CA, Meiners KM. 2011b. Iron fractionation in pack and fast ice in East Antarctica: Temporal decoupling between the release of dissolved and particulate iron during spring melt. *Deep Res Part II Top Stud Oceanogr* 58:1222–1236. doi:10.1016/j.dsr2.2010.10.036

Vancoppenolle M, Goosse H, de Montety A, Fichefet T, Tremblay B, Tison J-L. 2010. Modeling brine and nutrient dynamics in Antarctic sea ice: The case of dissolved silica. *J Geophys Res Ocean* 115:C02005. doi:10.1029/2009JC005369

Vancoppenolle M, Meiners KM, Michel C, Bopp L, Brabant F, Carnat G, Delille B, Lannuzel D, Madec G, Moreau S, Tison J-L, van der Merwe P. 2013. Role of sea ice in global biogeochemical cycles: emerging views and challenges. *Quat Sci Rev* 79:207–2030. doi:10.1016/j.quascirev.2013.04.011

Verbeke V. 2005. Concentrations en gaz ds la glace de mer: developpements techniques et implications environmentales. PhD thesis. Universite Libre de Bruxelles.

Verdugo P, Alldredge A, Azam F, Kirchman D, Passow U, Santschi P. 2004. The oceanic gel phase: a bridge in the DOM-POM continuum. *Mar Chem* 92:67–85. doi:10.1016/j.marchem.2004.06.017

Von Quillfeldt CH, Ambrose Jr WG, Clough LM. 2003. High number of diatom species in first-year ice from the Chukchi Sea. *Polar Biol* 26:806–818. doi:10.1007/s00300-003-0549-1

Waite TD. 2001. Thermodynamics of the iron system in seawater. (in) The biogeochemistry of iron in seawater. Eds: Hunter KA, Turner DR. IUPAC Series on Analytical and physical chemistry of environment systems, Wiley, New York, USA. pp:291-342

Wagener T, Guieu C, Losno R, Bonnet S, Mahowald N. 2008. Revisiting atmospheric dust export to the Southern Hemisphere ocean: Biogeochemical implications. *Global Biogeochem Cycles* 22:1–13. doi:10.1029/2007GB002984

Wang S, Bailey D, Lindsay K, Moore K, Holland M. 2014. Impacts of sea ice on the marine iron cycle and phytoplankton productivity. *Biogeosciences* 11:4713–4731. doi:10.5194/bg-11-4713-2014

Weeks W, Ackley SF. 1982. The growth, structure, and properties of sea ice. US Army Corps of Engineers, *Cold Regions Research & Engineering Laboratory*, Hanover NH.

Weissenberger J. 1998. Arctic Sea ice biota: design and evaluation of a mesocosm experiment. *Polar Biol* 19:151–159. doi:10.1007/s003000050228

Weissenberger J, Grossmann S. 1998. Experimental formation of sea ice: Importance of water circulation and wave action for incorporation of phytoplankton and

bacteria. *Polar Biol* 20:178–188. doi:10.1007/s003000050294

Westerlund S, Öhman P. 1991. Iron in the water column of the Weddell Sea. *Mar Chem* 35:199–217. doi:10.1016/S0304-4203(09)90018-4

Winton VHL, Dunbar GB, Atkins CB, Bertler NAN, Delmonte B, Andersson PS, Bowie A, Edwards R. 2016. The origin of lithogenic sediment in the south-western Ross Sea and implications for iron fertilization. *Antarct Sci* 28:1–11. doi:10.1017/S095410201600002X

Zhou J, Delille B, Kaartokallio H, Kattner G, Kuosa H, Tison J-L, Autio R, Dieckmann GS, Evers K-U, Jørgensen L, Kennedy H, Kotovitch M, Luhtanen A-M, Stedmon CA, Thomas DN. 2014. Physical and bacterial controls on inorganic nutrients and dissolved organic carbon during a sea ice growth and decay experiment. *Mar Chem* 166:59–69. doi:10.1016/j.marchem.2014.09.013

CHAPTER 2

Incorporation of iron and organic matter into young Antarctic sea ice during its initial growth stages

This chapter was published as an article under the same title in Elementa, Science of the Anthropocene, part of the special issue Biogeochemical Exchange Processes at Sea-Ice Interfaces (BEPSII), 4:000123. doi:10.12952/journal.elementa.000123

Supplemental material for this paper has been included in this chapter to facilitate the reading.

2.1 Introduction

It is now well established that sea ice represents an important reservoir of iron (Fe) to the Fe-depleted waters of the Southern Ocean (e.g., Sedwick et al., 1997; Lancelot et al., 2009; Lannuzel et al., 2010; Wang et al., 2014). The seasonal cycle of sea-ice formation and retreat in Antarctica affects approximately 40% of the entire Southern Ocean and impacts the whole Antarctic ecosystem (Arrigo, 2014). During formation, sea ice has a generally low capacity to incorporate salts and impurities such as biotic or abiotic particles and dissolved components (Cox and Weeks, 1975). The growing sea-ice crystals reject impurities into the liquid brine found within the ice. Small amounts of seawater can be trapped in the advancing ice interface, entraining some impurities, but most of the seawater is rejected at the ice-seawater interface. However, Antarctic field studies have shown Fe and organic matter enrichment of 1 to 2 orders of magnitude over seawater (Grotti et al., 2005; Lannuzel et al., 2007; 2008; 2014a; 2014b; van der Merwe et al., 2009; 2011a; 2011b; de Jong et al., 2013; 2015). The co-occurrence of high concentrations of Fe and organic matter in the ice suggests coupled processes leading to their enrichment (Lannuzel et al., 2007; 2015;

Schoemann et al., 2008). Specifically, van der Merwe et al. (2009) proposed that Fe can be associated with extracellular polymeric substances (EPS) and co-incorporated into the ice.

A combination of biological and physical mechanisms could explain incorporation of biogenic and lithogenic materials into sea ice. These mechanisms include: (1) sediment entrapment in newly formed sea ice (e.g., Nürnberg et al., 1994; Lindemann et al., 1997; Lindemann, 1998; Smedsrud, 1998; Dethleff and Kempema, 2007; Dethleff and Kuhlmann, 2009); (2) dissolved macro-nutrient entrapment (Riedel et al., 2007; Zhou et al., 2014); (3) dissolved organic matter entrapment (e.g., Giannelli et al., 2001; Ewert and Deming, 2011; Müller et al., 2013); and (4) entrapment of particulate biogenic material (e.g., Garrison et al., 1989; Gradinger and Ikävalko, 1998; Weissenberger and Grossmann, 1998; Rózańska et al., 2008).

The proposed processes for incorporation of particulate impurities into sea ice are as follows. When the first crystals of frazil ice form in the water column, they are thought to harvest or scavenge the particulate matter present in the water column during their rise to the surface (Weeks and Ackley, 1982; Osterkamp and Gosink, 1983; Garrison et al. 1989; Reimnitz et al., 1993; Dethleff, 2005). Microorganisms and detritus can act as nucleation sites for the ice crystals (Weeks and Ackley, 1982; Knopf et al., 2011). Once particles associated with frazil ice crystals have accumulated in the surface water, they can be concentrated under the action of Langmuir circulation cells and trapped in newly forming ice (Martin and Kauffman, 1981). Although this process has not been particularly well studied in Antarctica, it is considered to be a leading mechanism in the formation of sediment-laden sea ice in the Arctic (Dethleff, 2005; Dethleff and Kempema, 2007; Dethleff et al., 2009). Young Arctic sea ice with high sediment content also contains high dissolved metal

concentrations, including dissolved Fe (Hölemann et al., 1997). Similarly, the suspended material can be concentrated by wave-field pumping passing through the freshly formed layer of frazil ice (Lindemann et al., 1997). These particles then become attached to, or trapped in or between, the ice crystals (Weissenberger and Grossmann, 1998). Once a layer of ice isolates the water from the atmosphere, thermodynamic ice-growth processes dominate, and congelation ice starts to form. When congelation ice grows, exchange of sea salts and macro-nutrients between seawater and ice are controlled by convective fluid movement induced by strong salinity gradients across the ice-water interface (e.g., Vancoppenolle et al., 2010). These convective movements could be responsible for the aggregation at the seawater/sea-ice boundary of living and dead microorganisms, which then can become incorporated into the sea ice as the ice continues to grow (Lannuzel et al., 2010). The organic matter observed in columnar ice could alternatively originate from *in situ* biological processes; e.g., algal growth within the ice cover (Lizotte, 2003). Bio-accumulation through ice algal growth was suggested by Spindler (1994) as a key driver of high concentrations of organic matter (living and dead) in columnar ice. Because organic matter contains Fe, this bioaccumulation mechanism would lead to the incorporation of Fe in sea ice together with organic matter.

Due to the varying processes involved in sea-ice formation, frazil ice should theoretically be more enriched in Fe and organic matter than columnar ice, which forms more slowly and therefore expels impurities more effectively. However, this rationale only relies on initial incorporation processes and does not take into account *in situ* biogeochemical, transport and other processes. To date, no relationship between Fe content and ice texture has been clearly established (Lannuzel et al., 2007; 2014a; van der Merwe et al., 2009), and the relationships between sea-ice formation

and the Fe cycle in surface polar oceans remain poorly understood.

The aim of this study was to investigate the potential occurrence and pathways of Fe and organic matter enrichment in newly formed sea ice during two *in situ* time-series ice-growth experiments in the Weddell Sea during austral winter. We also explored the entrapment signature in different types of young sea ice collected opportunistically during the voyage. To our knowledge, this study is the first attempt to investigate the initial pathways leading to Fe enrichment in Antarctic sea ice.

2.2 Methods

2.2.1 Cleaning procedures for trace metal work

All sampling bottles (Nalgene, of low-density polyethylene, LDPE), melting containers (polypropylene, PP) and equipment were cleaned following the GEOTRACES recommendations (Cutter et al., 2010). In short, they were immersed for one week in 2% (v:v) Decon90 and then rinsed four times with reverse osmosis water (ROW) and three times with ultra high purity water (UHP water, Barnstead International, NANOpure Diamond polisher) before being soaked in a 50% (v:v) HCl bath (analytical grade Merck EMSURE, Germany) for one month. Bottles were then rinsed five times with UHP water in a class-100 laminar flow hood before being filled with 10% (v:v) HCl (Ultrapure, Seastar Baseline) and triple-bagged until used on the voyage. Before use, bottles were rinsed three times with UHP water and three times with the sample. During the voyage, filtration sets and other plastic equipment (Teflon filtration set, tubing, scoop, PP melting containers, etc.) were immersed in 20% (v:v) HCl between stations. Equipment used for Fe filtrations was thoroughly rinsed with UHP water, 10% (v:v) HCl and UHP water between the processing of the samples.

2.2.2 Sampling area

Sea-ice early growth experiments and young ice sampling were conducted during the Antarctic Winter Ecosystem and Climate Study (AWECS/ANT-XXIX/6) voyage with RV *Polarstern* to the Weddell Sea in June–August 2013 (Lemke, 2014; Figure 2.1). The first time-series ice-growth experiment (Station 506) started on 12 July 2013 in the middle of the Weddell Sea and ended on 14 July 2013. The second experiment (Station 517) was performed closer to the Antarctic Peninsula and the continental shelf between 29 and 31 July 2013 (Table 2.1). Natural young ice was also collected at five other stations (Stations 486–500; Figure 2.1).

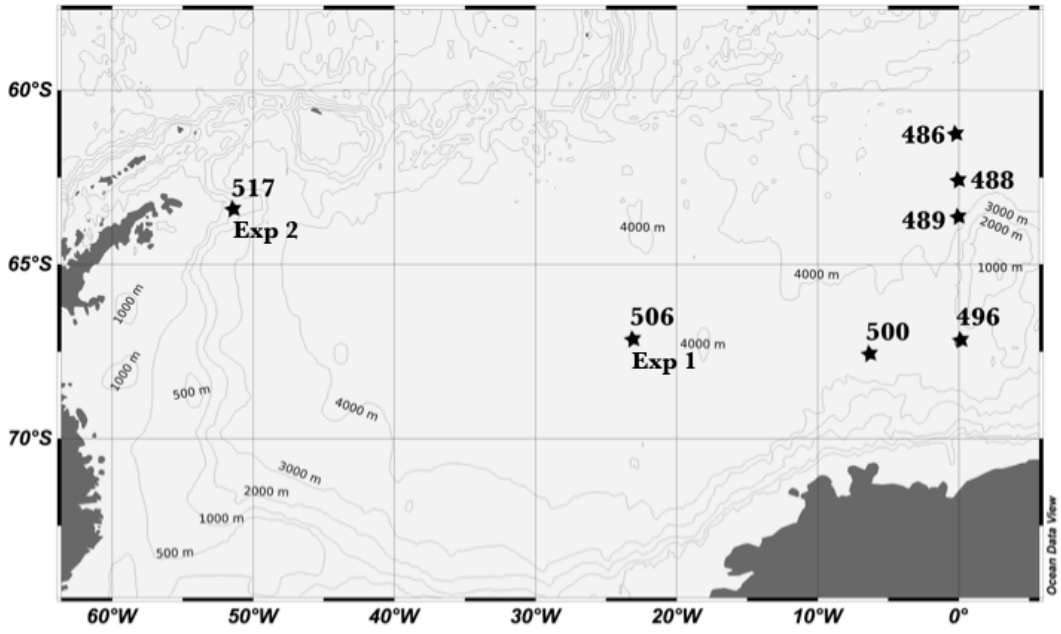

Figure 2.1 Location of the young ice sampling stations (Stations 486, 488,489, 496 and 500) and the two *in situ* ice-growth time-series experiments (Stations 506 and 517 for Experiments 1 and 2, respectively) of the AWECS cruise in the Weddell Sea during June-August 2013. Note that only the stations pertaining to this dataset are shown.

2.2.3 In situ ice-growth time-series experiments

Experiments were conducted in areas of level ice, upwind from the ship and other

activities on the ice to avoid contamination. Prior to ice coring, snow was removed using an acid-clean plastic shovel. Collection and processing of ice and water samples were conducted using the methods outlined by Lannuzel et al. (2006). Seawater was collected from the ice-water interface using a peristaltic pump (E/S Portable Sampler, Masterflex) equipped with acid-clean silicon tubes. For each experiment, four rows of holes (Figure 2.2) were drilled through the ice using a trace metal (TM) clean electro-polished stainless steel ice corer previously tested for TM sampling (14 cm internal diameter, Lichtert Industry, Belgium; Lannuzel et al., 2006). Each row corresponds to an increasing time step and each core (A to F, Figure 2.2) was allocated to measure one of the parameters described below. Holes were cleared of coring debris and slush with an acid-clean plastic scoop, which denoted the start of an experiment (T_0 = 0 h). Ice was then allowed to grow in each hole and subsequently collected at increasing time steps (T_1 = 6 h, T_2 = 12 h, T_3 = 24 h and T_4 = 48 h). The T_1 samples were collected using a titanium (Ti)-coated handsaw (Clauss Titanium). Titanium is a material commonly used for trace metal sampling (de Baar et al., 2008; Cutter et al., 2010). T_2, T_3 and T_4 rows were collected using the TM-clean corer. No snow precipitation was observed throughout the duration of the experiments. Ice samples were melted for a suite of parameters for rows T_1, T_2 and T_3. For T_4, the core was long enough to cut it into two sections using the Ti-coated handsaw (top = 0.1 m and bottom = the rest of the core). The procedure was achieved under a class-100 laminar flow hood (AirClean 600 PCR workstation, Model 300 Controller, AirClean System).

With the exception of the ice texture sample, ice samples were placed in individual PP melting containers and melted rapidly onboard in the dark at room temperature,

according to Rintala et al. (2014). During melting, the sample was gently homogenised to help redistribute the heat evenly and keep the melt cool. Melted ice cores and seawater samples were then immediately processed for particulate organic carbon (POC) and nitrogen (PON), dissolved organic carbon (DOC), the inorganic macro-nutrients ammonium (NH_4^+), silicic acid ($Si(OH)_4^-$), phosphate (PO_4^{3-}) and nitrate + nitrite (NO_3^- + NO_2^- = NO_x), chlorophyll *a* (Chl *a*), extracellular polymeric substances (EPS), bacterial counts, particulate iron (PFe) and dissolved iron (DFe), and bulk salinity.

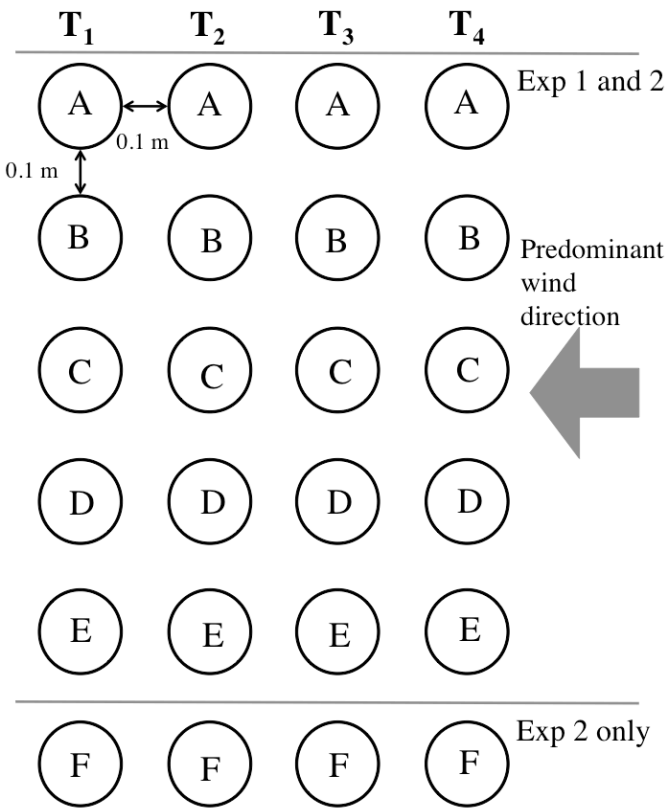

Figure 2.2 Layout of the set-up for Exp 1 and 2 (aerial view). Cores were separated by 0.1 m. For each time step, one row (cores A-E for Exp 1 and A-F for Exp 2) was sampled for a suite of parameters T_1 sampling was at 6 hours, T_2 at 12 hours, T_3 at 24 hours and T_4 at 48 hours. Cores allocation was as follows for Exp 1: core A, temperature and ice texture; core B, salinity and bacterial counts; core C, POC/PON, macro-nutrients and Chl a; core D, EPS; and core E, PFe and DFe. Core allocation during Exp 2 was: core A, temperature and ice texture; core B, salinity and bacterial count; core C, POC/PON, macro-nutrients; core D, Chl a; core E, EPS; and F, PFe and DFe.

2.2.4 Young natural ice sampling

Seawater was sampled 1 m below the ice using a 5-L polyvinylidene fluoride Pristine sample bottle (NIOZ) attached to a kevlar hydrographic wire and activated by a Teflon messenger. A subsample was then drawn into LDPE bottles, triple-bagged and brought back to the ship. The methods used to collect natural young ice were adapted to the type of ice (Table 2.1). Unconsolidated pancake ice was collected from a cage hanging over the sea ice (Station 486). The ice blocks were collected directly by hand, wearing clean-room nitrile gloves and clean sleeves (Kanna et al., 2014). Semi-consolidated pancake ice (Station 488) and consolidated pancake ice (Station 489) were sampled from the cage using the TM-clean corer. Young ice (Station 496) and grey ice (Station 500) were collected upwind from the ship from a refrozen lead. Grey ice is a type of newly formed sea ice with a thickness of 0.10–0.15 m. It is usually less elastic than nilas (thin sheet of transparent ice) and rafts under pressure. Young ice was collected using a SIPRE-type corer (Kovacs, 9-cm internal diameter). Approximately 1.5 cm of the outer layer of the core was scraped off using a Ti-blade to collect the clean inner core section (Kanna et al., 2014). Grey ice was sampled using the Ti-coated handsaw directly from the ice edge. Only the bottom 0.1 m of the core was analyzed for the semi-consolidated pancake ice, the consolidated pancake and the young ice. Cutting was processed on site to minimize brine loss. The entire core was placed on a trace-metal clean plastic board and cut using a Ti-coated handsaw immediately after sampling. For each station, the collected ice sections were placed in individual TM-clean PP melting containers and brought back to the ship. With the exception of the ice texture sample, samples were allowed to melt onboard in the dark at room temperature (Rintala et al., 2014). The melting time varied from 6 hours to approximately 16 hours for the thicker sections. Seawater and natural sea-ice

samples were processed for the same variables as the ice-growth experiments, except for bacterial count, which has been measured in the *in situ* ice-growth experiment only.

2.2.5 Analytical techniques

2.2.5.1 Physical variables

In situ ice temperatures were measured using a calibrated probe (Testo 720, precision ± 0.1 °C) inserted into 4-mm diameter holes freshly drilled into the side (2-cm intervals) of ice core A (Figure 2.2). Bulk salinity (Practical Salinity, S_P) of melted ice samples and seawater samples were measured using an Orion Star 3 conductivity meter (precision ± 0.1). Using the temperature and bulk salinity measurements (core B), brine volume fractions (V_b/V) were calculated according to Cox and Weeks (1988), neglecting sea-ice air content. Vertical thin sections of ice cores A were prepared (–25 °C in a ship-board cold room) and analyzed using cross-polarized light to identify ice textures (granular vs. columnar; Langway, 1958).

2.2.5.2 Particulate organic carbon and nitrogen, dissolved organic carbon, and macro-nutrients

All glassware in contact with POC, PON and DOC samples was combusted at 450°C for 12 hours prior to the cruise. Onboard and immediately after fully melted, ice and seawater samples were gently shaken to homogenize before filtration (200–2,500 mL) onto pre-combusted (450°C, 12 hours) 25-mm quartz filters (Sartorius). Forty-mL subsamples of the filtrate were stored in glass vials at –20°C in the dark for later DOC analysis. In addition, 20-mL filtrate subsamples were collected in two plastic tubes kept frozen at –20°C for macro-nutrient analyses. For DOC

Table 2.1 Young ice sampling locations and physical parameters

Station number	Location	Sampling date, 2013	Type of ice	Sampling method	Snow thickness (m)	Ice thickness (m)	Ice temperature (°C)	Bulk ice salinity (S_P)[a]	V_b/V (%)[b]
486	61°31 S, 00°05 W	17-Jun	Unconsolidated pancake	Cage + gloved hands	No snow	0.06–0.07	–5.0	23.7	26
488	62°54 S, 00°00 W	18-Jun	Semi-consolidated pancake	Cage + TM corer	< 0.01	0.30–0.36	–4.1	5.3	6
489	63.54° S, 00.01°W	19-Jun	Consolidated pancake	Cage + TM corer	0.03	0.30–0.36	–3.4	6.3	9
496	67.26° S, 00°01 W	24-Jun	Thin ice	Kovacs corer + Ti-coated handsaw	0.04	0.42–0.46	–3.2	8.3	13
500	67°57 S, 06°39 W	5-Jul	Grey ice	Ti-coated handsaw	No snow	0.05–0.06	–3.3	18.5	28
506	67°11 S, 23°00 W	12–14 July	*In situ* Exp 1	Ti-coated handsaw + TM corer	Snow removed	See Table 2.2	See Table 2.2	See Table 2.2	See Table 2.2
517	63°34 S, 51°10 W	29– 31 July	*In situ* Exp 2	Ti-coated handsaw + TM corer	Snow removed	See Table 2.2	See Table 2.2	See Table 2.2	See Table 2.2

[a] Seawater salinity (S_P) was 34.2, 34.5, 34.8, 34.2, and 34.2 at stations 486, 488, 489, 496, and 500, respectively.
[b] V_b/V = Brine volume fraction

analysis, frozen samples were melted overnight in the dark, and DOC concentrations were determined by high-temperature catalytic oxidation using a TOC analyzer (Total Organic Carbon Analyzer TOC-L CPH, Shimadzu) following the method of Qian and Mopper (1996). Quality controls were run using a standard of potassium hydrogen phtalate (reagent grade, Nakalai Tesque, Kyoto, Japan) and a solution of hydrogen carbonate and sodium carbonate (reagent grade, Nakalai Tesque, Kyoto, Japan). Detection limit for DOC was 0.33 μmol L^{-1} and precision was 1.5%. Filters for determination of POC/PON were stored at –20°C until analysis. After drying the filters at 60°C, inorganic carbon was removed by adding 30 µL of 10% (v:v) HCl (Ajax Finichem) to the filters. POC and PON contents on the filter were determined using a Thermo Finnigan EA 1112 Series Flash Elemental Analyzer (detection limit 0.1 μg, precision 1%). Certified standards of sulphanilamide OAS (Elemental Microanalysis Limited, Okehampton, UK) were run every 12 samples to ensure the quality of the POC and PON concentrations. The macro-nutrients $Si(OH)_4^-$, PO_4^{3-}, NH_4^+, and NO_x were analyzed at Analytical Service Tasmania following the methods recommended by Grasshoff et al. (1999). Phosphates, NH_4^+ and NO_x were analyzed with a Lachat Flow injection analyser (precision 0.5%). The detection limit is 0.002 mg L^{-1} for each parameter. Silicic acid was analyzed using a photometric analyzer (Aquakem 250) with a detection limit of 0.1 mg L^{-1} and precision of 2%. Measured certified reference material for nutrients in seawater (RMNS, Kanso, Japan) were run to ensure the quality of the nutrient concentrations. Theoretical dilution lines (TDL; Figure 2.4) were calculated using the macro-nutrient concentration of the underlying seawater sampled at the beginning of each experiment (Meese, 1989).

2.2.5.3 Iron

All onboard manipulations for Fe determinations were conducted under a class-100 laminar flow hood (AirClean 600 PCR workstation, Model 300 Controller, AirClean System). Sea-ice samples were allowed to melt in acid-clean PP buckets at room temperature in the dark. Immediately after melting, dissolved Fe (DFe < 0.4 μm) was obtained by collecting 60 mL of the filtrate passed through a 0.4-μm pore size 47-mm diameter polycarbonate (PC) membrane filter (Sterlitech) using a Teflon perfluoroalkoxy (PFA) filtration apparatus (Savillex, USA) under gentle vacuum (< 0.13 bar) to avoid cell lysis. Polycarbonate filters retaining the particulate Fe fraction (PFe > 0.4 μm) were transferred into acid-clean petri-dishes, double-bagged and stored at −20°C in the dark until analysis after return to Australia. DFe samples were collected in LDPE bottles (Nalgene) and acidified to pH 1.8 using 12 M ultra pure hydrochloric acid (Seastar Baseline, Choice Analytical). Samples were stored double-bagged at room temperature for at least 24 hours before measurement by flow injection analysis with chemiluminescent detection (FIA-CL).

2.2.5.3.1 Dissolved Fe

DFe samples were analyzed using a FIA-CL instrument. FIA-CL followed procedures by Obata et al. (1993) and de Jong et al. (1998), as described in detail by van der Merwe et al. (2009). The detection limit of the FIA-CL method is calculated as three times the standard (SD) of the procedural blank. Quality controls were run using international seawater reference samples (Sampling and Analysis of Fe (SAFe), deep (D2) and shallow (S), with consensus values of 0.960 ± 0.024 nmol L^{-1} and 0.096 ± 0.082 nmol L^{-1}, n = 4, respectively).

2.2.5.3.2 Particulate Fe

PFe polycarbonate filters were digested in 15 mL Teflon PFA vials (Savillex, USA), heated at 95°C for 12 hours on a Teflon coated hotplate (SCP Science), within an ISO 5 ducted laminar flow bench, housed within an ISO 7 clean room, using a mixture of 250 µL HCl (12 M, Seastar Baseline, Choice Analytical), 250 µL HNO_3 (16 M, Seastar Baseline, Choice Analytical) and 500 µL HF (29 M, Seastar Baseline, Choice Analytical). The PFA vials were allowed to cool down before being dry evaporated for 4 hours at 60°C. The samples were then re-suspended in 10 mL ultrapure 2% (v:v) HNO_3 with addition of indium as an internal standard to a final concentration of 10 ppb. Concentrations of PFe were determined at the Central Science Laboratory (University of Tasmania) using an Inductively Coupled Plasma Mass Spectrometer (ICP-MS, Element 2) according to Bowie et al. (2010). Prior to analysis, the instrument was purged with alternate 5% (v:v) HCl and 5% (v:v) HNO_3 solutions for 1 hour. Finally a 2% (v:v) HNO_3 solution was used to condition the instrument. A linear calibration curve was created using solutions of 0, 1, 5 and 10 ppb of a mixed standard (QCD Analysts, MISA suite of solutions, Spring Lake, USA). Samples were handled in a class-100 laminar flow bench. To ensure a low background recovery the instrument was rinsed with a solution of 2% (v:v) HNO_3, and a calibration blank (0 ppb) was analyzed as an unknown (n = 3). A 10 ppb mixed standard used to monitor instrument drift showed good instrument stability during analysis. Analyses of a certified reference material (BCR-414) resulted in a measured mean Fe value (± SD, n = 3) of 1.76 ± 0.04 g kg^{-1} compared to the certified (indicative) value of 1.85 g kg^{-1}, for a recovery of 95.2 ± 2.07%. The mean value for procedural digested acid blanks (n = 3) was 0.146 ± 0.028 μg Fe L^{-1}; the mean value for filter blanks (n

= 3) was 3.255 ± 0.829 μg Fe L^{-1}. The limit of detection was calculated as three times the standard deviation of the blank, which was 0.085 μg Fe L^{-1} for the acid blank and 2.488 μg Fe L^{-1} for the filter blank.

2.2.5.5 Extracellular polymeric substances

Melted ice and seawater samples were homogenized and filtered in triplicate onto 25-mm 0.4-µm pore size PC membranes (Millipore) under low vacuum (< 0.13 bar). A volume of 500 µL of 0.2-µm pre-filtered 0.02% Alcian Blue (AB, GX8 Sigma) in 0.06% acetic acid was added directly onto the filter and drawn through at low vacuum. If the AB stayed on the sample for more than 2 seconds, the filter was considered clogged and discarded. The filters were rinsed with 2 mL of Milli-Q water (Millipore, Gradient A10) to remove excess dye, placed in a PCR-well and stored in the dark at –20°C until further analysis. A calibration curve was performed at the start and the end of the cruise. The calibration curve was achieved by filtering 0, 5, 10 and 12 mL of a stock solution of 100 mg L^{-1} of xanthan gum (Sigma-Aldrich). One filter blank was collected on every sampling day. EPS concentrations were determined using the colorimetric AB method (Passow and Alldredge, 1995) modified by van der Merwe et al. (2009). The semi-quantitative AB method is based on the affinity of the AB stain for acid polysaccharides. The method targets particles > 0.4 µm and does not penetrate cells. Briefly, samples were extracted in 3 mL of 80% (v:v) sulphuric acid (H_2SO_4) (reagent grade, Merck Germany), measured spectrophotometrically with a Halo RB-10 spectrophotometer, and expressed in units of xanthan gum equivalents (xeq). The standard deviation between triplicates was < 10%.

2.2.5.6 Chlorophyll *a* and bacterial counts

Ice cores were melted rapidly, with gentle shake, at room temperature in the dark for Chl *a* analysis (Rintala et al., 2014). Melted samples were filtered under low vacuum (< 0.13 bar) and low light immediately after melting. To distinguish the contribution of larger autotrophs (*l*Chl *a* > 10 μm) and smaller autotrophs (10 μm > *s*Chl *a* > 0.8 μm), samples were size-fractionated by sequentially filtering the sample first onto 10-µm and then 0.8-µm polycarbonate filters (Millipore, 47-mm diameter). Filters were extracted in acetone and measured fluorometrically using a Turner Designs 10AU fluorometer (in vitro detection limit 0.02 µg L^{-1}) according to Arar and Collins (1997). Volumes of 20 mL of sea ice and seawater samples from the two *in situ* experiments were fixed with Glutaraldehyde (microscopy grade, final concentration of 1%) for bacterial counting. Samples were stored at 4°C until analysis at the Finnish Environmental Institute. They were then stained with Acridine Orange and counted by epifluorescence microscopy using a Leitz Aristoplan epifluorescence microscope equipped with I3 filter and PL Fluotar 100 x 12.5/20 oil immersion objective.

2.2.6. Cross-variable statistics

To evaluate the relationships between variables, non-parametric Spearman's rank correlations were used. For $p < 0.05$, the strength of the relationship was determined according to Cohen (1988). Data from *in situ* growth experiments and natural young ice samples were pooled together for analysis.

2.2.7 Enrichment index

For each parameter we calculated the enrichment index, EI_x (Gradinger and Ikävalko, 1998). This index is based on the effective segregation coefficient k_{effx} of the

component x and is normalized to salinity to detect specific incorporation processes that differ from conservative behavior with bulk salinity.

$$EI_x = \frac{[Sal]_{source}}{[Sal]_{ice}} \cdot \frac{[X]_{ice}}{[X]_{source}} \quad (2.1)$$

where $[Sal]_{source}$ and $[Sal]_{ice}$ are the salinity of the underlying seawater and the bulk salinity of the ice, respectively, $[X]_{ice}$ is the concentration of the component in the ice and $[X]_{source}$ is the concentration of the component x in the underlying seawater. Values of 1, < 1 or > 1 will correspond to conservative, specifically depleted or specifically enriched as compared to bulk salinity, respectively.

2.3 Results

2.3.1 In situ ice-growth time-series experiments

2.3.1.1 Basic sea-ice properties

Experiment 1 (Exp 1) was carried out on a first-year sea-ice floe in the central Weddell Sea (Station 506, Figure 2.1). Ice thickness and snow thickness ranged between 0.45 m and 0.71 m (average ± SD: 0.58 ± 0.09 m, n = 15), and between 0.12 m and 0.17 m (average ± SD: 0.145 ± 0.018 m, n = 10), respectively.

Experiment 2 (Exp 2) was located in the western part of the Weddell Sea (Station 517, Figure 2.1), closer to the continental shelf. The site had a more rafted and ridged ice cover, and a thicker snow cover (average ± SD: 0.34 ± 0.02 m, n = 10).

During the experiments, total ice thickness after 48 hours reached 0.24 m in Exp 1 and 0.22 m in Exp 2. The ice thickness and ice-growth rate at the end of each time step are summarized in Table 2.2. We observed a thin layer of granular ice at the surface of the newly formed sea ice (0.030 m in Exp 1 and 0.025 m in Exp 2)

Table 2.2 Physical properties of the *in situ* ice-growth time-series samples from Experiments 1 and 2

Sampling time		**Ice thickness (m)**		**Growth rate (cm h^{-1})**		**Temperature (°C)**		**Bulk salinity (S_P)**		**V_b/V (%)[a]**	
Designation	Time step (h)	Exp 1	Exp 2	Exp 1	Exp 2	Exp 1	Exp 2	Exp 1	Exp 2	Exp 1	Exp 2
T_1	0–6	0.03	0.045	0.5	0.75	–4.2	–5.2	15.9	18.4	18	17
T_2	0–12	0.065	0.06	0.54	0.5	–4.2	–5.9	12	15.7	14	13
T_3	0–24	0.085	0.095	0.35	0.4	–4.0	–6.9	9.3	11.2	12	9
T_4	0–48	0.24	0.225	0.5	0.4	–6.7	–9.9	8	10.4	7	6

[a] V_b/V = Brine volume fraction

followed by columnar ice in both experiments. Columnar ice started to grow after 6 hours in Exp 1 and less than 6 hours in Exp 2, reflecting the pattern of natural ice formation (Figure 2.3 a, b).

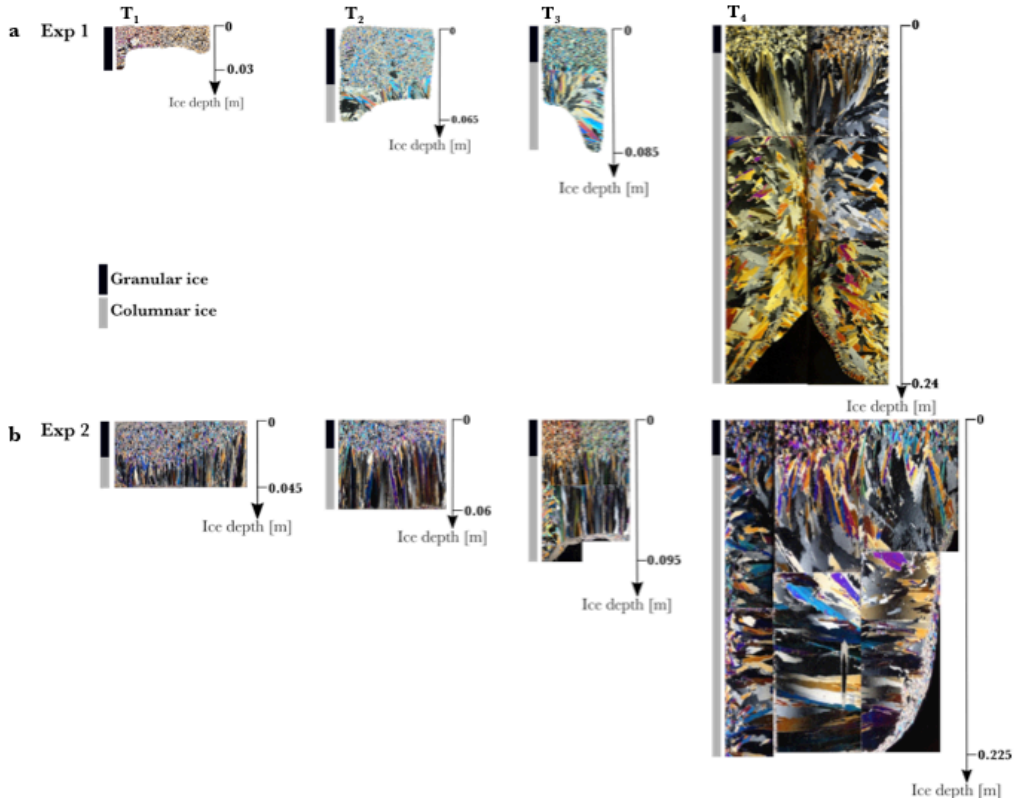

Figure 2.3 Ice texture for a) Exp 1 and b) Exp 2 for each time step. The black bar represents the granular ice and the grey bar the columnar ice. Total ice thickness (in m) and time steps are indicated.

Given the geometry of the experimental set up, however, it is worth noting that as the new columnar ice started to grow, progressive insulation from the ice at the top introduced competition with lateral growth from the cold sides of the initial core hole (surrounding ice floe); the effect actually dominated from a depth comparable to the diameter of the initial hole. The bulk ice salinity decreased from T_1 to T_4 as expected for growing sea ice (Table 2.2). Ice temperatures were slightly lower during Exp 2 driven by colder air temperatures (Table 2.2). Average air temperature was –18.3 ± 2.0°C (n = 297) during Exp 1 and –24.8 ± 2.7°C during Exp 2 (n = 294). Despite the low ice temperatures, brine volumes (V_b/V) were all

above the 5% theoretical percolation threshold for columnar ice, indicating a high porosity and therefore permeable nature of the newly formed ice (Golden et al., 1998). Note that V_b/V, temperature and salinity values were averaged for the entire core in T_4 (n = 2). Mean ± SD reported for the results described below refer to one value per time-step (n = 4).

2.3.1.2 Macro-nutrients, particulate and dissolved organic carbon and nitrogen

Nitrate + nitrite (NO_x), PO_4^{3-} and $Si(OH)_4^-$ showed similar temporal trends in both experiments (data not shown). The highest macro-nutrient concentrations were found in the T_1 cores, while the lowest concentrations were found in the T_4 cores. When plotted against salinity, NO_x, PO_4^{3-} and $Si(OH)_4^-$ followed theoretical dilution lines (TDL) (Figure 2.4 a–c). Ammonium concentrations in sea ice behaved differently compared to the other macro-nutrients, deviating from the TDL (Figure 2.4 d). Concentrations above the TDL suggest that different processes are involved in the incorporation or production of NH_4^+, leading to the enrichment of NH_4^+ in the ice. Unlike macro-nutrients, POC was enriched in sea ice compared to underlying seawater. In general, POC and PON exhibited a bell-shaped temporal development in both experiments. POC concentrations in the ice in Exp 1 and 2 ranged from 2.9 to 13.6 μmol L^{-1} and from 8.5 to 15.0 μmol L^{-1}, respectively (Figure 2.5 a, b). The underlying seawater concentrations were an order of magnitude lower, with 1.5 μmol L^{-1} and 0.5 μmol L^{-1} for Exp 1 and 2, respectively.

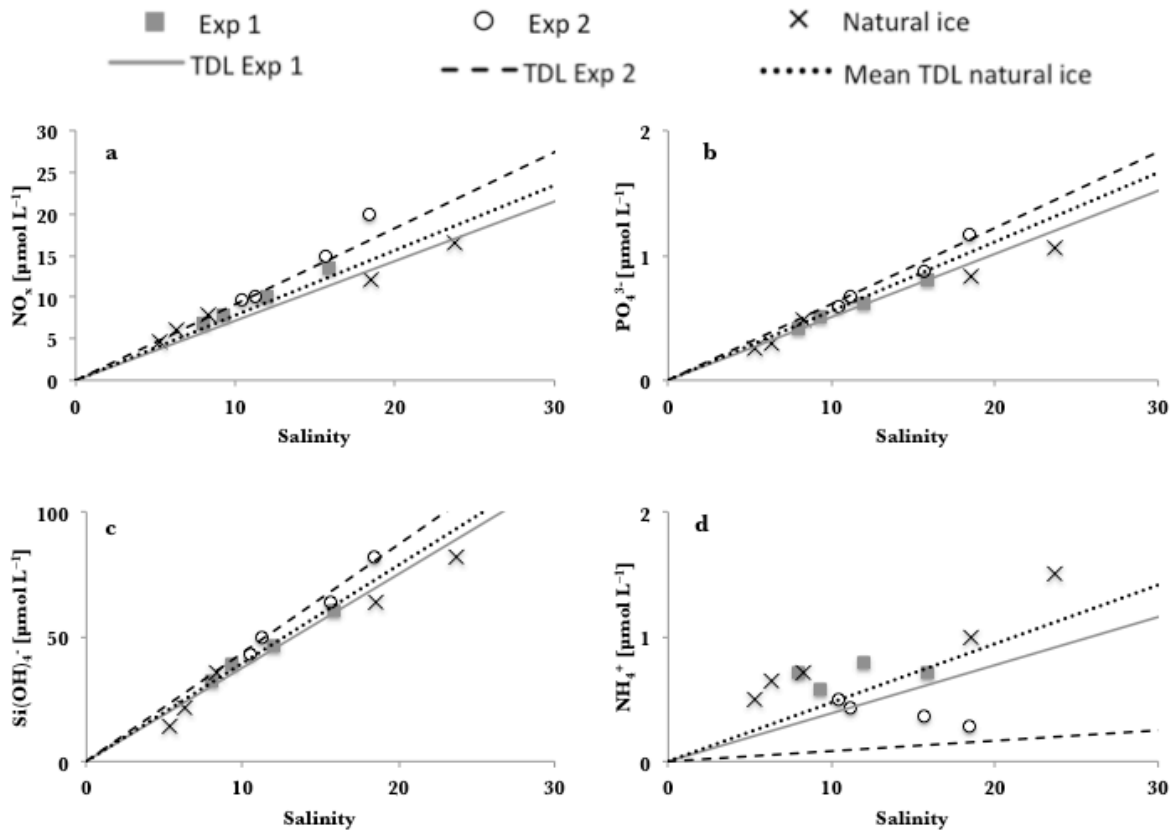

Figure 2.4 Concentration (μmol L^{-1}) of a) nitrate + nitrite (NO_x), b) phosphate (PO_4^{3-}), c) silicic acid ($Si(OH)_4^-$) and d) ammonium (NH_4^+) plotted against salinity for Exp 1 and 2 and the natural young ice. The solid grey line represents the theoretical dilution line (TDL) for Exp 1, the dashed dark line represents the TDL for Exp 2 and the dotted dark line represents the mean TDL for the natural young ice samples (n = 5). The TDLs are based on the salinity and respective macro-nutrient concentrations in underlying seawater.

In both experiments, PON concentrations were higher than the underlying seawater concentrations. Molar POC:PON ratios in the underlying seawater were below the typical Redfield ratio of 6.6 for phytoplankton, while ratios were consistently higher in the ice, with mean values of 12.5 $\pm$ 5.1 and 11.7 $\pm$ 2.1 for Exp 1 and 2, respectively. DOC concentrations were below the detection limit of 0.33 µmol L^{-1} in underlying seawater and sea ice in both experiments.

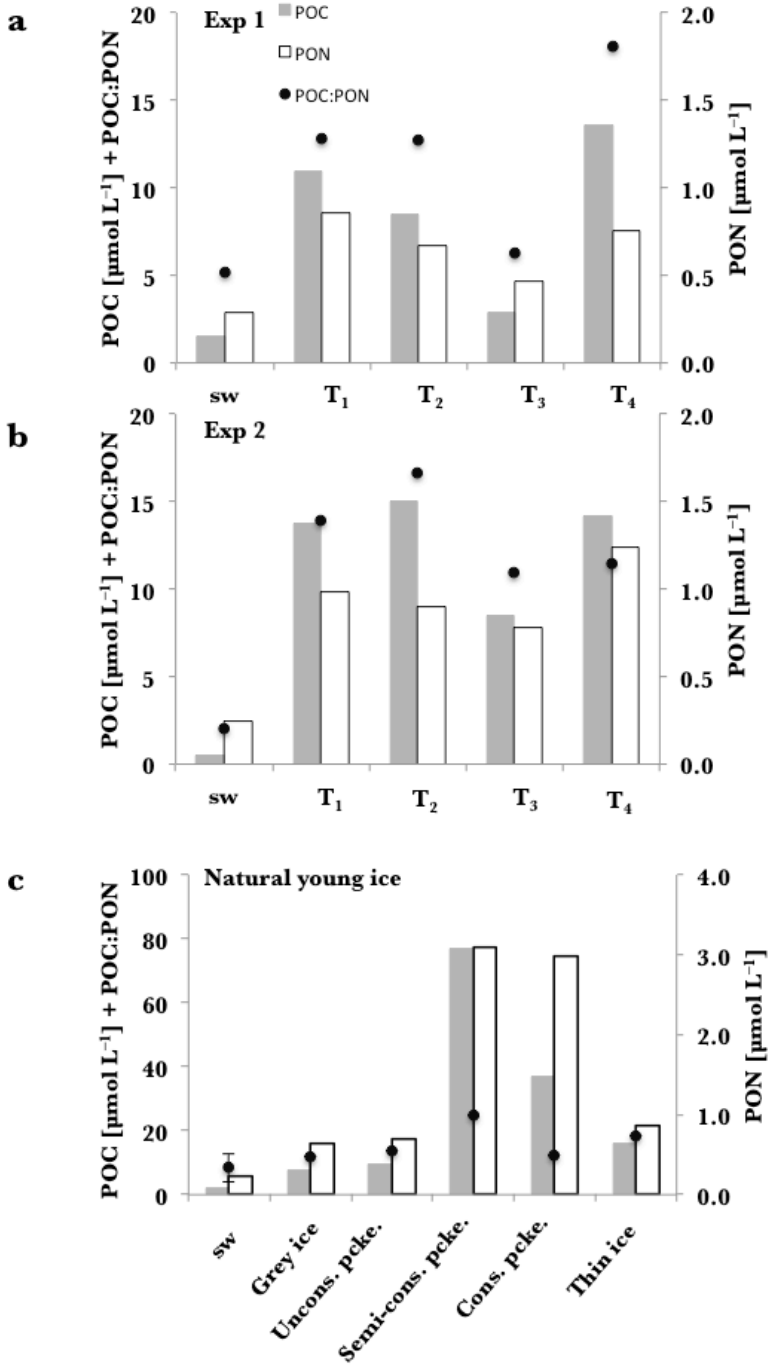

Figure 2.5 Particulate organic carbon (POC, grey rectangle, in μmol L^{-1}) and particulate organic nitrogen (PON, white rectangles, in μmol L^{-1}) concentrations in the ice and the seawater for each time step and during a) Exp 1, b) Exp 2 and c) in the natural young ice samples. The black dots are the molar POC:PON ratios. In the natural ice samples, the seawater concentration is the mean of each seawater concentration corresponding to the different ice samples (n = 5). The error bars correspond to the standard deviation of the seawater concentrations (n = 5). Sw refers to seawater, Uncons. pcke.: unconsolidated pancake, Semi-cons. pcke.: semi-consolidated pancake, Cons. pcke.: consolidated pancake.

2.3.1.3 EPS, Chl *a* and bacterial counts

Even when filtering for EPS at low pressure (< 0.13 bar) using the AB method, only a fraction of the material is retained on the filter (Passow and Alldredge, 1995). We computed EPS concentrations using a filter-capture efficiency for xanthan gum of 4.4% (van der Merwe et al., 2009). Although the EPS concentrations were higher in Exp 2 than in Exp 1, their evolution as a function of time was similar and displayed a bell-shaped development. Concentrations in the ice varied from 0.17 to 0.66 μg xeq L^{-1} (average: 0.38 ± 0.21 μg xeq L^{-1}) in Exp 1. In Exp 2, the concentrations ranged from 0.54 to 0.98 μg xeq L^{-1} (average: 0.75 ± 0.23 μg xeq L^{-1}). Concentrations in the underlying seawater were 0.22 μg xeq L^{-1} and 0.66 μg xeq L^{-1} for Exp 1 and 2, respectively (Figure 2.6 a, b).

The total Chl *a* (*Tot*Chl *a* = *l*Chl *a* + *s*Chl *a*) concentration in sea ice showed large variations with a peak at T_3 in Exp_1 (Figure 2.6 a). No corresponding peak was observed in Exp 2 (Figure 2.6 b). Concentrations in sea ice varied between 0.04 and 0.52 μg L^{-1} in Exp 1, and 0.03 and 0.17 μg L^{-1} in Exp 2 (Figure 2.6 b). *Tot*Chl *a* concentrations in underlying seawater were low: below the detection limit for Exp 1, and 0.02 μg L^{-1} for Exp 2 (Figure 2.6 a, b). Large autotrophs were virtually absent in the water but often made up the largest fraction in the ice, representing 57–92% (average: 78 ± 15%) of the *Tot*Chl *a* concentration in Exp 1 and 22–57% (average: 39 ± 15%) in Exp 2.

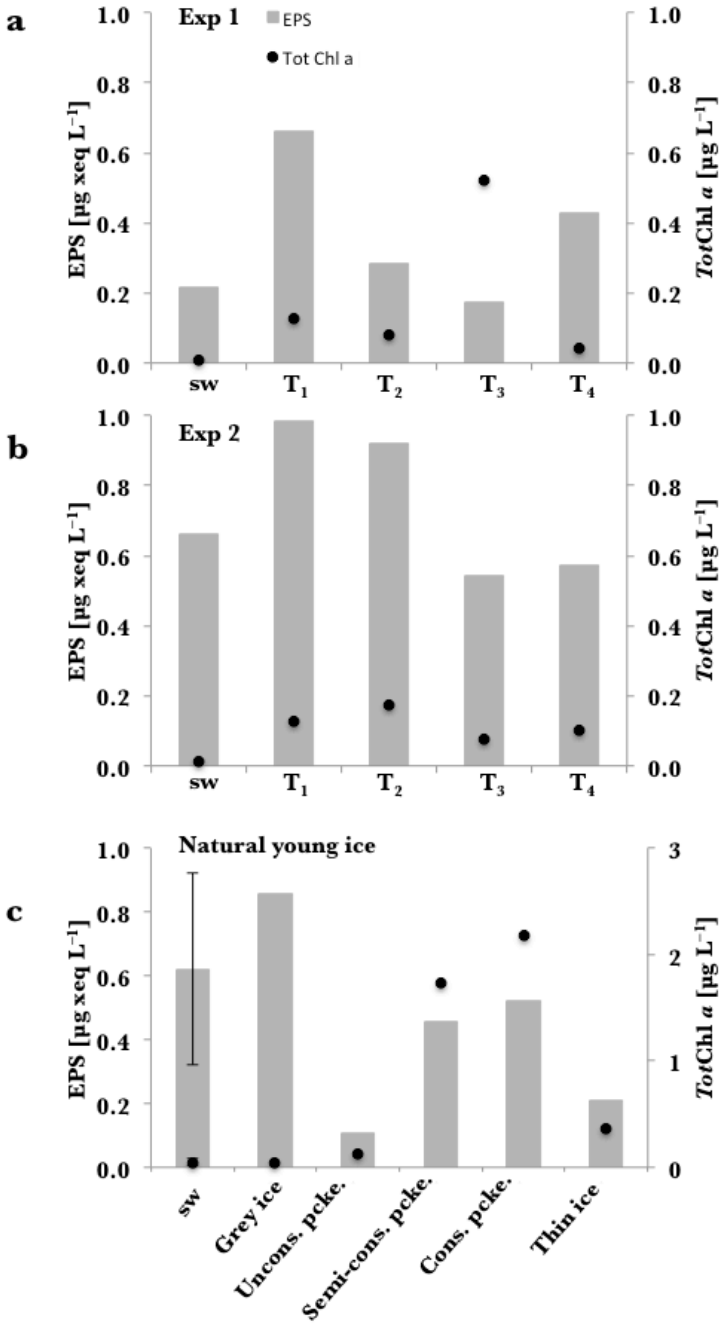

Figure 2.6 Extracellular polymeric substances (EPS) concentrations (grey rectangles, in μg xeq L^{-1}) and Total Chl *a* concentration (*TotChl a*, black dots, in μg L^{-1}) in the ice and the seawater for each time step and during a) Exp 1, b) Exp 2 and c) in the natural young ice samples. The *Tot*Chl a concentration in seawater during Exp 1 was below the detection limit (BDL). In the natural ice samples, the seawater concentration is the mean of each seawater concentration corresponding to the different ice samples (n = 5). The error bars correspond to the standard deviation of the seawater concentrations (n = 5). Sw refers to seawater, Uncons. pcke.: unconsolidated pancake, Semi-cons. pcke.: semi-consolidated pancake, Cons. pcke.: consolidated pancake.

Bacterial concentrations in the ice varied between 1.15 x 10^5 and 2.90 x 10^5 cells mL^{-1} in Exp 1 and 9.53 x 10^4 and 2.22 x 10^5 cells mL^{-1} in Exp 2. The temporal evolution of bacterial numbers in the ice was similar in both experiments with highest concentrations found at T_1 and the lowest at T_4. Bacterial concentrations in underlying seawater were 2.95 x 10^5 cells mL^{-1} for Exp 1 and 1.96 x 10^5 cells mL^{-1} for Exp 2 (Figure 2.7).

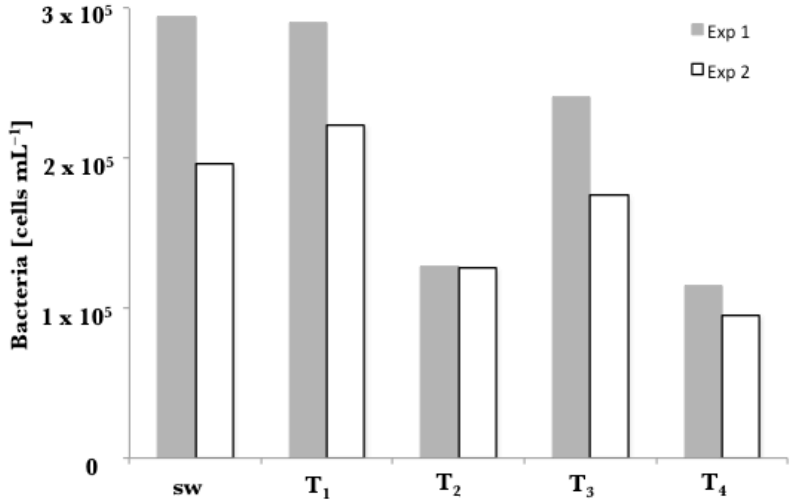

Figure 2.7 Bacteria concentration (in cells mL^{-1}) in seawater and ice for each time step during Exp 1 (grey bar) and Exp 2 (white bar).

2.3.1.4 Iron

Similar to the other particulate fractions, PFe was enriched in sea ice compared to underlying seawater. Particulate Fe concentrations ranged from 7.8 to 55.5 nmol L^{-1} in Exp 1 and 10.1 to 62.5 nmol L^{-1} in Exp 2 (Figure 2.8 a, b). Average concentrations were similar in both experiments (Exp 1: 23.7 $\pm$ 21.5 nmol L^{-1}; Exp 2: 26.1 $\pm$ 24.4 nmol L^{-1}). Underlying seawater values were 4.5 nmol L^{-1} in Exp 1 and 1.6 nmol L^{-1} in Exp 2. The highest values were observed at T_2 in both experiments. Dissolved Fe was also enriched in sea ice compared to seawater and the temporal evolution of DFe concentrations was similar in both experiments (Figure 2.8 a, b). Average DFe concentrations in Exp 1 and 2 were 1.0 $\pm$ 0.2 nmol L^{-1} and 1.7 $\pm$ 1.3 nmol L^{-1},

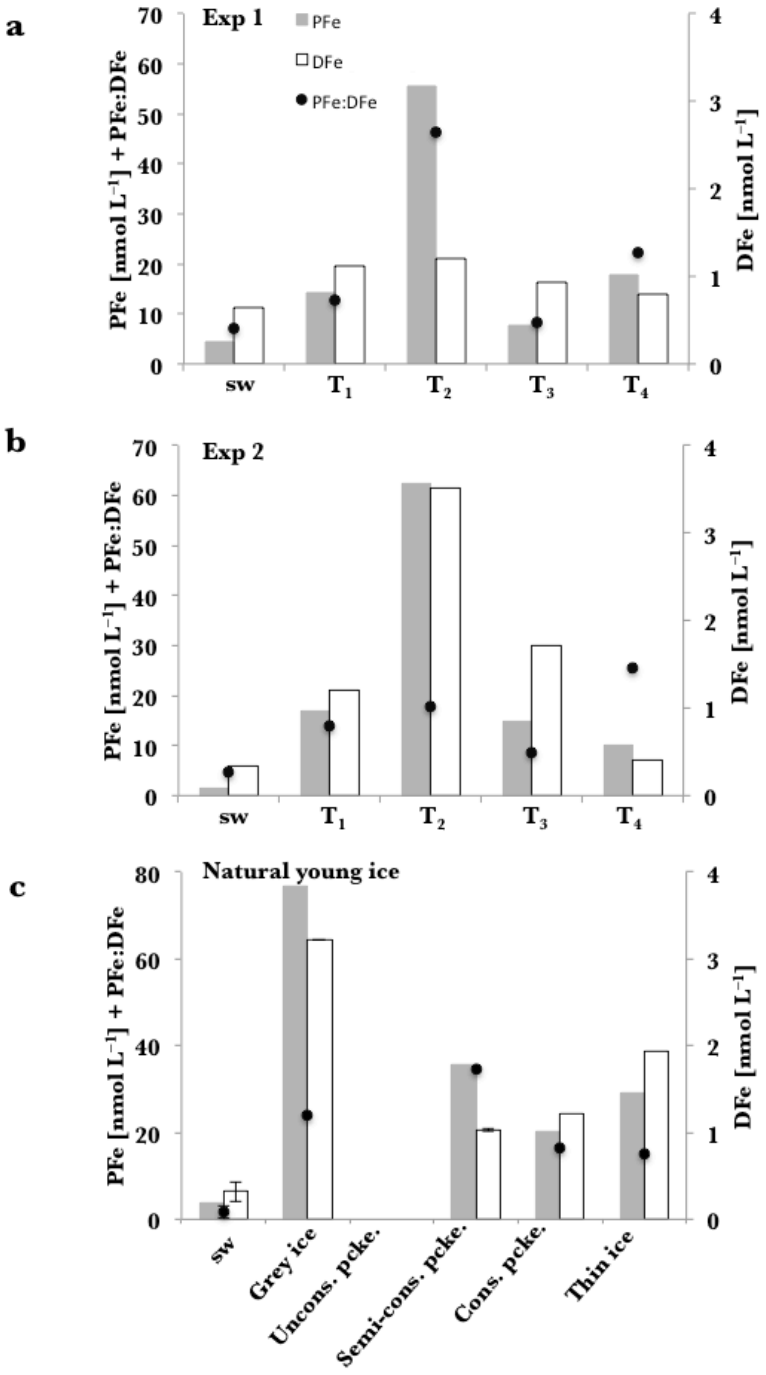

Figure 2.8 Particulate Fe (PFe) concentrations (grey, in nmol L^{-1}), dissolved Fe (DFe) concentrations (white, in nmol L^{-1}) and PFe:DFe ratio (black dots) in the ice and the sea water for each time step and during a) Exp 1, b) Exp 2 and c) in the natural young ice samples. In the natural ice samples, the seawater concentration is the mean of each seawater concentration corresponding to the different ice samples (n = 4). The error bars correspond to the standard deviation of the seawater concentrations (n = 4). No iron data (ND) are available for the unconsolidated pancake. Sw refers to seawater, Uncons. pcke.: unconsolidated pancake, Semi-cons. pcke.: semi-consolidated pancake, Cons. pcke.: consolidated pancake.

respectively. PFe:DFe ratios behaved similarly. All ratios in the ice were higher (22.4 ± 16.9 in Exp 1 and 16.5 ± 7.2 in Exp 2) than the underlying seawater ratios (7.0 in Exp 1 and 4.7 in Exp 2).

2.3.2 Natural young ice

In this section, when discussing seawater concentrations and TDLs we refer to the average seawater concentration (n = 5) using under-ice seawater data from the five sampling sites where natural young sea ice was collected, unless mentioned otherwise.

2.3.2.1 Basic sea-ice properties

The ice samples collected at stations 486, 488 and 489 represented different stages of pancake ice formation (Table 2.1). The first stage sampled (Station 486) was a large, thin and unconsolidated pancake with a thickness of 0.06–0.07 m. The second stage was a semi-consolidated pancake (Station 488) of 0.30–0.36 m in thickness. Snow was absent on the unconsolidated pancake and less than 0.01 m thick on the semi-consolidated pancake. At station 489, the snow cover was 0.03 m and the ice 0.30–0.36 m thick. Here pancakes were highly consolidated. Thin ice was also collected at station 496 with a 0.45 m average thickness and covered with 0.04 m of snow (Table 2.1). The grey ice (Station 500) was 24 hours old and 0.05–0.07 m thick (Table 2.1).

Elongated crystals of granular ice were observed in the unconsolidated pancake. Ice textures of the semi-consolidated and consolidated pancake exhibited classic patterns of granular ice underlain with columnar ice. We observed an intrusion of granular ice between 0.23 and 0.26 m in the consolidated pancake, suggesting rafting events (Figure 2.9 c). The bottom of the thin ice core (Station 496) was columnar (data not

shown) and the grey ice sample (Station 500) was too soft to process for ice texture analysis.

Bulk ice salinities of natural ice samples ranged from 5.3 (semi-consolidated pancake) to 23.7 (unconsolidated pancake) with an average of 12.4 ± 8.2 (n = 5). Computed brine volumes of natural ice samples ranged from 6.2 to 28.0% (average: 16.5 ± 9.9%, n = 5; Table 2.1).

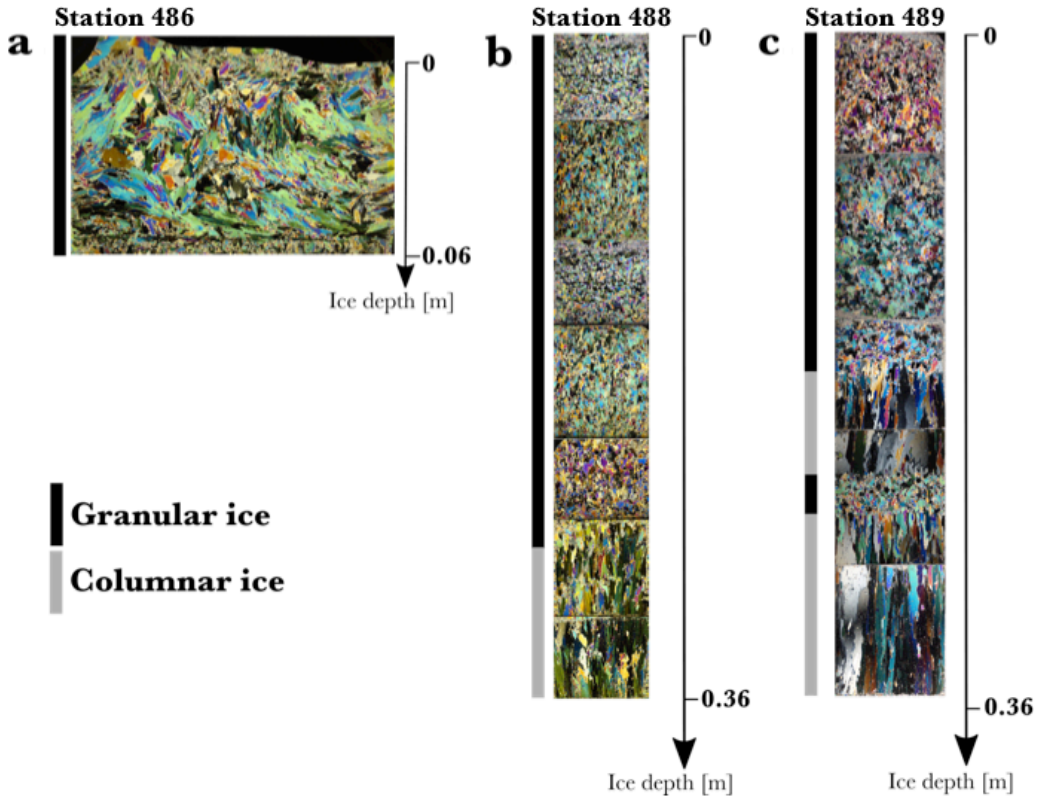

Figure 2.9 Ice texture and ice thickness (in m) of the natural young ice at a) unconsolidated pancake station 486, b) semi-consolidated pancake station 488 and c) consolidated pancake station 489. Note that the entire core is represented here while only the bottom part of the core has been analyzed for biogeochemical parameters. The black bar represents the granular ice and the grey bar the columnar ice.

2.3.2.2 Macro-nutrients, particulate organic matter and dissolved organic carbon and nitrogen

Macro-nutrient concentrations in natural young ice were lower than in the underlying seawater, except for NH_4^+ in the unconsolidated pancake. Ammonium ranged from

0.50 µmol L^{-1} to 1.50 µmol L^{-1}; NO_x, from 4.71 µmol L^{-1} to 16.4 µmol L^{-1}; PO_4^{3-}, from 0.26 µmol L^{-1} to 1.06 µmol L^{-1}; and $Si(OH)_4^-$, from 14.2 µmol L^{-1} to 81.9 µmol L^{-1}. Similar to Exp 1 and 2, all macro-nutrients followed TDLs, except for NH_4^+ which showed elevated concentrations in sea ice compared to background seawater levels (Figure 2.4). POC and PON concentrations were one order of magnitude higher in sea ice than in the underlying seawater (Figure 2.5 c). Average underlying seawater concentrations for POC and PON were 2.1 ± 1.3 µmol L^{-1} and 0.24 ± 0.05 µmol L^{-1}, respectively. Molar POC:PON ratios were of the same order of magnitude in the ice and the underlying seawater and higher than the Redfield ratio in all collected natural ice samples (Figure 2.5 c). DOC were below the detection limit of 0.33 μmol L^{-1} for all natural ice and underlying seawater samples, except in two ice bottom sections (data not shown).

2.3.2.3 Biological data: EPS and Chl *a*

The average EPS concentration in underlying seawater was 0.62 ± 0.30 µg xeq L^{-1} (Figure 2.6 c). Except for the bottom part of the consolidated pancake ice, EPS concentrations were higher in the underlying seawater than in the young ice for each station. The highest concentration in the ice was observed in the grey ice sample (0.86 µg xeq L^{-1}) and the lowest in the unconsolidated pancake (0.11 µg xeq L^{-1}; Figure 2.6 c).

Similar to POC, PON and EPS, salinity-normalized Chl *a* in sea ice was enriched in comparison to underlying seawater (Figure 2.6 c). The bottom section of the consolidated pancake ice displayed the highest *Tot*Chl *a* concentration (2.2 µg L^{-1}) while the lowest concentration was detected in the grey ice (< 0.1 µg L^{-1}). Compared to the small autotrophs, large autotrophs were more enriched in the young ice. *l*Chl *a* contributed up to 86% (average: 70 ± 15%, n = 5) of the *Tot*Chl

a in the natural young ice.

2.3.2.4 Iron

Because of possible contamination occurring during sampling, the Fe data for the unconsolidated pancake and associated seawater sample (254 nmol L^{-1} and 52.8 nmol L^{-1} of PFe, respectively) were discarded from the dataset. The dissolved Fe concentration in the seawater at this sampling site was 1.9 nmol L^{-1}, while there was no sea-ice DFe data available for this station.

For all other stations, PFe was enriched in sea ice with concentrations ranging from 20.1 to 76.7 nmol L^{-1} (average: 40.4 $\pm$ 25.0 nmol L^{-1}, n = 4) compared to 0.3 to 0.9 nmol L^{-1} (average: 0.6 $\pm$ 0.4 nmol L^{-1}, n = 4) in the underlying seawater (Figure 2.8 c). Dissolved Fe was also enriched in natural sea ice compared to its underlying seawater. DFe concentrations in the ice ranged from 1.0 nmol L^{-1} in the semi-consolidated pancake to 3.2 nmol L^{-1} in grey ice. The average sea-ice DFe concentration was 1.8 $\pm$ 1.0 nmol L^{-1} (n = 4). Underlying seawater concentrations ranged from 0.2 nmol L^{-1} to 0.4 nmol L^{-1} (average of 0.3 $\pm$ 0.1 nmol L^{-1} (n = 4), Figure 2.8 c). For both PFe and DFe, the highest concentration was detected in the grey ice sample. The average PFe and DFe concentrations in natural young ice were of the same order of magnitude as in Exp 1 and 2. Similar to our observations in Exp 1 and 2, PFe:DFe ratios in the ice were elevated relative to the ratio in the underlying seawater (Figure 2.8 c). The average ratio (22.5 $\pm$ 9.0, n = 4) in young ice was comparable to the experimental average.

2.3.3 Property–property relationships

Using the combined dataset from both experiments and natural ice samples, significant correlations (Spearman's rho, $p < 0.05$) were observed for PFe and DFe

(rho = 0.829, n = 14) and bacteria and brine volume (rho = 0.830, n = 10) for *in situ* samples and natural samples. There were strong inverse correlations between EPS and NH_4^+ (rho = –0.828, n = 15), and POC and brine volume (rho = –0.593, n = 15). Temperature was strongly inversely correlated with macro-nutrients except for NH_4^+. Bacteria, *Tot*Chl *a* and EPS were positively correlated with temperature (rho = 0.733, n = 10; rho = 0.529, n = 15; and rho = 0.518, n = 15, respectively). No correlations were observed between EPS and *Tot*Chl *a*, EPS and DFe, and EPS and PFe.

2.3.4 Enrichment indices

The enrichment indices for Exp 1 and 2 and natural young ice are summarized in Table 2.3. Because the Chl *a* concentrations in seawater in Exp 1 were below the detection limit, enrichment indices for Chl *a* in this experiment were not calculated. Enrichment indices for natural samples were calculated using the corresponding seawater concentrations. The enrichment indices confirmed the conservative behavior of all macro-nutrients, except NH_4^+. Enrichment indices for all other variables were higher, with values ranging from 1.4 to greater than 200 confirming a non-conservative behavior relative to salinity. In Exp 2, *l*Chl *a* showed the highest overall enrichment index (average: 125 ± 74.2, n = 4). Particulate Fe was most enriched in the natural young ice with an average EI of 301 ± 240 (n = 4).

2.4 Discussion

Our *in situ* ice-growth experiments provide a new approach to study the incorporation of Fe and organic matter into sea ice. Each experiment can be interpreted as a time-series mimicking the onset of sea-ice formation. In addition to these experiments, we collected natural young ice at several locations.

Table 2.3 Enrichment indices[a] for biogeochemical parameters of *in situ* ice-growth time-series[b] experiments and natural young ice samples

Parameter	Experiment 1				Experiment 2				Natural young ice[c]
	T_1	T_2	T_3	T_4	T_1	T_2	T_3	T_4	
NH_4^+	1.2	1.7	1.6	2.3	1.9	2.7	4.6	6	1.8±0.8
NO_x	1.2	1.2	1.2	1.2	1.2	1	1	1.1	1.1±0.2
PO_4^{3-}	1	1	1.1	1	1	0.9	1	1	0.9±0.1
$Si(OH)_4^-$	1	1	1.1	1.1	1	0.9	1	1	0.9±0.1
POC	0.3	3.2	3.3	4.3	51	65	52	95	61.3±49.1
PON	7.3	7.6	6.8	13	7.4	7.9	9.6	17	36.18±36.55
EPS	7.5	4.2	3.3	9.7	2.8	3	2.5	3	3.2±3.0
*l*Chl *a*[d]	ND[g]	ND	ND	ND	52	220	80	150	194.7±194.0
*s*Chl *a*[e]	ND	ND	ND	ND	18	16	16	20	50.8±125.8
*Tot*Chl *a*[f]	ND	ND	ND	ND	21	34	22	35	115.1±125.8
Bacteria	2.4	1.4	3.4	1.9	2.1	1.4	2.8	1.7	ND
PFe	7.7	40	7.3	19	20	88	30	22	301.4±239.6
DFe	4.3	6.1	6.1	6	6.9	23	16	4.1	23.93±9.7

[a] Values of 1, < 1 or > 1 correspond to conservative, specifically depleted or specifically enriched, respectively, relative to bulk salinity.
[b] Sampling times, T_1–T_4, were at 6, 12, 24, and 48 hours.
[c] Average ± SD is provided for the natural young ice samples, where n = 5 for macro-nutrients, POC, PON, EPS, *l*Chl *a*, *s*Chl *a*, *Tot*Chl *a*; n = 4 for PFe and DFe.
[d] *l*Chl *a* refers to Chl *a* > 10 μm.
[e] *s*Chl *a* refers to 10 μm > Chl *a* > 0.8 μm.
[f] *Tot*Chl *a* refers to *l*Chl *a* + *s*Chl *a*.
[g] ND = No data; seawater values for Chl *a* were below detection limit or not available for bacteria.

The thickest natural ice sample was 0.45 m thick. Therefore, we believe that our natural samples are only hours or a few days old, as sea ice thermodynamically can only grow up to 0.1 m in a single day (Petrich and Eicken, 2010).

2.4.1 Sea-ice physical properties during experimental and natural conditions

The development of granular ice at the sea-ice surface during the onset of sea-ice formation followed by columnar ice growth, e.g., as observed during Exp 1 and 2, is typical for natural sea-ice growth under calm conditions (Petrich and Eicken, 2010).

Ice crystal orientation at T_4 suggests that some 'side-freezing', due to heat exchange with the surrounding ice floes, occurred in our experiments after 24 h. This effect was also observed in the bottom section of the T_3 core in Exp 1 (Figure 2.3 a). As discussed further in section 4.3.1, 'side-freezing' may have affected initial incorporation of material and brine dynamics in the bottom part of the cores.

Columnar ice formation is generally slower than granular ice formation through frazil accretion (Petrich and Eicken, 2010), and thus impurities are rejected more efficiently (Palmisano and Garrison, 1993; Weissenberger and Grossmann, 1998; Weeks, 2010). In accordance with these previous studies, ice bulk salinities were higher for the first experimental time steps when granular ice was the dominating ice type.

The lower air temperatures during Exp 2 resulted in a faster ice-growth rate during the first 6 hours of the experiment. Despite the cold air temperatures, the ice was relatively warm in both experiments. Indeed ice surface temperatures generally decrease slowly after the initial stage of formation (e.g., Notz and Worster, 2008). Under these conditions, the ice is permeable and gravity drainage possibly occurs within the ice cover.

The irregular size and shape of ice crystals observed in the unconsolidated pancake resembled the texture of the first stages of pancake ice formation (Lange et al., 1989; Figure 2.9 a). Conditions at station 486 were very dynamic physically, which may explain the differences in this sample compared to other ice samples collected under calmer conditions further from the ice edge. These differences are revealed by the ratio between granular and columnar ice in the natural samples decreasing with increasing distance from the ice edge: granular ice represented 83% of the total ice in the unconsolidated pancake and 53% in the consolidated pancake. Brine volumes

(V_b/V) were always higher than the 5% percolation threshold for columnar ice (Golden et al., 1998) indicating the permeable nature of the ice in all samples.

2.4.2 Incorporation of dissolved constituents: conservative and non-conservative behavior

Macro-nutrient concentrations in sea ice are controlled by both physical and biological processes, including convective exchange, nutrient assimilation and remineralization by organisms. Both high macro-nutrient concentrations and no deviation from the TDL exclude biological incorporation/accumulation processes in our study. Macro-nutrient EI values close or equal to 1 indicate that the incorporation of macro-nutrients was coupled with sea salt dynamics (i.e., conservative behavior), except for NH_4^+ (Table 2.3). Conservative behavior of macro-nutrients has been observed previously in young sea ice (e.g., Dieckmann et al., 1991), which suggests that the processes involved in our ice-growth experiments were similar to those occurring in "naturally" forming ice. Although N, Si and P behaved conservatively with salinity, NH_4^+ was generally enriched relative to salts. This observation is in line with findings from previous studies (Becquevort et al., 2009; Zhou et al., 2013). The causes for NH_4^+ enrichment remain unclear, but it has been suggested that, due to its molecular size and shape, NH_4^+ could become incorporated into the ice crystal structure and not rejected into the brine system like other macro-nutrients (Gross, 2003).

It has been suggested that the seasonal stages of sea-ice formation control the stocks of DFe in sea ice (Lannuzel et al., 2010). Although our DFe concentrations are relatively low compared to other studies collected in winter, spring and summer (Westerlund and Öhman, 1991; de Jong et al., 1998; Lannuzel et al., 2007; 2008; 2013; 2014a; van der Merwe et al., 2009; 2011a), our study provides the first

evidence that sea ice begins to accumulate DFe as soon as it forms and grows in late autumn and early winter. Following this initial physico-chemical enrichment, DFe concentrations in sea ice subsequently increase as the ice ages through the season, likely due to biogenic processes (Lizotte, 2003; Thomas et al., 2010) or detrital remineralization processes, e.g., transformation of PFe into DFe.

Ammonium and DFe were the only two dissolved components in our study showing a non-conservative behavior by enrichment in the ice. Lannuzel et al. (2015) suggested that negatively charged dissolved EPS would complex DFe and, aided by their stickiness, lead to the enrichment of DFe in sea ice. Similar processes have been suggested for NH_4^+ (e.g., Gradinger and Ikävalko, 1998; Krembs et al., 2002). The lack of correlation between EPS and DFe, as well as between EPS and NH_4^+ in our study, does not support this hypothesis, and these processes remain unclear at this stage.

Some studies have reported a conservative behavior of DOC with salinity during ice formation (Giannelli et al., 2001; Amon, 2004), while other studies report elevated stocks of DOC within the ice (e.g., Carlson and Hansell, 2003; Riedel et al., 2008; Zhou et al., 2014). We believe that the extremely low DOC concentrations in seawater in our study led to the low DOC levels observed in newly formed sea ice. The two DOC peaks observed in the ice may be a result of a local solubilization, e.g., destruction of cells incorporated into the ice (Ewert and Deming, 2013).

2.4.3 Incorporation of particulate constituents: Factors influencing enrichment

High EI values for POC, PON, Chl *a*, EPS and PFe indicate that the desalinization processes occurring after initial entrapment in growing sea ice impact dissolved sea salts but not particulate materials. While dissolved sea salts are efficiently flushed out

of the ice and rejected to the water column, a disproportionate fraction of particulate materials remain in the ice, possibly attached to the walls of the brine channels.

2.4.3.1 Growth rate and ice texture

Enrichment indices from our experiments suggest that frazil ice incorporates less POC than columnar ice. The same trend is observed in the natural young ice samples: unconsolidated pancake ice and grey ice showed lower EI values for POC than columnar ice. This trend is contrary to the classical theory of organic matter incorporation into sea ice (scavenging and harvesting; e.g., Reimnitz et al., 1993), but consistent with previous field data where granular ice is not necessarily more enriched than columnar ice (Lannuzel et al., 2014a). The slightly lower POC concentrations found in our samples compared to other studies later in the season (e.g., Lannuzel et al., 2008; Dumont et al., 2009) support observations of seasonal accumulation of POC in Antarctic sea ice.

Furthermore, the relatively high underlying seawater PFe concentrations in our study compared to values measured later in the season support the hypothesis that organic matter and Fe from previous summers can remain in suspension in the water column during autumn (Lannuzel et al., 2010). We note that the PFe (and POC, PON and EPS) concentrations in columnar ice seem to be impacted by the ice-growth rate (Table 2.2 and Figure 2.8). We observed a decrease in the PFe concentration between T_2 and T_3 of Exp 1 followed by an increase in PFe between T_3 and T_4, when the local growth rate increased. This increase in PFe was not observed in Exp 2 where the growth rate remained stable throughout the experiment (Table 2.2). Less effective rejection of impurities associated with a faster growth rate could explain this observation, but this explanation may need clarification with longer experiments in future. Alternatively, the increase of POC, PON, EPS and PFe in the T_4 core of Exp 1

might reflect the increased influence of 'side-freezing', as evidenced by the thin section of the ice core (Figure 2.3). 'Side-growth' would likely decrease the efficiency of the gravity-driven brine drainage, resulting in increased bulk ice concentrations. Supporting this inference, the effect is enhanced in Exp 1, where 'side-freezing' started earlier. Also, the combination of vertical and lateral heat sinks might explain the increase in the ice-growth rate observed in the bottom part of the core. Nonetheless, due to the very young age of the ice and the low POC (and Chl *a*) concentrations, we believe that physical incorporation at the very onset of sea-ice formation was the main mechanism responsible for PFe enrichment. Our data suggest that granular ice growth does not incorporate more Fe than columnar ice growth (no general trend in EI values for PFe in granular or columnar ice), confirming previous results in Antarctic pack ice (Lannuzel et al., 2007; 2008; 2014a; van der Merwe et al., 2009).

2.4.3.2. Biological material: Chl *a* and EPS

Consistent with previous studies of young sea ice (Grossmann and Dieckmann, 1994), *Tot*Chl *a* concentrations in both experiments and the sampled natural young sea ice were low. During the experiments, the photoperiod was short (approximately 3.5 hours during Exp 1 and 7 hours during Exp 2) with irradiance not exceeding 6.9 W m^{-2} and 123.4 W m^{-2} during Exp 1 and 2, respectively. Given this environmental setting, we consider that *in situ* autotrophic growth or increase in intracellular Chl *a* following the incorporation into sea ice (Aguilera et al., 2002) was unlikely. Decreasing *Tot*Chl *a*:Phaeopigment ratios from seawater to sea ice (data not shown) support this hypothesis. Peaks of Chl *a* in Exp 1 and 2 could be the result of a combination of contamination by surrounding older ice (i.e., corer not completely vertical when sampling) and a potential effect of spatial patchiness of Chl *a* in the ice and the

seawater from which the ice formed (e.g., Meiners et al., 2012). Spatial heterogeneity is inherent to sea ice and was minimized by sampling cores close to each other (e.g., 0.10 m). Nonetheless, separate cores were needed to obtain sufficient material for analysis of the various parameters.

Sea ice and seawater EPS concentrations were also low compared to previous reports (e.g., Meiners et al., 2004; van der Merwe et al., 2009). Very low EPS production in early spring has been observed together with low biomass when low stress conditions were encountered in Antarctic pack ice (Ugalde et al., 2016). Although concentrations were low, Chl *a* and EPS were both enriched in the ice.

Unlike previous studies (Krembs and Engel, 2001; Meiners et al., 2003; Riedel et al., 2006), EPS did not correlate positively with either Chl *a* or bacteria, suggesting that the EPS in young ice measured in this study did not originate from production in the ice. Exopolymers can form abiotically from dissolved precursors (Passow, 2002; Orellana et al., 2011). Combined processes of low biomass and the absence of EPS precursors, such as DOC, could explain the low EPS concentrations encountered in our study. Also, Riedel et al. (2007) suggested that during the winter period, sea-ice EPS may be broken down or change chemically so that these EPS would not be detected by the AB method. We conclude that in our study, only abiotic processes were responsible for EPS enrichment in sea ice, leading to relatively low enrichment compared to previous studies where biotic and abiotic processes acted in combination (Meiners et al., 2003; Riedel et al., 2007).

2.4.3.3. Size of the particles

Overall, dissolved components were much less enriched in the ice than the particulate components, with bigger cells (or aggregated cells) showing particularly high enrichment indices (Table 2.3). This trend has been observed in Arctic sea ice

(Gradinger and Ikävalko, 1998; von Quillfeldt et al., 2003; Riedel et al., 2007) and has also been reported from an Antarctic fast ice study, where 97% of Fe incorporated in sea ice was in the form of PFe (Lannuzel et al., 2014b). In their study, large particles (> 10 μm) represented 80% of the PFe pool, indicating that the size of the particles is important.

The higher EI for large autotrophs compared to smaller autotrophs suggests that the size of the algae, or potential chain formation and aggregation, is a key factor in enrichment of autotrophs within sea ice. Preferential incorporation of algae ≥ 5 μm has been reported previously (Gradinger and Ikävalko 1998; Riedel et al., 2007) and cell-associated EPS may contribute to the selection of large autotrophs during sea-ice formation (Gradinger and Ikävalko, 1998).

2.4.3.4. Role of organic ligands

It has been shown that dissolved organic ligands (e.g., EPS) control the concentration of DFe and maintain it at threshold concentrations in natural Antarctic sea ice (Lannuzel et al., 2015). This mechanism is also potentially the case in our ice-growth experiments, with low EPS concentrations in our samples leading to aggregation/precipitation of DFe into PFe. The potential and multiple roles that EPS play in the incorporation of dissolved and particulate matter into sea ice clearly require further investigation (Lannuzel et al., 2015).

2.4.4 Decoupling between PFe and DFe, and POC and PON during ice growth

A decoupling between the PFe and DFe pools has been observed during the melting of sea ice (van der Merwe et al., 2011a). Our study shows a decoupling between PFe and DFe in the early stage of sea-ice formation, therefore suggesting a decoupling between the two fractions throughout the entire year. During ice formation, and

assuming absence of biological activity, the PFe:DFe ratio in ice and seawater should be similar unless these two size fractions are incorporated into the ice differently. Higher ratios in the ice, in both experiments and the natural samples, demonstrate that the sea ice is more enriched in PFe compared to DFe during the early stages of its formation. One way to explain this increase in PFe would be preferential retention of the particulate fraction during brine convection. Also, since brine convection remains active within the skeletal layer during ice growth (Notz and Worster, 2008; 2009), it provides both a continuous input of Fe to the brine channel system and selective return of DFe to the underlying seawater. Supporting this scenario is the fact that the grey ice sample, the thinnest of our dataset, is the one displaying the highest PFe, DFe and EPS concentrations. We could be witnessing the importance of EPS in scavenging PFe (and DFe) at the very early stages of ice formation. Lowest concentrations in thicker samples could be the result of a 'dilution' compared to what we observed at the sea ice/seawater interface.

A similar decoupling was observed for POC and PON, with POC:PON lower than Redfield in the seawater and above Redfield in the ice (Figure 2.5). This decoupling could indicate a preferential incorporation of particulate carbon in sea ice relative to particulate nitrogen. Extracellular polymeric substances C:N ratios lie above the Redfield ratio (Riedel et al., 2007; Niemi and Michel, 2015). The slight enrichment in EPS in the ice is therefore considered to contribute to this change in C:N ratios. The time scales during which both experiments were conducted and the age of the natural sea ice are indeed very short to induce any changes in the phytoplankton/sea-ice algal community and metabolism leading to a modification of the C:N ratio. Decoupling of DOC and DON has been previously observed (e.g., Thomas et al., 2001; Krell et al.,

2003; Papadimitriou et al., 2007), but to our knowledge, this is the first time a decoupling of POC and PON has been reported.

2.5 Conclusion

Our results show that only physical processes lead to the enrichment of particles and DFe in the very early stages of ice formation. The size of the particles plays a key role, with larger particles being preferentially enriched in sea ice. Combined with previous studies, the observed decoupling of PFe and DFe when trapped in the ice suggest a decoupling between PFe and DFe throughout the whole year. Our study is unique in its specific dedication to understanding the incorporation processes of Fe into newly formed sea ice, which are critical to understand in a changing sea ice environment. However, a few key questions remain open: what, specifically, is the role of EPS and organic ligands in the incorporation of Fe into sea ice, and what is the impact of ice-growth rate on these enrichment processes? The next steps towards improving understanding would be through the combination of controlled laboratory studies of sea-ice growth under varying initial conditions, small-scale studies of location and characterization of particulate matter within the sea-ice microstructure, and Fe-based biogeochemical modelling for sea ice.

References

Aguilera J, Bischof K, Karsten U, Hanelt D, Wiencke C. 2002. Seasonal variation in ecophysiological patterns in macroalgae from an Arctic fjord. II. Pigment accumulation and biochemical defence systems against high light stress. *Mar Biol* 140:1087–1095. doi: 10.1007/s00227-002-0792-y.

Amon RMW. 2004. The role of dissolved organic matter for the carbon cycle in the Arctic Ocean, in Stein R, Macdonald RW, eds., *The Organic Carbon Cycle in the Arctic Ocean*. Berlin: Springer: pp. 83–99.

Arar EJ, Collins GB. 1997. Method 445.0: In vitro determination of chlorophyll *a* and pheophytin *a* in marine and freshwater algae by fluorescence. Cincinnati: Office of Research and Development, U.S. Environemental protection Agency. #445.0.

Arrigo KR. 2014. Sea ice ecosystems. *Ann Rev Mar Sci* 6:439–467. doi: 10.1146/annurev-marine-010213-135103.

Becquevort S, Dumont I, Tison J-L, Lannuzel D, Sauvée M-L, et al. 2009. Biogeochemistry and microbial community composition in sea ice and underlying seawater off east Antarctica during early spring. *Polar Biol* 32:879–895. doi: 10.1007/s00300-009-0589-2.

Bowie AR, Townsend AT, Lannuzel D, Remenyi TA, van der Merwe P. 2010. Modern sampling and analytical methods for the determination of trace elements in marine particulate material using magnetic sector inductively coupled plasma-mass spectrometry. *Anal Chim Acta* 676:15–27. doi: 10.1016/j.aca.2010.07.037.

Carlson CA, Hansell DA. 2003. The contribution of dissolved organic carbon and nitrogen to the biogeochemistry of the Ross sea, in Ditullio GR, Dunbar RB, eds., *Biogeochemistry of the Ross Sea, Antarctic Research Series*. Washington, D. C.: American Geophysical Union: pp. 123–142. doi: 10.1029/078ars08

Cohen J. 1988. *Statistical Power Analysis for the Behavioral Sciences*. 2nd ed. New York, USA:Lawrence Erlbaum Associates.

Cox GFN, Weeks WF. 1975. Brine drainage and initial salt entrapment in sodium chloride ice. U.S. Army corps of engineers Cold Regions Research & Engineering Laboratory. Hanover, N.H.:CRREL-RR-345.

Cox GFN, Weeks WF. 1988. Numerical simulations of the profile properties of undeformed first-year sea ice during the growth season. *J Geophys Res-Ocean* 93:12449–12460. doi: 10.1029/JC093iC10p12449.

Cutter G, Andersson P, Codispoti L, Croot P, Francois R, et al. 2010. Sampling and sample-handling protocols for GEOTRACES cruises.

de Baar HJW, Timmermans KR, Laan P, De Porto HH, Ober S, et al. 2008. Titan: A new facility for ultraclean sampling of trace elements and isotopes in the deep oceans in the international Geotraces program. *Mar Chem* 111:4–21. doi: 10.1016/j.marchem.2007.07.009.

de Jong JTM, den Das J, Bathmann U, Stoll MHC, Kattner G, et al. 1998. Dissolved iron at subnanomolar levels in the Southern Ocean as determined by ship-board analysis. *Anal Chim Acta* 377:113–124. doi: 10.1016/S0003-2670(98)00427-9.

de Jong J, Schoemann V, Maricq N, Mattielli N, Langhorne P, et al. 2013. Iron in land-fast sea ice of McMurdo Sound derived from sediment resuspension and

wind-blown dust attributes to primary productivity in the Ross Sea, Antarctica. *Mar Chem* 157: 24-40. doi: 10.1016/j.marchem.2013.07.001.

de Jong JTM, Stammerjohn SE, Ackley SF, Tison J-L, Mattielli N, et al. 2015. Sources and fluxes of dissolved iron in the Bellingshausen Sea (West Antarctica): The importance of sea ice, icebergs and the continental margin. *Mar Chem* 177: 518-535. doi: 10.1016/j.marchem.2015.08.004.

Dethleff D. 2005. Entrainment and export of Laptev Sea ice sediments, Siberian Arctic. *J Geophys Res-Ocean* 110:C07009. doi: 10.1029/2004JC002740.

Dethleff D, Kempema EW. 2007. Langmuir circulation driving sediment entrainment into newly formed ice: Tank experiment results with application to nature (Lake Hattie, United States; Kara Sea, Siberia). *J Geophys Res-Ocean* 112: C02004. doi: 10.1029/2005JC003259.

Dethleff D, Kempema EW, Koch R, Chubarenko I. 2009. On the helical flow of Langmuir circulation - Approaching the process of suspension freezing. *Cold Reg Sci Technol* 56:50–57. doi: 10.1016/j.coldregions.2008.10.002.

Dethleff D, Kuhlmann G. 2009. Entrainment of fine-grained surface deposits into new ice in the southwestern Kara Sea, Siberian Arctic. *Cont Shelf Res* 29:691–701. doi: 10.1016/j.csr.2008.11.009.

Dieckmann GS, Lange MA, Ackley SF, Jennings Jr JC. 1991. The nutrient status in sea ice of the Weddell Sea during winter: effects of sea ice texture and algae. *Polar Biol* 11:449–456. doi: 10.1007/bf00233080.

Dumont I, Schoemann V, Lannuzel D, Chou L, Tison J-L, et al. 2009. Distribution and characterization of dissolved and particulate organic matter in Antarctic pack ice. *Polar Biol* 32:733–750. doi: 10.1007/s00300-008-0577-y.

Ewert M, Deming JW. 2011. Selective retention in saline ice of extracellular polysaccharides produced by the cold-adapted marine bacterium *Colwellia psychrerythraea* strain 34H. *Ann Glaciol* 52:111–117. doi: 10.3189/172756411795931868.

Ewert M, Deming JW. 2013. Sea ice microorganisms: environmental constraints and extracellular responses. *Biology* 2:603–628. doi: 10.3390/biology2020603.

Garrison DL, Close AR, Reimnitz E. 1989. Algae concentrated by frazil ice: evidence from laboratory experiments and field measurements. *Antarct Sci* 1:313–316. doi: 10.1017/S0954102089000477.

www.geotraces.org

Giannelli V, Thomas DN, Haas C, Kattner G, Kennedy H, et al. 2001. Behaviour of dissolved organic matter and inorganic nutrients during experimental sea-ice formation. *Ann Glaciol* 33:317–321. doi: 10.3189/172756401781818572.

Golden KM, Ackley SF, Lytle VI. 1998. The percolation phase transition in sea Ice. *Science* 282:2238–2241. doi: 10.1126/science.282.5397.2238.

Gradinger R, Ikävalko J. 1998. Organism incorporation into newly forming Arctic sea ice in the Greenland Sea. *J Plankton Res* 20:871–886. doi: 10.1093/plankt/20.5.871.

Grasshoff K, Kremling K, Ehrhardt M. 1999. *Methods of Seawater Analysis*. 3rd ed. Germany: Wiley-VCH.

Gross GW. 2003. Nitrates in ice: uptake; dielectric response by the layered capacitor method. *Can J Phys* 81:439–450. doi: 10.1139/p02-143.

Grossmann S, Dieckmann GS. 1994. Bacterial standing stock, activity, and carbon production during formation and growth of sea ice in the Weddell Sea, Antarctica. *Appl Environ Microbiol* 60:2746–2753.

Grotti M, Soggia F, Ianni C, Frache R. 2005. Trace metals distributions in coastal sea ice of Terra Nova Bay, Ross Sea, Antarctica. *Antarct Sci* 17:289–300. doi: 10.1017/s0954102005002695.

Hölemann JA, Schirmacher M, Prange A. 1997. Dissolved and particulate major and trace elements in newly formed ice from the Laptev Sea (Transdrift III, October 1995), in Kassens H, Bauch HA, Dmitrenko I, Eicken H, Hubberten H-W, et al., eds. *Land-ocean systems in the Siberian Arctic: Dynamics and history.* Berlin: Springer-Verlag: pp. 101–111.

Kanna N, Toyota T, Nishioka J. 2014. Iron and macro-nutrient concentrations in sea ice and their impact on the nutritional status of surface waters in the southern Okhotsk Sea. *Prog Oceanogr* 126:44–57. doi: 10.1016/j.pocean.2014.04.012.

Knopf DA, Alpert PA, Wang B, Aller JY. 2011. Stimulation of ice nucleation by marine diatoms. *Nat Geosci* 4:88–90. doi: 10.1038/ngeo1037.

Krell A, Ummenhofer C, Kattner G, Naumov A, Evans D, et al. 2003. The biology and chemistry of land fast ice in the White Sea, Russia - A comparison of winter and spring conditions. *Polar Biol* 26:707–719. doi: 10.1007/s00300-003-0543-7.

Krembs C, Eicken H, Junge K, Deming JW. 2002. High concentrations of exopolymeric substances in Arctic winter sea ice: Implications for the polar ocean carbon cycle and cryoprotection of diatoms. *Deep-Sea Res Part I* 49:2163–2181. doi: 10.1016/S0967-0637(02)00122-X.

Krembs C, Engel A. 2001. Abundance and variability of microorganisms and transparent exopolymer particles across the ice-water interface of melting first-year sea ice in the Laptev Sea (Arctic). *Mar Biol* 138:173–185. doi: 10.1007/s002270000396.

Lancelot C, de Montety A, Goosse H, Becquevort S, Schoemann V, et al. 2009. Spatial distribution of the iron supply to phytoplankton in the Southern Ocean: a model study. *Biogeosciences* 6:2861-2878. doi: 10.5194/bg-6-2861-2009.

Lange MA, Ackley SF, Wadhams P, Dieckmann GS, Eicken H. 1989. Development of sea ice in the Weddell Sea. *Ann Glaciol* 12:92–96.

Langway CC. 1958. Ice fabrics and the universal stage. Illinois: U.S. Armay Snow, ice and permafrost Research Establishment.

Lannuzel D, Chever F, van der Merwe PC, Janssens J, Roukaerts A, et al. 2014a. Iron biogeochemistry in Antarctic pack ice during SIPEX-2. *Deep Sea Res Part II* 131, 111-122. doi: 10.1016/j.dsr2.2014.12.003.

Lannuzel D, de Jong J, Schoemann V, Trevena A, Tison J-L, et al. 2006. Development of a sampling and flow injection analysis technique for iron determination in the sea ice environment. *Anal Chim Acta* 556:476–483. doi: 10.1016/j.aca.2005.09.059.

Lannuzel D, Grotti M, Abelmoschi ML, van der Merwe P. 2015. Organic ligands

control the concentrations of dissolved iron in Antarctic sea ice. *Mar Chem* 174:120–130. doi: 10.1016/j.marchem.2015.05.005.

Lannuzel D, Schoemann V, de Jong J, Chou L, Delille B, et al. 2008. Iron study during a time series in the western Weddell pack ice. *Mar Chem* 108:85–95. doi: 10.1016/j.marchem.2007.10.006.

Lannuzel D, Schoemann V, de Jong J, Pasquer B, van der Merwe P, et al. 2010. Distribution of dissolved iron in Antarctic sea ice: Spatial, seasonal, and inter-annual variability. *J Geophys Res* 115:G03022. doi: 10.1029/2009JG001031.

Lannuzel D, Schoemann V, de Jong J, Tison J-L, Chou L. 2007. Distribution and biogeochemical behaviour of iron in the East Antarctic sea ice. *Mar Chem* 106:18–32. doi: 10.1016/j.marchem.2006.06.010.

Lannuzel D, Schoemann V, Dumont I, Content M, de Jong J, et al. 2013. Effect of melting Antarctic sea ice on the fate of microbial communities studied in microcosms. *Polar Biol* 36:1483–1497. doi: 10.1007/s00300-013-1368-7.

Lannuzel D, van der Merwe PC, Townsend AT, Bowie AR. 2014b. Size fractionation of iron, manganese and aluminium in Antarctic fast ice reveals a lithogenic origin and low iron solubility. *Mar Chem* 161:47–56. doi: 10.1016/j.marchem.2014.02.006.

Lemke P, Participants of the ANT-XXIX/6 cruise. 2014. The expedition of the research vessel "Polarstern" to the Antarctic in 2013 (ANT-XXIX/6). Berichte zur Polar-und Meeresforschung. Bremerhaven: Helmoltz Gemeinschaft: Reports polar Mar Res 679.

Lindemann F. 1998. Sediments in Arctic sea ice - entrainement, characterization and quantification [PhD thesis]. Kiel University, Germany, Mathematisch-Naturwissenschaftliche Fakultaet.

Lindemann F, Holemann JA, Korablev A, Zachek A. 1997. Particle entrainment into newly forming sea ice - Freeze-up studies in October 1995, in Kassens H, Bauch HA, Dmitrenko IA, Eicken H, Hubberten H-W, et al., eds., *Land-ocean systems in the Siberian Arctic: Dynamics and history*. Berlin: Springer-Verlag: pp. 113–125.

Lizotte MP. 2003. The microbiology of sea ice, in Thomas DN, Dieckmann GS, eds., *Sea Ice: An introduction to its physics, chemistry, biology and geology*. Blackwell Science: pp. 184–210.

Martin S, Kauffman P. 1981. A field and laboratory study of wave damping by grease ice. *J Glaciol* 27:283–313.

Meese DA. 1989. The chemical and structural properties of sea ice in the southern Beaufort sea. U.S. Army corps of engineers Cold regions Research & Engineering Laboratory. Hanover, N.H.:CRREL Report 89-25.

Meiners K, Brinkmeyer R, Granskog MA, Lindfors A. 2004. Abundance, size distribution and bacterial colonization of exopolymer particles in Antarctic sea ice (Bellingshausen Sea). *Aquat Microb Ecol* 35:283–296. doi: 10.3354/ame035283.

Meiners K, Gradinger R, Fehling J, Civitarese G, Spindler M. 2003. Vertical distribution of exopolymer particles in sea ice of the Fram Strait (Arctic) during autumn. *Mar Ecol-Prog Ser* 248:1–13. doi: 10.3354/meps248001.

Meiners KM, Vancoppenolle M, Thanassekos S, Dieckmann GS, Thomas DN, et al. 2012. Chlorophyll *a* in Antarctic sea ice from historical ice core data. *Geophys Res Lett* 39:L21602. doi: 10.1029/2012GL053478.

Müller S, Vähätalo AV, Stedmon CA, Granskog MA, Norman L, et al. 2013. Selective incorporation of dissolved organic matter (DOM) during sea ice formation. *Mar Chem* 155:148–157. doi: 10.1016/j.marchem.2013.06.008.

Niemi A, Michel C. 2015. Temporal and spatial variability in sea-ice carbon:nitrogen ratios on Canadian Arctic shelves. *Elem Sci Anth* 3: 000078. doi: 10.12952/journal.elementa.000078.

Notz D, Worster MG. 2008. In situ measurements of the evolution of young sea ice. *J Geophys Res-Ocean* 113:C03001.doi: 10.1029/2007JC004333.

Notz D, Worster MG. 2009. Desalination processes of sea ice revisited. *J Geophys Res-Ocean* 114:C05006. doi: 10.1029/2007JC004333.

Nürnberg D, Wollenburg I, Dethleff D, Eicken H, Kassens H, et al. 1994. Sediments in Arctic sea ice: Implications for entrainment, transport and release. *Mar Geol* 119:185–214. doi: 10.1016/0025-3227(94)90181-3.

Obata H, Karatani H, Nakayama E. 1993. Automated determination of iron in seawater by chelating resin concentration and chemiluminescence detection. *Anal Chem* 65:1524–1528. doi: 10.1021/ac00059a007.

Orellana MV, Matrai PA, Leck C, Rauschenberg CD, Lee AM, et al. 2011. Marine microgels as a source of cloud condensation nuclei in the high Arctic. *P Natl Acad Sci* 108:13612–13617. doi: 10.1073/pnas.1102457108.

Osterkamp TE, Gosink JP. 1983. Frazil ice formation and ice cover development in interior Alaska streams. *Cold Reg Sci Technol* 8:43–56. doi: 10.1016/0165-232X(83)90016-2.

Palmisano AC, Garrison DL. 1993. Microorganisms in Antarctic sea ice, in Friedmann EI, ed., *Antarctic microbiology*. New-York: Wiley: pp. 167–218.

Papadimitriou S, Thomas DN, Kennedy H, Haas C, Kuosa H, et al. 2007. Biogeochemical composition of natural sea ice brines from the Weddell Sea during early austral summer. *Limnol Oceanogr* 52:1809–1823. doi: 10.4319/lo.2007.52.5.1809.

Passow U. 2002. Transparent exopolymer particles (TEP) in aquatic environments. *Prog Oceanogr* 55:287–333. doi: 10.1016/s0079-6611(02)00138-6.

Passow U, Alldredge AL. 1995. A dye-binding assay for the spectrophotometric measurement of transparent exopolymer particles (TEP). *Limnol Oceanogr* 40:1326–1335. doi: 10.4319/lo.1995.40.7.1326.

Petrich C, Eicken H. 2010. Growth, structure and properties of sea ice, in Thomas DN, Dieckmann GS, eds., *Sea Ice*. 2nd ed., Oxford: Wiley-Blackwell: pp. 23–77.

Qian J, Mopper K. 1996. Automated high-performance, high-temperature combustion total organic carbon analyzer. *Anal Chem* 68:3090–3097. doi: 10.1021/ac960370z.

Reimnitz E, Clayton JR, Kempema EW, Payne JR, Weber WS. 1993. Interaction of rising frazil with suspended particles: tank experiments with applications to nature. *Cold Reg Sci Technol* 21:117–135. doi: 10.1016/0165-232X(93)90002-

P.

Riedel A, Michel C, Gosselin M. 2006. Seasonal study of sea-ice exopolymeric substances on the Mackenzie shelf: Implications for transport of sea-ice bacteria and algae. *Aquat Microb Ecol* 45:195–206. doi: 10.3354/ame045195.

Riedel A, Michel C, Gosselin M, LeBlanc B. 2007. Enrichment of nutrients, exopolymeric substances and microorganisms in newly formed sea ice on the Mackenzie shelf. *Mar Ecol-Prog Ser* 342:55–67. doi: 10.3354/meps342055.

Riedel A, Michel C, Gosselin M, LeBlanc B. 2008. Winter–spring dynamics in sea-ice carbon cycling in the coastal Arctic Ocean. *J Mar Syst* 74:918–932. doi: 10.1016/j.jmarsys.2008.01.003.

Rintala J-M, Piiparinen J, Blomster J, Majavena M, Müller S, et al. 2014. Fast direct melting of brackish sea-ice samples results in biologically more accurate results than slow buffered melting. *Polar Biol* 37:1811–1822. doi: 10.1007/s00300-014-1563-1.

Różańska M, Poulin M, Gosselin M. 2008. Protist entrapment in newly formed sea ice in the coastal Arctic Ocean. *J Mar Syst* 74:887–901. doi: 10.1016/j.jmarsys.2007.11.009.

Schoemann VS, de Jong JTM, Lannuzel D, Tison J-L, Delille B, et al. 2008. Microbiological control on the cycling of Fe and its isotopes in Antarctic sea ice. *Geochim Cosmochim Acta* 72:A837.

Sedwick PN, DiTullio GR. 1997. Regulation of algal blooms in Antarctic shelf waters by the release of iron from melting sea ice. *Geophys Res Lett* 24:2515–2518. doi: 10.1029/97GL02596.

Smedsrud LH. 1998. Estimating aggregation between suspended sediments and frazil ice. *Geophys Res Lett* 25:3875-3878. doi: 10.1029/1998GL900051.

Spindler M. 1994. Notes on the biology of sea ice in the Arctic and Antarctic. *Polar Biol* 14:319–324. doi: 10.1007/BF00238447.

Thomas DN, Kattner G, Engbrodt R, Giannelli V, Kennedy H, et al. 2001. Dissolved organic matter in Antarctic sea ice. *Ann Glaciol* 33:297-303. doi: 10.3189/172756401781818338.

Thomas DN, Papadimitriou S, Michel C. 2010. Biogeochemistry of sea ice, in Thomas DN, Dieckmann GS, eds., *Sea Ice*. 2nd ed., Oxford: Wiley-Blackwell: pp. 425–467.

Ugalde SC, Westwood KJ, Van Den Enden R, McMinn A, Meiners KM. 2016. Characteristics and primary productivity of East Antarctic pack ice during the winter-spring transition. *Deep Res Part II*, in press. doi: 10.1016/j.dsr2.2015.12.013.

Vancoppenolle M, Goosse H, de Montety A, Fichefet T, Tremblay B, et al. 2010. Modeling brine and nutrient dynamics in Antarctic sea ice: The case of dissolved silica. *J Geophys Res-Ocean* 115:C02005. doi: 10.1029/2009JC005369.

van der Merwe P, Lannuzel D, Bowie AR, Mancuso Nichols CA, Meiners KM. 2011a. Iron fractionation in pack and fast ice in East Antarctica: Temporal decoupling between the release of dissolved and particulate iron during spring melt. *Deep Sea Res Part II* 58: 1222-1236. doi: 10.1016/j.dsr2.2010.10.036.

van der Merwe P, Lannuzel D, Bowie AR, Meiners KM. 2011b. High temporal resolution observations of spring fast ice melt and seawater iron enrichment in East Antarctica. *J Geophys Res* 116:G03017. doi: 10.1029/2010JG001628.

van der Merwe P, Lannuzel D, Mancuso Nichols CA, Meiners K, Heil P, et al. 2009. Biogeochemical observations during the winter–spring transition in East Antarctic sea ice: Evidence of iron and exopolysaccharide controls. *Mar Chem* 115:163–175. doi: 10.1016/j.marchem.2009.08.001.

von Quillfeldt CH, Ambrose Jr WG, Clough LM. 2003. High number of diatom species in first-year ice from the Chukchi Sea. *Polar Biol* 26:806–818. doi: 10.1007/s00300-003-0549-1.

Wang S, Bailey D, Lindsay K, Moore JK, Holland M. 2014. Impacts of sea ice on the marine iron cycle and phytoplankton productivity. *Biogeosciences* 11:4713–4731. doi: 10.5194/bg-11-4713-2014.

Weeks W, Ackley SF. 1982. The growth, structure, and properties of sea ice. U.S. Army corps of engineers Cold Regions Research & Engineering Laboratory. Hanover, N.H.: Monog. 82-1.

Weeks WF. 2010. *On sea ice*. Fairbanks: University of Alaska Press.

Weissenberger J, Grossmann S. 1998. Experimental formation of sea ice: Importance of water circulation and wave action for incorporation of phytoplankton and bacteria. *Polar Biol* 20:178–188. doi: 10.1007/s003000050294.

Westerlund S, Öhman P. 1991. Iron in the water column of the Weddell Sea. *Mar Chem* 35:199–217. doi: 10.1016/S0304-4203(09)90018-4.

Zhou J, Delille B, Eicken H, Vancoppenolle M, Brabant F, et al. 2013. Physical and biogeochemical properties in landfast sea ice (Barrow, Alaska): Insights on brine and gas dynamics across seasons. *J Geophys Res-Ocean* 118:3172–3189. doi: 10.1002/jgrc.20232.

Zhou J, Delille B, Kaartokallio H, Kattner G, Kuosa H, et al. 2014. Physical and bacterial controls on inorganic nutrients and dissolved organic carbon during a sea ice growth and decay experiment. *Mar Chem* 166:59–69. doi: 10.1016/j.marchem.2014.09.013.

CHAPTER 3

Insights into the incorporation of iron and organic matter in sea ice from laboratory-based ice-growth experiments

3.1 Introduction

Sea ice is an important reservoir of iron (Fe) in the Southern Ocean (e.g., Sedwick and DiTullio, 1997; Lancelot et al., 2009; Lannuzel et al., 2010; Wang et al., 2014). Every spring, Fe contained in sea ice is released into surface waters and can trigger phytoplankton blooms in the marginal ice zone (Sullivan et al., 1993; Lannuzel et al., 2007; 2010). However the processes leading to Fe enrichment in sea ice are yet to be fully understood.

The co-occurrence of enrichment of organic matter and Fe suggest that they are coupled (Grotti et al., 2005; de Jong et al., 2013, 2015; Lannuzel et al., 2007, 2008, 2014a; van der Merwe et al., 2009, 2011a, 2011b). It has been proposed that the Fe concentration in the ice depends on the concentration in the parent seawater during sea ice formation (van der Merwe et al., 2009). These authors also proposed that the Fe can be associated with extracellular polymeric substances (EPS) and incorporated into the ice together with EPS. Extracellular polymeric substances are produced by algae and bacteria (Meiners et al., 2004; Mancuso Nichols et al., 2005a) and have been found to be enriched in sea ice (e.g., Krembs et al., 2011; 2002; Meiners et al., 2004; 2003; Riedel et al., 2006; Underwood et al., 2010; van der Merwe et al., 2009;

Ewert and Deming, 2011; Aslam et al., 2012; chapter 2, Janssens et al., 2016). Their high stickiness, and negatively charged surface (Decho, 1990; Underwood et al., 2010) make them a good candidate for metallic anion binding (Croot and Johansson, 2000; Verdugo et al., 2004). Extracellular polymeric substances exists in a continuum of sizes from the dissolved and colloid to the particulate fractions (Verdugo et al., 2004). Dissolved organic ligands are thought to control the dissolved Fe (DFe) distribution in sea ice and might be a crucial actor in Fe enrichment in sea ice (Lannuzel et al., 2015).

Chapter 2 was dedicated to the study of Fe and organic matter enrichment during an *in situ* ice-growth experiment. We showed that ice formation leads to physical enrichment of these compounds, with larger particles being preferentially enriched compared to smaller particles (chapter 2, Janssens et al., 2016). Nonetheless the simultaneous investigation of physical, chemical and biological processes is extremely difficult due to the complex interaction between them. In this context, laboratory ice-growth experiments are useful to shed light on specific processes. These experiments allow to form ice in a controlled environment and from chosen source solutions.

Ice tank experiments and laboratory ice-growth experiment are numerous (e.g., INTERICE experiments in Germany – e.g., Geilfus et al., 2012; Krembs et al., 2002; Weissenberger and Grossmann, 1998; Zhou et al., 2014; CRREL experiments in the United State of America – e.g., Kovacs, 1996; Loose et al., 2009; or SERF experiments in Canada – e.g., Else et al., 2015; Galley et al., 2013). To our knowledge, none of them have been conducted under the trace metal clean conditions needed to study Fe-associated processes. This study aims at understanding the basic processes leading to the incorporation of Fe into growing sea ice, and specifically the

role of organic matter as a carrier of Fe. We adapted a cold-finger apparatus (Kuiper et al., 2003; Ewert and Deming, 2011) for use under carbon and trace metal non-contaminating conditions. We conducted two sets of experiments to understand the role of EPS and organic matter in the enrichment of Fe in sea ice. The first set of experiment aimed at quantifying EPS, organic matter and inorganic macro-nutrients (hereafter referred as macro-nutrients) entrapment into sea ice. The second set of experiments targeted the role that organic matter plays in the enrichment of Fe (DFe and particulate Fe, PFe) into sea ice. Furthermore, the addition of desert dusts and sea ice algae was included in the source solutions to investigate the difference between lithogenic and biogenic PFe incorporation in sea ice. To our knowledge, this work constitutes the first laboratory ice-growth experiments conducted in trace metal clean conditions.

3.2 Methods

3.2.1 Experiments

3.2.1.1 Ice texture experiments

The first set of experiments was ran onboard the RV Polarstern, and aimed at identifying the effects of different ice growth rates on ice crystal structure, i.e., ice texture. Seawater used for this experiment was collected during a winter cruise in the Weddell Sea onboard the RV Polarstern (ANT-XXIX/6, Lemke and Participants, 2014), using the ship water intake line. The ice was grown at -10°C, -15°C and -20°C and processed for ice texture analysis onboard the ship (Table 3.1).

Table 3.1 Summary of the different experiments ran using the cold-finger. In each experiment seawater was collected at different locations and different treatments were used as source solution

Experiment name	Treatment name	Source Solution	Addition and/or treatment	Freezing T (˚C)	Parameters
Ice texture Exp.	Texture -10°C	RV Polarstern SW intake line, Weddell Sea	-	-10	Ice fabrics and dimensions of the ice formed
	Texture -15°C		-	-15	
	Texture -20°C		-	-20	
EPS, POC, PON and macro-nut. Exp.	Surface SW	RV Polarstern SW intake line, 67°39 S, 5°31 W	-	-15	Salinity, POC, DOC, macro-nutrients and EPS
	Deep SW	Deep SW (4300 m), 68°01 S, 6°40 W	-		
	Surface SW + XG	Surface SW, 67°11 S, 13°14 W	5 mg/L Xangtan gum		
Iron Exp.	FSW + PFe	Prefiltered (0.4 μm) surface SW from Trumpeter Bay, (Tasmania), 43°16 S, 147°39 E.	30 μM PFe	-15	Salinity, PFe, PAl, DFe, POC, PON, DOC
	UV-FSW + PFe		30 μM PFe + 15 min UV		
	FSW + DFe		30 μM DFe		
	UV-FSW + DFe		30 μM DFe + 15 min UV		
	FSW + Algae		sea ice algae		

Where SW is seawater; XG is xangtan gum; POC and PON are particulate organic carbon and nitrogen; DOC is dissolved organic carbon, EPS is extracellular polymeric substances, FSW is filtered seawater; UV is ultra-violet; DFe is dissolved Fe, PFe is particulate Fe and PAl is particulate aluminium.

3.2.1.2 Extracellular polymeric substances, POC, PON and macro-nutrient experiments

A second set of experiments, *EPS, POC, PON and macro-nut. Exp*., was run onboard the RV Polarstern during a winter cruise to the Weddell Sea (ANT-XXIX/6, Lemke and Participants, 2014). Seawater was collected using the ship water intake line, a CTD or a peristaltic pump (E/S Portable Sampler, Masterflex) at different locations and different depths (Table 3.1) to study the incorporation of extracellular polymeric substances (EPS), particulate organic carbon (POC) and nitrogen (PON) and inorganic macro-nutrients (nitrate+nitrite: NO_2+NO_3=NO_x, silicic acid: $Si(OH)_4^-$, phosphate: PO_4^{3-}, and ammonium: NH_4^+). The first source solution was surface seawater (Surface SW, ship water intake line). The second source solution (Deep SW) was deep seawater collected with the CTD at 4300 m deep. In the third source solution (Surface SW + XG), 5 mg L^{-1} of xanthan gum (XG) from *Xanthomonas campestris* (Sigma-Aldrich) was added to the surface seawater sampled with a peristaltic pump (E/S Portable Sampler, Masterflex) at the ice-water interface. To do so, a stock solution of 1000 mg L^{-1} XG was made and sonicated for 60 min using a Bandelin Sonopuls sonicator. The stock solution was then diluted 10 times in Ultra High Purity (UHP) water (Millipore, Gradient A10) and sonicated for 30 min before being added to the surface seawater.

3.2.1.3 Iron experiments

A third set of experiments aimed at assessing the role of organic matter in the incorporation of Fe into growing sea ice. Experiments were conducted under trace metal clean conditions. Surface seawater was collected on the 9th of October 2015 from Trumpeter Bay, (Tasmania – 43°16 S, 147°39 E) using a shore-line, and stored

in acid-clean low-density polyethylene (LDPE, Nalgene) carboys. The sampling depth was approximately 2.5 m. In the home laboratory, seawater was filtered through polycarbonate (PC) membranes (Sterlitech, pore size: 0.4 μm) at low vacuum (< 0.13 bar) using an acid-clean PC filtration apparatus (Sartorius) under a class-100 laminar flow hood (AirClean 600 PCR workstation, Model 300 Controller, AirClean System). Filtered seawater (FSW) was divided into separate bottles for separate sets of treatments. Triplicates bottles were then spiked with different Fe sources. Added concentrations were selected to reach detectable Fe signals during analyses. The first source solution, 'FSW + PFe', was obtained by adding 30 μM of lithogenic PFe (PFe > 0.4 μm) to the FSW. We used dusts particles < 20 μm, collected in the Atacama desert, Chile (European Southern Observatory, Paranal) and assumed a composition of 5% (w:w) of Fe, similar to the Earth's Crust (Taylor, 1964).

A second source solution, 'FSW + DFe', was obtained by adding 30 μM of DFe (DFe < 0.4 μm) into the FSW using a commercial solution of $FeCl_3$ 1,000ppm (Merck).

Two complementary sets of experiments were run after UV-treatment of the FSW. Filtered seawater was dispensed into acid-clean 500 mL Teflon fluorinated ethylene propylene (FEP) bottles (Nalgene) and placed between ultraviolet lamps inside a black PVC chamber for 15 min. This step of UV exposure ensured the destruction of any dissolved organic matter (DOM) present in the solution (Queroue et al., 2014). After UV exposure, PFe or DFe was added to the source solution following the steps adopted in treatments 'FSW + PFe' and 'FSW + DFe'. The latter treatments are referred to as 'UV-FSW + PFe' and 'UV-FSW + DFe'.

A final experiment was carried out using FSW to which 44 mL of melted bottom sea ice containing algae was added. The ice sample was collected at Davis station, Antarctica in November 2015. This treatment, named 'FSW + Algae', aimed at

studying the incorporation of biogenic PFe in sea ice. A list of the treatments is given in Table 3.1.

3.2.2 Sea-ice growth set-up

The experimental set-up and manipulations were conducted in a custom-made clean plastic bubble onboard the RV Polarstern (*Ice texture Exp*., *EPS, POC, PON and mcro-nut*. *Exp*.); and under a class-100 laminar flow hood in the home-laboratory (AirClean 600 PCR workstation, Model 300 Controller, AirClean System) for experiments on the incorporation of Fe (*Iron Exp*.). Ice was grown using a cold-finger apparatus first described by Kuiper et al. (2003) and Ewert and Deming (2011), modified for use under carbon and trace metal non-contaminant conditions. The cold-finger was fully made of titanium (Ti) and cooled with a circulating bath (Wise Circu, WCR-P22) using ethanol as coolant. (Figure 3.1).

The cold-finger was immersed straight in a custom-cut square acid-clean 2 L PC container (Nalgene) filled with different source solutions of seawater (Table 3.1). The PC container was placed into an insulated box made of foam insulation sheet (TechLite®) and placed on a magnetic stirrer to insure the homogeneity of the source solutions during the experiments.

At the end of each experiment, the ice was carefully removed from the remaining seawater and removed from the cold-finger. Ice was allowed to melt at room temperature in an acid-clean PC container. A diagram of the experimental set up and workflow is shown in Figure 3.1. Both remaining seawater and melted ice were analyzed for the list of parameters described below. Prior to each treatment a T_0 sample was collected for measurements of the same parameters in the source solutions

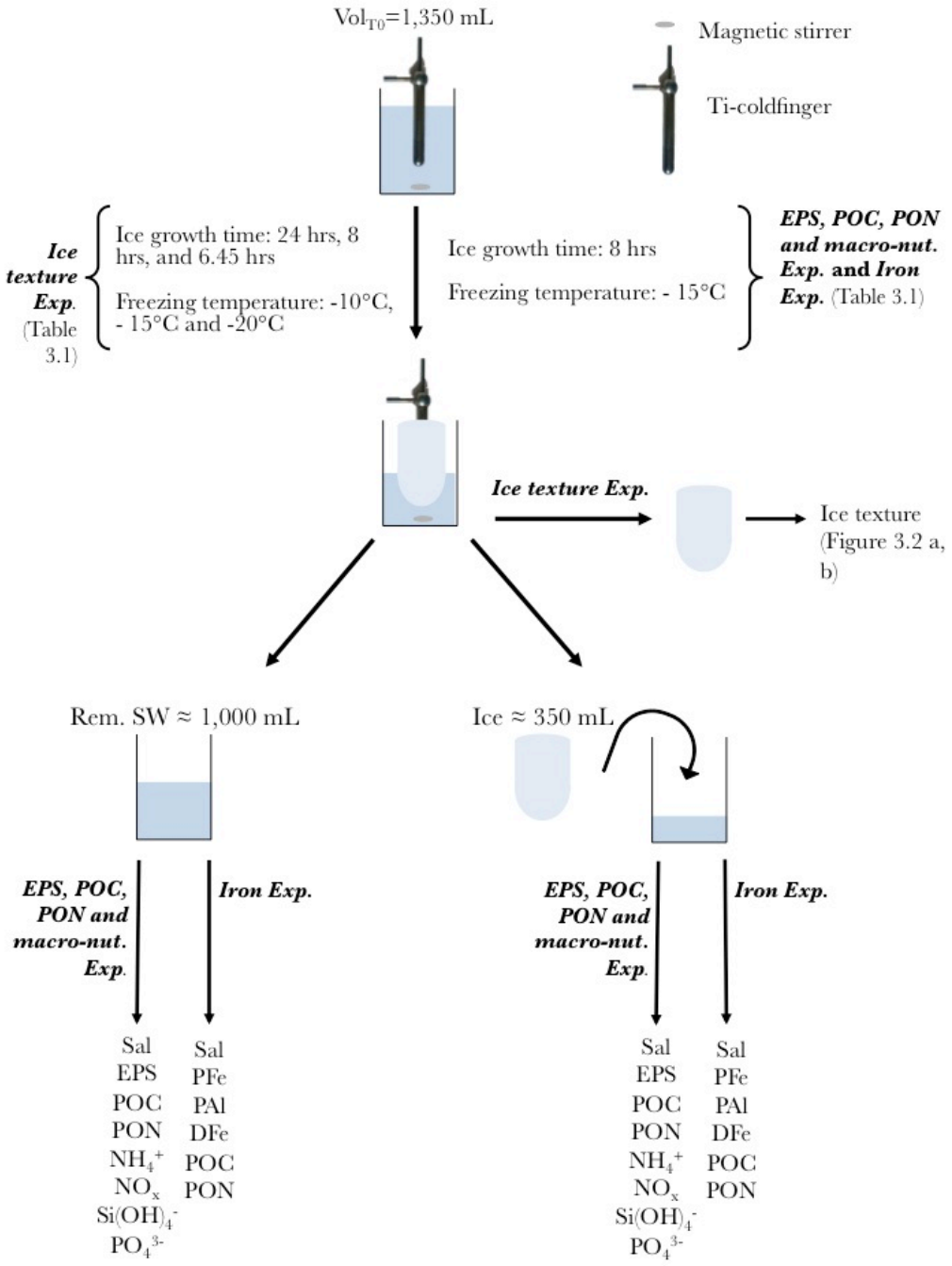

Figure 3.1 Schematic of the cold-finger experiment for the Ice texture Experiment (*Ice texture Exp.*), the Exopolysaccharides, POC, PON and macro-nutrients experiment (*EPS, POC, PON and marco-nut Exp.*) and the iron experiment (*Iron Exp.*). The entire set-up was placed in a custom-made clean plastic bubble (*Ice texture Exp.* and *EPS, POC, PON and macro-nut. Exp.*), or under a laminar flow hood (*Iron Exp.*). The cold-finger was connected to a circulating water bath with ethanol at -15°C (not represented). Experiments were run in triplicates. For each experiment the volume at T_0 was 1350 mL. The ice was formed at -10°C, -15°C and -20°C for 24, 8 and 6.45 hours respectively for the *Ice texture Exp.*, and -15°C for 8 hours for the *EPS, POC, PON and marco-nut. Exp.* and the *Iron Exp.*. Once formed, the ice was removed from the cold-finger, and processed for ice texture (*Ice texture Exp.*), or allowed to melt at room temperature before further processing (*EPS, POC, PON and macro-nut. Exp.* and *Iron Exp.*). Both remaining seawater (Rem. SW) and ice were processed for parameter described in the method section.

3.2.3 Physical variables: salinity and ice texture

Salinities (practical salinity, S_P) of seawater, bulk ice and remaining seawater were measured using a portable salinity probe (YSI Incorporated model 30, precision $\pm$0.1). Vertical and horizontal thin sections of the ice were prepared following the method of Langway (1958). Thin sections were observed through 2 cross-polarized filters and photographed following methods described in detail in chapter 2.

3.2.4 Biogeochemical variables

3.2.4.1 Extracelullar polymeric substances

Melted ice and seawater samples were homogenized and filtered onto PC membranes (0.4 μm, Millipore) under low vacuum (< 0.13 bar) to avoid cell lysis. Filters were stained with 500 μL of a solution of Alcian Blue (AB, GX8 Sigma, 0.02% AB in 0.06% acetic acid). Excess dye was removed by rinsing the membrane with 2 mL of UHP water (Millipore, Gradient A10). Membranes were then stored individually at –20°C in the dark until analysis. Concentrations were determined colorimetrically using the method of Passow and Alldredge (1995) and modified by van der Merwe et al. (2009). Concentrations were computed using the filter capture efficiency of 4% from van der Merwe et al. (2009).

3.2.4.2 Dissolved and particulate organic material and macro-nutrients

All glassware used for POC and DOC analysis were soaked in a 2% (v:v) HCl solution (analytical grade Merck EMSURE Germany), rinsed with UHP water, wrapped in aluminium foil and combusted at 450°C for 4 hours. In between triplicates and treatments, glassware was rinsed with UHP water, soaked in a 2% (v:v) HCl solution (analytical grade, Merck EMSURE Germany) for 8 hours and rinsed thoroughly with UHP water. Samples for POC were filtered onto pre-combusted 25

mm quartz filters (Sartorius). A subsample of 40 mL of the filtrate was collected in a pre-combusted glass vial for DOC analysis. 20 mL of the filtrate was subsampled in two 10 mL plastic tubes for macro-nutrient (NO_x, $Si(OH)_4^-$, PO_4^{3-}, and NH_4^+) analysis. Dissolved organic carbon and POC samples were stored at –20°C in the dark until analysis. After acidification of the filters (30 μL of 10 % (v:v) HCl, Ajax Finichem) to remove inorganic carbon, POC and PON concentrations were determined using a Thermo Finnigan EA 1112 Series Flash Elemental Analyser (precision 1%) at Central Science Laboratory (CSL, University of Tasmania). Dissolved organic carbon concentrations were measured by high-temperature catalytic oxidation using a TOC analyzer (Total Organic Carbon Analyser TOC-L CPH, Shimadzu), following the method by Qian and Mopper (1996). Silicic acid was analyzed using a photometric analyzer (Aquakem 250) and PO_4^{3-}, NO_x and NH_4^+ were analyzed with a Lachat Flow injection analyzer following the methods by Grasshoff et al. (2009). Detection limits were 0.1 mg L^{-1} and 0.002 mg L^{-1} respectively for each method.

3.2.4.3 Iron and aluminium

All sampling LDPE bottles, PC containers, PC filtration sets, petri-dishes and other equipment in contact with the samples were cleaned following GEOTRACES recommendations (Cutter et al., 2010). Polycarbonate membranes for PFe and PAl were soaked in a 10% (v:v) HCl for a week, thoroughly rinsed with UHP water (Barnastead International, NANOpure Diamond polisher) and stored in UHP water until use. Before and between treatments and triplicates, the cold-finger was thoroughly rinsed with UHP water. Between triplicates, equipment used for Fe filtrations was thoroughly rinsed with UHP water, soaked in a 10% (v:v) HCl solution for 16 hours and rinsed 5 times with UHP water.

Immediately after removing the ice from the PC bottle, the remaining seawater was filtered onto 0.4 μm pore size 47 mm diameter PC membrane filters (Sterlitech) using an acid-clean PC filtration set (Sartorius) under gentle vacuum (< 0.13 bar). The filter was collected for measurements of PFe and PAl (particles > 0.4 μm) concentrations and placed in acid-clean petri-dishes. 60 mL of the filtrate was collected in LDPE bottles (Nalgene) and acidified to pH 1.8 for DFe analysis. Once fully melted, the same process was applied to the melted sea ice. Filters were stored individually in acid-clean petri-dishes, triple bagged and kept at –20°C in the dark until analysis. The LDPE bottles containing the dissolved fraction were kept at ambient temperature until analysis.

Filters for PFe and PAl determination were digested using a mixture of strong acids following the method described in Bowie et al. (2010). Dissolved Fe samples were diluted 10 times to reduce sea salt interference on the analyzer. Particulate metals and DFe concentrations were then measured at the Central Science Laboratory (University of Tasmania) using an Inductively Coupled Plasma Mass Spectrometer (ICP-MS, Element 2) following methods described in Bowie et al. (2010).

3.2.5 Segregation coefficient and enrichment index

The partition coefficient, K_{eff} is used to describe the proportion of solute that is retained in sea ice.

$$K_{effX} = \frac{[X]_{ice}}{[X]_{source\ solution}} \qquad (3.1)$$

where $[X]_{ice}$ and $[X]_{source\ solution}$ is the concentration of the component X in the ice and in the source solution respectively.

To assess the enrichment of the ice in each component compared to sea salt, we calculated the enrichment index (EI_x, Gradinger and Ikävalko, (1998)).

$$EI_x = \frac{[Sal]_{source}}{[Sal]_{ice}} . \frac{[X]_{ice}}{[X]_{source}} \qquad (3.2)$$

where $[Sal]_{source}$ is the salinity of the source solution, and $[Sal]_{ice}$ is the salinity of the ice. Enrichment index of 1, <1 or >1 will correspond to conservative, depletion or enrichment, respectively, of the component X as compared to bulk salinity.

3.3 Results

3.3.1 Ice texture and salinity

The ice texture was dominated by columnar ice (Figure 3.2 a, b). The texture reflected the geometry of the cold-finger. Except for small differences in the size of the ice crystals, temperature had no effect on the texture.

Salinities of bulk-ice samples, as well as in the remaining seawater, were consistent throughout the experiments, with a mean bulk-ice salinity

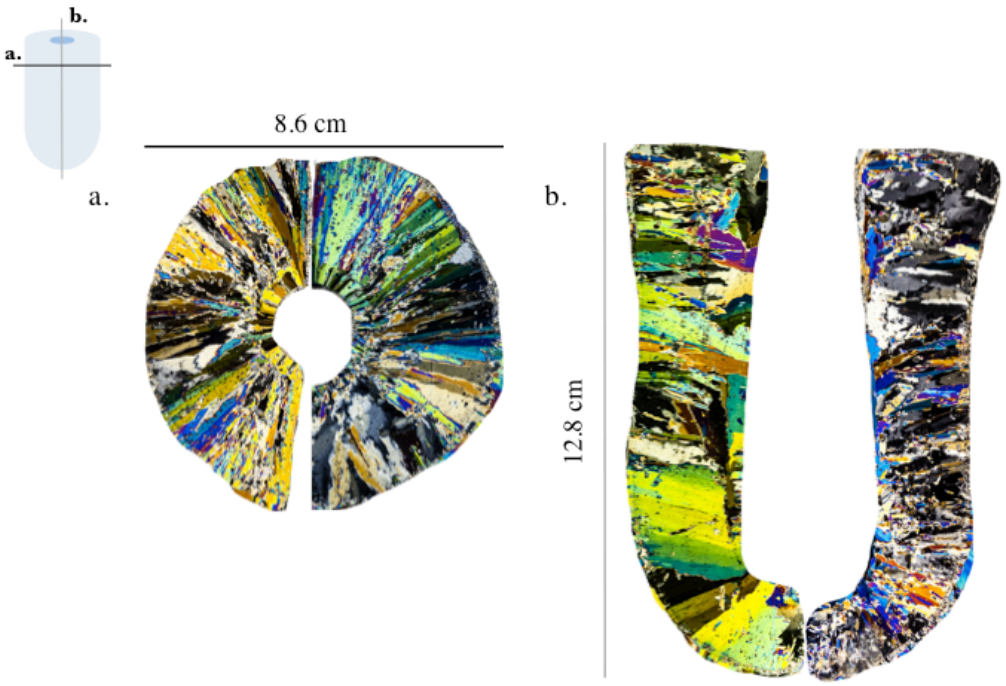

Figure 3.2 Thin section of a. the horizontal (black line) and b. vertical (grey line) cross-section of the sea ice grown at -15°C.

of 14.5 ± 1.3 S_P (mean ± standard deviation (SD), n = 24) and a mean salinity of 39.6 ± 1.3 (n = 24) for remaining seawater. The different growth temperatures applied to the samples did not affect the way that sea salts were incorporated into sea ice (mean K_{eff} = 0.43 ± 0.04).

In the rest of the section, we present the results of the 3 different treatments (Surface SW, Deep SW, and Surface SW + XG) in the *EPS, POC, PON and macro-nut. Exp*. This is followed by the results on UV and Fe treatments of the *Iron Exp*. ((UV-)FSW + PFe, (UV-)FSW + DFe and FSW + Algae).

3.3.2 Extracellular polymeric substances, POC, PON and macro-nutrients experiments

3.3.2.1 Enrichment indices of macro-nutrients and EPS

Enrichment indices were close or equal to one for the macro-nutrients in Surface SW, Deep SW and Surface SW + XG in each treatment (mean±SD = 1.0±0.09, n = 9), except NH_4^+ that was enriched in the ice in each treatment. Highest EI_{NH4+} was found in the Deep SW treatment (Figure 3.3). Extracellular polymeric substances enrichment was variable between treatments. Lowest EI_{EPS} was observed in the Deep SW treatment, while highest EI_{EPS} was observed in the Surface SW treatment (Figure 3.3). Highest EI_{NH4+} corresponded to the lowest EI_{EPS} and vice versa.

.

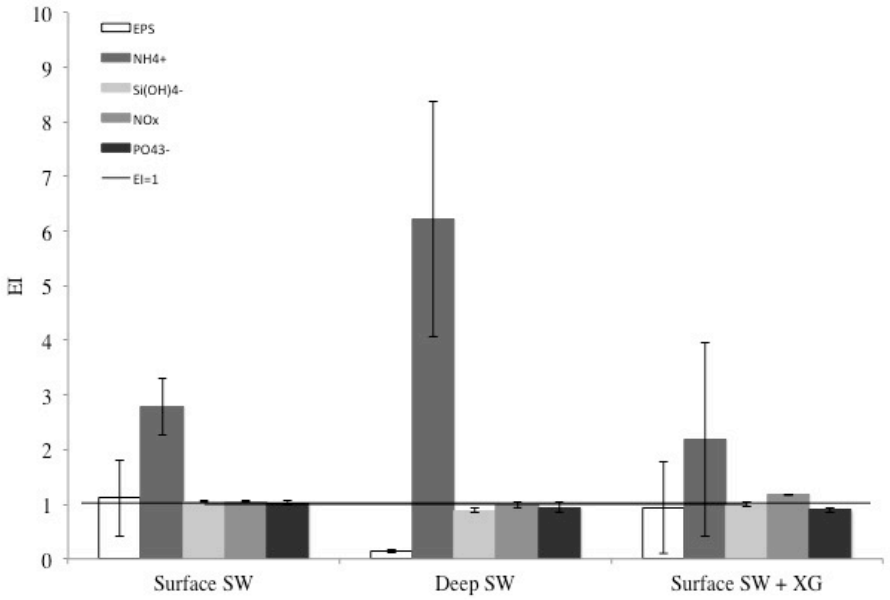

Figure 3.3 Enrichment indices (EI) of exopolysaccharides (EPS), ammonium (NH_4+), silicic acid ($Si(OH)_4^-$), nitrate + nitrite (NO_x) and phosphates (PO_4^{3-}) in the *EPS, POC, PON and macro-nut. Exp*. The error bars represent the standard deviation between triplicates (n = 3). The black line shows the limit between enrichment (EI>1) or depletion (EI<1) of each compound.

3.3.2.2 Enrichment indices of POC and PON

All EI_{POC} and EI_{PON} were well above 1 indicating an enrichment of POC and PON in newly formed ice (Figure 3.4). Mean EI_{POC} and EI_{PON} were 50.5±35.7 (n = 9) and 8.9±6.4 (n = 9), respectively.

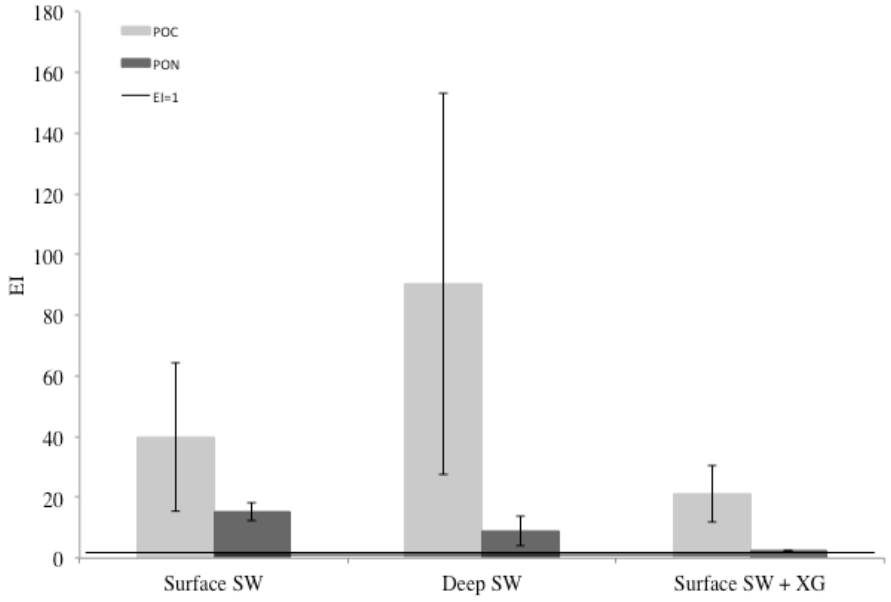

Figure 3.4 Enrichment indices (EI) of particulate organic carbon (POC) and nitrogen (PON) in the *EPS, POC, PON and macro-nut. Exp*. The error bars represent the standard deviation between triplicates (n = 3). The black line shows the limit between enrichment (EI>1) or depletion (EI<1) of POC or PON.

3.3.3 Iron experiments

3.3.3.1 Enrichment indices of PFe and DFe

Dissolved Fe was enriched in sea ice compared to the source seawater solution in each treatment (EI_{DFe} > 1) and relatively stable between treatments (mean EI_{DFe} = 2.2±0.9, Figure 3.3). Dissolved Fe was more enriched than PFe in all treatments, except in the FSW + Algae treatment (Figure 3.5). The incorporation rate of DFe decreased when UV treatment was applied (Figure 3.5).

Ice was enriched in PFe in the treatments where lithogenic or biogenic PFe was added: FSW + PFe (EI_{PFe} = 1.3±1.41, n = 3) and FSW + Algae (EI_{PFe} = 4.7±2.8, n = 3; Figure 3.5). When lithogenic PFe was added and UV treatment applied, less PFe was incorporated in sea ice (UV-FSW + PFe, EI_{PFe} = 0.5±0.3, n = 3) than without UV-treatment. The treatment where biogenic PFe was added (FSW + Algae) showed the highest EI_{PFe} of all treatments (EI_{PFe} = 4.7±2.8, n = 3). The lowest EI_{PFe} and EI_{DFe} were found in the treatment where DFe was added and exposed to UV (UV-FSW + DFe), with EI_{PFe}=0.2±0.0 (n = 3) and EI_{DFe}=1.2±1.1 (n = 3), respectively.

3.3.3.2 Enrichment indices of POC and PON

Particulate organic matter (POC and PON) was enriched in sea ice in treatments where PFe was added. Unlike other parameters, POC was the only compound showing a higher EI in UV-treated than in its non-UV treated equivalent.

The enrichment index of PON (EI_{PON}) was always lower than EI_{POC} (Figure 3.6).

Overall, the FSW + DFe and UV-FSW + DFe treatments had the lowest EIs and the lowest variability (1.1±0.7, n = 3 and 0.8±0.5, n = 3, respectively).

The treatments with addition of lithogenic and biogenic PFe (FSW + PFe and FSW + Algae) were the only ones where enrichment in all compounds (DFe, PFe, POC and PON) was observed relative to the source solution (Figures 3.5 and 3.6). This was not the case with the treatments were DFe was added (FSW + DFe and UV-FSW + DFe), or when UV light was applied, where, depending on the compound, enrichment or depletion was observed.

3.3.3.3 Particulate Fe to particulate Al ratios

Aluminium can be used as a tracer of lithogenic Fe inputs. The PFe/PAl molar ratio in the ice was elevated in all treatments compared to the Earth crustal ratio of 0.33

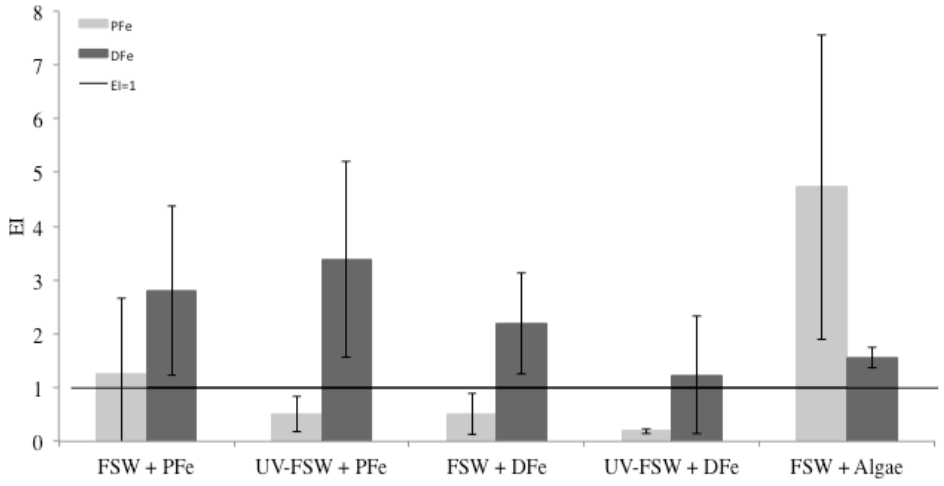

Figure 3.5 Enrichment indices (EI) of particulate iron (PFe) and dissolved iron (DFe) in each treatment of the *Iron Exp*. The error bars represent the standard deviation between triplicates (n = 3). The black line shows the limit between enrichment (EI>1) or depletion (EI<1) of PFe or DFe.

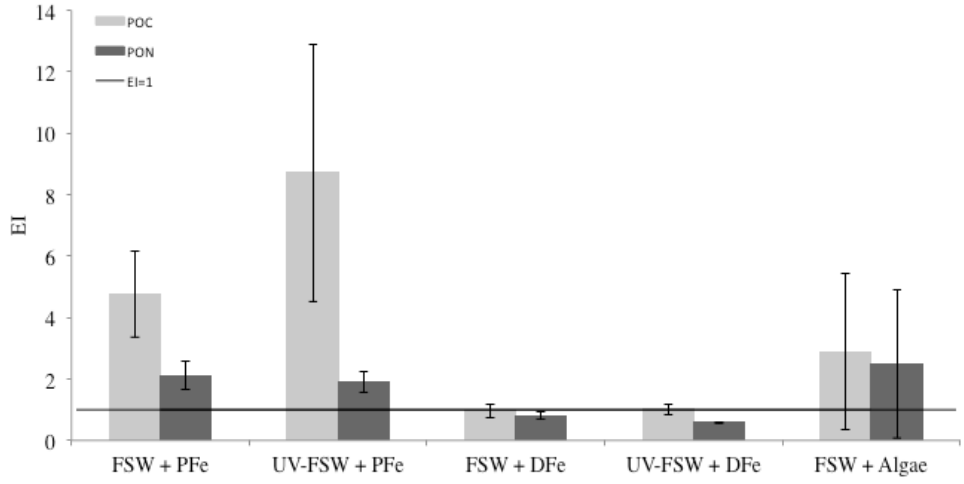

Figure 3.6 Enrichment indices (EI) for POC and PON in each treatment of the in the *Iron Exp*. The error bars represent the standard deviation between triplicates (n = 3). The black line shows the limit between enrichment (EI>1) or depletion (EI<1) of POC or PON.

(Taylor, 1964). We observed two different patterns. In the treatments with addition of PFe (FSW + PFe, UV-FSW + PFe and FSW + Algae), PFe/PAl was higher in the ice than in the remaining seawater (Figure 3.7a). In these treatments, the PFe/PAl ratio was 2 to 3 times higher than the crustal ratio, suggesting that an enrichment in PFe occurred relative to PAl (Figure 3.7a). The opposite was observed in the treatment

where DFe was added (FSW + DFe and UV-FSW + DFe), where the ratio in the ice was lower than in the remaining seawater, and PFe/PAl ratios two to three orders of magnitudes higher than the crustal ratio (Figure 3.7b).

3.3.3.4 Correlations

When pooled together (no distinction between treatments), EI_{PFe} was positively correlated to EI_{PON} (Spearman, $p < 0.05$, $R^2=0.50$, $n = 16$). Also EI_{POC} and EI_{PON} were positively correlated (Spearman test, $p < 0.05$, $R^2=0.89$, $n = 16$). Generally standard deviations between successive triplicates were higher when PFe was added to the source solution compared to DFe addition. This increase in Fe concentrations from one replicate treatment to the next, could reflect the release of soluble Fe after the addition of dust to the sample bottle.

3.4 Discussion

The similarity in ice and remaining seawater salinities between the different sets of experiments shows the reproducibility of our experimental set up. Despite the unusual ice texture of the samples, representative processes of the natural environment are shown with the conservative behaviour of major macro-nutrients, except NH_4^+ as previously observed in natural young ice samples (Chapter 2, Janssens et al., 2016) and sea-ice tank experiments (Zhou et al., 2014).

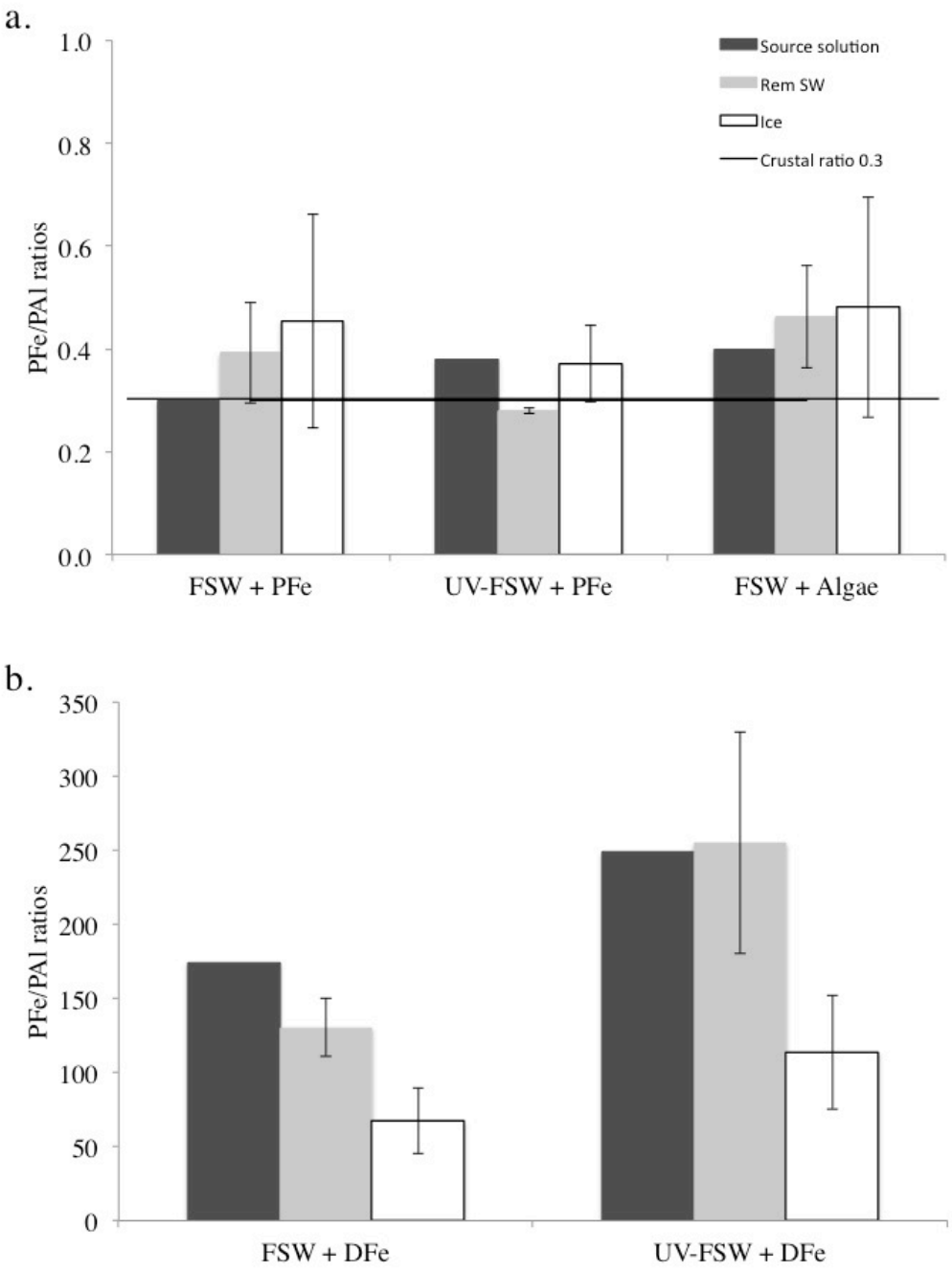

Figure 3.7 PFe/PAl ratio in the source solution (dark grey), the remaining seawater (light grey) and in the ice (white) in a) FSW + PFe, UV FSW + PFe and FSW + Algae treatments, and b) FSW + DFe and UV FSW + DFe treatments. The dark line represents the Earth crustal PFe/PAl ratio (Taylor, 1964). The error bars represent the standard deviation between triplicates (n = 3).

3.4.1 Extracellular polymeric substances, POC, PON and macro-nutrients experiments

3.4.1.1 POC, PON and EPS

Experimental results indicate that the quantity of EPS in the source solution do not dictate its rate of incorporation into newly-formed sea ice. Extracellular polymeric substances from deep-seawater was the least enriched in the ice, although it had the highest initial concentration (0.10 μg xeq L^{-1}). Also, the addition of XG, a reference standard for EPS in marine environments (Passow and Alldredge, 1995), did not favour a preferential enrichment compared to the natural EPS in other treatments. Deep-sea bacteria have been found to produce EPS (Mancuso Nichols et al., 2005a), and it could be that deep water EPS have different surface properties (e.g., number of an-ionic groups) or molecular weights than EPS produced in surface waters. Decho (1990) found that physicochemical characteristics of EPS are indeed influenced by their tertiary structure, itself dependent on the frequency and type of functional groups presence on the EPS. This could also affect the incorporation efficiency, with stickier EPS being more enriched. These divergences in surface properties of EPS could also play an important role in the incorporation of NH_4^+. The highest NH_4^+ enrichment was found when EI_{EPS} was the lowest (Figure 3.3). In an ice tank study, Krembs et al. (2011) found that concentrations of EPS were higher in the ice when *Melosira arctica*, a diatom found in Arctic sea ice, was added in the source solution compared to ice grown from saline solution containing different concentrations of XG, even if the concentration of XG was higher than the concentration of EPS produced by the diatom. Similarly, using a cold-finger apparatus similar to ours, Ewert and Deming (2011) showed that only the native EPS produced by a cold-adapted marine bacterium commonly found in sea ice, was preferentially incorporated in sea ice. Our findings of

EPS from surface seawater being the most enriched in sea ice is in line with these previous findings, suggesting that the quality of EPS is a key parameter for its entrapment into sea ice.

Higher EI_{POC} than EI_{PON} are in line with previous reports of POC and PON concentrations in young Antarctic sea ice (chapter 2, Janssens et al., 2016). Here, POC and PON were more enriched in experiments using Antarctic unfiltered seawater compared with experiments conducted with filtered source solutions from Tasmania (*Iron* Exp.). The presence of biogenic material (phytoplankton, bacteria and EPS) in the unfiltered Antarctic sample could explain this higher enrichment compared to the filtered Tasmanian seawater sample. Also, similar to EPS, the quality of POC determines the degree of enrichment in sea ice. Due to its location, the coastal Tasmanian sampling site is under influence of terrestrial and anthropogenic input bringing large amounts of allochtonous material to the pool of organic matter. This is opposed to the Antarctic sampling sites, where the organic matter in the water column is mainly autochtonous, and therefore the likelihood of terrestrial input is extremely low, if existent. Zhou et al. (2014) revealed that the riverine DOM was less enriched in sea ice compared to autochtonous DOM, due to different molecular composition, different affinity with the other compounds, and with sea ice. Similarly, Müller et al. (2013) showed that the degree of DOC enrichment depends on the chemical characteristics of the DOM. Our results suggest that the POC of potential terrestrial origin is less enriched in sea ice than the allochtonous Antarctic POC, by an order of magnitude.

3.4.2 Iron experiments

3.4.2.1 Lithogenic vs biogenic iron: role of EPS produced by ice algae and bacteria

EI_{PFe} in FSW + Algae has been found to be up to 4 times higher than in any other treatment, suggesting a better incorporation of the biogenic PFe compared to the lithogenic PFe. The bottom ice sample added to the FSW + Algae treatment was dominated by pennate diatoms such a *Nitzschia stellate, N. lecointei, Fragillariopsis spec*. and *Entomoneis kjellmanii* (data not shown).

An effect of the size of the particles may have lead to the preferential enrichment of biogenic PFe (or Fe-bearing algae) relative to lithogenic PFe (or Fe-bearing dust). The dusts added were thieved through 20 μm nylon mesh, while mentioned diatom species can be as large as 150 μm in cell size (Scott and Marchant, 2005), and can form colonies and ribbon-chain like assemblages (Scott and Marchant, 2005; Aslam et al., 2012). Better incorporation of larger cells and impurities has been previously observed in natural young sea ice (Gradinger and Ikävalko, 1998; Riedel et al., 2007; Różańska et al., 2008; chapter 2, Janssens et al., 2016). We could also be witnessing the role of EPS in the incorporation of PFe into sea ice.

Assemblages of diatoms are predominant in autotrophic-dominated sea-ice habitats and known to be associated to, and also be the principal producer of EPS (Krembs and Engel, 2001; Meiners et al., 2003; 2004; Mancuso Nichols et al., 2005a, 2005b; Underwood et al., 2010, 2013). Particulate EPS have been shown to be likely of algal origin and quickly enriched into sea ice (Meiners et al., 2003; Riedel et al., 2007). Extracellular polymeric substances enrichment has been previously observed in a similar cold-finger experiment (Ewert and Deming, 2011), and tank experiments (Krembs et al., 2011). The overall negatively charged surface of EPS (Decho, 1990;

Mancuso Nichols et al., 2005b) is considered to be important to bind to cationic metals such as Fe. In exchange, Fe provides stability to the network by acting as bridging ion (e.g., Brown and Lester, 1982; Decho, 1990).

Moreover, EPS are two to four orders of magnitude stickier than other particles (Passow, 2002), therefore potentially further helping the adhesion of PFe to ice surfaces. We can therefore assume that EPS were an important component of the added melted bottom ice sample to the source solution in the FSW + Algae treatment, resulting in the preferential enrichment in biogenic PFe compared to lithogenic PFe. Krembs et al. (2011) have shown that the presence of EPS in the ice changes the microstructure of the ice and alters it physical properties. Thus it is also possible that these modified properties are beneficial for PFe incorporation (more adapted shape of the pores and increased internal sea ice surface area) but this requires further investigation.

Another argument supporting the preferential incorporation of biogenic PFe is found when investigating the PFe/PAl ratio. Assuming that Al is purely of lithogenic origin, and comparing the PFe/PAl molar ratio to the Earth crustal ratio of 0.33 (Taylor, 1964), the excess of PFe represents the biogenic fraction (Lannuzel et al., 2014a). Assuming a similar incorporation of lithogenic PFe and lithogenic PAl, the change of PFe/PAl molar ratio in the ice can be attributed to the incorporation of the biogenic fraction of PFe, or the precipitation of DFe into PFe in the ice. Yet we observed an increase of the PFe/PAl ratio in the ice in the FSW + Algae and FSW + PFe treatments, indicating a preferential incorporation of the PFe, particularly the biogenic PFe fraction (FSW + Algae), and the fraction associated with non-UV-destroyed organic ligands (FSW + PFe).

The DFe fraction was less affected by the addition of algae than the PFe fraction. Sea ice algae are known to produce EPS in the colloidal and soluble form (Aslam et al., 2012). In this study, we work with a size distinction of 0.4 μm between dissolved and particulate fraction. This definition is however operationally defined and organic matter consists of a size continuum spanning across the soluble, colloidal and particulate fractions. The colloidal material is operationally in the dissolved fraction as it is defined as the fraction that can pass through a filter with pore size of 0.1 to 0.46 μm (Chin et al., 1998). Extracellular polymeric substances range in size from microns to hundreds of microns in the marine environment (Sullivan and Palmisano, 1984; Passow and Alldredge, 1995). Van der Merwe et al. (2009) suggested that organically-bound DFe in the ice can reduce their loss to the water column when brine drainage occurs by being associated with particles or cells (Sunda, 2001). The retention of DFe by EPS would explain the lower EI_{DFe} in the UV-treated FSW + DFe.

3.4.2.2 Effect of UV treatment on Fe incorporation efficiency: importance of organic ligands

When subject to high UV exposure, dissolved organic matter is degraded and ultimately transformed into carbon dioxide (CO_2) and water (H_2O). The difference between the UV- and non UV-treated treatments aimed at understanding the role of organic matter, including organic ligands, in the incorporation of Fe into sea ice. It has been shown that photochemical reactions alter the concentration and reactivity of the organic ligands involved in the complexation/solubilisation of trace metals (Moffett, 1995). More specifically, photochemical reduction of organically bound Fe decreases ligand-binding strength, rendering the complex Fe more labile and increasing its bioavailability (Barbeau et al., 2001).

In this chapter, Fe was added to seawater solutions after UV treatment. Different enrichment behaviours for Fe and organic matter were observed between UV-treated and non-UV treated source solutions.

As expected, DFe (and PFe) enrichment decreased when UV treatment was applied to FSW + DFe. This experiment highlights that the presence of organic matter favours the incorporation of DFe into growing sea ice. However, DFe enrichment increased when UV treatment was applied to FSW + PFe. In the former treatments, the DFe was not present in excess, as such precipitation of DFe into PFe was not observed (see section 3.4.2.3). We suggest that, in the latter case the UV treatment resulted in the release of dissolved organic ligands from the degradation of particulate organic matter (POM).

These "newly-formed" ligands were then able to complex with DFe and carry the DFe into sea ice leading to higher EI_{DFe} in UV-FSW + PFe than in FSW + PFe, where dissolved organic ligands were more sparse. We explain the difference in enrichment efficiency of DFe in (UV-)FSW+ PFe and (UV-)FSW + DFe by a combined effect of "ligand saturation" and precipitation of DFe into PFe (see section 3.4.2.3). The UV-broken bound effect might have been compensated by the production of new dissolved organic ligand available for DFe. However, not enough dissolved organic ligands were present in solution to keep the added 30 μM of DFe in solution in the FSW + DFe treatment. Free DFe remaining in seawater therefore precipitated into PFe, leading to the high PFe/PAl ratios observed.

As observed in the case of DFe incorporation in the (UV-)FSW + DFe treatments, PFe enrichment decreased when UV treatment was applied to FSW + PFe and FSW + DFe. This indicates the role of organic matter in the incorporation of PFe in growing sea ice. Unlike EI_{PFe} and EI_{DFe}, EI_{POC} increased when UV treatment was applied to

FSW + PFe. It has been proposed that UV-B radiation breaks down not only DOC but also POC (Report Montreal protocol, 1999), although the effect of UV on particulate organic matter is not clearly defined. Our results show that UV could impact on the quality of POC (including large EPS) leading to different incorporation behaviours. It is likely that the POC becomes smaller and is then more easily incorporated into the ice. This argument however contradicts what has been previously observed in the field, where large particles are preferentially incorporated in sea ice (Gradinger and Ikävalko, 1998; Riedel et al., 2007; Lannuzel et al., 2014b; Janssens et al., 2016).

One explanation is that UV-radiations changes the physico-chemical properties of organic matter in a way that the PFe-organic matter binding capacity would be altered, but the enrichment of POC would be favoured. Organic-free PFe would therefore be hardly incorporated, while the UV-induced modifications in the POC facilitate its incorporation. It has been shown that the binding potential of EPS is greatly influenced by their physico-chemical properties (Krembs and Deming, 2008; Verdugo, 2012), properties that are likely to be altered by UV irradiation. Therefore, more than the size, the important factor for enrichment of particles would be their physico-chemical properties and the tertiary structure/molecular composition/shape of the particles. Zhou et al., (2014) suggested that organic matter is initially incorporated as particulate organic matter and then converted into dissolved organic matter once in the ice. We could be witnessing this process in the FSW + Algae treatment, with the transformation of POC into DOC by heterotrophic organisms, leading to lower EI_{POC} than in (UV-)FSW + PFe. Zhou et al. (2014) also showed that different quality of DOC impacts the incorporation efficiency. We suggest that this mechanism is also applicable to particulate constituents as discussed in section 3.4.2.1.

3.4.2.3 Precipitation of dissolved Fe

The PFe/PAl ratios measured in our samples can give an indication on the level of precipitation of DFe into PFe. The addition of DFe into seawater led to very high PFe/PAl ratios in the FSW + DFe and UV-FSW + DFe experiments (Fig. 3.7 b). A significant amount of DFe (30 μM) was added to these 2 solutions, without addition of organic ligands (e.g., EDTA) to balance the addition of DFe and keep it in solution. Organic ligands can be produced *in situ* by sea ice algae and bacteria (Lannuzel et al., 2015) or supplied externally from sediment resuspension (Croot and Johansson, 2000; Buck et al., 2007). EDTA is synthetically produced and is therefore not an adequate model ligand of the natural environment.

We observed here the precipitation of the non-organically bound excess of DFe into the PFe pool (Lannuzel et al., 2014a, 2015), leading to the high PFe/PAl ratios observed. This process is even more expressed in the UV-FSW + DFe treatment, where the UV exposure breaks the bounds of the Fe-ligand complexes already present in the source solution before addition of DFe. The precipitated PFe and remaining DFe were then less prone to incorporation into sea ice, as observed by lower EI_{PFe} and EI_{DFe}. Two explanations are possible: (1) As previously observed in our study, biogenic PFe (low in these experiments) is preferentially enriched in the newly-formed ice compared to lithogenic PFe. Also, the high PFe concentrations might have reached a threshold where the ice is saturated and more incorporation becomes impossible. We may observe a decoupling between biogenic and lithogenic PFe incorporation. Extracellular polymeric substances have been proposed to be acting as a plug retaining salinity in the ice (Krembs et al., 2011). If the biogenic PFe is incorporated first, helped by the association to, and then retained in the ice by, EPS, the incorporation of lithogenic PFe might not be as efficient and could reach a

concentration threshold in the ice. The association of Fe with EPS, as well as the room available in the brine channels would therefore determine the incorporation, retention, and threshold of PFe in the ice.

(2) We might witness the key role of organic ligands in transferring DFe from seawater to sea ice. Organically-bound Fe would take advantage of the properties of the particles it is attached to, to get trapped in the ice as discussed previously (section 3.4.2.2). It is difficult to distinguish the contribution of each process in these experiments and it is likely a combination of both. We note, that Fe concentrations in these experiments were above the range of concentrations encountered in the Southern Ocean. Nonetheless, these results shed light on the general chemistry of the processes.

3.4.3 Limitations of laboratory ice-growth experiments

Laboratory ice-growth experiments are a great asset to the field of polar oceanography for many reasons. They are logistically easier and cheaper to conduct than field experiment and field sampling. Laboratory ice-grown offers a unique opportunity to study ice growth from its initial stage of ice formation while the history of a natural ice floe is difficult to assess. This type of experiments allows us to isolate processes occurring at the onset of ice formation, and study the influence of specific parameters, while monitoring the others and keeping them under control. Most importantly, replicate measurements are possible in the laboratory while field sampling of a natural ice floe always carries the uncertainty of high spatial heterogeneity (e.g., Meiners et al., 2012, Williams et al., 2015).

However laboratory based ice-growth experiments also present drawbacks. First, ice growth is limited in space (a few cm^3) and time (a few hours). In the cold-finger case, the geometry of the system is different from natural ice. Ice crystals are mainly

growing horizontally (Figure 3.2), while natural columnar ice exhibits vertical ice crystals. Nonetheless, the good agreement of our laboratory-based results with field studies shows that the initial incorporation of solutes and particles over a short period of time was not affected by the geometry of the ice. The cold-finger setup is, therefore, a useful tool to refine and complete field data, and isolate processes that can be then included in biogeochemical models. Although laboratory ice-growth experiments cannot replace field campaigns, they are a key step towards the understanding of biogeochemical cycles associated with sea ice.

3.5 Conclusion

This chapter represents the first study dedicated to Fe enrichment in sea ice under controlled conditions. The investigation highlights the role of EPS and POC in the enrichment of PFe in sea ice. Results also showed that biogenic PFe is preferentially enriched compared to lithogenic PFe. Rather than the quantity, it is the quality of EPS and POC that determines their entrapment in the ice, with autochtonous POC being more enriched than allochtonous POC. The reasons are still unclear, but characterisations of these particles would be a step forward to understand the complex links between Fe and POM incorporation into sea ice. The quality of POM determines its association with PFe, and ultimately the efficiency of PFe incorporation in sea ice. UV treatment clearly alters POM and modifies the association of Fe (PFe and DFe) with organic matter. This ultimately affects their degree of enrichment. Organic ligands responsible for DFe enrichment are also affected by UV treatment. In the context of dramatically changing sea-ice environments, it is important to clearly identify drivers and quantify processes that affect ice-associated Fe and carbon biogeochemical cycling in polar waters.

References

Aslam SN, Cresswell-Maynard T, Thomas DN, Underwood GJC. 2012. Production and characterization of the intra- and extracellular carbohydrates and polymeric substances (EPS) of three sea-ice diatom species, and evidence for a cryoprotective role for EPS. *J Phycol* 48:1494–1509. doi:10.1111/jpy.12004

Barbeau K, Rue EL, Bruland KW, Butler A. 2001. Photochemical cycling of iron in the surface ocean mediated by microbial iron(III)-binding ligands. *Nature* 413:409–413. doi:10.1038/35096545

Bowie AR, Townsend AT, Lannuzel D, Remenyi TA, van der Merwe P. 2010. Modern sampling and analytical methods for the determination of trace elements in marine particulate material using magnetic sector inductively coupled plasma-mass spectrometry. *Anal Chim Acta* 676:15–27. doi:10.1016/j.aca.2010.07.037

Brown MJ, Lester JN. 1982. Role of bacterial extracellular polymers in metal uptake in pure culture and activated sludge-1. Effect of metal concentration. *Water Res* 16:1539–1548. doi:10.1016/0043-1354(82)90206-8

Buck KN, Lohan MC, Berger CJM, Bruland KW. 2007. Dissolved iron speciation in two distinct river plumes and an estuary: Implications for riverine iron supply. *Limnol Oceanogr* 52:843–855. doi:10.4319/lo.2007.52.2.0843

Chin W-C, Orellana MV, Verdugo P. 1998. Spontaneous assembly of marine dissolved organic matter into polymer gels. *Nature* 391:568–572. doi:10.1038/nature01582.1

Croot PL, Johansson M. 2000. Determination of Iron Speciation by Cathodic Stripping Voltammetry in Seawater Using the Competing Ligand. *Electroanalysis* 12:565-576. doi:10.1002/1521-4109)200005)12

Cutter G, Andersson P, Codispoti L, Croot P, Francois R, Lohan M, Obata H, Rutgers M. 2010. Sampling and sample-handling protocols for GEOTRACES cruises.

de Jong J, Schoemann V, Maricq N, Mattielli N, Langhorne P, Haskell T, Tison J-L. 2013. Iron in land-fast sea ice of McMurdo Sound derived from sediment resuspension and wind-blown dust attributes to primary productivity in the Ross Sea, Antarctica. *Mar Chem* 157:24–40. doi:10.1016/j.marchem.2013.07.001

de Jong JTM, Stammerjohn SE, Ackley SF, Tison J-L, Mattielli N, Schoemann V. 2015. Sources and fluxes of dissolved iron in the Bellingshausen Sea (West Antarctica): The importance of sea ice, icebergs and the continental margin. *Mar Chem* 177:518–535. doi:10.1016/j.marchem.2015.08.004

Decho AW. 1990. Microbial exopolymer in ocean environments: their roles in food webs and marine processes. *Ocean Mar Biol Annu. Rev* 28:73–153

Else B, Rysgaard S, Attard K, Campbell K, Crabeck O, Galley R, Geilfus N-X, Lemes M, Lueck R, Papkyriakou T, Wang F. 2015. Under-ice eddy covariance flux measurements of heat, salt, momentum, and dissolved oxygen in an artificial

sea ice pool. *Cold Reg Sci Technol* 119:158–169. doi:10.1016/j.coldregions.2015.06.018

Ewert M, Deming JW. 2011. Selective retention in saline ice of extracellular polysaccharides produced by the cold-adapted marine bacterium Colwellia psychrerythraea strain 34H. *Ann Glaciol* 52:111–117. doi:10.3189/172756411795931868

Executive summary of the 1998 report of the environmental assessment panel, in synthesis of the reports of the scientific, environmental effects, and technologies and economic assessment panels of the Montreal protocol, UNEP, United Nations Environment Programme Ozone secretariat, February 1999

Galley R, Else B, Geilfus N-X, Hare A, Isleifson D, Ryner L, Barber D, Rysgaard S. 2013. Morphology and distribution of liquid inclusions in young sea ice as imaged by magnetic resonance. *Cryosph Discuss* 7:4977–5006. doi:10.5194/tcd-7-4977-2013

Geilfus N-X, Delille B, Verbeke V, Tison J-L. 2012. Towards a method for high vertical resolution measurements of the partial pressure of CO_2 within bulk sea ice. *J Glaciol* 58:287–300. doi:10.3189/2012JoG11J071

Gradinger R, Ikävalko J. 1998. Organism incorporation into newly forming Arctic sea ice in the Greenland Sea. *J Plankton Res* 20:871–886. doi:10.1093/plankt/20.5.871

Grasshoff K, Kremling K, Ehrhardt M. 2009. Methods of Seawater Analysis. 3rd ed. Germany. Wiley-VCH. doi:10.1002/9783527613984

Grotti M, Soggia F, Ianni C, Frache R. 2005. Trace metals distributions in coastal sea ice of Terra Nova Bay, Ross Sea, Antarctica. *Antarct Sci* 17:289–300. doi:10.1017/s0954102005002695

Janssens J, Meiners KM, Tison J-L, Dieckmann G, Delille B, Lannuzel D. 2016. Incorporation of iron and organic matter into young Antarctic sea ice during its initial growth stages. *Elem Sci Anthr* 4:123. doi:10.12952/journal.elementa.000123

Kovacs A. 1996. Sea ice. Part 1. Bulk salinity versus ice floe thickness.

Krembs C, Deming JW. 2008. The role of exopolymers in microbial adaptation to sea ice, (in) Psychrophiles: From Biodiversity to Biotechnology. Eds: Margesin R, Schinner F, Marx JC, Gerday C. Springer-Verlag, New-Yortk, pp. 247–264.

Krembs C, Eicken H, Deming JW. 2011. Exopolymer alteration of physical properties of sea ice and implications for ice habitability and biogeochemistry in a warmer Arctic. *Proc Natl Acad Sci U.S.A* 108:3653–8. doi:10.1073/pnas.1100701108

Krembs C, Eicken H, Junge K, Deming JW. 2002. High concentrations of exopolymeric substances in Arctic winter sea ice: Implications for the polar

ocean carbon cycle and cryoprotection of diatoms. *Deep Res Part I Oceanogr Res* 49:2163–2181. doi:10.1016/S0967-0637(02)00122-X

Krembs C, Engel A. 2001. Abundance and variability of microorganisms and transparent exopolymer particles across the ice-water interface of melting first-year sea ice in the Laptev Sea (Arctic). *Mar Biol* 138:173–185. doi:10.1007/s002270000396

Krembs C, Tuschling K, Juterzenka K. 2002. The topography of the ice-water interface - its influence on the colonization of sea ice by algae. *Polar Biol* 25:106–117. doi:10.1007/s0030000100318

Kuiper MJ, Lankin C, Gauthier SY, Walker VK, Davies PL. 2003. Purification of antifreeze proteins by adsorption to ice. *Biochem Biophys Res Commun* 300:645–648. doi:10.1016/S0006-291X(02)02900-5

Lancelot C, de Montety A, Goosse H, Becquevort S, Schoemann V, Pasquer B, Vancoppenolle M. 2009. Spatial distribution of the iron supply to phytoplankton in the Southern Ocean: a model study. *Biogeosciences Discuss* 6:4919–4962. doi:10.5194/bgd-6-4919-2009

Langway C, 1958. Ice fabrics and the universal stage, U.S. Snow, Ice and Permafrost Research Establishment. Illinois.

Lannuzel D, Chever F, van der Merwe PC, Janssens J, Roukaerts A, Cavagna A-J, Townsend AT, Bowie AR, Meiners KM. 2014a. Iron biogeochemistry in Antarctic pack ice during SIPEX-2. *Deep Sea Res Part II Top Stud Oceanogr* 131:111-122. doi:10.1016/j.dsr2.2014.12.003

Lannuzel D, Grotti M, Abelmoschi ML, van der Merwe P. 2015. Organic ligands control the concentrations of dissolved iron in Antarctic sea ice. *Mar Chem* 174:120–130. doi:10.1016/j.marchem.2015.05.005

Lannuzel D, Schoemann V, de Jong J, Chou L, Delille B, Becquevort S, Tison J-L. 2008. Iron study during a time series in the western Weddell pack ice. *Mar Chem* 108:85–95. doi:10.1016/j.marchem.2007.10.006

Lannuzel D, Schoemann V, de Jong J, Pasquer B, van der Merwe P, Masson F, Tison J-L, Bowie A. 2010. Distribution of dissolved iron in Antarctic sea ice: Spatial, seasonal, and inter-annual variability. *J Geophys Res* 115:G03022. doi:10.1029/2009JG001031

Lannuzel D, Schoemann V, de Jong J, Tison J-L, Chou L. 2007. Distribution and biogeochemical behaviour of iron in the East Antarctic sea ice. *Mar Chem* 106:18–32. doi:10.1016/j.marchem.2006.06.010

Lannuzel D, van der Merwe PC, Townsend AT, Bowie AR. 2014b. Size fractionation of iron, manganese and aluminium in Antarctic fast ice reveals a lithogenic origin and low iron solubility. *Mar Chem* 161:47–56. doi:10.1016/j.marchem.2014.02.006

Lemke P, Participants of the ANT-XXIX/6 cruise. 2014. The expedition of the research vessel "Polarstern" to the Antarctic in 2013 (ANT-XXIX/6), Berichte zur Polar-und Meeresforschung. Bremerhaven: Helmoltz Gemeinschaft: Reports polar Mar Res 679.

Loose B, McGillis WR, Schlosser P, Perovich D, Takahashi T. 2009. Effects of freezing, growth, and ice cover on gas transport processes in laboratory seawater experiments. *Geophys Res Lett* 36:1–5. doi:10.1029/2008GL036318

Mancuso Nichols CA, Guezennec J, Bowman JP. 2005a. Bacterial exopolysaccharides from extreme marine environments with special consideration of the Southern Ocean, sea ice, and deep-sea hydrothermal vents: A review. *Mar Biotechnol* 7:253–271. doi:10.1007/s10126-004-5118-2

Mancuso Nichols CA, Garon Lardière S, Bowman JP, Nichols PD, Gibson JAE, Guézennec J. 2005b. Chemical characterization of exopolysaccharides from Antarctic marine bacteria. *Microb Ecol* 49:578–589. doi:10.1007/s00248-004-0093-8

Meiners K, Brinkmeyer R, Granskog MA, Lindfors A. 2004. Abundance, size distribution and bacterial colonization of exopolymer particles in Antarctic sea ice (Bellingshausen Sea). *Aquat Microb Ecol* 35:283–296. doi:10.3354/ame035283

Meiners K, Gradinger R, Fehling J, Civitarese G, Spindler M. 2003. Vertical distribution of exopolymer particles in sea ice of the Fram Strait (Arctic) during autumn. *Mar Ecol Prog Ser* 248:1–13. doi:10.3354/meps248001

Meiners KM, Vancoppenolle M, Thanassekos S, Dieckmann GS, Thomas DN, Tison J-L, Arrigo KR, Garrison DL, McMinn A, Lannuzel D, van der Merwe P, Swadling KM, Smith Jr WO, Melnikov I, Raymond B. 2012. Chlorophyll a in Antarctic sea ice from historical ice core data. *Geophys Res Lett* 39:L21602. doi:10.1029/2012GL053478

Moffett JW. 1995. Temporal and spatial variability of copper speciation in the Sargasso Sea. *Deep Res Part I Oceanogr Res* 42:1273–1295. doi:10.1016/0967-0637(95)00060-j

Müller S, Vähätalo AV, Stedmon CA, Granskog MA, Norman L, Aslam SN, Underwood GJC, Dieckmann GS, Thomas DN. 2013. Selective incorporation of dissolved organic matter (DOM) during sea ice formation. *Mar Chem* 155:148–157. doi:10.1016/j.marchem.2013.06.008

Passow U. 2002. Transparent exopolymer particles (TEP) in aquatic environments. *Prog Oceanogr* 55:287–333. doi:10.1016/S0079-6611(02)00138-6

Passow U, Alldredge AL. 1995. A dye-binding assay for the spectrophotometric measurement of transparent exopolymer particles (TEP). *Limnol Oceanogr* 40:1326–1335. doi:10.4319/lo.1995.40.7.1326

Qian J, Mopper K, 1996. Automated high-performance, high-temperature combustion total organic carbon analyzer. *Anal Chem* 68:3090–3097. doi:10.1021/ac960370z

Queroue F, Townsend A, van der Merwe P, Lannuzel D, Sarthou G, Bucciarelli E, Bowie A. 2014. Advances in the offline trace metal extraction of Mn, Co, Ni, Cu, Cd, and Pb from open ocean seawater samples with determination by sector field ICP-MS analysis. *Anal Methods* 6:2837–2847. doi:10.1039/C3AY41312H

Riedel A, Michel C, Gosselin M. 2006. Seasonal study of sea-ice exopolymeric substances on the Mackenzie shelf: Implications for transport of sea-ice bacteria and algae. *Aquat Microb Ecol* 45:195–206. doi:10.3354/ame045195

Riedel A, Michel C, Gosselin M, LeBlanc B. 2007. Enrichment of nutrients, exopolymeric substances and microorganisms in newly formed sea ice on the Mackenzie shelf. *Mar Ecol Prog Ser* 342:55–67. doi:10.3354/meps342055

Różańska M, Poulin M, Gosselin M. 2008. Protist entrapment in newly formed sea ice in the coastal Arctic Ocean. *J Mar Syst* 74:887–901. doi:10.1016/j.jmarsys.2007.11.009

Scott JF, Marchant JH. 2005. Antarctic marine protists. Australian Biological Ressources Study and Australian Antarctic Division, Canderra, Hobart.

Sedwick PN, DiTullio R. 1997. Regulation of algal blooms in Antarctic shelf waters by the release of iron from melting sea ice. *Geophys Res Lett* 24:2515–2518. doi:10.1029/97GL02596

Sullivan CW, Arrigo KR, McClain CR, Comiso JC, Firestone J. 1993. Distributions of phytoplankton blooms in the Southern Ocean. *Science* 262:1832–1837. doi:10.1126/science.262.5141.1832

Sullivan CW, Palmisano AC. 1984. Sea ice microbial communities: distribution, abundance, and diversity of ice bacteria in McMurdo Sound, Antarctica, in 1980. *Appl Environ Microbiol* 47:788–95

Sunda WG. 2001. Bioavailability and bioaccumulation of iron in the sea. (in) The Biogeochemistry of Iron in Seawater. Eds: Turner DR, Hunter KH. IUPAC Series on Analytical and physical chemistry of environment systems, Wiley. pp: 41–84.

Taylor SR. 1964. Abundance of chemical elements in the continental crust : a new table. *Geochim Cosmochim Acta* 28:1273–1285. doi:10.1016/0016-7037(64)90129-2

Underwood GJC, Aslam SN, Michel C, Niemi A, Norman L, Meiners KM, Laybourn-Parry J, Paterson H, Thomas DN. 2013. Broad-scale predictability of carbohydrates and exopolymers in Antarctic and Arctic sea ice. *Proc Natl Acad Sci U.S.A* 110:15734–15739. doi:10.1073/pnas.1302870110

Underwood GJC, Fietz S, Papadimitriou S, Thomas DN, Dieckmann G. 2010. Distribution and composition of dissolved extracellular polymeric substances (EPS) in Antarctic sea ice. *Mar Ecol Prog Ser* 404:1–19. doi:10.3354/meps08557

van der Merwe P, Lannuzel D, Bowie AR, Meiners KM. 2011a. High temporal resolution observations of spring fast ice melt and seawater iron enrichment in East Antarctica. *J Geophys Res* 116:G03017. doi:10.1016/2010JG001628

van der Merwe P, Lannuzel D, Mancuso Nichols CA, Meiners K, Heil P, Norman L, Thomas DN, Bowie AR. 2009. Biogeochemical observations during the winter–spring transition in East Antarctic sea ice: Evidence of iron and exopolysaccharide controls. *Mar Chem* 115:163–175. doi:10.1016/j.marchem.2009.08.001

Verdugo P. 2012. Marine Microgels. *Ann Rev Mar Sci* 4:375–400. doi:10.1146/annurev-marine-120709-142759

Verdugo P, Alldredge A, Azam F, Kirchman D, Passow U, Santschi P. 2004. The oceanic gel phase: a bridge in the DOM-POM continuum. *Mar Chem* 92:67–85. doi:10.1016/j.marchem.2004.06.017

Wang S, Bailey D, Lindsay K, Moore K, Holland M. 2014. Impacts of sea ice on the marine iron cycle and phytoplankton productivity. *Biogeosciences* 11:4713–4731. doi:10.5194/bg-11-4713-2014

Weissenberger J, Grossmann S. 1998. Experimental formation of sea ice: Importance of water circulation and wave action for incorporation of phytoplankton and bacteria. *Polar Biol* 20:178–188. doi:10.1007/s003000050294

Williams G, Maksym T, Wilkinson J, Kunz K, Murphy C, Kimball P, Singh H. 2015. Thick and deformed Antarctic sea ice mapped with autonomous underwater vehicles. *Nature geoscience* 8:61-67. doi:10.1038ngeo2299

Zhou J, Delille B, Kaartokallio H, Kattner G, Kuosa H, Tison J-L, Autio R, Dieckmann GS, Evers K-U, Jørgensen L, Kennedy H, Kotovitch M, Luhtanen A-M, Stedmon CA, Thomas DN. 2014. Physical and bacterial controls on inorganic nutrients and dissolved organic carbon during a sea ice growth and decay experiment. *Mar Chem* 166:59–69. doi:10.1016/j.marchem.2014.09.013

CHAPTER 4

First representation of iron in a sea-ice biogeochemical model

4.1 Introduction

Sea ice plays a critical role in regulating the Earth's climate, and its seasonal cycle constitutes one of the biggest changes on the planet's surface (Arrigo, 2014; Thomas 2016). The physical interactions of sea ice with the climate have been largely represented in global Earth System Models (ESM, e.g., Holland et al., 2006; Serreze et al., 2007). In contrast, sea ice impacts on biogeochemical cycles are currently not represented in global ESMs even though they are considered to have significant influence on the climate system (Vancoppenolle et al., 2013). Sea ice is generally represented as a biologically and chemically inert layer between the atmosphere and the ocean, and generally considered as impermeable to gas exchanges (Vancoppenolle et al., 2013). Exceptions are the recent study from Moreau et al. (2016) investigating the carbon cycle associated with sea ice growth and melt using the NEMO-LIM-PISCES (Nucleus for European Modelling of the Ocean – Louvain-la-Neuve sea Ice Model – Pelagic Interactions Scheme for Carbon and Ecosystem Studies) model, and the implementation of the Biogeochemical Flux Model (BFM) model with a sea ice component by Tedesco et al. (2010).

The Southern Ocean is a high-nutrient, low-chlorophyll (HNLC) area, with surface waters limited in iron (Fe) (e.g., Boyd and Ellwood, 2010). Despite low Fe concentrations in Antarctic surface waters, sea ice is enriched in Fe compared to its

parent seawater (Aguilar-Islas et al., 2008; de Jong et al., 2013, 2015; Grotti et al., 2005; Janssens et al., 2016; Kanna et al., 2014; Lannuzel et al., 2014a, 2008, 2007; Tovar-Sánchez et al., 2010; van der Merwe et al., 2011a, b). Iron, together with other nutrients and organic matter, is seasonally stored in the ice in autumn and winter and transformed by autotrophic and heterotrophic activity (Lannuzel et al., 2010; Meiners and Michel, 2016). Under winds and ocean currents forces, sea ice drifts and redistributes this biogeochemical material before the ice melts in spring and summer. Sea ice acts therefore as a temporal reservoir of Fe for waters of the Southern Ocean (e.g., Lancelot et al., 2009; Lannuzel et al., 2010; Sedwick and DiTullio, 1997). Sea ice meltwaters can contribute up to 70% of the total input of Fe into Antarctic open waters in spring (Lannuzel et al., 2007), thereby exerting a strong control on Southern Ocean primary productivity. It is therefore crucial to include sea-ice Fe biogeochemical processes into models as a mean to better understand and predict the Fe and carbon budget of the Southern Ocean.

While sea ice has been included in biogeochemical (BGC) ocean models as a source of Fe to surface waters of the polar oceans (Lancelot et al., 2009; Wang et al., 2014), these models consider vertically homogenous concentrations of dissolved Fe (DFe) in the ice and do not include the particulate Fe fraction (PFe). However, the bioavailability of Fe is determined by its chemical speciation and physical fractionation and is thus an important specificity to represent in models. Moreover, Lannuzel et al. (2014a) found that 71% of the PFe incorporated into Antarctic pack ice is biogenic, and that the flux of biogenic PFe released from sea ice is 10 times higher than the DFe flux. Biogeochemical processes occurring within the ice and affecting the concentrations of Fe in the dissolved and particulate pools are currently not represented in models (e.g., Lannuzel et al., 2016; Vancoppenolle and Tedesco,

2016). In addition, the existing models are using simplistic parameterisations of the mechanisms of Fe incorporation into and release from the sea ice; this is because field based work has so far failed to clearly identify and quantify these processes. Many uncertainties therefore remain in model studies, such as the quantification of the influence of melting sea ice as a Fe source to surface waters, underestimation of the DFe input into sea ice or missing mechanisms.

In order to reduce these uncertainties, we implemented a one-dimensional modelling framework to study the vertical processes in the ice in a single location, and compute the budget of Fe. Here, we use a one-dimensional halo-thermodynamic sea ice model (LIM-1D, Vancoppenolle et al., 2010; 2007) to investigate the key processes driving Fe dynamics in sea ice. To our knowledge, this is the first biogeochemical sea ice model incorporating brine dynamics between layers within the ice, and exchange with the ocean (Vancoppenolle et al., 2010), required for the representation of dissolved tracer transport in the ice. We investigate the following: (1) the processes leading to Fe enrichment in sea ice and, (2) the physical and biological processes driving the Fe dynamics within sea ice. Specifically, the questions addressed in this chapter are: (1) How can we robustly model Fe dynamics in sea ice and particularly the initial entrapment of Fe and the adsorption of Fe in the brine system? (2) What are the important parameters that must be constrained to reproduce observed Fe concentrations in sea ice? (3) Is it possible to reproduce the temporal evolution of Fe using a sea ice model of reasonable complexity?

The first part of this study, addressing the first question, is based on model simulations of observations carried out during *in situ* ice-growth experiments in the Weddell Sea during Austral winter (chapter 2, Janssens et al., 2016). Using parameterisations based on these experiments, the second part of this study

investigates the Fe dynamics in sea ice and the main mechanisms driving the DFe and PFe concentrations in undeformed first-year sea ice. These model simulations are evaluated using observations from two different sea ice stations, sampled off East Antarctica in early spring 2003 (ARISE, Lannuzel et al., 2007) and 2007 (SIPEX, van der Merwe et al., 2011b).

4.2 The model

4.2.1 Sea ice physics and thermodynamics

The LIM-1D model used in this study is a one-dimensional (vertical) sea ice model configured to reproduce the typical thermodynamic regimes of first-year Antarctic pack ice. The physics are based on the structure introduced by Maykut and Untersteiner (1971) and implemented for energy-conservation by Bitz and Lipscomb (1999). The brine dynamics follow Vancoppenolle et al. (2010), and snow-ice formation occurs when the snow load is heavy enough to depress the ice below seawater level, and the flooded surface refreezes (Vancoppenolle et al., 2009). The ice is represented by an uniform multi-layer (N layers = 10) column of ice, with thickness h_i, a bulk-salinity profile S, and temperature profile, T. The thickness of each layer increase (ice growth simulation) or decrease (ice decay simulation) at each time step. The temperature is computed by solving the heat diffusion equation in the N layers of ice (Vancoppenolle et al., 2007). Salt advection-diffusion equations are used to compute the change in ice salinity and simulate natural brine convection and percolation (Vancoppenolle et al., 2010). Each layer of ice is characterised by a brine volume, e_z, and a bulk- and brine salinity, Sz and σ_z, respectively. The heat budget between the ocean, the ice, and the atmosphere determines the change in ice and snow thickness.

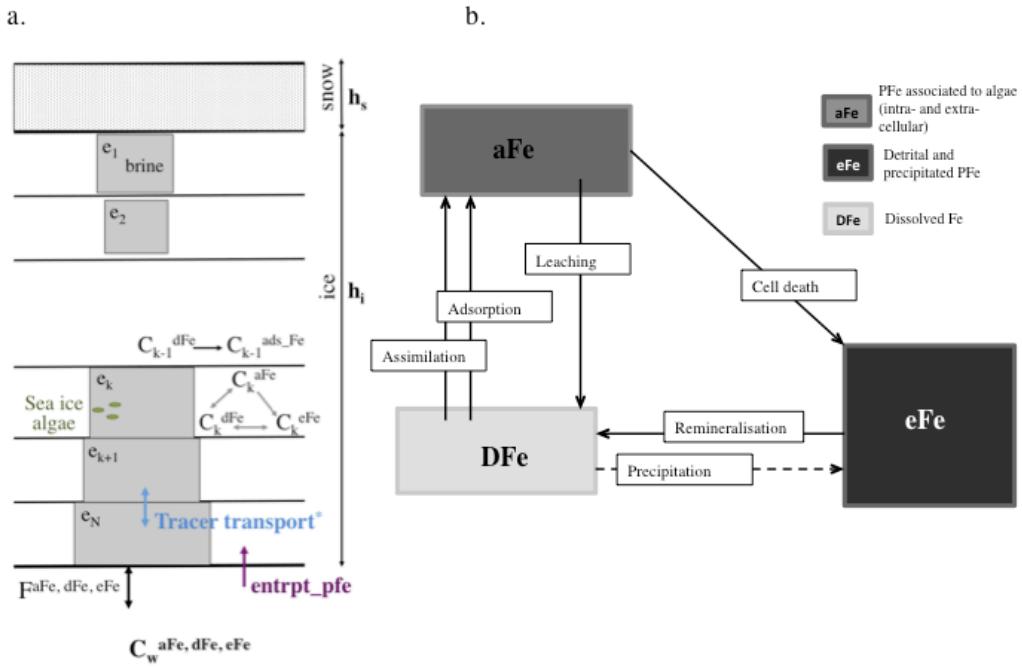

Figure 4.1 Schematic representation of a) the vertical grid in the LIM-1D model, where C_k (k = 1, …, N) refers to bulk (= ice + brine) tracer concentrations in the kth layer. h_s is the snow thickness and h_i is the ice thickness, $F^{aFe, dFe, eFe}$ the ocean-ice aFe, dFe and eFe flux, $C_w^{aFe,dFe,eFe}$ the seawater aFe, dFe, eFe concentrations, e_k the brine of volume of the kth layer. The blue arrow represents the transport of tracer between layers of ice. The purple arrow represents the initial entrapment of PFe (aFe + eFe) when sea ice grows, and b) the biogeochemistry of Fe in the model. The squares represent the pool of Fe (aFe, eFe and dFe). The arrows between pools represent the processes affecting the different pools of Fe. Note that the precipitation is represented with dashed line because currently not used in the model.

4.2.2 Representation of Fe in the model

4.2.2.1 Sources of Fe in the model

The main source of Fe to sea ice comes from the Fe-depleted seawater (Lannuzel et al., 2016). In this study we consider the ocean as an infinite reservoir of Fe for sea ice. Atmospheric dust input in the Southern Ocean is generally considered small (Gao et al., 2013; Mahowald et al., 2005; Wagener et al., 2008) except in localised areas near the coast (de Jong et al., 2013). We therefore do not consider any potential input of Fe to the uppermost layer of sea ice as a result of dust deposition, precipitation, snow ice formation or surface flooding.

4.2.2.2 Initial Fe enrichment in sea ice

4.2.2.2.1 Entrapment of PFe

Observations have shown that only physical processes are responsible for Fe enrichment at the onset of sea ice formation (chapter 2, Janssens et al., 2016). Therefore, we simulate the fraction of particulate material incorporated in the ice during ice growth as being proportional to its original seawater concentration (C_{sw}). Based on results from *in situ* ice-growth experiments, we introduce an entrapment factor for PFe (and particulate organic carbon, POC) which is equivalent to the enrichment index introduced by Gradinger and Ikävalko (1998), entpt_pfe > 1, to reproduce the initial enrichment of PFe in sea ice, as.

$$\text{entpt\_pfe} = \frac{C_{ice}^{PFe}}{C_{sw}^{PFe}} \frac{Sal_{sw}}{Sal_{ice}} \quad (4.1)$$

$$\text{entpt\_poc} = \frac{C_{ice}^{POC}}{C_{sw}^{POC}} \frac{Sal_{sw}}{Sal_{ice}} \quad (4.2)$$

where $C_{ice}^{PFe/POC}$ and $C_{sw}^{PFe/POC}$ are the bulk PFe and POC concentration in the ice and in the seawater, respectively. $Sal_{ice}$and $Sal_{sw}$are the bulk-ice salinity and the salinity of the seawater, respectively.

4.2.2.2.2 Adsorption of DFe

Dissolved biogeochemical tracers follow existing brine dynamics evolution and biogeochemistry theory, already implemented in the model. In previous versions of the model the adsorption of dissolved tracers, onto brine walls and/or organic matter, was not represented. Lannuzel et al. (2016) calculated the theoretical concentration of DFe in brines $[DFe]^{br}$ using the equation 5.3, and have shown that up to 90% of DFe in sea ice is not expunged by brine drainage but is actually retained within the ice.

$$[DFe]^{br} = \frac{[DFe]}{\Phi_{br}} \quad (4.3)$$

Where $[DFe]^{br}$ is the theoretical concentration of DFe in the brines (in nmol L^{-1}), $[DFe]$ is the concentration of DFe in the bulk sea-ice sample (in nmol L^{-1}), and Φ_{br} is the brine fraction.

As such, we implement the model with an adsorption factor for DFe, 0 < ads_dfe < 1, determined from observations as:

$$\text{ads\_dfe} = \frac{MeasuredC_{brine}^{DFe}}{[DFe]^{br}} \quad (4.4)$$

At every time step, the fraction of DFe that is subject to brine dynamics is (1-ads_dfe)*DFe.

4.2.2.3 Biogeochemistry and dynamic of Fe in the model

Three pools of Fe are represented in the model (Figure 4.1 b): (1) The particulate iron associated with algae (both intracellular and extracellular), aFe, (2) the detrital and precipitated particulate iron, eFe, and (3) the dissolved iron, DFe. In the model, we diagnose the particulate Fe as PFe = aFe + eFe. Exchanges between the three pools in the sea ice are governed by the main biogeochemical processes described below.

Assimilation (referred here as synthesis, syn_fe) by microorganisms transfers the DFe into the aFe pool.

$$\text{syn\_fe} = f_{syn}^{Fe}.r_{syn}.C_{DFe} \quad (4.5)$$

Precipitation of DFe increases the eFe concentration via

$$\text{pcp\_fe} = 0 \quad (4.6),$$

and is set to zero due to lack of observational data for parameterisation.

Cells death (lysis) transfers the aFe to the eFe fraction.

$$\text{lys\_fe} = f_{lys}^{Fe}.r_{lys}.C_{aFe} \quad (4.7)$$

The DFe fraction is replenished by respiration of the aFe fraction,

$$\text{rsp\_fe} = f_{rsp}^{Fe}.r_{rsp.}C_{aFe} \quad (4.8)$$

and by remineralisation of the eFe fraction (Figure 4.1 b);

$$\text{rem\_fe} = f_{rem}^{Fe}.r_{rem}.C_{eFe} \quad (4.9)$$

Where r_x in equations (4.5), (4.7), (4.8) and (4.9) is the rate of the process x (s^{-1}) as computed for carbon; f_x^{Fe} (dimensionless) specifies how much faster (>1) or slower (<1) the process transfers Fe from a pool to the other as compared to carbon transfer. This illustrates the decoupling between the carbon cycle and the Fe cycle. This representation allows to vary the Fe:C ratio in algae and detrital organic matter. For example, if f_{rem}^{Fe} = 10, Fe is remineralised 10 fold faster than carbon. C_{dFe}, C_{aFe}, and C_{eFe} are concentrations of DFe, PFe associated to algae and detrital particulate Fe (nmol L^{-1}) in the layer N, respectively (Fig. 4.1 a, b).

4.3 Experiments/ model set-up

4.3.1 Observations used for model evaluation

The model was parameterised with *in situ* data from the AWECS voyage and model outputs were compared with results from two field-studies conducted off East Antarctica.

1. Antarctic Winter Ecosystem Climate Study (AWECS) voyage

The rates of entrapment of PFe and adsorption of DFe were calibrated using results from two *in situ* ice-growth experiments (referred here as AWECS Exp 1 and AWECS Exp 2) carried out under trace metal clean conditions in the Weddell Sea, during Antarctic winter 2013 (July – August) onboard *RV Polarstern*. These experiments were designed to reproduce the first 48 hours of sea ice growth. Over the period, samples from both the ice and the underlying seawater were analyzed for physical (temperature, salinity, ice texture) and biogeochemical properties (chlorophyll *a* (Chl *a*), macro-nutrients, PFe and DFe, extracellular polymeric

substances (EPS) and bacterial count). A full description of the experimental set-up is given in chapter 2 (Janssens et al., 2016).

2. Antarctic Remote Ice Sensing Experiment (ARISE) voyage

Ice cores and seawater were sampled from a pack-ice floe during the ARISE voyage onboard *RV Aurora Australis* in September/October 2003 between 64˚- 65˚ S and 112˚ - 119˚ E. Trace metal sampling strategy and biogeochemical regimes are described in detail in Lannuzel et al. (2007) and Becquevort et al. (2009). In this study we target stations characterised by thermodynamic ice growth (i.e., they showed no deformation (e.g., rafting or ridging which cannot be represented in LIM-1D) as determined by thin section analysis), and where adequate atmospheric forcing was available.

3. Sea Ice Physics and Ecosystems eXperiment (SIPEX) voyage

Similarly, ice cores and seawater were sampled during the SIPEX voyage onboard the *RV Aurora Australis*. This third field campaign took place in September – October 2007 in the East Antarctic sector (110˚ - 130˚ E). A description of the physics and biogeochemistry of the ice relevant for this study is presented in van der Merwe et al. (2011b). Similar to ARISE, we selected appropriate stations characterised by thermodynamic growth and suitable atmospheric forcing.

4.3.2 Forcing and initialization

4.3.2.1 Forcings

AWECS: autumn - winter

External atmospheric forcing (air temperature, wind speed, air humidity, precipitations, incident short and long wave radiations) during AWECS were extracted from the shipboard data for the duration of both experiments.

ARISE and SIPEX: winter - spring

We used backward motion trajectories to retrace the initial locations of the sampled ice floes during ARISE and SIPEX, and then applied appropriate atmospheric forcing. Backward trajectories were calculated using a dataset of AMSR-E-derived maximum cross correlation sea ice motion vectors (Kimura, 2004). For each floe we obtain one position/day going back to up to 200 days preceding the actual sampling day (Figure 4.2). Using these dates and locations we extracted the corresponding atmospheric forcing using NCEP-NCAR reanalysis for air temperature, air humidity and wind speed (Kalnay et al. (1996), 4-time daily values averaged into daily values), monthly snowfall values and daily values for incident short and long waves radiations. Start of the sea ice formation denotes the start of the simulation. The simulation stops on the day of sampling. The duration of the simulation is determined by the number of days of simulation that leads to a match between the modelled and observed ice thickness (Table 4.1).

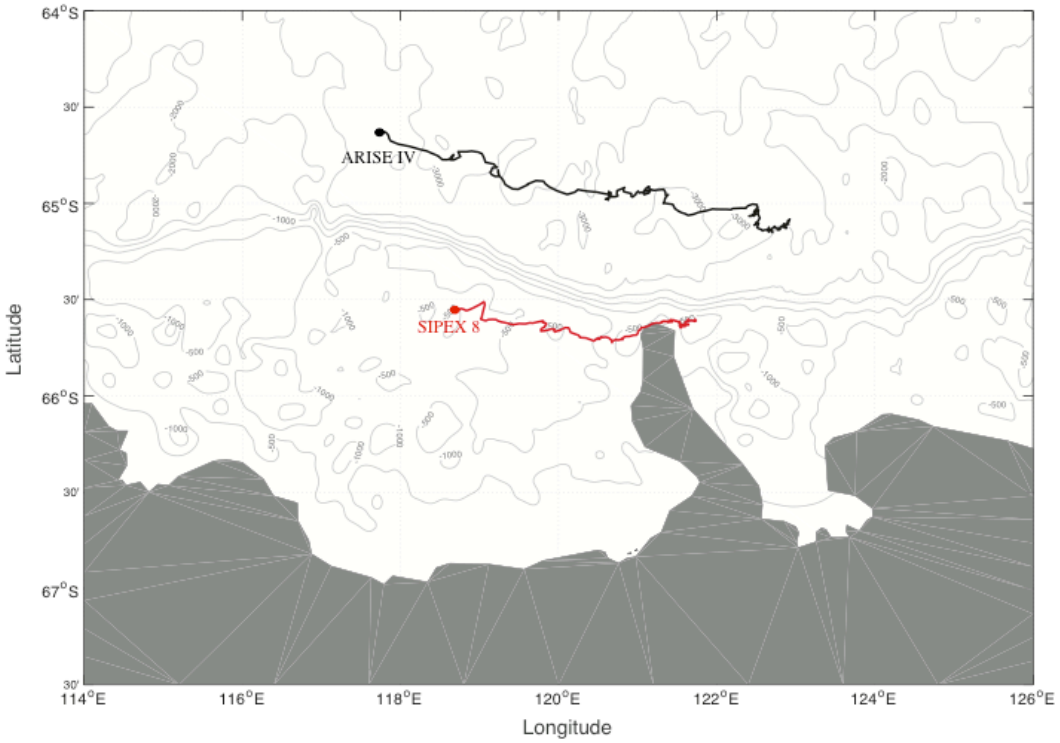

Figure 4.2 Back trajectories of station ARISE IV (in back) and SIPEX 8 (in red) in the sea ice zone. Sampling location is denoted with the dot.

4.3.2.2 Initialization of the model

The model is initialized with 0.02 m of ice for AWECS simulations and 0.05 m for the ARISE and SIPEX simulations.

Dissolved macro-nutrients (nitrate + nitrite = NO_x, silicic acid = $Si(OH)_4^-$, and phosphate = PO_4^{3-}), POC, Chl *a* and Fe concentrations in sea ice are initialized using averaged sea ice concentration measured during the 4 time steps of each AWECS experiments (Exp 1 and Exp 2). We used *in situ* seawater concentrations measured at the start of each AWECS experiments, which were considered constant in time.

Similarly, concentrations measured during AWECS Exp 1 (average sea ice and seawater concentrations) were used to initialize the model for the 'CTRL_awecs' run for ARISE and SIPEX simulations. We use AWECS Exp 1 initialization because the fit of the model with the observations was slightly better than in AWECS Exp 2.

Since we used back trajectories it was not possible to know what was the concentration of the seawater at the time of sea ice formation. Our choice of initializing with AWECS measurements is justified by that fact that they are the only Southern Ocean Fe data available for seawater and young Antarctic sea ice for late autumn/early winter. We performed sensitivity analysis of the model to different initial sea ice and seawater conditions (see section 4.3.3.2). Initial conditions are summarised in Tables 4.1 and 4.3.

Table 4.1 Parameters used to initialize stations ARISE IV and SIPEX 8, and final ice thickness vs modelled ice thickness for stations ARISE IV and SIPEX 8

Station name	**Start of the simulation**	**End of the simulation[a]**	**Simulation length (days)**	**H_{i0} (m)**	**Observed ice thickness (m)**	**Modelled ice thickness (m)**
ARISE IV	05. 05. 2003	01. 10. 2003	150	0.05	0.48 - 0.52	0.52
SIPEX 8	07. 06. 2007	25. 09. 2007	110	0.05	0.345	0.33

[a] End of the simulation = sampling day

4.3.3 Sensitivity analysis

4.3.3.1. AWECS experiments: calibration of Fe entrapment and adsorption

Parameters and initial concentrations in the model were weakly constrained. To illustrate how the processes represented in the model influence the DFe and PFe concentrations at the onset of sea ice formation, several sets of values for entpt_pfe and ads_dfe were tested (Table 4.2). We use ranges from *in situ* time-series ice-growth experiments for entpt_pfe (chapter 2, Janssens et al., 2016), and *in situ* data from Lannuzel et al. (2016) for ads_dfe. Entpt_pfe ranged between 3 and 40 (average = 10, n = 8) during AWECS Exp 1 and AWECS Exp 2. Ads_dfe can be up to 0.9 (which means that up to 90 % of the DFe is retained in the brine system). The control run ('CTRL_awecs') for AWECS Exp 1 and AWECS Exp 2 is calibrated to

reproduce concentrations as close as possible to concentrations observed during both field experiments, using one set of parameters.

Table 4.2 Runs performed to test the sensibility of the model to the representation of entpt_pfe and ads_dfe, and the ability of the model to represent dissolved and particulate Fe in young sea ice. Entpt_pfe is the entrapment of PFe (chapter 2), and ads_dfe is the adsorption of DFe (Lannuzel et al., 2016).

Run	Name	entpt_pfe	ads_dfe
1	CTRL_awecs	6	0.75
2	low_entpt-low_ads	3	0.5
3	high_entpt-low_ads	10	0.5
4	low_entpt-mid_ads	3	0.75
5	high_entpt-mid_ads	10	0.75
6	low_entpt-high_ads	3	0.9
7	high_entpt-high_ads	10	0.9

Values were fixed at entpt_pfe = 6 and ads_dfe = 0.75. The 'CTRL_awecs' run is compared to series of runs with lower and higher entpt_pfe and ads_dfe. The combinations tested are summarised in Table 4.2.

4.3.3.2 ARISE and SIPEX

We now evaluate the ability of the model to simulate Fe concentrations in sea ice collected in late winter to early spring, compared to AWECS, which was collected much earlier in the season. A first set of simulations was run to evaluate the effect of the initial concentrations on the vertical profiles of macro-nutrients, Chl *a*, POC and DFe and PFe. In the model, the POC = AoC + eoC (4.10), where AoC is the particulate organic carbon associated with algae (biogenic), and eoC is the detritic particulate organic carbon. The Chl *a* concentration is calculated using the AoC concentration:

$$Chl\ a = AoC \times r^{Chla/C} \times 12 \quad (4.11)$$

Where $r^{Chla/C}$ = 0.05 is the Chl *a*/C ratio in POC from Sarthou et al., (2005).

Beside the initiation analysis described above, we tested the influence of the remineralisation of PFe into DFe and the effects of high algal biomass on the Fe cycle. These runs are compared to the 'CTRL_awecs' run set-up (entpt_pfe = 6 and ads_dfe = 0.75). Table 4.3 provides an overview of the different runs and their parameterisations.

4.4 Results

4.4.1 AWECS experiments

4.4.1.1 Sea ice thermodynamics

Simulated ice temperature, ice salinity and brine volume were compared to mean observations. During the AWECS Exp 1 and Exp 2, one measurement was made per parameter for time step 6 hours, 12 hours and 24 hours. In the 48 hours time step, parameters were measured in the top and in the bottom section of the ice core. The average observation in the top section of the ice core in Figure 4.3, 4.4 and 4.5 represents the average observed concentration for steps 6 hours to 24 hours, and the top section of time step 48 hours (n = 4), and associated standard deviation. The

Table 4.3 Runs and parameterization performed for the stations ARISE IV and SIPEX 8. f^{Fe}_{rem} is the factor of transfer from Fe between different pools of Fe, as compared to the transfer of carbon between pools of carbon, dFe refers to the dissolved Fe in the model (DFe is the observed dissolved Fe), eFe is the detrital and precipitated particulate Fe, aFe is the particulate Fe associated with algae (both intracellular and extracellular), eoC is the detritic particulate organic carbon, and AoC is the particulate organic carbon associated with algae (biogenic).

Run	Name	f^{Fe}_{rem}	dFe ice (nmol L^{-1})	dFe sw (nmol L^{-1})	eFe ice (nmol L^{-1})	eFe sw (nmol L^{-1})	aFe ice (nmol L^{-1})[a]	aFe sw (nmol L^{-1})	eoC ice (μmol L^{-1})	eoC sw (μmol L^{-1})	AoC ice (μg L^{-1})	AoC sw (μg L^{-1})	NO_x ice (μmol L^{-1})	NO_x sw (μmol L^{-1})	PO_4^{3-} ice (μmol L^{-1})	PO_4^{3-} sw (μmol L^{-1})	$Si(OH)_4^-$ ice (μmol L^{-1})	$Si(OH)_4^-$ sw (μmol L^{-1})
1a	CTRL_awecs	1	1.12	0.64	14.18	4.51	4.	0.002	9.91	1.49	0.27	0.02	8.99	27.86	0.55	1.97	41.99	145.91
2a	sw_obs	1	18.6	2.40	49.15	0.50	4.	0.002	144	5.0	8.41	0.05	61.55	29.1	19.68	1.96	113.95	62.1
3a	bott_ice	1	18.6	16.7	49.15	69.39	4.	0.002	144	358	8.41	32.08	61.55	98.92	19.68	71.5	113.95	55.58
4a	low_rem_fe	0.1	18.6	2.40	49.15	0.50	4.	0.002	144	5.0	8.41	0.05	61.55	29.1	19.68	1.96	113.95	62.1
5a	high_rem_fe	2	18.6	2.40	49.15	0.50	4.	0.002	144	5.0	8.41	0.05	61.55	29.1	19.68	1.96	113.95	62.1
6a	high_biol	1	18.6	2.40	49.15	0.50	4	2.00	144	5.0	80.0	5.0	61.55	29.1	19.68	1.96	113.95	62.1
1s	CTRL_awecs	1	1.12	0.64	14.18	4.51	4.	0.002	9.91	1.49	0.27	0.02	8.99	27.86	0.55	1.97	41.99	145.91
2s	sw_obs	1	1.04	1.00	9.36	1.90	4.	0.002	13.86	1.98	0.189	0.01	8.57	27.93	0.55	1.67	11.78	59.16
3s	bott_ice	1	1.04	1.82	9.36	11.11	4.	0.002	13.86	13.28	0.189	0.789	8.57	8.28	0.55	0.48	11.8	13.1
4s	low_rem_fe	0.1	1.04	1.00	9.36	1.90	4.	0.002	13.86	1.98	0.189	0.01	8.57	27.93	0.55	1.67	11.78	59.16
5s	high_rem_fe	2	1.04	1.00	9.36	1.90	4.	0.002	13.86	1.98	0.189	0.01	8.57	27.93	0.55	1.67	11.78	59.16
6s	high_biol	1	1.04	1.00	9.36	1.90	4	2.00	13.86	1.98	80.0	5.0	8.57	27.93	0.55	1.67	11.78	59.16

bottom observation is the concentration measured in the bottom section of the ice core in time step 48 hours (n = 1). An exception is the temperature, which was measured every 0.02 m in the four ice cores. Thermodynamic properties of the ice are well represented by the model (Figure 4.3 a, b). Simulated temperatures range from ≈-12°C/-14°C (Exp 1/Exp 2) at the surface of the ice to ≈-2°C at the ice-water interface. Modelled salinity profiles show the expected increase of salinity at the bottom of the ice, associated with an increase in brine volume, which was computed from temperature and salinity according to Cox and Weeks (1988). Therefore, the slight overestimation of the temperature at the bottom of the ice is reflected in the brine volume, as illustrated in Figure 4.3 a, b for Exp 1 and Exp 2, respectively.

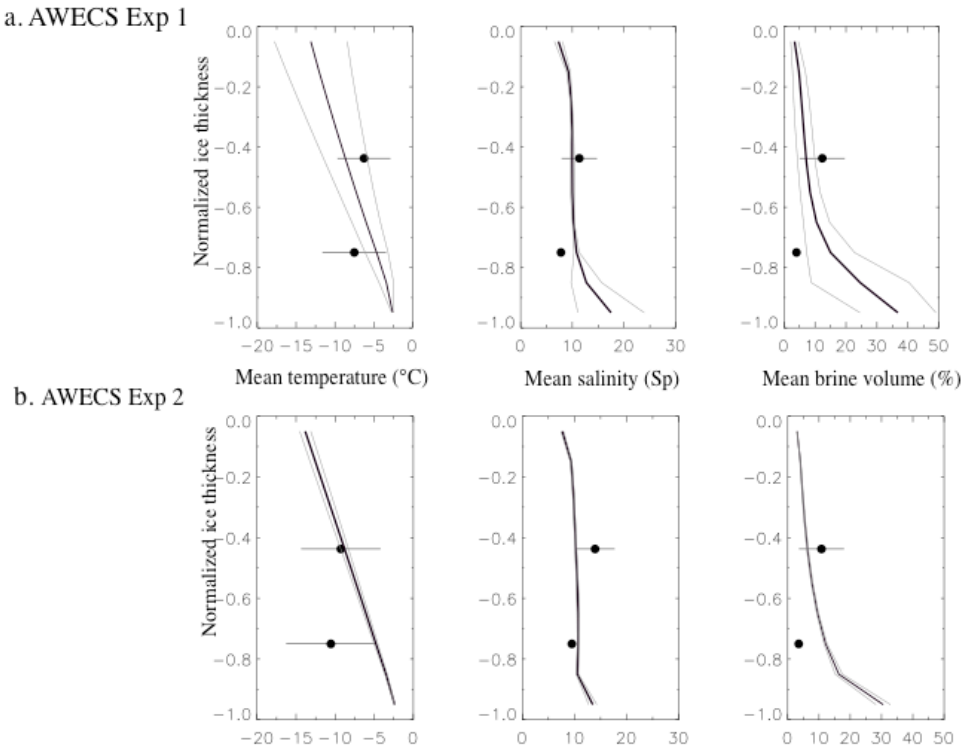

Figure 4.3 Normalized vertical profiles of mean (in black), minimum, and maximum (in grey) temperature (°C), salinity (S_p) and brine volume (%) for a) AWECS Exp 1 and b) AWECS Exp 2. The black dots are the mean observations and their associated standard deviation (n=4).

4.4.1.2 Macro-nutrients, particulate organic carbon and Chl *a*

Simulated concentrations of dissolved macro-nutrients are also in good agreement with observations (Figure 4.4 a, b). Similar to salinity, modelled macro-nutrient concentrations were slightly overestimated at the bottom of the ice. Generally, the model underestimates Chl *a* concentrations, which however remain in the same order of magnitude as the field observations in both experiments. Simulations are consistent between Exp 1 and Exp 2, and the shape of the macro-nutrients and Chl *a* profiles are similar in both experiments.

Particulate organic carbon concentrations are overestimated in Exp 1, and underestimated in Exp 2. In contrast to the macro-nutrient vertical profiles, the shape of the POC vertical profiles are not similar in Exp 1 and Exp 2. Particulate organic carbon concentration increases slightly with depth in Exp 1. In contrast with Exp 1, the minimum POC concentration is found at the bottom of the ice (4.81 μmol L^{-1}) and the maximum concentration near the surface of the ice (8.85 μmol L^{-1}). In these simulations, the processes controlling the initial incorporation of PFe and DFe (entpt_pfe and ads_dfe) do not affect the initial incorporation of dissolved macro-nutrients, Chl *a* and POC concentrations (Figure 4.4 a, b).

4.4.1.3 Dissolved and particulate iron

We analyzed the sensitivity of the model to the initial entrapment of PFe, and the adsorption of DFe in the brine system. First we notice that the entpt_pfe generates straight vertical profiles of PFe (except in the 'high_entpt – high_ads' run in AWECS Exp 1). Runs with low entpt_pfe showed flattened vertical profiles of both DFe and PFe. The lower the entpt_pfe is, the straighter the DFe vertical profile becomes. Implementation of higher entpt_pfe led to a stronger increase of modelled DFe in the middle of the ice cores, reflected by a decrease of the PFe concentration at the same

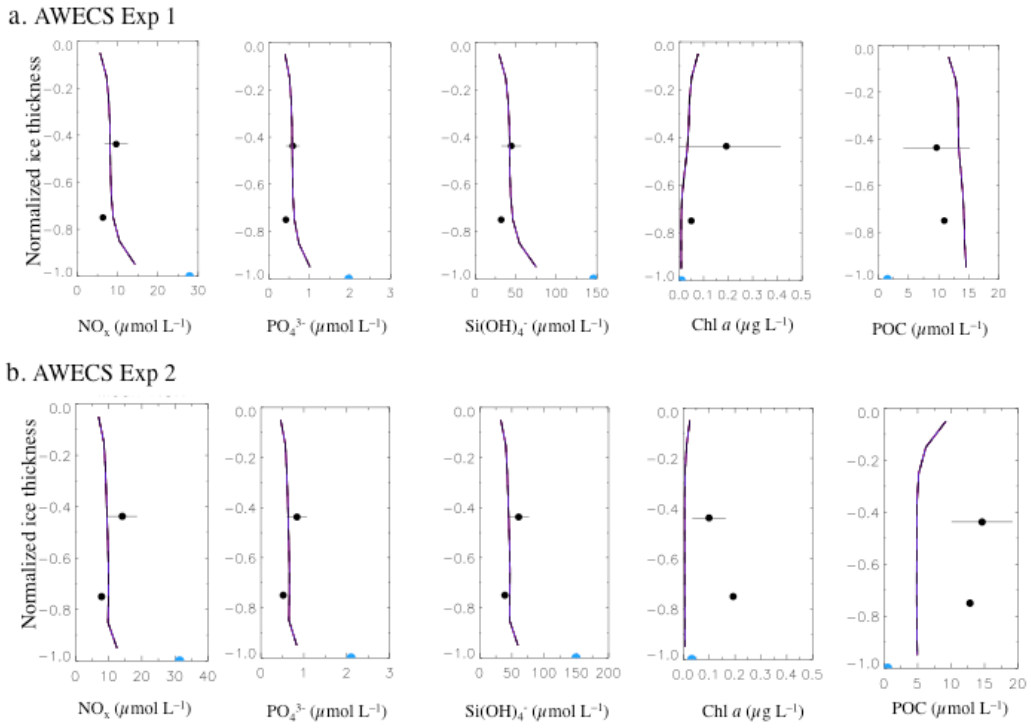

Figure 4.4 Normalized vertical profiles of mean concentrations of macro-nutrients (NO_x, $Si(OH)_4^-$ and PO_4^{3-}), Chl *a* (μg L^{-1}) and POC (in μmol L^{-1}) for a) AWECS Exp 1 and b) AWECS Exp 2. The black dots are the mean concentrations observed, the horizontal black line is the standard deviation (n=4), and the blue dot is the seawater concentration.

depth. Maximum observed values for entpt_pfe = 40 and ads_dfe = 0.9 led to unrealistically high PFe and DFe concentrations (results not shown). In contrast, the observed concentrations were not reproduced when using minimum values of entpt_pfe = 3 and ads_dfe = 0.1. Dissolved Fe profiles are affected by the strength of the entrapment of PFe and the strength of the adsorption of DFe, while PFe profiles are affected only by the strength of the entrapment of PFe. The DFe profile shows a "D-shape" (minimum concentration near the surface and in the bottom ice, maximum concentration in the middle of the ice column) in Exp 1. The DFe profile shows a straight vertical profile in Exp 2. Combined values of entpt_pfe = 6 and ads_dfe = 0.75 ('CTRL_awecs') led to the best estimation of both PFe and DFe profiles in both experiments. Mean simulated DFe concentrations in the 'CTRL_awecs' run ranged

from 1.14 to 2.17 nmol L^{-1} (average 1.77 nmol L^{-1}, n=10) in AWECS Exp 1, and 0.56 and 0.95 nmol L^{-1} (average 0.77 nmol L^{-1}, n=10) in AWECS Exp 2. These results are in the same order of magnitude as the observed DFe concentrations (Figure 4.5, black dashed line). The simulated PFe concentrations in AWECS Exp 1 varied between 20.20 nmol L^{-1} and 26.10 nmol L^{-1} (average 24.89 nmol L^{-1}, n=10), and between 8.82 nmol L^{-1} and 15.40 nmol L^{-1} (average 9.72 nmol L^{-1}, n=10) in AWECS Exp 2.

Note that for PFe profiles the 'low_entpt-low_ads' and the 'low_entpt-high_ads' runs are both masked behind the 'low_entpt-high_ads' profile in Figure 4.5 a, b. Similarly, 'low_entpt-low_ads' and 'low_entpt-mid-ads' runs are hidden behind the 'high_entpt-high' run in Figure 4.5 a, b.

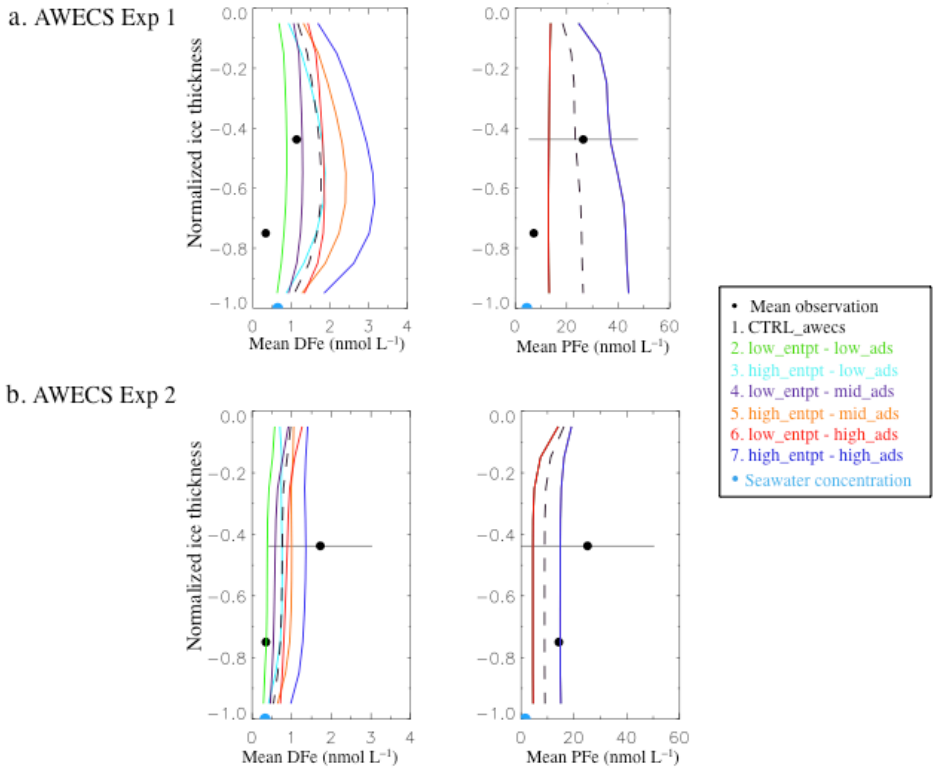

Figure 4.5 Normalized vertical profiles of mean dissolved (DFe, nmol L^{-1}) and particulate Fe (PFe = eFe + aFe, nmol L^{-1}) concentrations for a) AWECS Exp 1, and b) AWECS Exp 2. The black dots are the mean concentrations (nmol L^{-1}) observed and the horizontal line is the standard deviation (n=4), and the blue dot is the seawater concentration (nmol L^{-1}). The CTRL_awecs run is represented by the dashed black line.

4.4.2 Representation of ARISE and SIPEX stations

4.4.2.1 Sea ice thermodynamics

Station ARISE IV and SIPEX 8 were the 2 only stations fulfilling the selection criteria of thermodynamic growth conditions and available adequate forcing. Start and end times of the simulations for each station are summarised in Table 4.1. Modelled final ice thicknesses match the observations within the centimetre-scale for both stations (Table 4.1). The model reproduces the vertical profiles of ice temperature, bulk-salinity and brine volume for both stations with good accuracy (Figure 4.6 a for ARISE IV, and 4.7 a for SIPEX 8).

The model shows rapid ice growth until the end of July, when the ice growth eases for a few days, and then starts again to reach its maximum ice thickness (≈ 0.63 m) during the end of July for station ARISE IV. Ice melt is moderate between end of July and September. During the last month of the simulation, the ice thickness stays relatively constant (Figure 4.6 b). A similar pattern is observed for SIPEX 8. Here, the maximum ice thickness was reached in mid-July, and was approximately 0.5 m (Figure 4.7 b). Temperatures in the ice are colder earlier in the season and match closer to atmospheric temperatures at the sea ice surface than at the ice-ocean interface. For both stations, we observed a warming event of the ice in July, and a corresponding increase of brine volume. As expected, brine volume followed the same pattern than the ice temperature.

4.4.2.2 Representation of the sea ice biogeochemistry

4.4.2.2.1 Effect of initial concentrations

Using the same values for parameters and initial concentrations as the 'CTRL_awecs' run in AWECS Exp 1, the model performs relatively poorly to quantitatively, and qualitatively, reproduce macro-nutrient observations (Figure 4.8 and 4.9, black dashed

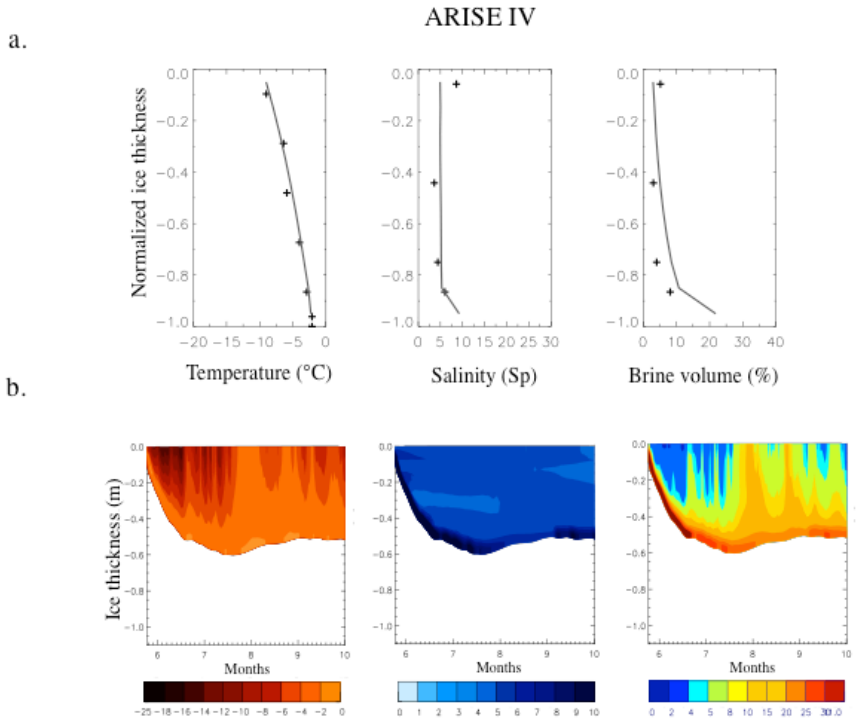

Figure 4.6 a) Normalized vertical profiles of temperature (°C), salinity (S_p) and brine volume (%) (dark grey lines) and corresponding observations (black crosses) for ARISE IV. The ice thickness is normalized. b) Contoured temperature (°C), salinity (S_p) and brine volume (%). Horizontal and vertical axes refer to months and ice thickness (m), respectively. Contours plots show the evolution of sea ice from the start of the simulation to the end of the simulation (sampling date).

line). Dissolved macro-nutrients concentrations are generally underestimated in both stations (except for $Si(OH)_4^-$ in SIPEX 8), and the general C-shape of their profiles is not represented by the model. Both PO_4^{3-} and NO_x are underestimated in ARISE IV and SIPEX 8, but to a lesser extent in SIPEX 8. Similar results are observed for Chl *a* and POC concentrations. In an attempt to get closer to the observed concentration, in the 'sw_obs' run, the ice is initialized with the averaged ice concentrations measured

on the respective stations rather than AWECS data. Similarly, seawater is initialized with respective underlying seawater measured on the sampling day. However, the shape of the modelled profile is not affected by this modification in neither ARISE IV

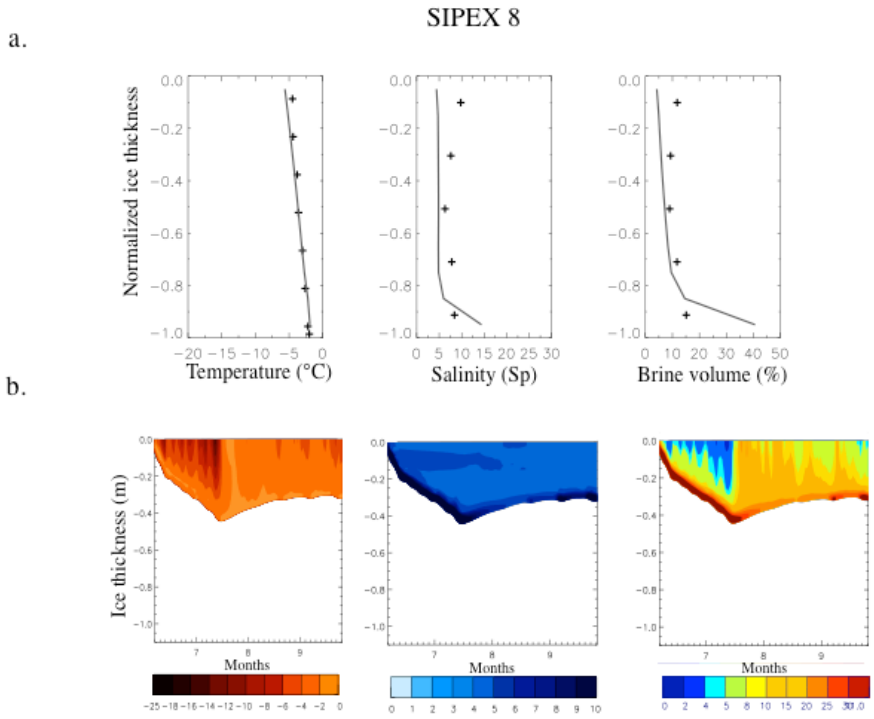

Figure 4.7 a) Normalized vertical profiles of temperature, (°C), salinity (Sp) and brine volume (%) (dark grey lines) and corresponding observations (black crosses) for SIPEX 8, b) contoured temperature (°C), salinity (S_p) and brine volume (%). Horizontal and vertical axes refer to months and ice thickness (m), respectively. Contours plots show the evolution of sea ice from the start of the simulation to the end of the simulation (sampling date).

nor SIPEX 8 (Figure 4.8 and 4.9, green dotted line). The L-shape of the macro-nutrients (and POC) vertical profiles remains in SIPEX 8. The L-shape is less distinct in ARISE IV.

Simulation of DFe portraits two different profiles between ARISE IV and SIPEX 8 (see also Figure 4.10 for a zoom in). The 'CTRL_awecs' run overestimates the DFe concentrations in both ARISE IV and SIPEX 8. The 'sw_obs' run led to a better simulation of the DFe profile, but still overestimated DFe in SIPEX 8. Simulated PFe

concentrations remain considerably below observed concentrations at both stations and for each run (Figure 4.8 and 4.9).

In the 'bott_ice' run, the initial seawater concentration is set to be equivalent to the bottom ice concentration observed at station ARISE IV (Figure 4.8, dotted blue line) and SIPEX 8 (Figure 4.9, dotted blue line). The initial concentration of ice stays unchanged compared to the 'sw_obs' run. Macro-nutrients, Chl *a* and POC vertical profiles are strongly affected by this modification, both qualitatively and quantitatively. This parameterisation results in simulated concentrations that are much higher than the observed concentrations (except Chl *a*, which does not increase strongly in ARISE IV). The general shape of the profiles fluctuates as well. A S-shape is observed for the macro-nutrient profiles in ARISE IV, a Z-shape for POC, and Chl *a* stays very low with a slight increase at the bottom of the ice and around 0.6 (normalized ice thickness). The increase of macro-nutrients and Chl *a* all occur at the same depth. For station SIPEX 8, the 'bott_ice' run leads to the closest match between modelled profiles and observations.

The general shape of Fe profiles is relatively similar for both stations. However, the 'bott_ice' run drives large overestimation of the DFe concentrations, e.g., up to 2 orders of magnitude in ARISE IV. Here, the effect of the 'bott_ice' run on the PFe is limited to an increase of PFe in the bottom ice section only (Figure 4.8 and 4.9, blue dotted line). Despite the large increase of the PFe concentration in the seawater, profiles in the ice are consistently underestimated by the model. The bottom ice section in SIPEX 8 is the only portion accurately represented by the model using this set-up. Although the profiles need to be refined, these results show that the initialization is crucial to reproduce observed concentrations with the model.

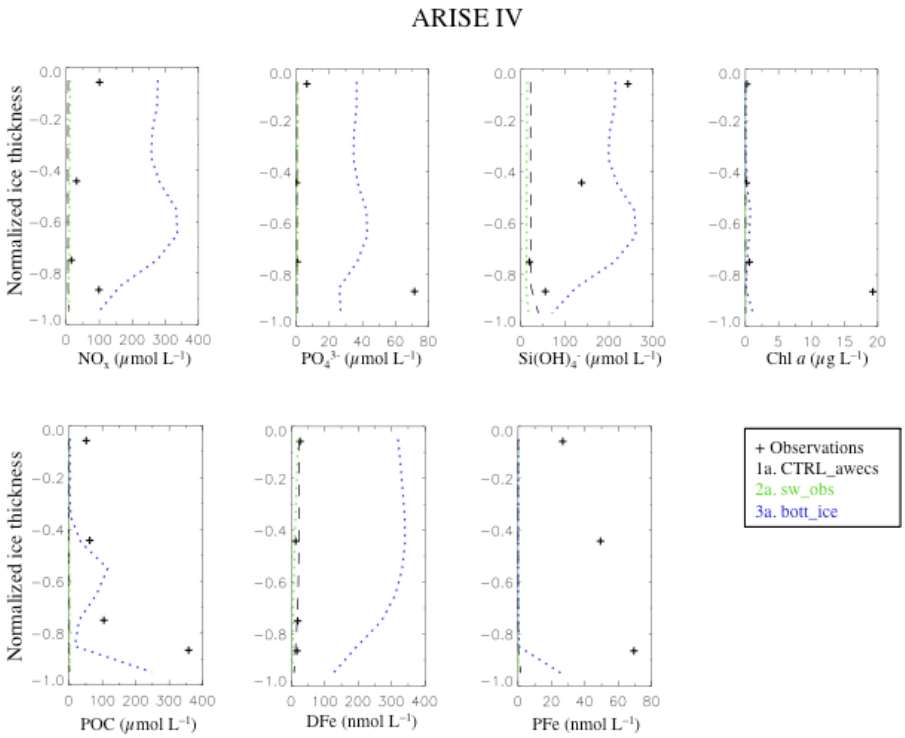

Figure 4.8 Normalized vertical profiles of macro-nutrients (NO_x, $Si(OH)_4^-$ and PO_4^{3-} in μmol L^{-1}), Chl *a* (μg L^{-1}), POC (μmol L^{-1}) and dissolved and particulate Fe (nmol L^{-1}) in ARISE IV when varying the initial concentrations. Observed concentrations are shown with the black crosses.

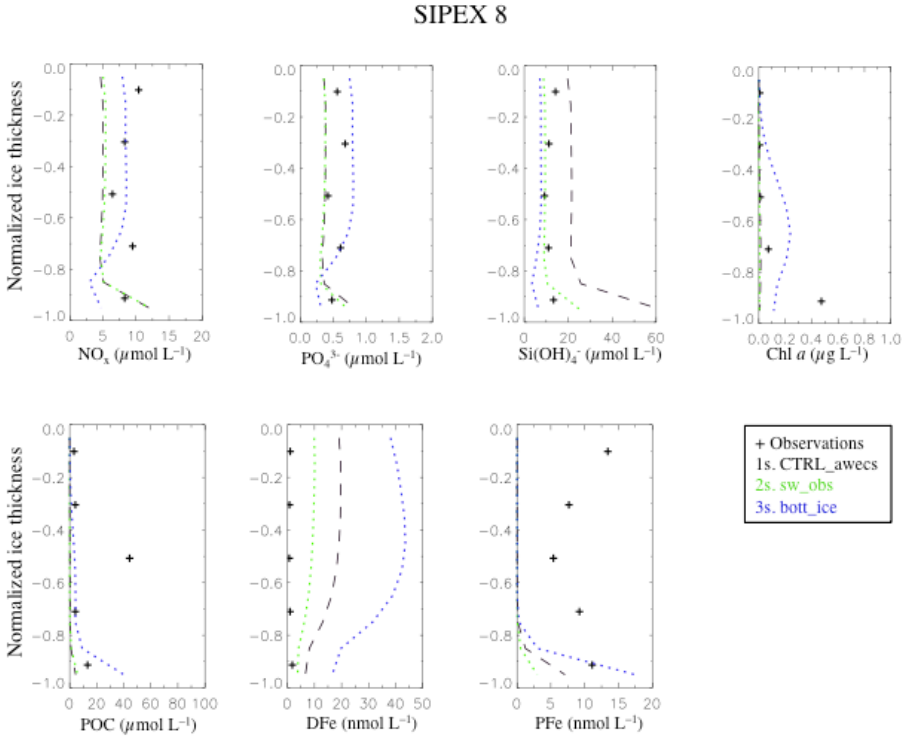

Figure 4.9 Normalized vertical profiles of macro-nutrients (NO_x, $Si(OH)_4^-$ and PO_4^{3-} in μmol L^{-1}), Chl *a* (μg L^{-1}), POC (μmol L^{-1}) and dissolved and particulate Fe (nmol L^{-1}) in SIPEX 8 when varying the initial concentrations. Observed concentrations are shown with the black crosses.

4.4.2.2.2 Key parameters controlling the biogeochemistry of Fe

This part focuses on refining the representation of Fe in sea ice. Therefore, for the sake of clarity, only DFe and PFe profiles are displayed for the following runs. In this set of runs, we varied the value of the f_{rem}^{Fe} (equation (4.10)), which is equivalent to modifying the remineralisation rate of Fe as compared to the remineralisation of carbon. The 'low_rem_fe' (Figure 4.10, plain purple line) run and the 'high_rem_fe' run (Figure 4.10, plain orange line) were initialized with the same concentrations than the 'sw_obs' run (Figure 4.10, dotted green line). For easier comparison, 'CTRL_awecs' run and 'sw_obs' run are also represented in Figure 4.10. As expected, lower remineralisation increases the concentration of PFe, and slightly decreases the DFe concentrations compared to the 'sw_obs' run. Particulate Fe and DFe vertical profiles are mirrored in SIPEX 8: the maximum PFe concentration corresponds to the minimum DFe concentration and vice versa (Figure 4.10 b). The observed high concentration of PFe near the ice surface is not accurately represented in SIPEX 8, in any of the runs. However, this is well represented by the 'low_rem_fe' run in ARISE IV.

In the previous runs, aFe (particulate Fe associated to algae) concentration was negligible compared to eFe concentration (eFe >> aFe). In the last run, 'high_biol', the initial conditions of aFe are significantly increased in both the ice and the seawater (Table 4.3). Simultaneously, we also increased the initial sea ice and seawater Chl *a* concentration. Although DFe concentration remains too low in the bottom ice, the representation of the profile of DFe is improved in ARISE IV. The shape of the DFe profile in SIPEX 8 stays unchanged, but slightly higher concentrations are observed compared to the previous runs. Particulate Fe is not affected by the higher initial sea ice and seawater Chl *a* concentration in ARISE IV. A

slight increase of the PFe at depth > 0.2 (normalized thickness) slightly improved the representation of PFe profile in SIPEX 8 compared to the "high_rem_fe' and 'CTRL_awecs' runs. A similar increase is observed in the Chl *a* and POC profiles (result not shown). Parameterization of processes driving Fe dynamics in sea ice has therefore a bigger impact on PFe and DFe profiles than the increase of Chl *a* (used as a proxy for sea ice algae) in the model.

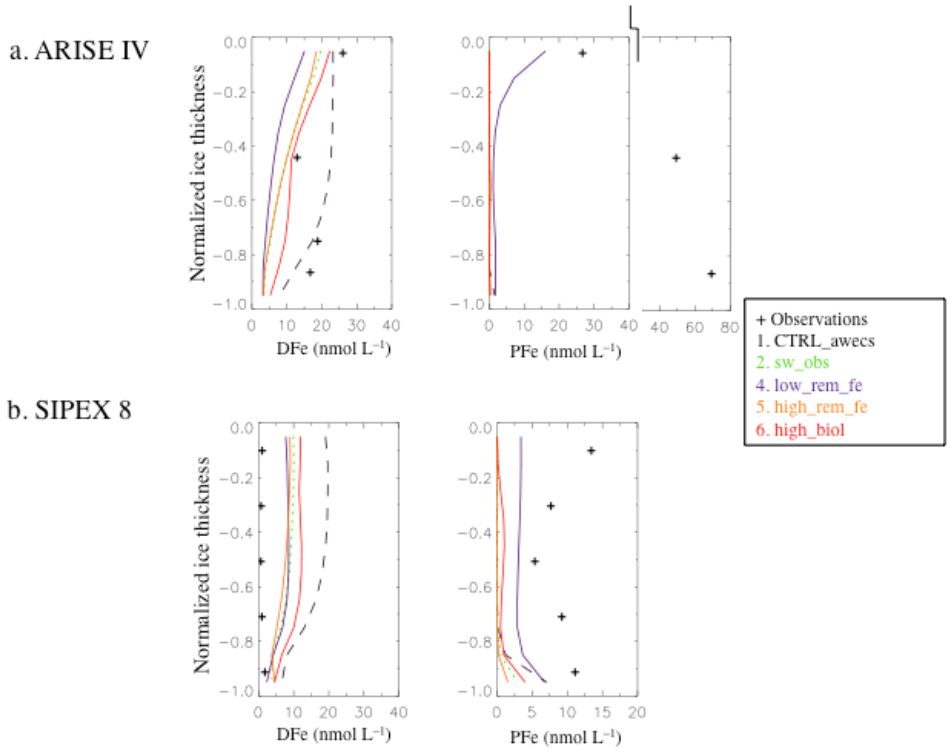

Figure 4.10 Normalized vertical profiles of dissolved and particulate Fe (nmol L^{-1}) in a) ARISE IV, and b) SIPEX 8 when varying parameters affecting the biogeochemistry of Fe. They are compared to the CTRL_awecs run (dashed black line) and the sw_obs run (dotted green line). The black crosses show the observations. In ARISE IV, the observed concentration of PFe being much higher than the simulated PFe concentration, the observations are shown on a different portion of plot using a larger scale.

4.5 Discussion

4.5.1 Sea ice thermodynamic and biogeochemistry

The modelled temperature, salinity and brine volume profiles are in quantitative and qualitative agreement with the observations for both young ice (AWECS) and older

ice (ARISE IV and SIPEX 8). The loss of brine due to the extraction of the core is known to underestimate the bulk salinity of the sample (Notz et al., 2005). This could explain the slight difference between the modelled and the observed salinity (and therefore brine volume) profiles during AWECS simulations.

Although the dissolved macro-nutrients follow the brine dynamic in the model (Vancoppenolle et al., 2010), the model performs poorly at reproducing their vertical profiles in ARISE IV. On the contrary, nutrients profiles are relatively well represented in SIPEX 8, AWECS Exp 1 and Exp 2. It is considered that the ice in AWECS Exp 1, Exp 2 and SIPEX 8 was unaltered by biological activity (van der Merwe et al., 2011b; chapter 2, Janssens et al., 2016), as opposed to a more important biomass in ARISE IV (Lannuzel et al., 2007). Given the difficulty to initialize with the correct nutrients and POC profiles in back trajectory model simulations, and the coarse representation of primary production in the model (Moreau et al., 2015; Vancoppenolle et al., 2010; Vancoppenolle and Tedesco, 2016), the lack of biomass in SIPEX 8, AWECS Exp 1 and AWECS Exp 2 may explain the better representation by the model of the biologically unaltered *in situ* nutrients profiles. The poor representation of Chl *a* could likely be improved by the addition of a parameter accounting for the initial physical enrichment of algae observed in newly formed sea ice, similar to what has been introduced in this work for PFe and POC. Gradinger and Ikävalko (1998) and chapter 2 show that algae are highly enriched in the ice at the start of sea ice formation. This process is currently not represented in any model.

As the purpose of this chapter is to investigate the representation of Fe dynamic in sea ice, rather than an investigation of the nutrient, POC and Chl *a* profiles, and the sources of error for their misrepresentation, the following discussion will focus on Fe, unless the other parameters provide additional support for elucidating Fe dynamics.

4.5.2 Discussion on the representation of Fe profiles

The analysis of the simulated DFe and PFe profiles provides valuable information on the relative importance of the different processes driving the budget of Fe in the ice.

4.5.2.1 Young ice vs older ice

In this section the main discrepancy between the representation in young ice (AWECS experiments) and older ice (ARISE IV and SIPEX 8) are discussed.

While chapter 2 (Janssens et al., 2016) has shown that only physical processes were significant to account for the initial enrichment of Fe in young sea ice, as the season progresses, biological activity (and later melting) is an important process in controlling the size fractionation and concentrations of Fe in sea ice (Lannuzel et al., 2007). Consequently, the model performs well at representing the accumulation of PFe in young sea ice. Profiles resulting from entrapment during basal ice formation are reasonably well represented by the model (AWECS). However, the model performs poorly when the observed concentrations are the results of both physical and biological processes (ARISE IV and to a lesser extent, SIPEX 8). For AWECS, although the initial physical enrichment is not represented in the model for DFe (other than the enrichment due to brine convection), the ads_dfe prevents most of the DFe from being rejected by brine convection into the ocean, consequently leading to enrichment of Fe in sea ice. Although the adsorption of DFe in Lannuzel et al. (2016) accounts for ice collected later in the season, these runs show that mechanisms responsible for adsorption of DFe in the brine system (either on the walls or associated to organic matter) are also valid for very young sea ice. One of the proposed reasons for the high adsorption of DFe is the association of DFe with sticky organic matter (e.g., EPS, Lannuzel et al., 2015; van der Merwe et al., 2009, chapter 2). These results suggest that DFe would be directly enriched and retained in the ice

with the EPS, or rapidly binding to EPS once in the ice. This result contrasts with macro-nutrients which strictly follow brine dynamics when no biological activity is represented (Vancoppenolle et al., 2010). The relative high uncertainties associated to the bottom ice DFe and PFe concentrations are attributed to the low resolution of the observations in AWECS Exp 1 and AWECS Exp 2. Overall, modelled concentrations and general shape of the vertical Fe profiles are relatively well represented by the model in the case of newly formed sea ice.

We might therefore consider that the amendment of the model with an entpt_pfe and and ads_dfe factor is a reasonable approach to reproduce the physical enrichment of both PFe and DFe in young sea ice. Unfortunately, this is not sufficient to accurately represent Fe concentration profiles in older sea ice. Other processes must be represented (Figures 4.8, 4.9 and 4.10). The following paragraphs explain the approaches adopted to improve the Fe representation in sea ice collected later in the season.

4.5.2.2 Effect of the initial Fe concentration

Similar to macro-nutrients, POC and Chl *a*, DFe and PFe concentrations are not accurately represented by the model in ARISE IV and SIPEX 8 when using the AWECS Exp 1 'CTRL_awecs' run. Van der Merwe et al. (2009) found that the concentration of Fe in the ice depends on the concentrations in the seawater from which the sea ice had formed. To test that hypothesis, we changed the initial Fe concentrations of seawater in the 'sw_obs' and 'bott_ice' runs (and concentrations of macro-nutrients, POC and Chl *a*). The model results support the hypothesis that seawater and initial sea ice concentrations play a strong role in Fe distribution in sea ice. Moreover, the 'bott_ice' run is the most affected by these modifications. Importantly, these runs also show that the seawater concentration has a greater

influence on results than the sea ice concentration initialization set-up. When seawater is initialized with concentrations equivalent to the bottom ice concentration ('bott_ice' run), and initial ice concentration stays unchanged compared to previous run ('sw_obs'), both shape and magnitude of the macro-nutrients and DFe profiles are affected. At this stage, the seawater column in the model has fixed concentrations (no profile), and thus it remains difficult to evaluate the best concentration to use to force the model. It might be more realistic to set the seawater concentration with concentrations measured a few meters under the ice; alternatively concentration measured in the skeletal layer, e.g., directly at the ice-ocean interface, could be used? The model shows that different compounds respond differently to this initialization, as illustrated for DFe, and also Chl *a* (Figure 4.8 and 4.9). Finally, it is important to keep in mind that the seawater concentrations are constant throughout the entire duration of the simulations, while in the field, is it likely that this concentration varies through the seasonal ice cycle, leading to varying enrichment efficiency.

Contrary to DFe, PFe is not well represented in any of these three runs, in any of the ARISE IV and SIPEX 8 stations (Figure 4.8 and 4.9). The PFe profiles for all three simulations are very similar, with the exception of the bottom ice in the 'bott_ice' run. Despite this, the simulated concentrations remain much lower than the observations. Specifically, higher concentrations of PFe near the surface of the ice are currently not well represented by the model. This can be partially explained by the fact that mechanisms supplying Fe to the upper layer of the ice are not taken into account in this study. Flooding of the ice replenishes the uppermost parts of the ice in Fe from seawater (Lannuzel et al., 2007; Meiners and Michel, 2016). Moreover, when sea ice growth stops (mid-to-end of July), the physical enrichment of PFe stops, and mechanisms driving the fluxes between the different sea ice reservoirs of Fe take

over, depleting the PFe pool in the current parameterization set-up. Therefore, at the end of the simulation, the initial enrichment of PFe is considered to be 'concealed' by the biogeochemical transformations encountered by PFe. Contrary, DFe supply to sea ice occurs during the entire simulation, through convective exchange with seawater and the bottom layers of the ice. This could be an explanation for the overestimations of the DFe concentrations and the under-respresentation of PFe concentrations in the model.

4.5.2.3 Influence of the biologically mediated processes between PFe and DFe

We have seen previously that when dynamics of Fe is governed by physical processes only, the model performs well at representing the vertical profiles. Currently biological processes, such as e.g., remineralisation of PFe into DFe by heterotrophic organisms and conversion of DFe into biogenic PFe via uptake by sea ice algae, are not well constrained. In this section the uncertainties in coefficients chosen to represent the biological activity in the model and their effects on PFe and DFe profiles are discussed. In the 'low_rem_fe' and 'high_rem_fe' runs the remineralisation rate of PFe into DFe has been decreased to 10% of the rate of the carbon remineralisation, and increased to 200% of the rate of carbon remineralisation, respectively to evaluate the influence of this parameter. The value used for remineralisation of carbon is probably too high, which could partially explained why the simulated profiles are not very accurate. With the 'low_rem_fe' run we expect to see an increase in the PFe concentration and a decrease of the DFe concentration. This is what is observed in the model results, although the *in situ* profiles are not accurately represented. Generally, runs 'low_rem_fe' and 'high_rem_fe' overestimate the DFe and underestimate de PFe concentrations. There are four possible explanations for these results: (1) First, the constant used to compute the

remineralisation of PFe is likely to be too high, even in the "low_rem_fe' run. If the remineralisation is too important, the PFe pool is over-depleted, and the replenishment of DFe is too important. This is what we observed in the PFe and DFe profiles (Figure 4.10 a and b).

(2) Secondly, in these simulations, precipitation of DFe into PFe is set to 0. When not bond to organic ligands, DFe can precipitate and form oxyhydroxides in the particulate size range (Boye et al., 2001; de Baar and de Jong, 2001). Although no observations are currently available about the rate of this mechanism in sea ice, it is possibly that Fe precipitation is a significant process transforming DFe into PFe, therefore impacting the dynamics of Fe in sea ice. An accurate representation of the precipitation rate would be a major step forward towards a better representation of the balance of the fluxes between these two reservoirs in the model.

(3) Thirdly, conversion of DFe to PFe does not only happen as a result of precipitation. Van der Merwe et al. (2011b) observed conversion of DFe into biogenic PFe via uptake by ice algae in basal layers during the SIPEX voyage. Therefore, better parameterization of the biologically mediated exchanges between pools of Fe is of primary importance to improve the representation of Fe profiles, and investigate bioaccumulation of DFe in ice algae and bacteria. (4) Finally, lithogenic PFe can be an important contribution to the pool of PFe in the ice, especially in the fast ice, or in the pack ice formed on the continental shelf (Lannuzel et al., 2014a). Current version of the model does not depict the lithogenic PFe, potentially missing an important source of PFe to the ice. This is particularly true for SIPEX 8 that formed and drift very close to the Antarctic continent (Figure 4.2), and was therefore under the influence of more Fe of lithogenic origin than ARISE IV (Lannuzel et al., 2014b, 2007; van der Merwe et al., 2011a).

A recent study from Lannuzel et al. (in prep) found that the decrease of DFe in sea ice cannot be fully explained by biological uptake only. The reduction of DFe concentration is likely a combination of both sea ice algae consumption and thermodynamical processes, which is in the line with findings from the model.

Finally, in the last run, 'high_biol' the initial concentration of the PFe associated to algae (aFe) was increased to 4 nmol L^{-1} and 2 nmol L^{-1} in the ice and the seawater, respectively. Concurrently, the carbon associated to algae (AoC) was increased to mimic the increase in primary productivity. This last result shows that, both PFe and DFe profiles are strongly influenced by autotrophic processes in the model. The change of these variables slowly shapes the PFe and DFe profiles towards a better representation of the observations. In summary, we have shown that initial concentrations, remineralisation of PFe into DFe, and autotrophic activity act in combination, and need further investigation to better decipher the Fe dynamics in sea ice.

4.5.3 Suggested improvements for further development of the model

Considering, that this is the first representation of Fe in a sea ice biogeochemical model, a few improvements are suggested to further the development of this model.

Introduction of an 'entpt_chla'

We believe that, with the better parameterisation of the fluxes between the different reservoirs of Fe, a better representation of the biological activity in the model is a key element toward an accurate representation of the Fe dynamic by the model. A first step is to enrich the ice in primary producers at the onset of sea ice formation. The introduction of an 'entpt_chla' would stand to represent the physical enrichment of sea ice in algae as observed in Gradinger and Ikävalko (1998), and in chapter 2 (Janssens et al., 2016).

Coupling Fe cycle with carbon cycle

Marine carbon and Fe cycles are tightly coupled and controlled by complex interactions of competition and synergy between different members of the microbial community (Fourquez et al., 2015). Moreover, many studies suggest that the enrichment of organic matter and Fe are coupled when trapped in the ice (Lannuzel et al., 2015, 2007; Schoemann et al., 2008). As currently represented in the model, the Fe cycle is independent of the carbon cycle. It would be advantageous to better connect these two essential cycles in the model, e.g., by the addition of a relationship between POC and Fe. Schoemann (personal communication) found two relationships between POC and detrital PFe in the ice. The relationships are different depending on the season (autumn/winter vs spring). Improvement of the model with this relation would likely improve the representation of both PFe and POC.

Precipitation of Fe and role of organic ligands

We have seen that the accurate estimation of the precipitation of Fe is a key element for a better representation of the PFe and DFe profiles. Organic ligands have been shown to control the DFe concentration in sea ice (Lannuzel et al., 2016), and keep the DFe in solution (Boye et al., 2001; de Baar and de Jong, 2001). Therefore, an accurate representation of the organic ligands (including EPS) in the model is a necessity to be able to parameterize the precipitation.

Lithogenic Fe

Presently PFe is represented by the intra and extra cellular Fe associated to algae (aFe) and the detritic PFe (eFe). PFe from lithogenic origin is currently not depicted in the model. However, (Lannuzel et al., 2014b) showed that 79 % of PFe in Antarctic fast ice can be of lithogenic origin. This contribution is believed to be less in the pack ice (modelled in this study) due to the remoteness of the ice from near-shore sources

(Lannuzel et al., 2014b). Nonetheless, an improved implementation of the model, which includes a reservoir of lithogenic Fe and associated fluxes, would contribute to a better representation of the Fe profiles.

Interaction between physical and biogeochemical processes in sea ice

All the runs performed in this study show that the thermodynamic and physics of the ice are not affected by the changing biogeochemical parameters. However EPS have been found to affect the habitability of the ice, altering the physical properties of the ice and the saline retention (Krembs et al., 2011). As currently represented in the model, dissolved nutrients follow the brine dynamic (Vancoppenolle et al., 2010). In return, the brine dynamic is not affected by the presence of organic matter, which therefore, limit the accuracy of the representation of the observations. This needs further investigation, and is an improvement that could be made in future version of the model.

4.6 Conclusion

To conclude, the model performs well in representing the vertical distribution in Fe in young sea ice and in older sea ice not altered by biological activity. The introduction of the entpt_pfe and ads_dfe is an acceptable way to account for the physical enrichment of PFe and DFe. Nonetheless, the model performs relatively poorly when biological processes are affecting *in situ* concentrations.

Initial sea ice and seawater concentrations are of paramount importance to simulates the sea ice vertical profiles of macro-nutrients, Chl *a*, POC and Fe. Later in the simulation however, it is crucial to better constrain the parameters regulating the fluxes between pools of Fe, and introduce a representation of the lithogenic PFe. In future versions of the model it is central to introduce a more realistic representation of

the biological processes by a better parameterization of the rate of each processes (e.g., remineralisation, lyse, precipitation). At this early stage of the development of the model this is not possible to reproduce the temporal evolution of Fe using this setup and parameterisation. Indeed, more work needs to be done firstly to be able to accurately reproduce the observed vertical profiles.

This work highlights the difficulty of representing and constraining the complex mechanisms driving Fe dynamic in sea ice, mechanisms that are themselves currently not well quantified. Nonetheless we have presented a good first representation of Fe in sea ice and suggested improvement for future work.

References

Aguilar-Islas AM, Rember RD, Mordy CW, Wu J. 2008. Sea ice-derived dissolved iron and its potential influence on the spring algal bloom in the Bering Sea. *Geophys Res Lett* 35:10–14. doi:10.1029/2008GL035736

Arrigo KR. 2014. Sea ice ecosystems. *Ann Rev Mar Sci* 6:439–67. doi:10.1146/annurev-marine-010213-135103

Becquevort S, Dumont I, Tison J-L, Lannuzel D, Sauvée M-L, Chou L, Schoemann V. 2009. Biogeochemistry and microbial community composition in sea ice and underlying seawater off east Antarctica during early spring. *Polar Biol* 32:879–895. doi:10.1007/s00300-009-0589-2

Bitz CM, Lipscomb WH. 1999. An energy-conserving thermodynamic model of sea ice. *J Geophys Res* 104:15669. doi:10.1029/1999JC900100

Boyd PW, Ellwood MJ. 2010. The biogeochemical cycle of iron in the ocean. *Nat Geosci* 3:675–682. doi:10.1038/ngeo964

Boye M, Van Den Berg CMG, de Jong JTM, Leach H, Croot P, de Baar HJW. 2001. Organic complexation of iron in the Southern Ocean. *Deep Res Part I Oceanogr Res* 48:1477–1497. doi:10.1016/S0967-0637(00)00099-6

Cox GFN, Weeks WF. 1988. Numerical simulations of the profile properties of undeformed first-year sea ice during the growth season. *J Geophys Res* 93:2449–12460. doi:10.1029/JC093iC10p12449

de Baar HJW, de Jong JTM. 2001. Distributions, Sources and Sinks of Iron in Seawater. (in) The biogeochemistry of iron in seawater. Eds: Turner DR, Hunter KA. IUPAC Series on Analytical and physical chemistry of environment systems, Wiley. pp:123–253.

de Jong J, Schoemann V, Maricq N, Mattielli N, Langhorne P, Haskell T, Tison J-L. 2013. Iron in land-fast sea ice of McMurdo Sound derived from sediment resuspension and wind-blown dust attributes to primary productivity in the Ross Sea, Antarctica. *Mar Chem* 157:24–40. doi:10.1016/j.marchem.2013.07.001

de Jong JTM, Stammerjohn SE, Ackley SF, Tison J-L, Mattielli N, Schoemann V. 2015. Sources and fluxes of dissolved iron in the Bellingshausen Sea (West Antarctica): The importance of sea ice, icebergs and the continental margin. *Mar Chem* 177:518–535. doi:10.1016/j.marchem.2015.08.004

Fourquez M, Obernosterer I, Davies DM, Trull TW, Blain S. 2015. Microbial iron uptake in the naturally fertilized waters in the vicinity of the Kerguelen Islands : phytoplankton – bacteria. *Biogeosciences* 12:1893–1906. doi:10.5194/bg-12-1893-2015

Gao Y, Xu G, Zhan J, Zhang J, Li W, Lin Q, Chen L, Lin H. 2013. Spatial and particle size distributions of atmospheric dissolvable iron in aerosols and its input to the Southern Ocean and coastal East Antarctica. *J Geophys Res Atmos*

118:12634–12648. doi:10.1002/2013JD020367

Gradinger R, Ikävalko J. 1998. Organism incorporation into newly forming Arctic sea ice in the Greenland Sea. *J Plankton Res* 20:871–886. doi:10.1093/plankt/20.5.871

Grotti M, Soggia F, Ianni C, Frache R. 2005. Trace metals distributions in coastal sea ice of Terra Nova Bay, Ross Sea, Antarctica. *Antarct Sci* 17:289–300. doi:10.1017/s0954102005002695

Holland MM, Bitz CM, Tremblay B. 2006. Future abrupt reductions in the summer Arctic sea ice. *Geophys Res Lett* 33:1–5. doi:10.1029/2006GL028024

Janssens J, Meiners KM, Tison J-L, Dieckmann G, Delille B, Lannuzel D. 2016. Incorporation of iron and organic matter into young Antarctic sea ice during its initial growth stages. *Elem Sci Anthr* 4:123. doi:10.12952/journal.elementa.000123

Kalnay E, Kanamitsu M, Kistler R, Collins W, Deaven D, Gandin L, Iredell M, Saha S, White G, Woollen J, Zhu Y, Chelliah M, Ebisuzaki W, Higgins W, Janowiak J, Mo KC, Ropelewski C, Wang J, Leetmaa A, Reynolds R, Jenne R, Joseph D. 1996. The NCEP/NCAR 40-year reanalysis project. *Bull Am Meteorol Soc* 77:437–471. doi:10.1175/1520-0477(1996)077<0437:TNYRP>2.0CO;2

Kanna N, Toyota T, Nishioka J. 2014. Iron and macro-nutrient concentrations in sea ice and their impact on the nutritional status of surface waters in the southern Okhotsk Sea. *Prog Oceanogr* 126:44–57. doi:10.1016/j.pocean.2014.04.012

Kimura N. 2004. Sea ice motion in response to surface wind and ocean current in the Southern Ocean. *J Meteor Soc Japan Ser. II* 82:1223-1231. doi: 10.2151/jmsj.2004.1223

Krembs C, Eicken H, Deming JW. 2011. Exopolymer alteration of physical properties of sea ice and implications for ice habitability and biogeochemistry in a warmer Arctic. *Proc Natl Acad Sci U.S.A* 108:3653–8. doi:10.1073/pnas.1100701108

Lancelot C, de Montety A, Goosse H, Becquevort S, Schoemann V, Pasquer B, Vancoppenolle M. 2009. Spatial distribution of the iron supply to phytoplankton in the Southern Ocean: a model study. *Biogeosciences Discuss* 6:4919–4962. doi:10.5194/bgd-6-4919-2009

Lannuzel D, Chever F, van der Merwe PC, Janssens J, Roukaerts A, Cavagna A-J, Townsend AT, Bowie AR, Meiners KM. 2014a. Iron biogeochemistry in Antarctic pack ice during SIPEX-2. *Deep Sea Res Part II Top Stud Oceanogr* 131:111-122. doi:10.1016/j.dsr2.2014.12.003

Lannuzel D, Grotti M, Luisa AM, van der Merwe P. 2015. Organic ligands control the concentrations of dissolved iron in Antarctic sea ice. *Mar Chem* 174:120-130. doi:10.1016/j.marchem.2015.05.005

Lannuzel D, Fourquez M, de Jong J, Tison J-L, Delille B, Schoemann V. in prep. Antarctic sea-ice algae: results from in situ and temperature controlled short-term radiotracer incubation.

Lannuzel D, Schoemann V, de Jong J, Chou L, Delille B, Becquevort S, Tison J-L. 2008. Iron study during a time series in the western Weddell pack ice. *Mar Chem* 108:85–95. doi:10.1016/j.marchem.2007.10.006

Lannuzel D, Schoemann V, de Jong J, Pasquer B, van der Merwe P, Masson F, Tison J-L, Bowie A. 2010. Distribution of dissolved iron in Antarctic sea ice: Spatial, seasonal, and inter-annual variability. *J Geophys Res* 115:G03022. doi:10.1029/2009JG001031

Lannuzel D, Schoemann V, de Jong J, Tison J-L, Chou L. 2007. Distribution and biogeochemical behaviour of iron in the East Antarctic sea ice. *Mar Chem* 106:18–32. doi:10.1016/j.marchem.2006.06.010

Lannuzel D, van der Merwe PC, Townsend AT, Bowie AR. 2014b. Size fractionation of iron, manganese and aluminium in Antarctic fast ice reveals a lithogenic origin and low iron solubility. *Mar Chem* 161:47–56. doi:10.1016/j.marchem.2014.02.006

Lannuzel D, Vancoppenolle M, van der Merwe P, de Jong J, Meiners KM, Grotti M, Nishioka J, Schoemann V. 2016. Iron in sea ice: Review and new insights. *Elem Sci Anthr* 4:130. doi:10.12952/journal.elementa.000130

Mahowald NM, Baker AR, Bergametti G, Brooks N, Duce RA, Jickells TD, Kubilay N, Prospero JM, Tegen I. 2005. Atmospheric global dust cycle and iron inputs to the ocean. *Global Biogeochem Cycles* 19:GB4025. doi:10.1029/2004GB002402

Maykut GA, Untersteiner N. 1971. Some results from a time-dependent thermodynamic model of sea ice. *J Geophys Res* 76:1550–1575. doi:10.1029/JC076i006p01550

Meiners KM, Michel C. 2017. Dynamics of nutriments, dissolved organic matter and exopolymers in sea ice. (in) Sea Ice, 3rd Edition. Eds: Thomas, DN. ISBN: 9781118778388

Moreau S, Vancoppenolle M, Bopp L, Aumont O, Madec G, Delille B, Tison J-L, Barriat P-Y, Goosse H. 2016. Assessment of the sea-ice carbon pump: Insights from a three-dimensional ocean-sea-ice biogeochemical model (NEMO-LIM-PISCES). *Elem Sci Anthr* 4:122. doi:10.12952/journal.elementa.000122

Moreau S, Vancoppenolle M, Delille B, Tison J-L, Zhou J, Kotovitch M, Thomas DN, Geilfus N-X, Goosse H. 2015. Drivers of inorganic carbon dynamics in first-year sea ice: A model study. *J Geophys Res Ocean* 120:471–495. doi:10.1002/2014JC010388

Notz D, Wettlaufer JS, Worster MG. 2005. Instruments and Methods A non-

destructive method for measuring the salinity and solid fraction of growing sea ice in situ. *J Glaciol* 51:159–166. doi:10.3189/172756505781829548

Sarthou G, Timmermans KR, Blain S, Tréguer P. 2005. Growth physiology and fate of diatoms in the ocean: a review. *Journal of Sea Research* 53:25-42. doi: 10.1016/j.seares.2004.01.007

Schoemann V, de Jong JTM, Lannuzel D, Tison J-L, Dellile B, Lei C, Lancelot C, Becquevort S. 2008. Microbiological control on the cycling of Fe and its isotopes in Antarctic sea ice. *Geochim Cosmochim Acta* 72:A837.

Sedwick PN, DiTullio R. 1997. Regulation of algal blooms in Antarctic shelf waters by the release of iron from melting sea ice. *Geophys Res Lett* 24:2515–2518. doi:10.1029/97GL02596

Serreze MC, Holland MM, Stroeve J. 2007. Perspectives on the Arctic's shrinking sea-ice cover. *Science* 315:1533–1536. doi:10.1126/science.1139426

Tedesco L, Vichi M, Haapala J, Stipa T. 2010. A dynamic Biologically Active Layer for numerical studies of the sea ice ecosystem. *Ocean Model* 35:89–104. doi:10.1016/j.ocemod.2010.06.008

Tovar-Sánchez A, Duarte CM, Alonso JC, Lacorte S, Tauler R, Galbán-Malagón C. 2010. Impacts of metals and nutrients released from melting multiyear Arctic sea ice. *J Geophys Res* 115:C07003. doi:10.1029/2009JC005685

van der Merwe P, Lannuzel D, Bowie AR, Meiners KM. 2011a. High temporal resolution observations of spring fast ice melt and seawater iron enrichment in East Antarctica. *J Geophys Res* 116:G03017. doi:10.1016/2010JG001628

van der Merwe P, Lannuzel D, Bowie AR, Mancuso Nichols CA, Meiners KM. 2011b. Iron fractionation in pack and fast ice in East Antarctica: Temporal decoupling between the release of dissolved and particulate iron during spring melt. *Deep Res Part II Top Stud Oceanogr* 58:1222–1236. doi:10.1016/j.dsr2.2010.10.036

van der Merwe P, Lannuzel D, Mancuso Nichols CA, Meiners K, Heil P, Norman L, Thomas DN, Bowie AR. 2009. Biogeochemical observations during the winter–spring transition in East Antarctic sea ice: Evidence of iron and exopolysaccharide controls. *Mar Chem* 115:163–175. doi:10.1016/j.marchem.2009.08.001

Vancoppenolle M, Bitz CM, Fichefet T. 2007. Summer landfast sea ice desalination at Point Barrow, Alaska: Modeling and observations. *J Geophys Res Ocean* 112:1–20. doi:10.1029/2006JC003493

Vancoppenolle M, Fichefet T, Goosse H, Bouillon S, Madec G, Maqueda MAM. 2009. Simulating the mass balance and salinity of Arctic and Antarctic sea ice. 1. Model description and validation. *Ocean Model* 27:33–53. doi:10.1016/j.ocemod.2008.10.005

Vancoppenolle M, Goosse H, de Montety A, Fichefet T, Tremblay B, Tison J-L. 2010. Modeling brine and nutrient dynamics in Antarctic sea ice: The case of dissolved silica. *J Geophys Res Ocean* 115:C02005. doi:10.1029/2009JC005369

Vancoppenolle M, Meiners KM, Michel C, Bopp L, Brabant F, Carnat G, Delille B, Lannuzel D, Madec G, Moreau S, Tison J-L, van der Merwe P. 2013. Role of sea ice in global biogeochemical cycles: emerging views and challenges. *Quat Sci Rev* 79:207–2030. doi:10.1016/j.quascirev.2013.04.011

Vancoppenolle M, Tedesco L. 2016. Numerical modelling of sea ice biogeochemistry Numerical models of sea ice biogeochemistry. (in) Sea Ice. Eds: Thomas, DN. *in press*. doi:10.13140/RG.2.1.2402.0324

Wagener T, Guieu C, Losno R, Bonnet S, Mahowald N. 2008. Revisiting atmospheric dust export to the Southern Hemisphere ocean: Biogeochemical implications. *Global Biogeochem Cycles* 22:1–13. doi:10.1029/2007GB002984

Wang S, Bailey D, Lindsay K, Moore K, Holland M. 2014. Impacts of sea ice on the marine iron cycle and phytoplankton productivity. *Biogeosciences* 11:4713–4731. doi:10.5194/bg-11-4713-2014

CHAPTER 5

General conclusion and perspectives

The aim of this thesis was to investigate the processes of incorporation of Fe and organic matter in newly-formed sea ice. In this thesis I combined measurements from a field study and results from laboratory sea-ice growth experiments to explore the pathways leading to the enrichment of Fe and organic matter in sea ice. Findings from chapters 2 and 3 were then used to implement the LIM 1-D sea ice biogeochemical model with the representation of Fe, and perform a first parameterization, and evaluation of the model.

5.1 General findings

Chapter 2 reports the first Fe measurements in the autumn/winter season, providing valuable insights in the Fe cycle associated with sea ice at the early stages of sea ice formation. The results clearly highlight that particles are enriched in sea ice from the onset of sea ice formation. Larger particles have higher enrichment indices than smaller sizes. Physical processes alone are responsible for this initial enrichment. Desalinisation processes did not impact particulate material. Particulate Fe and DFe seem to be decoupled when trapped in the ice. When combined with results from van der Merwe et al. (2011b) in spring, PFe and DFe distributions in sea ice are thought to be decoupled throughout the whole year.

In the next chapter I carried out laboratory-based ice-growth experiments under controlled conditions to explore the role of organic matter as a Fe carrier from seawater to the ice. These experiments constitute the first sea-ice formation experiments performed under trace metal clean conditions, and in laboratory-

controlled conditions. Results showed that the enrichment efficiency is regulated by the quality rather than the quantity of material present in the initial seawater. I first showed that the enrichment of autochtonous organic material was higher than the enrichment of allochtonous organic material. Biogenic PFe was more enriched than lithogenic PFe in the sea ice, and is likely driven by the presence of EPS of algal origin. UV exposure degraded the organic matter in the seawater (including organic ligands) and altered the association of Fe and organic material, leading to lower enrichment of PFe and DFe in sea ice. This suggests that organic ligands, such as EPS, could play an important role in the enrichment of Fe.

Natural and artificial enrichment indices obtained respectively from chapters 2 and 3 (Table 5.1) show that the initial enrichment of PFe is more variable than the initial enrichment of the DFe. This supports previous findings that sea ice DFe concentrations are more homogenous than the PFe concentrations (Lannuzel et al., 2016).

Table 5.1 Summary of enrichment indices for PFe and DFe in AWECS Exp 1 and 2 (chapter 2), natural young ice (chapter 2), and laboratory ice growth experiments (chapter 3)

	AWECS Exp 1	**AWECS Exp 2**	**Natural young ice**	**Lab experiment non-UV treated**	**Lab experiment UV treated**
PFe	18.5 ± 15.3	40.0 ± 32.3	301 ± 240	2.2 ± 2.2	0.35 ± 0.2
DFe	5.6 ± 0.88	12.5 ± 8.7	24 ± 10	2.2 ± 0.6	2.3 ± 1.5

Finally, preliminary results from the LIM 1-D study showed that the model is more sensitive to the initialization than the biogeochemical parameterisations chosen to drive the Fe dynamics within the sea ice. Although DFe and PFe are relatively well represented in young ice and older ice with low biomass, the model performs poorly in older sea ice (longer simulations) affected by biological activity. The poorly quantified parameters driving the Fe biogeochemical cycle (e.g., rate of Fe uptake,

role of organic ligands, remineralisation and precipitation), and the absence of representation of lithogenic PFe in the model are responsible for this gap between observation and simulated profiles.

5.2 Future work

Transferring the knowledge gained from biogeochemical processes studied here at the micro-scale (e.g., in the brine system or at the ice/water interface) to macro-scale (e.g., size of an ice floe), and then into global predictions in a changing environment (e.g., global modelling) is very challenging.

Although this work has shed some light on processes leading to enrichment in organic material and Fe in sea ice, new pressing questions have emerged. Based on the findings from this thesis, the following section suggests directions for future work to be carried out in order to improve the understanding of the Fe cycle associated to sea ice, and its role in the Southern Ocean, and develop future predictions in rapidly changing environment.

5.2.1 Improvement of spatial and temporal resolutions

Although this work provides the first Fe measurement of sea ice in austral winter, and despite the increasing amount of field studies in the past few years, Fe data around Antarctica remain sparse, and are principally limited to the spring and summer seasons. A better spatial (Pacific and Atlantic sector of the Southern Ocean) and temporal resolution (austral autumn and winter) would be an important step towards the resolution of the Fe cycle, and the improved understanding of its impacts and links on the carbon cycle and the Southern Ocean. There is a need for long-term observational platforms throughout the whole year to allow for monitoring of seasonal-decadal trends. Currently, the Year Round Ocean Sea Ice Atmosphere

Exchanges (YROSIAE) study carried out in Cape Evans is the only long-term (6 months) biogeochemical survey existing. For example an extension of the time-series work that has been done in the fast ice at Casey (van der Merwe et al., 2011a), and more recently at Davis would be particularly interesting. Moreover, Lannuzel et al. (2010) have observed inter-annual variability in the East Antarctic sector. More systematic studies would help to decipher the long terms trends as well as spatial and temporal variability (in both pack ice and fast ice), which are also needed to improve the parameterization and the initialization of sea ice biogeochemical models, and future implementation in global Earth System Models.

5.2.2 Role of organic ligands and EPS

In the light of the work carried out in chapter 2 and 3, additional laboratory ice-growth experiments are required. Small scale studies and characterisation of particles within the sea ice microstructure would be of great interest to elucidate the role played by organic ligands in the enrichment of Fe, and more generally in driving the speciation of Fe (and ultimately its bioavailability for autotrophs and heterotrophs) in the sea ice environment. In combination with a better characterisation of the particles in the sea ice micro-structure, further development and adaptation of the method developed by Middleton et al. (2016) to visualize the development of brine channels and convective processes in newly forming sea ice could provide further insights in the role played by EPS in altering physical properties of the ice, and could also lead to the improvement of mechanisms leading to Fe enrichment. Specifically, a better understanding of the processes occurring at the sea ice interface would be a great avenue for future research.

5.2.3 Fe cycle in a changing sea ice environment

At a larger scale, the influence of UV on the incorporation of material into newly-formed sea ice may have significant impacts under climate change scenarios (chapter 3). While the Antarctic sea ice extent has been increasing over the past 20 years (with regional contrast, e.g., Maksym et al., 2012; Williams, 2014), models predict a severe decline in sea-ice extent, thickness and ice-cover duration by the end of this century (Arzel et al., 2006; Smith et al., 2012). Strong changes in the timing of sea-ice formation in some areas of the Southern Ocean (e.g., Stammerjohn et al., 2012; Massom e al., 2013) will expose organic matter and Fe present in the surface waters to different intensities of UV. As a result, the incorporation and quality of these compounds could be affected, leading to significant changes in the biogeochemistry of sea ice. Changes in down-welling irradiance e.g., due to changes in cloud cover as well as snow thickness on the sea ice may further affect these processes. In this context it is critical to further understand of the role of UV on sea-ice biogeochemical processes, with particular focus on POC and PFe. Moreover, the incorporation of impurities is most likely affected by changes in the timing of sea-ice formation and retreat as well as the length of the sea ice season. Shifts in the seasonality of sea ice might impact the quality and quantity of materials released in spring. Changes in the quality and quantity of Fe delivered during spring melt would further impact the primary productivity associated with sea-ice retreat, with repercussions on the higher trophic levels, and the biological pump of carbon in the Southern Ocean.

The accurate modelling of the biogeochemical cycles associated with sea ice, and their contribution to marine biogeochemistry will therefore play a key role in predicting future climate scenarios. It is essential to focus efforts towards a better parameterization of sea ice biogeochemical models, and a better representation of the

processes driving the biogeochemical cycle associated with sea ice. Only, then will we be able to accurately implement global earth system models with sea ice biogeochemical processes, and improve the prediction of the response of marine ecosystems, and the carbon pump, in both polar and global oceans to past, present and future climate change scenarios.

References

Arzel O, Fichefet T, Goosse H. 2006. Sea ice evolution over the 20th and 21st centuries as simulated by current AOGCMs. *Ocean Model* 12:401–415. doi:10.1016/j.ocemod.2005.08.002

Lannuzel D, Schoemann V, de Jong J, Pasquer B, van der Merwe P, Masson F, Tison J-L, Bowie A. 2010. Distribution of dissolved iron in Antarctic sea ice: Spatial, seasonal, and inter-annual variability. *J Geophys Res* 115:G03022. doi:10.1029/2009JG001031

Lannuzel D, Vancoppenolle M, van der Merwe P, de Jong J, Meiners KM, Grotti M, Nishioka J, Schoemann V. 2016. Iron in sea ice: Review and new insights. *Elem Sci Anthr* 4:130. doi:10.12952/journal.elementa.000130

Maksym T, Stammerjohn SE, Ackley S, Massom R. 2012. Antarctic sea ice - A Polar opposite? *Oceanography* 25:140–151. doi:10.5670/oceanog.2012.88

Massom R, Reid P, Stammerjohn S, Raymond B, Fraser A, Ushio S. 2013. Change and Variability in East Antarctic Sea Ice Seasonality, 1979/80-2009/10. *PLoS One* 8. doi:10.1371/journal.pone.0064756

Middleton CA, Thomas C, De Wit A, Tison J-L. 2016. Visualizing brine channel development and convective processes during artificial sea-ice growth using Schlieren optical methods. *J Glaciol* 62:1–17. doi:10.1017/jog.2015.1

Smith KL, Polvani LM, Marsh DR. 2012. Mitigation of 21st century Antarctic sea ice loss by stratospheric ozone recovery. *Geophys Res Lett* 39:2–7. doi:10.1029/2012GL053325

Stammerjohn S, Massom R, Rind D, Martinson D. 2012. Regions of rapid sea ice change: An inter-hemispheric seasonal comparison. *Geophys Res Lett* 39:L06501. doi:10.1029/2012GL050874

van der Merwe P, Lannuzel D, Bowie AR, Meiners KM. 2011a. High temporal resolution observations of spring fast ice melt and seawater iron enrichment in East Antarctica. *J Geophys Res* 116:1–18. doi:10.1029/2010JG001628

van der Merwe P, Lannuzel D, Bowie AR, Mancuso Nichols CA, Meiners KM. 2011b. Iron fractionation in pack and fast ice in East Antarctica: Temporal decoupling between the release of dissolved and particulate iron during spring melt. *Deep Res Part II Top Stud Oceanogr* 58:1222–1236. doi:10.1016/j.dsr2.2010.10.036

Williams G. 2014. What is the paradox of increasing Antarctic sea ice really telling us? The conversation.

APPENDIX A

Iron biogeochemistry in Antarctic pack ice during SIPEX-2

This appendix contains an article published in Deep Sea Research II, 2014, volume 131, pages 111-122, doi: 10.1016/j.dsr2.2014.12.003.

Deep-Sea Research II 131 (2016) 111–122

Contents lists available at ScienceDirect

Deep-Sea Research II

journal homepage: www.elsevier.com/locate/dsr2

Iron biogeochemistry in Antarctic pack ice during SIPEX-2

Delphine Lannuzel [a,b,*], Fanny Chever [c], Pier C. van der Merwe [b], Julie Janssens [a], Arnout Roukaerts [d], Anne-Julie Cavagna [d], Ashley T. Townsend [e], Andrew R. Bowie [a,b], Klaus M. Meiners [b,f]

[a] Institute for Marine and Antarctic Studies, University of Tasmania, Locked Bag 129, Hobart, TAS 7001, Australia
[b] Antarctic Climate and Ecosystems CRC, University of Tasmania, Private Bag 80, Hobart, TAS 7001, Australia
[c] Ocean and Earth Science, National Oceanography Centre Southampton, University of Southampton, Southampton SO14 3ZH, United Kingdom
[d] Analytical, Environmental & Geo-Chemistry, Vrije Universiteit, Brussel, Pleinlaan 2, B-1050 Brussels, Belgium
[e] Central Science Laboratory, University of Tasmania, Private Bag 74, Hobart, TAS 7001, Australia
[f] Australian Antarctic Division, 203 Channel Highway, Kingston, TAS 7050, Australia

ARTICLE INFO

Available online 11 December 2014

Keywords:
Sea ice
Iron
Antarctica
Southern Ocean
Primary production

ABSTRACT

Our study quantified the spatial and temporal distribution of Fe and ancillary biogeochemical parameters at six stations visited during an interdisciplinary Australian Antarctic marine science voyage (SIPEX-2) within the East Antarctic first-year pack ice zone during September–October 2012. Unlike previous studies in the area, the sea ice Chlorophyll *a*, Particulate Organic Carbon and Nitrogen (POC and PON) maxima did not occur at the ice/water interface because of the snow loading and dynamic processes under which the sea ice formed. Iron in sea ice ranged from 0.9 to 17.4 nM for the dissolved (<0.2 μm) fraction and 0.04 to 990 nM for the particulate (>0.2 μm) fraction. Our results highlight that the concentration of particulate Fe in sea ice was highest when approaching the continent. The high POC concentration and high particulate iron to aluminium ratio in sea ice samples demonstrate that 71% of the particulate Fe was biogenic in composition. Our estimated Fe flux from melting pack ice to East Antarctic surface waters over a 30 day melting period was 0.2 μmol/m^2/d of DFe, 2.7 μmol/m^2/d of biogenic PFe and 1.3 μmol/m^2/d of lithogenic PFe. These estimates suggest that the fertilization potential of the particulate fraction of Fe may have been previously underestimated due to the assumption that it is primarily lithogenic in composition. Our new measurements and calculated fluxes indicate that a large fraction of the total Fe pool within sea ice may be bioavailable and therefore, effective in promoting primary productivity in the marginal ice zone.

1. Introduction

Marine phytoplankton fix aqueous carbon dioxide (CO_2) within the surface ocean through photosynthesis. This process increases the flux of CO_2 from the atmosphere into the ocean and therefore plays a key role in mitigating green house gas induced global warming (Sarmiento and Gruber, 2006). When light levels are sufficient, phytoplankton growth is limited by the availability of micro-nutrients such as iron (Fe) in remote regions like the Southern Ocean, where external inputs of Fe are low (Martin and Fitzwater, 1988; de Baar et al., 1990). Both laboratory and short-term artificial Fe fertilization experiments unequivocally showed the importance of Fe in controlling phytoplankton production and therefore Fe was one of the factors controlling carbon export into the ocean interior (Boyd et al., 2007). A drawback of artificial fertilization experiments is the difficulty of effectively quantifying carbon export into the ocean interior and estimates vary by 2 orders of magnitude (Blain et al., 2007; Pollard et al., 2009). Although variability in the estimates is high, the CROZEX study in the Southern Ocean showed that the efficiency of natural fertilization from the sub-Antarctic Crozet island was up to 20 times greater than that of an artificially Fe-enriched site (SERIES, Boyd et al., 2004) (Blain et al., 2007; Pollard et al., 2009).

Within Fe limited high nutrient—low chlorophyll waters, multiple naturally Fe-fertilized sites have been identified, including seasonal sea ice, which acts as a 'capacitor' to seasonally store Fe. Antarctic sea ice contains 1–2 orders of magnitude more Fe, organic matter, and chlorophyll *a* than under-ice seawater (Grotti et al., 2005; Lannuzel et al., 2007, 2008; van der Merwe et al., 2009, 2011a,b; de Jong et al., 2013) and triggers ice-edge phytoplankton blooms during the release of these constituents in austral spring (Sedwick et al., 1997; Lancelot et al., 2009). Given that sea-ice formation and retreat affects approximately 40% of the entire Southern Ocean area (Southern Ocean extent $=35\times10^6$ km^2;

* Corresponding author.
E-mail address: delphine.lannuzel@utas.edu.au (D. Lannuzel).

http://dx.doi.org/10.1016/j.dsr2.2014.12.003

maximum-minimum Antarctic sea ice extent = 15.2×10^6 km^2; Thomas and Dieckmann, 2003), the "frozen ocean" may therefore constitute the dominant source of Fe to polar waters during annual melting, and therefore plays a key role in drawing down atmospheric CO_2 levels in the climatically-important Southern Ocean. There is an urgent need to evaluate how modern-day climate change will affect the Antarctic sea-ice ecosystem. A pre-requisite for this is to describe and understand present-day sea-ice biogeochemical processes. In this context, new field measurements and sample collection approaches for characterization of sea-ice ecosystem dynamics should be a priority.

The East Antarctic is an ideal location to study the role of sea ice as an ocean fertilizer during the melting season because three consecutive field studies have been specifically dedicated to Fe biogeochemistry in this sector: ARISE in pack ice in 2003 (Sept/Oct, 63.5–65°S/109–117°E; Lannuzel et al., 2007), SIPEX-1 in pack ice in 2007 (Sept/Oct, 64–65.5°S/114–128°E; van der Merwe et al., 2009; 2011a) and a time series in fast ice in 2009 (Casey, Nov, 66°S/110°E; van der Merwe et al., 2011b; Lannuzel et al., 2014). The main outcomes from these studies were that (1) dissolved Fe concentrations vary seasonally rather than spatially (Lannuzel et al., 2010), (2) particulate Fe vary spatially, with higher concentrations observed near the continent or when higher biomass is present (van der Merwe et al., 2011a) and (3) dissolved Fe is released before particulate Fe during spring melt (van der Merwe et al., 2011a). Our previous work also suggested that during the melting season, dissolved Fe released from sea ice could account for 15 to 70% of the primary productivity in the East Antarctic sector, and that the additional Fe supplied in the form of particles may extend the longevity of the ice-edge bloom (Lannuzel et al., 2014). Building on our knowledge of Fe sea-ice biogeochemistry in the area, the major goal of this new field study was 3-staged. First, we wanted to determine if the mode of ice growth (i.e. thermodynamic versus dynamic growth) controls the concentration of dissolved and particulate Fe. The particulate Fe concentration in sea ice was highly variable during three previous field studies in East Antarctica. Therefore, our 2nd aim was to evaluate whether the previously observed variability in pack ice particulate Fe concentration could be explained by its biogenic or lithogenic composition and furthermore, can this differentiation of particulate Fe determine its availability for sea-ice algae and phytoplankton when released into seawater? Finally, based on measured rates of primary productivity in sea ice and ancillary parameters, our last aim was to assess whether macronutrients, Fe or light controlled the local productivity at this time of year.

2. Material and methods

2.1. Collection and handling of samples

Samples were collected during the Australian-led Sea Ice Physics and Ecosystem eXperiment-2 (SIPEX-2) marine science voyage in austral winter/spring 2012 (26 Sept–10 Nov, 64–65°S/116–121°E, Fig. 1). The acid-cleaning protocols for sample bottles and equipment followed the guidelines of GEOTRACES (www.geotraces.org). Contamination-free ice coring equipment developed by Lannuzel et al. (2006) was used to collect ice cores. Ice cores were triple bagged and stored at −18 °C until further processing in the home laboratory. Ice cores were then sectioned under a class-100 laminar flow hood (AirClean 600 PCR workstation, AirClean System) using a medical grade stainless steel bonesaw (Richards Medical), thouroughly rinsed with ultra-high purity water (18.2 MΩ), and ice sections were then allowed to melt at ambient temperature in acid-cleaned 3 L Polyethylene (PE) containers. Melted sea-ice sections were then homogenized by a gentle shake and filtered through 0.2 μm pore size polycarbonate filters (Sterlitech, 47 mm diameter) using Teflon® perfluoroalkoxy (PFA) filtration devices (Savillex, USA) connected to a vacuum pump set on < 2 bar to obtain the particulate (> 0.2 μm) and dissolved (< 0.2 μm) metal fractions. The collected filtrates (< 0.2 μm) were acidified to pH 1.8 using Seastar Baseline® HCl (Choice Analytical) and stored at ambient temperature until analysis in the home laboratory. The filters retaining the particulate material were stored frozen in acid-clean petri dishes until further processing.

Standard physico-chemical and biological parameters such as sea-ice and snow thicknesses, in situ ice temperature, sea-ice and brine salinities, ice texture, chlorophyll *a* (Chl*a*), macro-nutrients (nitrate + nitrite (NO_x), phosphate (PO_4^{3-}), silicic acid ($Si(OH)_4^-$) and ammonium (NH_4^+)), dissolved organic carbon (DOC), and particulate organic carbon and nitrogen (POC and PON) were also determined in each sample, following the methods described in van der Merwe et al. (2009). Theoretical brine volume fractions (V_b/V) were calculated using in situ ice temperatures and bulk ice salinities and relationships from Cox and Weeks (1983). The full ice core length was examined under crossed-polarized light to identify the texture (i.e. columnar vs. granular) according to the method of Langway (1958). Preparation of the thin sections took place in a container kept at −25 °C. The thin sections were obtained by cutting vertical sections of about 6 mm thick using a band saw. Ice sections were then thinned down using a microtome blade to reach a final thickness of 3–4 mm and observed under cross-polarized lights (Fig. 2).

2.2. Analysis of dissolved iron

The acidified filtrates were diluted 5 times, using 2% v-v ultrapure HNO_3 (Seastar Baseline, Choice Analytical) and Fe concentrations were determined directly using sector field inductively coupled plasma magnetic sector mass spectrometry (SF-ICP-MS; Element 2) following the method described in Lannuzel et al. (2014). Results for procedural blanks and limits of detection are presented in Table 1.

2.3. Analysis of particulate iron and aluminium

Filters retaining particulate material (> 0.2 μm) were digested in a mixture of strong, ultrapure acids (750 μL 12 N HCl, 250 μL 40% HF, 250 μL 14 N HNO_3) in 15 mL Teflon® perfluoroalkoxy (PFA) (Savillex, USA) on a Teflon coated graphite digestion hot plate housed in a bench-top fume hood (all *Digi*PREP from SCP Science, France) coupled with HEPA® filters to ensure clean air input at 95 °C for 12 h, then dry evaporated for 4 h and re-suspended in 2% v-v HNO_3 (Seastar Baseline, Choice Analytical). The procedure was applied to filter blanks and certified reference materials BCR-414 and MESS-3 to verify the recovery of the acid digestion treatment. The concentrations of particulate metals were then determined by SF–ICP–MS (Bowie et al., 2010). Results for procedural blanks, limits of detection and certified reference materials are presented in Tables 1 and 2 and were found fit for purpose. Although we obtained the concentrations of 18 elements in our sea-ice samples, we only dicuss Fe here, and used aluminium (Al) concentrations to fingerprint Fe sources. The other elements will be reported and discussed in a companion paper.

For statistical analysis, we used a Spearman's Rho correlation because the data was non-normally distributed (i.e. non-parametric), with Spearman's rho correlation coefficient R, the number of data points n, and the level of significance $p < 0.01$ or $p < 0.05$ (Table 3).

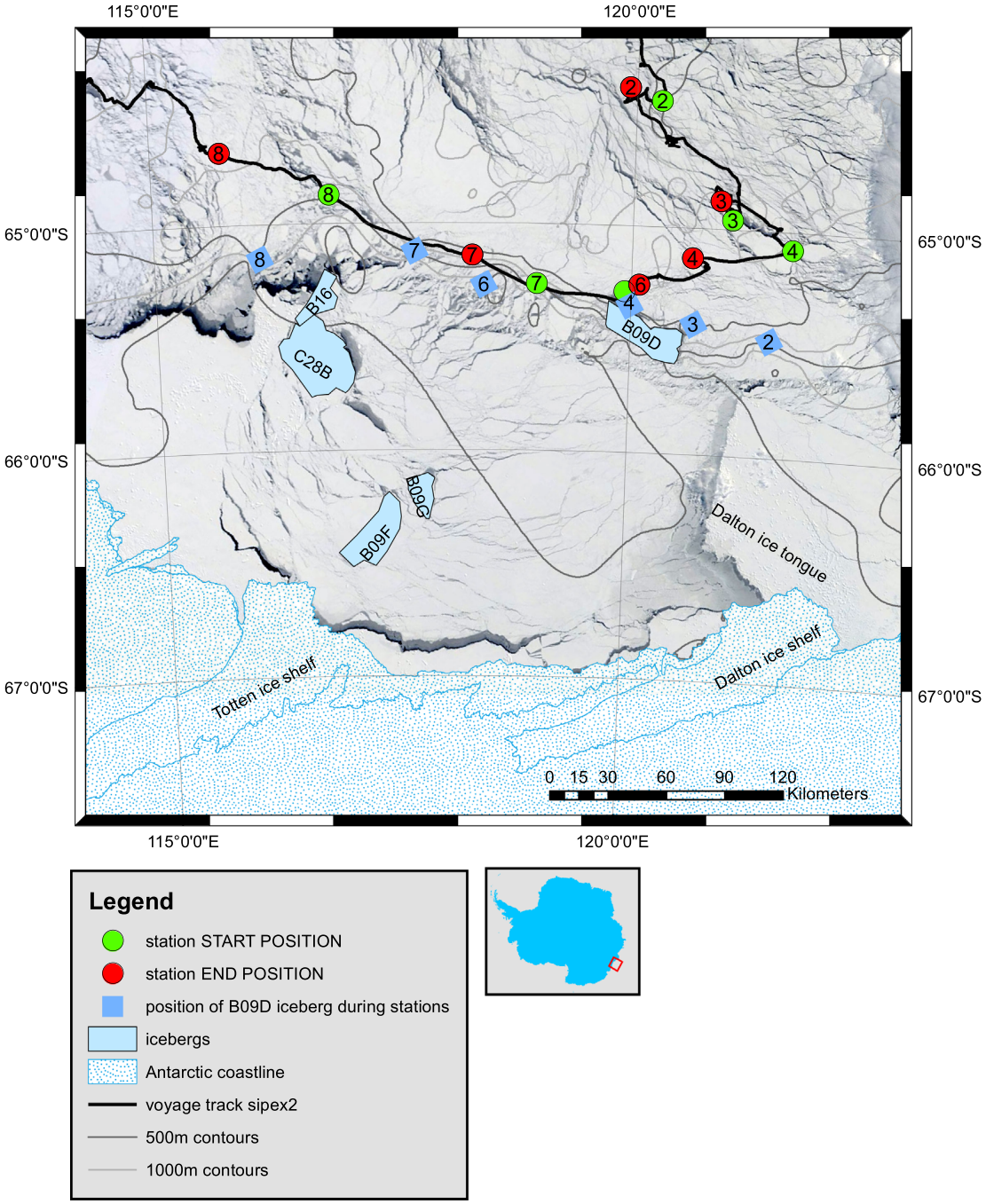

Fig. 1. Bathymetry, sea-ice cover, ship track and locations of the ice stations visited during the SIPEX-2 voyage. Due to the westward drift of pack ice, the start and end positions of each station are indicated on the map. Station 2 was sampled on 26.11.2012, station 3 on 03.10.2012, station 4 on 07.10.2012, station 6 on 13.10.2012, station 7 on 19.10.2012 and station 8 on 29.10.2012. Note the location of iceberg B09D during each ice station. The projection is South Pole Stereographic and the map has been rotated 118° CCW. All data was provided by the Australian Antarctic Data Centre (https://data.aad.gov.au/). Bathymetry data supplied by IBCSO project Arndt et al. (no date). Coastal polygon supplied by SCAR, Antarctic Digital Database is copyright © 1993–2014 Scientific Committee on Antarctic Research. MODIS images downloaded from NASA Worldview (https://earthdata.nasa.gov/labs/worldview/).

3. Results

3.1. Sea-ice physical properties

Apart from station 2 which had a thin cover of 0.05 m of snow, the rest of the sites were covered with a very thick layer of snow, ranging from 0.25 m at station 3 to 0.74 m at station 6 (Fig. 2, average 0.39 m). The sea-ice cores collected on our sites ranged from 0.72 to 1.43 m in thickness (average 0.93 m). Texture-wise, station 3 was the only typical first-year pack-ice station, with 0.02 m of granular ice underlain by columnar ice. Station 4 also showed some first year sea-ice features, with 0.29 m of granular ice underlain by 0.61 m of columnar ice. Overall, granular ice however dominated the overall ice textures at 64% (Fig. 2). The snow thickness represented on average 30% of the total ice thickness. Station 6 showed evidence of rafting processes with the superposition of granular ice on top of columnar ice in three consecutive layers.

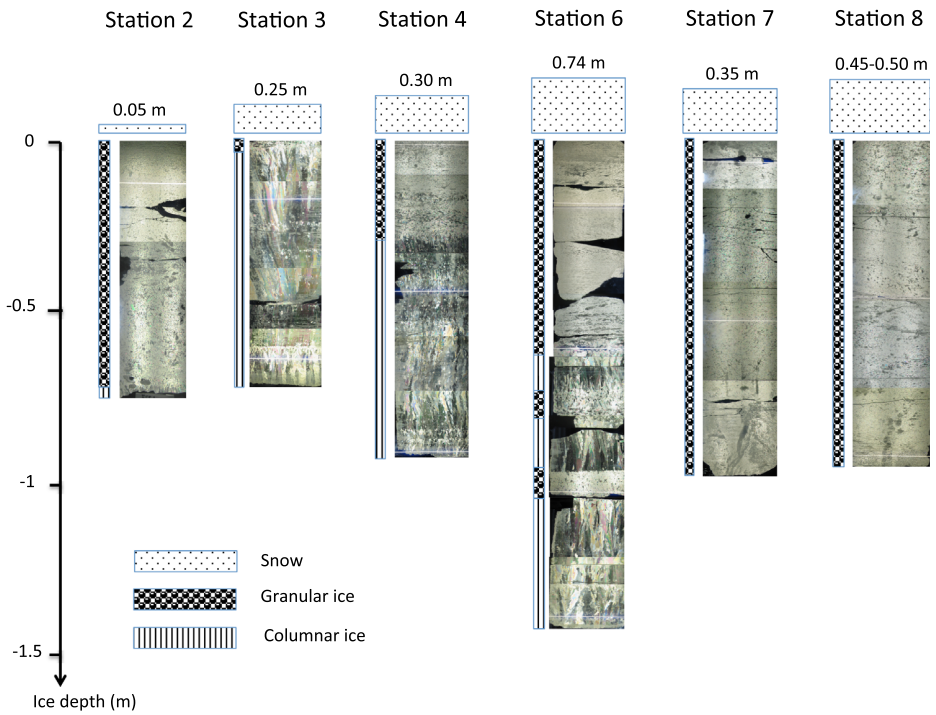

Fig. 2. Snow thickness (in m), ice thickness (in m) and sea-ice textures (granular and columnar) obtained from thin sections observed under polarized light.

Table 1
ICP–SFMS results in μg/L for procedural digest filter and rinse solution blanks. The limit of detection (LOD) is 3 times the standard deviation of the filter blank.

	Fe (μg/L)	Al (μg/L)
0.2 μm PC filter		
Average filter blank ($n=3$)	0.99 ± 0.25	1.38 ± 0.61
LOD	0.750	1.82
2% HNO_3		
Average blank ($n=10$)	0.04 ± 0.01	0.06 ± 0.03
LOD	0.03	0.09

Table 2
ICP-SFMS results in mg/kg for certified referenced material ($n=8$), [indicative value].

	Fe (mg/kg)	Al (mg/kg)
BCR-414		
[Indicative]	[1850 ± 190]	[1800 ± 30]
Measured	1880 ± 60	2639 ± 80
MESS-3		
Certified	43400 ± 1100	85900 ± 2300
Measured	39076 ± 1533	76439 ± 3321

The mean in situ sea-ice temperatures increased from −4.8 °C at station 3, to −3.0 °C at station 4 and up to −1.8 °C at the remaining sites. The ice temperature profiles were nearly isothermal for stations 2, 6, 7 and 8 (Fig. 3A), probably because of the thick snow cover pushing the ice deep into the ocean and insulating it against the atmosphere. The mean air temperature increased from −22.8 °C at station 3, to −10.7 °C at station 4 and up to −2.9 °C at station 6 (Fig. 3A).

Sea-ice salinities ranged from 3.9 to 18.5, and the vertical profiles were highly heterogeneous overall. Salinities were generally higher in the surface layers. Station 3 had the only "C-shaped" salinity profile of the voyage (Fig. 3B), which is typically observed in first year winter pack ice (van der Merwe et al., 2009).

The brine volume ratio V_b/V (where V_b=brine volume and V=volume of bulk sea ice) can be used as an indicator of sea ice permeability. Typically, in columnar ice, when $V_b/V < 5\%$ (for salinity of 5 and ice temperature of −5 °C), the ice is considered impermeable (Golden et al., 1998). Saenz and Arrigo (2012) have suggested that the permeability threshold of granular ice, formed by frazil ice accumulation or due to snow ice formation, may be higher than the permeability threshold of columnar ice, formed by congelation growth. This can be explained by a more random distribution of brine pockets and channels in granular sea ice. In our samples, granular ice dominated, and the mean brine volume ratio (V_b/V) was 8.3% on average at station 3, 12.0% at station 4 and 14.5–19.6% at the warmer sites. Significant correlations (non-parametric, Spearman's rho=0.56, $n=35$, $p<0.01$) were observed between brine volume and ice temperature. Therefore the increase in average brine volume appeared to be driven by an increase in average ice temperature, which is ultimately controlled by increasing ambient air temperatures (Fig. 3A). Station 3 had intermediate ice sections below the critical V_b/V of 5% for columnar ice, indicating the impermeable nature of these sections within the ice. All the other stations had $V_b/V > 10\%$, suggesting sea-ice melting was already underway at the time of sampling (Fig. 3C).

3.2. Sea-ice biogeochemistry

3.2.1. Macro-nutrients, Chla, DOC, POC and PON

Sea-ice concentration ranges of NO_x, $Si(OH)_4^-$, PO_4^{3-} and NH_4^+ were 0.1–8.2 μM, 1.7–26.6 μM, 0.1–1.9 μM and 0.1–14.3 μM, respectively (Fig. 4A–D). Macro-nutrient concentrations are also shown plotted versus sea-ice salinity (Fig. 4E–H). The theoretical dilution line (TDL) was plotted by using the salinity and macro-nutrients concentration in seawater collected at 1 m below the sea ice. Silicic acid behaved conservatively with salinity, although most of the data points were slightly above the TDL (Fig. 4F). The relationship between $Si(OH)_4^-$ and ice salinity was statistically significant (Table 3), however, all other macro-nutrients deviated from their respective TDL. NO_x concentrations were significantly reduced

Table 3
Spearman's rank correlation coefficients in sea ice. The number of samples (n) is the sum of all sections and sites used in the correlation analysis. The bold shading marks the significant correlations. Sigma 2-tailed with *=$p<0.05$; **=$p<0.01$.

		V_b/V	Chl*a*	POC	PON	DOC	NH_4^+	NO_x	PO_4^{3-}	$Si(OH)_4^-$	DFe	PFe
Salinity	Correlation	**0.377***	−0.010	0.000	0.158	0.202	0.259	0.261	0.318	**0.737****	0.130	0.099
	Sigma	0.023	0.952	0.999	0.358	0.238	0.127	0.136	0.059	0.000	0.448	0.568
	n	36	36	36	36	36	36	34	36	34	36	36
V_b/V	Correlation		−0.087	0.043	0.195	0.172	0.154	**0.722****	**0.347***	**0.520****	**0.549****	0.314
	Sigma		0.615	0.802	0.254	0.317	0.369	0.000	0.038	0.002	0.001	0.062
	n		36	36	36	36	36	34	36	34	36	36
Chl*a*	Correlation			**0.557****	**0.600****	0.185	**0.436****	0.048	**0.516****	−0.076	−0.056	0.251
	Sigma			0.000	0.000	0.280	0.008	0.789	0.001	0.669	0.746	0.139
	n			36	36	36	36	34	36	34	36	36
POC	Correlation				**0.891****	**0.666****	**0.684****	−0.113	**0.561****	0.049	0.022	**0.397***
	Sigma				0.000	0.000	0.000	0.525	0.000	0.784	0.898	0.016
	n				36	36	36	34	36	34	36	36
PON	Correlation					**0.514****	**0.736****	0.134	**0.770****	0.193	0.053	**0.376***
	Sigma					0.001	0.000	0.451	0.000	0.275	0.760	0.024
	n					36	36	34	36	34	36	36
DOC	Correlation						**0.386***	−0.141	0.250	0.119	0.113	**0.416***
	Sigma						0.020	0.426	0.141	0.503	0.513	0.012
	n						36	34	36	34	36	36
NH_4^+	Correlation							0.076	**0.531****	0.308	0.085	**0.428****
	Sigma							0.671	0.001	0.077	0.622	0.009
	n							34	36	34	36	36
NO_x	Correlation								**0.485****	**0.525****	0.323	**0.348***
	Sigma								0.004	0.002	0.063	0.044
	n								34	33	34	34
PO_4^{3-} –	Correlation									**0.478****	0.125	0.296
	Sigma									0.004	0.467	0.080
	n									34	36	36
$Si(OH)_4^-$	Correlation										**0.371***	0.245
	Sigma										0.031	0.163
	n										34	34
DFe	Correlation											**0.575****
	Sigma											0.000
	n											36

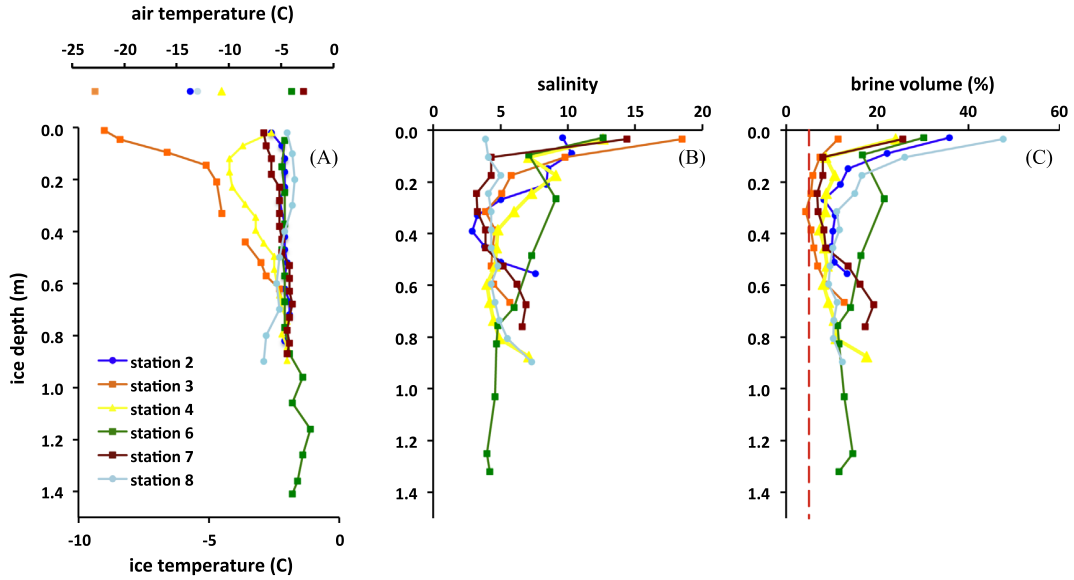

Fig. 3. (A) Air and sea-ice temperatures, (B) salinity and (C) brine volume ratios (%) during SIPEX-2. The red dashed line marks the 5% brine volume permeability threshold for columnar ice. (For interpretation of the references to color in this figure legend, the reader is referred to the web version of this article.)

relative to the TDL (Fig. 4E), indicating a drawdown of NO_x in sea ice, sometimes until complete exhaustion (station 7). Conversely, PO_4^{3-} deviated above and below the TDL while NH_4^+ concentrations were generally below the TDL (Fig. 4G and H), indicating accumulation of NH_4^+.

The Chl*a* concentration in sea ice ranged from <0.02 μg/L at station 6 to 13.7 μg/L at station 7, with an overall average Chl*a* concentration of 2.2 ± 2.5 μg/L (Fig. 5A). The highest Chl*a* concentrations occurred in sea-ice interior layers, except for station 6 where Chl*a* maximum was in the bottom ice layer.

Dissolved organic carbon in sea ice ranged from 0.15 and 2.66 mg/L (average 1.4 ± 0.7 mg/L). Stations 4 and 7 respectively exhibited the lowest and highest DOC values. Similar to Chl*a*, the DOC maxima did not occur at the ice/water interface (Fig. 5B).

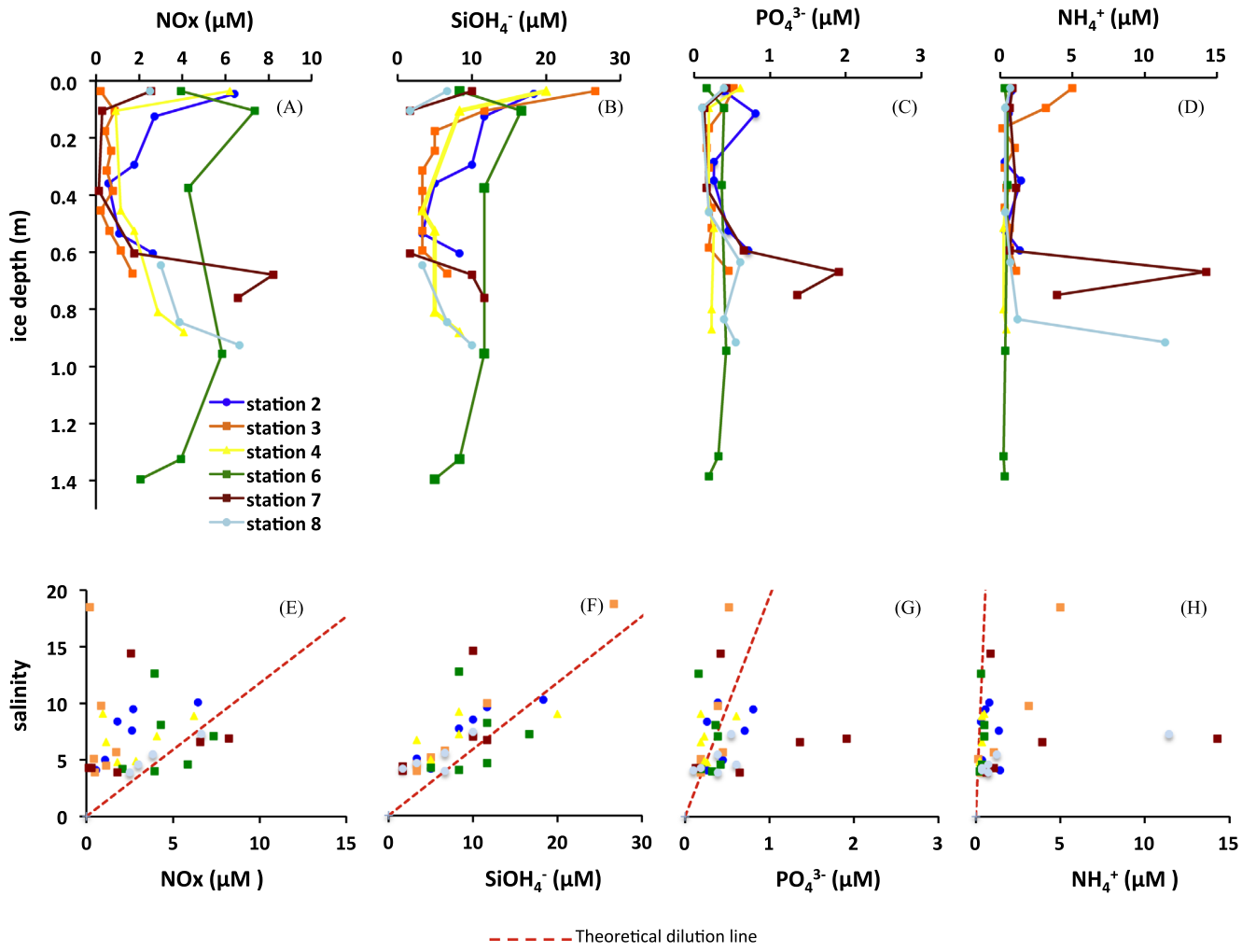

Fig. 4. Upper panel: concentrations (μM) in (A) nitrate+nitrate (NO_x), (B) silicic acid ($SiOH_4^-$), (C) phosphates (PO_4^{3-}) and (D) ammonium (NH_4^+), as a function of sea ice depth (m) during SIPEX-2. Lower panel: sea ice concentrations of (E) nitrate+nitrate (NO_x), (F) silicic acid ($SiOH_4^-$), (G) phosphate (PO_4^{3-}) and (H) ammonium (NH_4^+), plotted against salinity. The red dotted line represents the theoretical dilution line. (For interpretation of the references to color in this figure legend, the reader is referred to the web version of this article.)

Particulate organic carbon and PON concentrations in sea ice ranged, respectively, between 24 and 1088 μg/L (average 332 ± 298 μg/L) and between 2 and 156 μg/L (average 42 ± 41 μg/L). Similar to Chl*a* and DOC, the POC and PON maxima did not occur at the ice/water interface (Fig. 5C and D). In the top most and lower most sections of the ice cover, the POC:PON ratios were lower and close to the Redfield C:N molar ratio of 6.6 mol:mol typical of phytoplankton (Redfield, 1958). These ice sections therefore harbor autotrophic activity.

Significant correlations were observed between POC and PON, and PO_4^{3-} and Chl*a* across all sites (Table 3). Chlorophyll *a* also correlated significantly with PON, NH_4^+ and PO_4^{3-}.

3.2.2. Iron distributions

Fig. 6 shows the profiles of DFe and PFe concentrations in collected sea-ice cores. The DFe profiles are highly variable both between stations and within profiles. The PFe profiles differ greatly between sampling sites, with stations 7 and 8 noticeably different. The ranges in sea ice were 0.9–17.4 nM DFe (average 7.5 ± 4.5 nM) and 0.04–990 nM PFe (average 133 ± 215 nM). Similar to previous Antarctic studies, our results show high DFe concentrations in sea ice relative to under-ice seawater (range 0.09–3.05 nM DFe; 15–1000 m deep; Schallenberg et al., this issue). Significant correlations between DFe and V_b/V (R=0.55) and DFe and PFe (R=0.57) were observed (Table 3).

The fractional solubility of Fe (FS–Fe=ratio of dissolved to total Fe concentration) in sea ice varied between 0.01 and 0.98 (average FS–Fe=0.13 ± 0.16).

Based on the data collected at 6 sections within each core, we vertically integrated the concentrations of DFe and PFe at each station (Table 4). We also applied this integration to POC and Chl*a* concentrations. Depth integrated DFe was the highest at station 6 (16.9 μmol/m^2) and the lowest at station 3 (2.2 μmol/m^2). Depth integrated PFe was the highest at station 7 (294.3 μmol/m^2) and the lowest at station 3 (16 μmol/m^2). Station 7 also exhibited the highest depth integrated Chl*a* (3.6 mg/m^2) and POC (660 mg/m^2) concentrations.

4. Discussion

4.1. Sea-ice physical properties

Based on the ice temperatures and brine volume ratios in Fig. 3, three seasonal regimes during SIPEX-2 can be identified: station 3 was a cold winter station, station 4 a transition station, and the

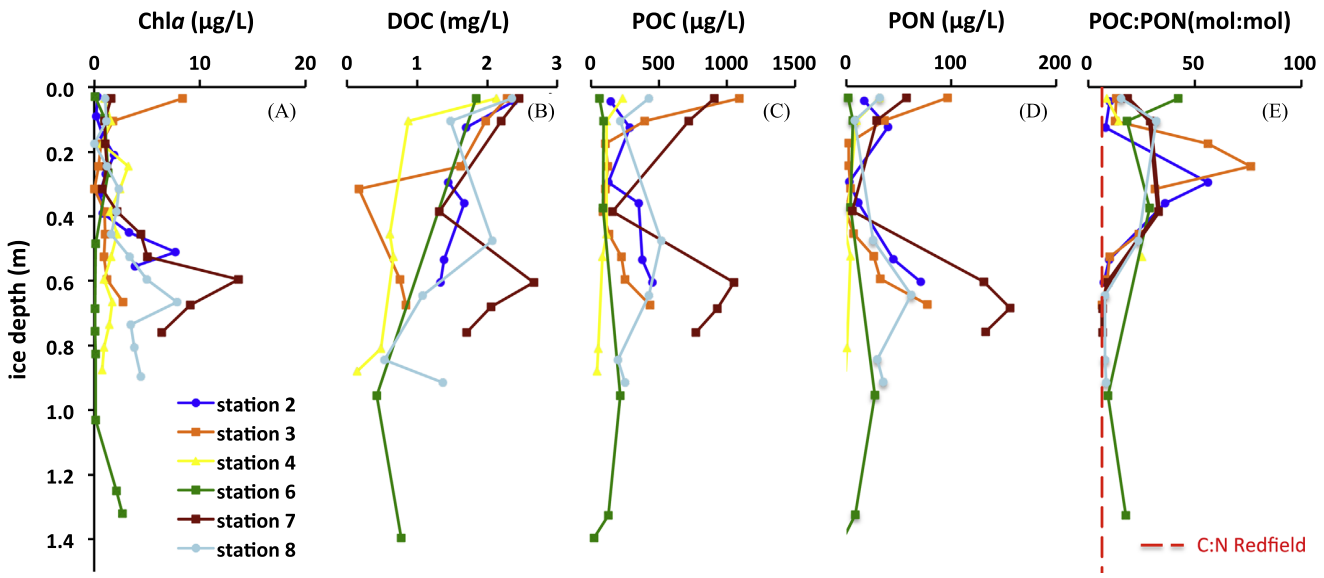

Fig. 5. Concentrations (µg/L) in (A) chlorophyll *a* (Chl*a*), (B) dissolved organic carbon (DOC), (C) particulate organic carbon (POC), (D) particulate organic nitrogen (PON) and (E) POC:PON ratios (mol:mol) as a function of sea-ice depth (m) during SIPEX-2. The red dotted line represents the C:N Redfield molar ratio (106:16). (For interpretation of the references to color in this figure legend, the reader is referred to the web version of this article.)

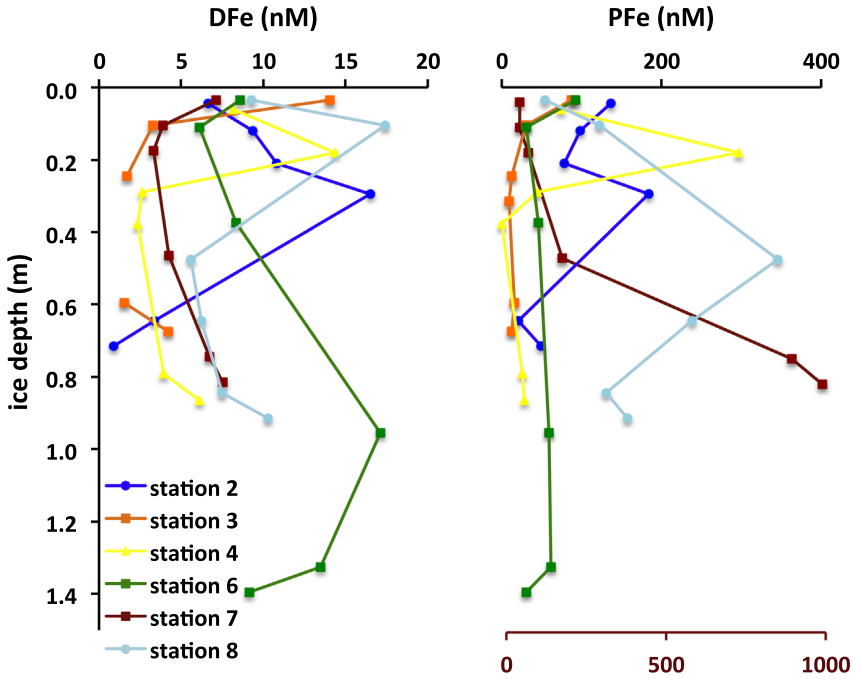

Fig. 6. Concentrations (in nM) in dissolved and particulate iron (DFe and PFe) as a function of sea-ice depth (in m) during SIPEX-2. The lower *x*-axis is the scale for PFe at station 7.

Table 4
Depth integrated concentrations of Fe (in µmol/m^2), Chl*a* and POC (in mg/m^2) in sea ice during SIPEX-2

stations	DFe	PFe	Biogenic PFe	Lithogenic PFe	Chl*a*	POC
2	6.6	73.4	56.6	16.7	2.3	230.7
3	2.2	16.0	10.0	6.0	1.3	233.7
4	4.9	57.2	44.8	12.4	1.2	90.3
6	16.9	74.9	28.1	47.9	1.2	190.2
7	4.3	294.3	250.0	44.3	3.6	657.4
8	8.9	197.0	89.7	107.3	3.0	339.5
Average	7.3	118.8	79.9	39.1	2.1	290.3
Stdev	5.2	105.1	87.6	37.6	1.1	197.0

other four stations were warm spring type stations. The increase in the mean air temperature most likely triggered the warming of the ice, from the top, as exemplified for stations 3, 4, 6 and 7 (Fig. 3A). Although the mean air temperatures at stations 2 and 8 were low, the in situ ice temperatures were relatively warm. The thick snow cover at station 8 probably insulated the sea ice from the cold atmospheric conditions. The snow layer was however thin at station 2. This suggests that the air temperature decreased recently and did not have time to affect the ice temperatures before we collected the samples.

Ice textures were dominated by granular ice, which highlights the presence of either snow ice or frazil ice crystals. Frazil ice

forms under dynamic turbulent conditions at high growth rates, concentrating micro-organisms (living and detrital) by nucleation of frazil ice crystals or by scavenging cells as frazil crystals float up through the water column (Garrison et al., 1989; Horner, 1996). Precipitation of snow and its redistribution through drifts are key features of the Antarctic pack ice zone (Sturm and Massom, 2010). Snow layers accumulate on top of the ice cover soon after its formation. Depending on the sea-ice thickness below, the snow cover may become thick enough to depress the sea-ice cover and seawater may then infiltrate into the snow pack. "Snow ice" then forms by refreezing of the flooded snow and creates a solid layer of ice on top of the ice floe, which is of granular type (Worby et al., 1998). Snow ice may then be underlain by frazil ice, which is also granular. Columnar ice forms slowly compared to granular ice (Eicken, 2003), and tends to efficiently reject micro-organisms in the early stage of ice growth (Palmisano and Garrison, 1993; Weissenberger and Grossmann, 1998). In our samples, no clear relationship between biological occurrence or Fe and ice textures was observed.

Ice texture observations suggest that the ice collected at stations 3 and 4 grew thermodynamically (i.e. due to a decrease in ambient temperature). Station 6 grew in thickness because of dynamic processes including rafting (where ice floes raft on top of each other) and ridging (blocks of ice are pushed onto, and below, the edge of ice floes). The repeated observation of deformed columnar ice crystals supports this rafting process. As a result, the ice core collected at station 6 which was subjected to rafting was thicker than at station 3 where the ice grew thermodynamically. The snow layer was thick throughout our study, leading to snow ice formation at several stations. Station 4 displayed 0.16 m of snow ice, underlain by 0.13 m of frazil ice, and then columnar ice. This is confirmed by the in situ ice temperatures and salinity for station 4 where the top 0.16 m of snow ice were warmer and saltier than the sea ice below (Fig. 3A and B). Snow ice also likely formed at the snow-ice interface at stations 6, 7 and 8 (Fig. 2). We did not measure $\delta^{18}O$ at the trace metal sampling sites to decipher snow ice from frazil ice. $\delta^{18}O$ was measured in sea ice by other research groups at the main sampling sites during SIPEX-2 and do highlight the recurrence of snow ice formation on their sites (Heil et al., 2016). We consider the same feature applies to the entire ice floes studied, including the trace metal sampling sites.

4.2. Biogeochemical comparison to previous studies: DFe and DOC thresholds in sea ice

The 24–1088 μg/L POC concentrations from SIPEX-2 were lower than the 28–4784 μg/L measured during ARISE (Becquevort et al., 2009) and 38–3309 μg/L during SIPEX-1 (van der Merwe et al., 2009) in the same sector, at the same time of the year. The POC:PON ratios were generally close to the Redfield ratio in bottom ice but elevated in the internal ice sections. This could be explained by the relative dominance of carbon associated with exopolysaccharides (EPS) over carbon associated with autotrophs in these ice layers (Ugalde, 2016). Exopolysaccharides are commonly enriched in carbon relative to nitrogen when compared to the Redfield ratio (26 mol:mol; Engel and Passow, 2001). However the very high POC:PON ratios observed in internal layers (up to 76 mol:mol at station 3, Fig. 5E) could reflect the extremely low PON concentrations (Fig. 5D) due to nitrogen limitation in these sections (Fig. 4A).

Unlike SIPEX-1 (van der Merwe et al., 2009), DOC did correlate significantly with POC ($R=0.67$) and PON ($R=0.51$) during SIPEX-2. The significant correlation between DOC and POC could indicate an algal origin for sea ice DOC, as previously observed during spring blooms in the Arctic (Bunch and Harland, 1990; Smith et al., 1997; Riedel et al., 2008). However, the measured DOC:POC ratio in sea ice averaged 7:1 (range of 1:1 to 32:1) which is lower than the mean global ocean value of 15:1 (Millero, 1996; Kepkay, 2000). One explanation may be an abiotic transformation of DOC into POC when a DOC threshold is reached (Becquevort et al., 2009). This transfer of DOC into POC would also explain the significance of the relationship observed in our study between DOC and POC (Table 3).

The DFe measured during SIPEX-2 (DFe = 0.9–17.4 nM) was within the ranges reported during ARISE (DFe = 2.1–26.1 nM; Lannuzel et al., 2007) and SIPEX-1 (DFe = 0.2–14.4 nM; van der Merwe et al., 2011a) which were studies located in the same sector and at the same time of the year. Therefore, although the sea ice conditions were very different in 2003, 2007 and 2012, the DFe interannual variability in late austral winter-spring seems low. Sea-ice thickness, texture and growth (i.e. thermodynamic versus dynamic) do not seem to control the concentrations of DFe in sea ice. One hypothesis is that the sources of new and regenerated DFe are very similar from one year to the other. Fast ice however, does not incorporate much more DFe than pack ice (Lannuzel et al., 2010), even when new sources of Fe are only a few tens of meters away from the collected ice (van der Merwe et al., 2011b). Another hypothesis is that DFe reaches a maximum concentration threshold in sea ice, which it cannot exceed. This would explain the lack of spatial variability in DFe concentrations between pack ice stations during SIPEX-2 (Fig. 6), and between pack-ice and fast-ice sites collected around Antarctica (Lannuzel et al., 2010). Similar to DOC and POC, DFe and PFe were also significantly correlated in sea ice during SIPEX-2 ($R=0.57$, $n=36$, $p<0.01$). We suggest that once a threshold is reached for the apparent DFe concentration in the brine channels, DFe is transformed into PFe. This theory is further supported by the low fraction of DFe relative to PFe concentrations typically encountered in sea ice (FS–Fe = 0.13 in pack ice and FS–Fe = 0.03 in fast ice) compared to open waters (FS–Fe = 0.52 ± 0.19, $n=31$, calculated from 0 to 150 m, SAZ-SENSE data published in Lannuzel et al. (2011)). This process is similar to what would happen in seawater, however the PFe cannot sink out in sea ice and therefore lead to the high PFe relative to DFe. To get an estimate of the DFe threshold value within the brine channels, we calculate the potential brine DFe concentrations as follows:

$$DFe_{brine} = \frac{DFe_{bulk} \times brinesalinity}{bulksalinity},$$

where DFe_{bulk} is the concentration of DFe in the melted ice section, bulk salinity is the salinity of the melted ice section and brine salinity is calculated as a function of bulk ice salinity and in situ temperature in that sea ice section.

Our DFe_{brine} concentrations however, do not reach a clear threshold number (DFe_{brine} range = 6.8–173.7 nM and average = 55.1 ± 39.0 nM). Biological uptake and remineralization, as well as organic ligand concentrations may control the equilibrium between the dissolved and particulate phase, and therefore shift the solubility threshold value. Recent work in Antarctic fast ice has shown a linear relationship between DFe and organic ligands (Lt) concentrations in sea-ice and brine samples, with [Lt] = 0.90 [DFe] + 4.24 in sea ice ($R^2=0.93$, $n=34$) and [Lt] = 1.08 [DFe] + 4.86 in brines ($R^2=0.98$, n = 12). These results suggest that organic ligands control the concentrations of DFe in sea ice. Once the ligands become saturated with Fe, non-organically bound DFe become scavenged onto particles (Lannuzel et al., under review).

In the case of PFe, the ranges measured during ARISE in 2003 (PFe = 2.0 –96.6 nM; Lannuzel et al., unpublished data) and SIPEX-1 in 2007 (PFe = 0.9–217.7 nM; van der Merwe et al., 2011a) were much lower than SIPEX-2 in 2012 (PFe = 0.04–990 nM). The highest PFe concentrations were observed at station 7 (Fig. 6), which is the closest station to drifting icebergs and the continental shelf. Note that the range from SIPEX-1 in 2007 includes one fast-ice

station, for which the PFe concentration was anomalously high at 217.7 nM. Fast ice typically incorporates more lithogenic PFe than pack ice because of its proximity to continental sources (Grotti et al., 2005; van der Merwe et al., 2011a,b; Lannuzel et al., 2014).

4.3. Lithogenic and biogenic particulate Fe

4.3.1. Icebergs

Several icebergs were sighted in the area (Fig. 1). Icebergs C28B, B16, B09F and B09G remained on the continental shelf during the SIPEX-2 expedition and we suggest that their influence on our ice stations was therefore minimal. However, Fig. 1 shows that iceberg B09D closely followed the shelf break during our study, suggesting it may have dragged along the shelf and stirred some sedimentary PFe in its path. Station 7 being within 30 km and directly in the lee of the B09D, the iceberg could have contributed to the incorporation of dissolved and particulate Fe into the sea-ice cover, either by direct melting or by stirring up some sediments (Raiswell et al., 2008). No under ice seawater PFe samples were collected during SIPEX2 to support this hypothesis. The under-ice seawater profiles did not indicate that B09D influenced the DFe concentrations at station 7 (Schallenberg et al., 2016). Note that the sea-ice data are difficult to directly compare to the under-ice seawater Fe data presented in Schallenberg et al. (2016). This is because sea-ice and seawater datasets are somewhat decoupled; i.e. sea ice collected at station 7 does not necessarily originate from the same location as seawater collected at station 7.

4.3.2. Lithogenic and biogenic contributions to PFe

One method to evaluate the lithogenic contribution to sea ice is to compare the Fe/Al ratios in collected samples to the Fe/Al ratios reported in lithogenic samples from the literature or from specific locations relevant to the study. Fig. 7 shows that the molar ratios Fe/Al (1.15 ± 0.93, $n=30$) in all pack-ice samples are above the crustal and sedimentary ratios of respectively 0.33 (Taylor, 1964) and 0.26–0.34 (Angino, 1969; Gasparon et al., 2007). This suggests that the PFe found in these pack-ice samples cannot be solely from atmospheric deposition and resuspended sediments. High fast ice Fe/Al ratios were observed by de Jong et al. (2013) when Chl*a* concentrations exceeded a threshold (>0.5 μg/L), suggesting a biogenic modification of the elemental ratios in the bottom ice. We further investigate relative lithogenic and biogenic contributions.

Assuming that Al is solely of lithogenic origin and using the mean crustal Fe/Al molar ratios typical of lithogenic samples (Fe/Al=0.33; Taylor, 1964), it is possible to calculate the lithogenic and biogenic PFe concentrations in sea ice (Frew et al., 2006).

$$[\mathrm{PFe}]_{\mathrm{lithogenic}} = [\mathrm{PAl}]_{\mathrm{ice}} \times 0.33$$

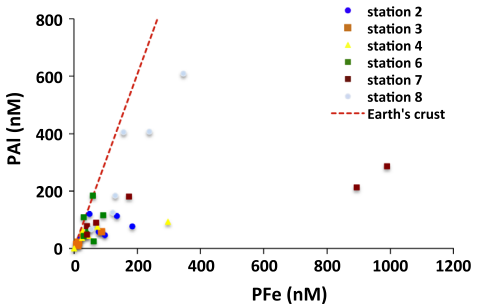

Fig. 7. Plot of particulate Fe (PFe) versus particulate Al (PAl) concentrations (in nM). Earth's crustal Fe/Al ratio=0.33 mol:mol is indicated by the red dotted line. (For interpretation of the references to color in this figure legend, the reader is referred to the web version of this article.)

$$[\mathrm{PFe}]_{\mathrm{biogenic}} = [\mathrm{PFe}]_{\mathrm{ice}} - [\mathrm{PFe}]_{\mathrm{lithogenic}}$$

The results show that 29% of PFe was lithogenic in origin (with $[\mathrm{PFe}]_{\mathrm{lithogenic}} = 35 \pm 40$ nM, $n=30$). Assuming that biogenic PFe is the difference between the total PFe and lithogenic PFe, then the concentration of biogenic PFe in pack ice was on average 93 ± 200 nM ($n=30$), which represents 71% of total PFe. The biogenic contribution represents 87% at station 7, which was the highest recorded on the voyage. This is consistent with POC and Chl*a* data which were also the highest at station 7 (Table 4). Rates of primary productivity in sea ice at station 7 were the second highest during the voyage with an average of 3.32 mg/C/m^2/d (range 0.04–5.5 mg/C/m^2/d), most of which was associated with the internal algal community (Roukaerts et al., 2016).

The concentrations of PFe in pack ice in the same sector were much lower in 2003 (2.0–96.6 nM; Lannuzel et al., unpublished data) and 2007 (0.9–77.7 nM; van der Merwe et al., 2011a) than in 2012 (0.04–990 nM; this study). When using the PFe and PAl concentrations measured in 2007, we find that the biogenic PFe concentrations varied greatly between 2007 (0.0–33.9 nM) and 2012 (0.0–895.5 nM). The high biogenic PFe concentrations recorded during SIPEX-2 illustrates the bio-accumulation of Fe in sea ice, potentially because of differences in the water column characteristics where/when sea ice formed in 2012. The bio-accumulation of Fe could be due to: (1) high DFe inputs originating from the continental shelf or icebergs (Schallenberg et al., 2016) being then actively taken up by sea-ice algae at the ice/water interface and transferred into PFe (Lannuzel et al., 2007; van der Merwe et al., 2011a), or (2) biogenic PFe directly incorporated in sea ice when it originally formed further East potentially on the continental shelf where productivity (and therefore biogenic PFe) may have been higher.

4.4. Role of seasonal sea ice as a natural ocean fertilizer

When using the depth integrated DFe, lithogenic PFe and biogenic PFe concentrations in East Antarctic pack ice from Table 4, and assuming a 1 m thick ice cover and 30 days of melting, the estimated Fe flux from melting pack ice to East Antarctic surface waters in spring 2012 would be 0.2 μmol/m^2/d for DFe, 2.7 μmol/m^2/d for biogenic PFe and 1.3 μmol/m^2/d for lithogenic PFe. Therefore, our study highlights that the biogenic and lithogenic PFe fluxes are an order of magnitude higher than the DFe flux. Particulate organic matter associated with Fe (=biogenic PFe) can be oxidized or remineralized, and release Fe into the dissolved phase, together with carbon, nitrogen and silicate. Remineralization processes have been recognized to play a major role in supplying available Fe to the phytoplankton community (Hurst and Bruland, 2007; Hutchins and Bruland, 1994). The flux of biogenic PFe released from sea ice being 10 times higher than the DFe flux. The importance of sea ice in supplying bio-available PFe to the Antarctic surface waters therefore cannot be ignored. If only 10% of biogenic PFe is regenerated, bio-available PFe can match the DFe flux, therefore doubling the flux of bio-available Fe supplied by melting sea ice to Antarctic surface waters. Iron associated with lithogenic material can also become bio-available, but to a much lesser extent than the biogenic fraction. The size and density of the particles, concentration of organic ligands, ocean mixing, rate of grazing by higher trophic levels and remineralization processes will control the concentration of bio-available PFe supplied by sea ice to surface waters.

Several DFe fluxes have been put forward in the Southern Ocean, and highlight that atmospheric dust input (continental+extraterrestrial) onto pack ice is generally low (i.e. 0.0016 μmol/m^2/d; from Lannuzel et al., 2007). Apart from regional exceptions, it is ack-

nowledged that the main source of Fe to Antarctic sea ice comes from below, either by entrainment from the mixed layer (=new+regenerated Fe) or from organic matter and associated Fe (=regenerated Fe) left floating in seawater from the preceding summer season (Lannuzel et al., 2010). Modeling studies have reported that diapycnal diffusion supplies to the Southern Ocean 0.0016–0.0157 μmol/m^2/d of DFe while deep winter mixing supplies 0.026–0.091 μmol/m^2/d (Tagliabue et al., 2014). With 0.2 μmol DFe /m^2/d released to Antarctic surface waters during the melt season, sea ice supplies more DFe than all the other mentioned sources put together. As sea ice covers 40% of the Southern Ocean, its role as a natural ocean fertilizer therefore cannot be ignored.

4.5. Sea-ice biogeochemistry during SIPEX-2: Iron versus light limitation

Due to favorable environmental conditions at the bottom of ice floes, ice algal communities typically develop at the ice/water interface, resulting in maximum Chl*a*, POC and PON, and a characteristic "L-shaped" vertical profile. However, surface flooding can result in accumulation of biogenic particulate matter in surface slush layers, leading to C-shaped profiles (Meiners et al., 2012). East Antarctic sea ice has been reported to harbor primarily bottom communities (Grose and McMinn, 2003; Meiners et al., 2011). Interestingly, this was not the case in our study. The complex sea-ice properties and ice growth mentioned earlier in the discussion led to heterogeneous distributions of Chl*a*, DOC, POC, PON and to a lesser extent macro-nutrient concentrations (Figs. 4 and 5).

Silicic acid did follow a conservative model of incorporation in sea ice i.e. in proportion with salinity gradients, whilst the other nutrients were either enriched (NH_4^+ and PO_4^{3-}) or consumed (NO_x and PO_4^{3-}) in sea ice. Stations 3 and 7 exhibited enhanced Chl*a*, POC and PON concentrations at the top of the ice cover, suggesting an active surface community. Station 7 displayed a 0.35 m thick snow cover on top of 0.72 m of granular ice (Fig. 2), suggesting some snow ice formed in the top of the ice cover and therefore some surface flooding occurred. The infiltration of seawater may have seeded the surface of the ice with nutrients and micro-organisms, leading to an active surface community at station 7 with a C:N close to the Redfield ratio and high POC, PON and Chl*a* (Fig. 5). In contrast, it is unclear at this stage what lead to the high POC and Chl*a* observed at station 3 in the top layer of the sea ice. The snow thickness was amongst the lowest measured during SIPEX-2 (0.25 m), the ice textures highlight thermodynamic growth (undeformed and level ice) and no snow ice formation. Furthermore, the ice temperatures and brine volumes indicate that the ice cover was typical of winter conditions. We suggest that the relatively thin snow cover led to increased light availability at station 3 compared to other sampling sites, which led to the development of a surface community which used the available nutrients initially incorporated during the early stage of sea-ice formation. This is exemplified by the complete drawdown in NO_x at the ice/snow interface (Fig. 4A and F), compared to the other ice stations where seawater infiltration replenished the surface community with macro-nutrients. However, the $SiOH_4^-$ concentration remained the highest at station 3 (Fig. 4B), suggesting the community developing was not dominated by diatoms, but most likely *Phaeocystis* such as *P. Antarctica* or *P. globulosa.* Interestingly, relatively high NH_4^+ concentrations observed at station 3 suggest strong recycling processes in surface sea ice (Fig. 4D), which supplied regenerated nitrogen needed for the autotrophic community to maintain growth rates. However, resupply of new NO_x through seawater infiltration, either by percolation or flooding, would be required for biomass to increase while maintaining Redfield stoichiometry.

Rates of primary production were measured using stable isotope uptake incubations on the trace metal site at stations 2, 3, 4, 6 and 7 (Roukaerts et al., 2016). The highest rates were measured at station 2 (5.5 mg/C/m^2/d) followed by station 7 (3.3 mg/C/m^2/d). Station 4 had the lowest rates of primary productivity (0.04 mg/C/m^2/d), in agreement with the low Chl*a*, POC and PON concentrations measured in sea ice at that station. A clear increase in primary production was observed during the one-month expedition, during which the daylight increased by about 3 h. Although we do observe an increase in C uptake rates as the season progresses, the levels are low and characteristic of pre-bloom conditions (Roukaerts et al., 2016).

Overall the availability of macro-nutrients and DFe was high throughout the study (i.e. non limiting concentrations except for NO_x < 0.2 μM at stations 3 and 7 in certain sections) and the warm ice temperatures and high permeability of the ice cover were favorable for algal growth. However, a common feature was the thick snow cover on top of the ice at most stations. This feature, on one hand, led to seawater infiltration which may have favored the growth of surface communities, but on another hand, may have restricted incoming light reaching the bottom communities. An increase of snow thickness by 0.2 m can restrict light transmission through sea ice by up to 80% (Arrigo, 2003). In our study, snow thickness averaged 0.4 m and represented almost 30% of the sea-ice thickness. We therefore suggest that, because of extensive snow cover witnessed during the expedition, the low light levels led to the low sea-ice primary productivity (see also Ugalde et al., 2016; Roukaerts et al., 2016).

The Fe demand of sea-ice algae can be estimated from cellular Fe:C and primary productivity (PP) (Fe_{demand} = new PP × $(Fe:C)_{cellular}$) where new PP = 0.5–6 mg/C/m^2/d (Roukaerts et al., 2016). To the best of our knowledge, no data on intracellular Fe:C ratios currently exist for sea-ice algae assemblages. In seawater, this ratio typically ranges from 10 to 40 μmol Fe:mol C (de Baar et al., 2008; Hassler and Schoemann, 2009; Sarthou et al., 2005) and not only does it vary in space and time, but it also varies with the type of phytoplankton. Iron fertilized sites tend to sit in the higher range of $(Fe:C)_{cellular}$ ratios (Sarthou et al., 2005). Using a conservative estimation of $(Fe:C)_{cellular}$ = 10–40 μmol:mol for sea ice algae, we obtain an Fe_{demand} = 0.4–20 nmol/m^2/d in sea ice. This Fe_{demand} is well below the DFe_{supply} in sea ice = 0.86 μmol/m^2/d estimated during the voyage, confirming that Fe did not limit the primary productivity in sea ice at this time of year. The DFe_{supply} in sea ice was approximated by substracting the lowest from the highest DFe inventory values reported in table 4 (=16.9–2.2 μmol/m^2), and dividing by the time elapsed between these 2 stations (17 days).

If the growth of the sea-ice community was not directly controlled by the lack of Fe, the under ice phytoplankton community may however have been limited by Fe supply later in the season, when light limitation was alleviated. In the marginal ice zone, a 0.2 μmol/m^2/d supply of DFe from melting pack ice and $(Fe:C)_{cellular}$ = 10–40 μmol:mol would sustain a gross primary productivity of 0.06–0.24 g/m^2/d in the East Antarctic sector. Our Fe-induced productivity estimate represents 10% to 40% of the 0.61 g/m^2/d measured in seawater in the marginal ice zone in spring 1996 (Nicol et al., 2000). The higher and lower ends of our estimate are controlled by the Fe:C range we used, which is based on phytoplankton cultures and therefore may not match the in situ ratios. Additionally, if 10% to 70% of biogenic PFe supplied from sea ice is soluble and therefore becomes available for phytoplankton uptake, then the Fe fertilization from sea ice can fully account for the primary productivity value reported by Nicol et al. (2000). Our estimates clearly demonstrate that the uncertainties on the intracellular Fe:C ratios and on the solubility of PFe have to be addressed before we can fully appreciate the role of sea ice-bearing Fe in controlling primary productivity in the marginal ice zone.

5. Conclusion

Concentrations of DFe in pack ice collected during SIPEX-2 were 2 to 3 orders of magnitude more concentrated than in ice-free East Antarctic waters (Schallenberg et al., 2016). The SIPEX-2 DFe ranges were found to lie between those previously reported from the ARISE and SIPEX-1 studies, even though the sea-ice conditions were very different. Sea-ice thickness, texture and growth (i.e. thermodynamic versus dynamic) do not control the concentrations of DFe in sea ice. Instead, we hypothesize that DFe precipitates into PFe when it reaches a certain in situ solubility threshold. This threshold may be controlled by the concentration of Fe-binding organic ligands present in sea ice. Particulate Fe concentrations did vary between stations, with station 7 displaying unique characteristics. A strong biogenic PFe signature was observed at all stations, especially at station 7. Iron supply estimates highlight the dominance of PFe over DFe in fertilizing the marginal ice zone, but questions remain regarding how bio-available PFe may become once released into seawater. The flooding and dynamic conditions under which sea ice grew during SIPEX-2, involving rafting and ridging processes, led to unusual biogeochemical profiles in sea ice. The availability of nutrients, favorable sea-ice conditions (warm and porous), low primary productivity and thick snow covers observed throughout the study suggest that light was the primary factor limiting growth in sea ice at this time of the year in the SIPEX-2 study area.

Acknowledgements

The authors would like to thank the officers and crew of the *RV Aurora Australis* for their logistic support during the SIPEX-2 voyage. We would like to acknowledge Olivier Lecomte for helping in the collection of the trace metal ice cores. This work was co-funded by the Australian Research Council (LE0989539 and DE120100030), the Australian Government Cooperative Research Centres Programme through the Antarctic Climate & Ecosystems (ACE CRC) and the Australian Antarctic Science (AAS) project no. 4051.

References

Angino, E.E., 1969. Geochemistry of Antarctic pleagic sediments. Geochim. Cosmochim. Acta 30, 939–961.

Arndt, J.E., Schenke, H.W., Jakobsson, M., Nitsche, F., Buys, G., Goleby, B., Rebesco, M., Bohoyo, F., Hong, J.K., Black, J., Greku, R., Udintsev, G., Barrios, F., Reynoso-Peralta, W., Morishita, T., Wigley, R., no date. The International Bathymetric Chart of the Southern Ocean (IBCSO) Version 1.0—a new bathymetric compilation covering circum-Antarctic waters, Geophys Res. Lett., http://dx.doi.org/10.1002/grl.50413.

Arrigo, K.R., 2003. Physical control of chlorophyll *a*, POC, and TPN distributions in the pack ice of the Ross Sea, Antarctica. J. Geophys. Res. 108 (C10), 3316. http://dx.doi.org/10.1029/2001JC001138.

Becquevort, S., Dumont, I., Tison, J.L., Lannuzel, D., Sauvée, M.L., Chou, L., Schoemann, V., 2009. Biogeochemistry and microbial community composition in sea ice and underlying seawater off East Antarctica during early spring. Polar Biol. 32 (6), 879–895. http://dx.doi.org/10.1007/s00300-009-0589-2.

Blain, S., Quéguiner, B., Armand, L., Belviso, S., Bombled, B., Bopp, L., Wagener, T., 2007. Effect of natural iron fertilization on carbon sequestration in the Southern Ocean. Nature 446 (7139), 1070–1074. http://dx.doi.org/10.1038/nature05700.

Bowie, A.R., Townsend, A.T., Lannuzel, D., Remenyi, T., van der Merwe, P., 2010. Modern sampling and analytical methods for the determination of trace elements in marine particulate material using magnetic sector inductively coupled plasma-mass spectrometry. Anal. Chim. Acta 676 (1-2), 15–27. http://dx.doi.org/10.1016/j.aca.2010.07.037.

Boyd, P.W., Law, C.S., Wong, C.S., Nojiri, Y., Tsuda, A., Levasseur, M., 2004. The decline and fate of an iron-induced subarctic phytoplankton bloom. Nature 428, 549–553. http://dx.doi.org/10.1029/2001JB001129.

Boyd, P.W., Jickells, T., Law, C.S., Blain, S., Boyle, E.a., Buesseler, K.O., Watson, AJ, 2007. Mesoscale iron enrichment experiments 1993–2005: synthesis and future directions. Science (New York, NY) 315 (5812), 612–617. http://dx.doi.org/10.1126/science.1131669.

Bunch, J.N., Harland, R.C., 1990. Bacterial production in the bottom surface of sea ice in the Canadian subarctic. Can J. Fish. Aquat. Sci. 47, 1986–1995.

Cox, G.F.N., Weeks, W.F., 1983. Equations for determining the gas and brine volumes in sea-ice samples. Ann. Glaciol. 29 (102), 306–316.

de Baar, H.J.W., Buma, A.G.J., Nolting, R.F., Cadée, G.C., Jacques, G., Tréguer, P., 1990. On iron limitation of the Southern Ocean: experimental observations in the Weddell and Scotia Seas. Mar. Ecol. Prog. Ser. 65, 105–122.

de Baar, H.J.W., Gerringa, L., Laan, P., Timmermans, K., 2008. Efficiency of carbon removal per added iron in ocean iron fertilization. Mar. Ecol. Prog. Ser. 364, 269–282. http://dx.doi.org/10.3354/meps07548.

de Jong, J., Schoemann, V., Maricq, N., Mattielli, N., Langhorne, P., Haskell, T., Tison, J., 2013. Iron in land-fast sea ice of McMurdo Sound derived from sediment resuspension and wind-blown dust attributes to primary productivity in the Ross Sea, Antarctica. Mar. Chem. , http://dx.doi.org/10.1016/j.marchem.2013.07.001.

Eicken, H., 2003. From the microscopic to the macroscopic to the regional scale, growth, microstrucutre and properties of sea ice. In: Sea Ice – an Introduction to Its Physics, Biology, Chemistry and Geology. Blackwell Science, London, pp. 22–81.

Engel, A., Passow, U., 2001. Carbon and nitrogen content of transparent exopolymer particles (TEP) in relation to their Alcian Blue adsorption. Mar. Ecol. Prog. Ser. 219, 1–10.

Frew, R.D., Hutchins, D., Nodder, S., Sanudo-Wilhelmy, S., Tovar-Sanchez, A., Leblanc, K., Boyd, P.W., 2006. Particulate iron dynamics during FeCycle in subantarctic waters southeast of New Zealand, Global Biogeochem CyBiogeochem. Cycles 20 (1), http://dx.doi.org/10.1029/2005GB002558, (n/a–n/a)!.

Garrison, D.L., Close, A.R., Reimnitz, E., 1989. Algae concentrated by frazil ice: evidence from laboratory experiments and field measurements. Antarct. Sci. 1 (4), 313–316.

Gasparon, M., Ehrler, K., Melles, M., 2007. Temporal and spatial variability of geochemical backgrounds in the Windmill Islands, East Antarctica: implications for climatic changes and human impacts. Appl. Geochem., *22*; , pp. 888–905. http://dx.doi.org/10.1016/j.apgeochem.2006.12.018.

Golden, K., Ackley, S.F., Lytle, V., 1998. The percolation phase transition in sea Ice. Science (New York, NY) 282 (5397), 2238–2241 (Retrieved from).

Grose, M., McMinn, A., 2003. Algal biomass in east Antarctic pack ice: how much is in the east. In: Huiskes, A.H.L., Gieskes, W.W.C., Rozema, J., Schorno, R.M.L., van der Vies, S.M., Wolff, W.J. (Eds.), Antarctic Biology in a Global Context. Proceedings of the VIIIth SCAR International Biology Symposium. Backhuys Publishers, Leiden, pp. 21–25.

Grotti, M., Soggia, F., Ianni, C., Frache, R., 2005. Trace metals distributions in coastal sea ice of Terra Nova Bay, Ross Sea, Antarctica. Antarct. Sci. 17 (2), 289–300. http://dx.doi.org/10.1017/S0954102005002695.

Hassler, C.S., Schoemann, V., 2009. Bioavailability of organically bound Fe to model phytoplankton of the Southern Ocean. Biogeosci. Discuss. 6, 1677–1712.

Heil, Hutchings, Massom, Stevens, Lecomte et al., 2016. Physical Characterization of the East Antarctic Pack Ice During SIPEX 2012. Deep Sea Res. Part II, 131, 7–21.

Horner, R., 1996. Ice algal investigations:historical perspective. In: NIPR Symp. Polar Biol., 1–12.

Hurst, M.P., Bruland, K.W., 2007. An investigation into the exchange of iron and zinc between soluble, colloidal, and particulate size-fractions in shelf waters using low-abundance isotopes as tracers in shipboard incubation experiments. Mar. Chem. 103 (3-4), 211–226. http://dx.doi.org/10.1016/j.marchem.2006.07.001.

Hutchins, D.A., Bruland, K.W., 1994. Grazer-mediated regeneration and assimilation of Fe, Zn and Mn from planktonic prey. Mar. Ecol. Prog. Ser. 110, 259–269.

Kepkay, P.F., 2000. Colloids and the ocean carbon cycle. In: Wangersky, P. (Ed.), The Handbook Of Environmental Chemistry, vol 5. Part D: Marine Chemistry. Springer, Berlin, pp. 35–56.

Lancelot, C., Montety, A., De, Goosse, H., Becquevort, S., Schoemann, V., 2009. Spatial distribution of the iron supply to phytoplankton in the Southern Ocean: a model study. Biogeosci. Discuss. 6, 4919–4962.

Langway, C.C., 1958. Ice Fabrics and the Universal Stage. USA Cold Regions Research and Engineering Laboratory, CRREL Technical Report, 62, .

Lannuzel, D., de Jong, J., Schoemann, V., Trevena, A., Tison, J.-L., Chou, L., 2006. Development of a sampling and flow injection analysis technique for iron determination in the sea ice environment. Anal. Chim. Acta 556 (2), 476–483. http://dx.doi.org/10.1016/j.aca.2005.09.059.

Lannuzel, D., Schoemann, V., de Jong, J., Tison, J.-L., Chou, L., 2007. Distribution and biogeochemical behaviour of iron in the East Antarctic sea ice. Mar. Chem. 106 (1-2), 18–32. http://dx.doi.org/10.1016/j.marchem.2006.06.010.

Lannuzel, D., Schoemann, V., de Jong, J., Chou, L., Delille, B., Becquevort, S., Tison, J.-L., 2008. Iron study during a time series in the western Weddell pack ice. Mar. Chem. 108 (1-2), 85–95. http://dx.doi.org/10.1016/j.marchem.2007.10.006.

Lannuzel, D., Schoemann, V., de Jong, J., Pasquer, B., van der Merwe, P.,, Masson, F., Bowie, A., 2010. Distribution of dissolved iron in Antarctic sea ice: Spatial, seasonal, and inter-annual variability. J. Geophys. Res. 115 (G3), G03022. http://dx.doi.org/10.1029/2009JG001031.

Lannuzel, D., Bowie, A.R., Remenyi, T., Lam, P., Townsend, A., Ibisanmi, E., Schoemann, V., 2011. Distributions of dissolved and particulate iron in the sub-Antarctic and Polar Frontal Southern Ocean (Australian sector). Deep Sea Res. Part II 58 (21-22), 2094–2112. http://dx.doi.org/10.1016/j.dsr2.2011.05.027.

Lannuzel, D., Merwe, P.C., Van Der, Townsend, A.T., Bowie, A.R., 2014. Size fractionation of iron, manganese and aluminium in Antarctic fast ice reveals a lithogenic origin and low iron solubility. Mar. Chem. 161, 47–56.

Lannuzel, D., Grotti, M., Abelmoshi, M.-L., van der Merwe, P.C. Organic ligands control the concentrations of dissolved iron in Antarctic sea ice. Mar. Chem., Under review.

Martin, J.H., Fitzwater, S.E., 1988. Iron deficiency limits phytoplankton growth in the north-east Pacific subarctic. Nature 331 (6154), 341–343.

Meiners, K.M., Norman, L., Granskog, M.A., Krell, A., Heil, P., Thomas, D.N., 2011. Physico-ecobiogeochemistry of East Antarctic pack ice during the winter-spring transition. Deep Sea Res. Part II 58 (9-10), 1172–1181. http://dx.doi.org/10.1016/j.dsr2.2010.10.033.

Meiners, K.M., Vancoppenolle, M., Thanassekos, S., Dieckmann, G.S., Thomas, D.N., Tison, J.-L., Raymond, B., 2012. Chlorophyll *a* in Antarctic sea ice from historical ice core data. Geophys. Res. Lett. *39* (21), http://dx.doi.org/10.1029/2012GL053478 (n/a–n/a).

Millero, F.J., 1996. Chemical Oceanography, second ed. CRC Press, Boca Raton, FL.

Nicol, S., Pauly, T., Bindoff, N.L., Wright, S., Thiele, D., Hosie, G.W., Woehler, E., 2000. Ocean circulation off east Antarctica affects ecosystem structure and sea-ice extent. Nature 406 (6795), 504–507. http://dx.doi.org/10.1038/35020053.

Palmisano, A.C., Garrison, D.L., 1993. Microorganisms in Antarctic sea-ice, Antarctic Microbiology. I. Friedman. Wiley-Liss, New York, pp. 167–218.

Pollard, R.T., Salter, I., Sanders, R.J., Lucas, M.I., Moore, C.M., Mills, R.A., Zubkov, M.V., 2009. Southern Ocean deep-water carbon export enhanced by natural iron fertilization. Nature 457 (7229), 577–580. http://dx.doi.org/10.1038/nature07716.

Raiswell, R., Benning, L.G., Tranter, M., Tulaczyk, S., 2008. Bioavailable iron in the Southern Ocean: the significance of the iceberg conveyor belt. Geochem. Trans. 9, 1–9. http://dx.doi.org/10.1186/1467-4866-9-7.

Redfield, A.C., 1958. The biological control of chemical factors in the environment. Am. Sci. 46 (3), 205–221.

Riedel, A., Michel, C., Gosselin, M., LeBlanc, B., 2008. Winter-spring dynamics in sea ice carbon cycling in the coastal Arctic Ocean. J. Mar. Syst. 74 (3-4), 918–932.

Roukaerts, A., Cavagna, A.J., Fripiat, F., Lannuzel, D., Mainers, K.M., Dehairs, F., 2016. Determination of the regimes of production in the Antarctic sea-ice during SIPEX-2 using N, & C stable isotope in-situ incubation experiments. Deep Sea Res. Part II, 131, 140–149.

Saenz, B.T., Arrigo, K.R., 2012. Simulation of a sea ice ecosystem using a hybrid model for slush layer desalination. J. Geophys. Res. 117 (C5), C05007. http://dx.doi.org/10.1029/2011JC007544.

Sarmiento, J.G., Gruber, N., 2006. Ocean Biogeochemical Dynamics. Princeton University Press, Princeton, Woodstock p. 503.

Sarthou, G., Timmermans, K.R., Blain, S., Tréguer, P., 2005. Growth physiology and fate of diatoms in the ocean: a review. J. Sea Res. 53 (1-2), 25–42. http://dx.doi.org/10.1016/j.seares.2004.01.007.

Schallenberg, C., van der Merwe, P.C., Chever, F., Cullen, J., Lannuzel, D., Bowie, A. 2016. Dissolved iron distribution in the water column beneath the pack ice in the Eastern Antarctic (120 E) during the winter/spring transition. Deep Sea Res. Part II, 131, 96–110.

Sedwick, P.N., Edwards, P.R., Mackey, D.J., Griffiths, F.B., Parslow, J.S., 1997. Iron and manganese in surface waters of the Australian subantarctic region. Deep Sea Res. Part I 44 (7), 1239–1253.

Smith, R.E.H., Gosselin, M., Kudoh, S., Robineau, B., Taguchi, S., 1997. DOC and its relationship to algae in bottom ice communities. J. Mar. Syst. 11, 71–80.

Sturm, M., R.A. Massom, 2010. Snow and sea ice. In: D. Thomas, G. Dieckman (Eds.), Sea Ice. second ed., Wiley-Blackwell, New York (USA) and Oxford (UK), 153-204.

Tagliabue, A., Sallée, J.-B., Bowie, A.R., Lévy, M., Swart, S., Boyd, P.W., 2014. Surface-water iron supplies in the Southern Ocean sustained by deep winter mixing. Nat. Geosci. *7* (4), 314–320. http://dx.doi.org/10.1038/ngeo21.

Taylor, S.R., 1964. Abundance of chemical elements in the continental crust: a new table. Geochim. Cosmochim. Acta 28, 1273–1285.

Thomas, D.N., Dieckmann, G.S., 2003. Sea Ice—An Introduction to its Physics, Chemistry, Biology and Geology. Blackwell Publishing, Oxford.

van der Merwe, P., Lannuzel, D., Mancuso Nichols, C.A., Meiners, K.M., Heil, P., Norman, L., Bowie, A.R., 2009. Biogeochemical observations during the winter–spring transition in East Antarctic sea ice: evidence of iron and exopolysaccharide controls. Mar. Chem. 115 (3-4), 163–175. http://dx.doi.org/10.1016/j.marchem.2009.08.001.

van der Merwe, P., Lannuzel, D., Bowie, A.R., Mancuso Nichols, C.A., Meiners, K.M., 2011a. Iron fractionation in pack and fast ice in East Antarctica: temporal decoupling between the release of dissolved and particulate iron during spring melt. Deep Sea Res. Part II 58, 1222–1236.

van der Merwe, P., Lannuzel, D., Bowie, A.R., Meiners, K.M., 2011b. High temporal resolution observations of spring fast ice melt and seawater iron enrichment in East Antarctica. J. Geophys. Res. 116 (G3), G03017. http://dx.doi.org/10.1029/2010JG001628.

Weissenberger, J., Grossmann, S., 1998. Experimental formation of sea ice: importance of water circulation and wave action for incorporation of phytoplankton and bacteria. Polar Biol. 20, 178–188.

Worby, A.P., Massom, R.A., Allison, I., Lytle, V.I., Heil, P., 1998. East Antarctic sea ice: A review of its structure, properties and drift, In: (Ed.) Jeffries, M.O., Antarctic Sea Ice: Physical Processes, Interactions and Variability, Antarct. Res. Ser., vol. 74, , AGU, Washington, DC, pp. 41–67.